KAUNAS UNIVERSITY OF TECHNOLOGY

MIGLĖ ŽAMOIT

ACRYLATED EPOXIDIZED SOYBEAN OIL-BASED POLYMERS AND POLYMERIC COMPOSITES FOR OPTICAL 3D PRINTING

Doctoral dissertation
Technological Sciences, Chemical Engineering (T 005)

Kaunas, 2023

Scientific Supervisor:
Prof. Dr. Jolita OSTRAUSKAITĖ (Kaunas University of Technology, Technological Sciences, Chemical Engineering, T 005).

Edited by: English language editor Dovilė Blaudžiūnienė (Publishing House *Technologija*), Lithuanian language editor Eglė Dumskytė (Publishing House *Technologija*)

Dissertation Defense Board of Chemical Engineering Science Field:
Prof. Dr. Raimundas ŠIAUČIŪNAS (Kaunas University of Technology, Technological Sciences, Chemical Engineering, T 005) – **chairperson**;
Assoc. Prof. Dr. Joana BENDORAITIENĖ (Kaunas University of Technology, Technological Sciences, Chemical Engineering, T 005);
Senior researcher Dr. Mindaugas GEDVILAS (Center for Physical Sciences and Technology, Technological Sciences, Materials Engineering, T 008);
Assoc. Prof. Dr. Anne-Sophie SCHULLER (University of Haute-Alsace, France, Technological Sciences, Chemical Engineering, T 005);
Prof. Dr. Virgilius VALEIKA (Kaunas University of Technology, Technological Sciences, Chemical Engineering, T 005).

The official defense of the dissertation will be held at 10 a.m. on 12 May, 2023 at the public meeting of Dissertation Defense Board of Chemical Engineering Science Field in the Meeting room A228 at Santaka Valley of Kaunas University of Technology.

Address: Baršausko 59–A228, Kaunas, LT-51423, Lithuania.
Phone: (+370) 608 28 527; e-mail doktorantura@ktu.lt

Doctoral dissertation was sent on 12 April, 2023.
The doctoral dissertation is available on the internet http://ktu.edu and at the library of Kaunas University of Technology (K. Donelaičio 20, Kaunas, LT-44239, Lithuania).

KAUNO TECHNOLOGIJOS UNIVERSITETAS

MIGLĖ ŽAMOIT

AKRILINTO EPOKSIDINTO SOJŲ ALIEJAUS POLIMERAI IR POLIMERINIAI KOMPOZITAI OPTINIAM 3D SPAUSDINIMUI

Kaunas, 2023

Mokslinis vadovas:
prof. dr. Jolita OSTRAUSKAITĖ (Kauno technologijos universitetas, technologijos mokslai, chemijos inžinerija, T 005).

Redagavo: anglų kalbos redaktorė Dovilė Blaudžiūnienė (leidykla „Technologija"), lietuvių kalbos redaktorė Eglė Dumskytė (leidykla „Technologija")

Chemijos inžinerijos mokslo krypties disertacijos gynimo taryba:
prof. dr. Raimundas ŠIAUČIŪNAS (Kauno technologijos universitetas, technologijos mokslai, chemijos inžinerija, T 005) – **pirmininkas**;
doc. dr. Joana BENDORAITIENĖ (Kauno technologijos universitetas, technologijos mokslai, chemijos inžinerija, T 005);
vyr. m. d. dr. Mindaugas GEDVILAS (Fizinių ir technologijos mokslų centras, technologijos mokslai, medžiagų inžinerija, T 008);
doc. dr. Anne-Sophie SCHULLER (Aukštutinio Elzaso universitetas, Prancūzija, technologijos mokslai, chemijos inžinerija, T 005);
prof. dr. Virgilijus VALEIKA (Kauno technologijos universitetas, technologijos mokslai, chemijos inžinerija, T 005).

Disertacija bus ginama viešame Chemijos inžinerijos mokslo krypties disertacijos gynimo tarybos posėdyje 2023 m. gegužės 12 d. 10 val. Kauno technologijos universiteto „Santakos" slėnyje, Posėdžių kambaryje A228.

Adresas: K. Baršausko g. 59-A228, Kaunas, LT-51423, Lietuva.
Tel. (+370) 608 28 527; el. paštas doktorantura@ktu.lt

Disertacija išsiųsta 2023 m. balandžio 12 d.
Su disertacija galima susipažinti interneto svetainėje http://ktu.edu ir Kauno technologijos universiteto bibliotekoje (K. Donelaičio g. 20, Kaunas, LT-44239, Lietuva).

Contents

LIST OF ABBREVIATIONS

AESO – acrylated epoxidized soybean oil

ABAPO – composition of acrylated epoxidized soybean oil with photoinitiator phenyl bis(2,4,6-trimethylbenzoyl) phosphine oxide

ADMPA – composition of acrylated epoxidized soybean oil with photoinitiator phenyl bis(2,4,6-trimethylbenzoyl) phosphine oxide

AS – the weight part of acrylated epoxidized soybean oil in the composition

ATPO – composition of acrylated epoxidized soybean oil with photoinitiator diphenyl (2,4,6-trimethylbenzoyl) phosphine oxide

ATPOL — composition of acrylated epoxidized soybean oil with photoinitiator ethyl (2,4,6-thimethylbenzoyl) phenyl phosphinate

BAPO – phenyl bis(2,4,6-trimethylbenzoyl) phosphine oxide

BRC – biorenewable carbon content

DMPA – 2,2-dimethoxy-2-phenyl acetophenone

DMTA – dynamic mechanical thermal analysis

DLP – digital light processing

DSC – differential scanning calorimetry

DVB – divinylbenzene

E_C – compressive modulus

E_E – elastic modulus

ECM – ethylcellulose macromonomer

FLGPCL02 – commercial photoresin Formlabs Clear FLGPCL02

G' – storage modulus

HDDA – 1,6-hexanediol diacrylate

I – the weight of isobornyl methacrylate in the composition

IBOMA – isobornyl methacrylate

LCA – life cycle assessment

LDW –laser direct writing

ME – methacrylic ester

MYR – myrcene

nHA – nano-hydroxyapatite

pAESO – homopolymer synthesized from pure acrylated epoxidized soybean oil

PR48 – commercial photoresin Aurodesk Clear PR48

REF — commercial photoresin Monocure3D Rapid Gray

RD – reactive diluent

SLA – stereolithography

$T_{dec.-10\%}$ – temperature at a weight loss of 10%

T_g – glass transition temperature

t_{gel} – gel point

TGA – thermogravimetric analysis

THFA – tetrahydrofurfuryl acrylate

THFMA – tetrahydrofurfuryl methacrylate

TMPTA – trimethylolpropane triacrylate

TPO – diphenyl (2,4,6-trimethylbenzoyl) phosphine oxide

TPOL – ethyl (2,4,6-thimethylbenzoyl) phenyl phosphinate

VDA – vanillin diacrylate

VDM – vanillin dimethacrylate

X – filler synthesized from silica gel and calcium oxide

XS – filler synthesized from silica gel-rich aluminum fluoride production waste material and calcium oxide

YIF – yield of the insoluble fraction

σ – tensile strength

ε – elongation at break

1. INTRODUCTION

In the past decade, 3D printing technologies have attained an immense amount of attention not only among scientists, but also between regular consumers. 3D printing, or additive manufacturing allows the direct fabrication of complex 3D structures with low raw material usage, making it a powerful technique for advanced manufacturing [1]. Relatively simple and vastly used 3D printing technology is fused deposition modelling (FDM) where melted thermoplastic polymer filament is extruded to form a layered printed object [2]. Optical 3D printing technologies employ light to harden layer-by-layer liquid photo-curable resin into complex-shaped polymeric objects, which cannot be cut, carved, or assembled [3]. While FDM technology indicates higher printing speed, higher printing resolution, more detailed object parts could be obtained in optical 3D printing [4] making it more suitable for precise product manufacturing. Although most of the commercially available 3D printing materials are environmentally stable petroleum-based materials. To reduce negative environmental impact, bio-based materials could be used in optical 3D printing. By combining various bio-based materials, partially or fully bio-based photocross-linked polymers for optical 3D printing could be obtained. Also, depending on the structure and functionality of bio-based materials, different properties of 3D printed polymeric object could be developed [5].

The introduction of reinforcements to photocross-linked polymers has received extensive attention due to the improved properties of 3D printed objects. Depending on the composition of the 3D printing resin and the reinforcement chosen, the improved properties of the polymer composite could be obtained, such as mechanical, thermal, electrical, or other properties [6]. By employing bio-based materials suitable for optical 3D printing with appropriate reinforcement, practicable biocomposites could be produced. Such materials could not only replace synthetic materials in optical 3D printing, but could also improve the properties of printed objects with an indicated biodegradability.

The development of acrylated epoxidized soybean oil (AESO)-based polymers with or without additional reinforcement suitable for optical 3D printing was the main object of this work. AESO is a low cost and low toxicity bio-based material used in UV-curing coatings and produced in high annual yields [7] making it a suitable bio-based material for this research. In the scope of this dissertation, the application of AESO in optical 3D printing producing bio-based polymers and polymer composites suitable for replacing commercial petroleum-based products was addressed. The experimental results have been presented in five publications.

The aim of the work was to develop acrylated epoxidized soybean oil-based photocross-linked polymers and polymer composites for optical 3D printing technologies.

The tasks proposed to achieve the above-stated aim were as follow:

1. To design and synthesize photocross-linked polymers composed of acrylated epoxidized soybean oil and plant-derived comonomers,

investigate their properties and compare with those of commercial products used in optical 3D printing technologies;

2. To investigate initiator-free photocuring of acrylated epoxidized soybean oil-based resins and the properties of the resulting polymers and apply them in laser direct writing lithography;

3. To determine the influence of acrylated epoxidized soybean oil on four photoinitiators, their concentration, and temperature on the photocuring kinetics and the properties of the resulting polymers;

4. To design and synthesize acrylated epoxidized soybean oil-based photocross-linked polymers with different plant-derived reactive diluents, investigate their properties and suitability for digital light processing 3D printing;

5. To determine the influence on calcium silicate hydrate (CaO and SiO_2 molar ratio 1:1) fillers on properties of photocross-linked acrylated epoxidized soybean oil-based polymer composites and determine their suitability for digital light processing 3D printing.

Scientific novelty

- For the first time, acrylated epoxidized soybean oil-based cross-linked polymers have been synthesized without the use of a photoinitiator, which retain the free-standing structure of polymeric objects and are suitable for laser direct writing lithography.

- Novel acrylated epoxidized soybean oil-based resins containing plant-derived comonomers exhibit high photosensitivity and cross-linking rate suitable for optical 3D printing.

- New functionalized calcium silicate hydrate fillers synthesized from aluminum fluoride production waste resulted in better mechanical and thermal properties of acrylated epoxidized soybean oil-based composites compared to fillers obtained from synthetic inorganic reagents.

Practical value of the work

Photocross-linked polymers and polymer composites suitable for different optical 3D printing technologies have been developed only from commercially available bio-based monomers. Six acrylated epoxidized soybean oil-based resins in total have been validated and tested in industrial digital light processing 3D printers in companies JSC "3D Creative" and "AmeraLabs". The properties of their 3D printed objects of complex structure were comparable to those printed from commercial synthetic materials. The Life Cycle Assessment (LCA) of acrylated epoxidized soybean oil photoresin with bio-based isobornyl methacrylate has been carried out for optically 3D printed dental models in collaboration with Centria University of Applied Sciences and "AmeraLabs" [8]. The comparison of the environmental impact of acrylated epoxidized soybean oil-based resin and conventional petroleum-based acrylic resin clearly showed the benefit of using bio-based materials for formulating the UV-curable 3D printing resin, as reduced environmental impact has been

determined in 12 out of 16 categories. All bio-based polymers designed, which were successfully applied in digital light processing 3D printing, showed biodegradability, although it was a slower process than that of cellulose at the same experimental conditions.

Contribution of the author

The author has designed, synthesized, and characterized five series of acrylated epoxidized soybean oil cross-linked polymers and polymeric composites described in Chapters 2.1–2.5. The author has performed and analyzed the results of photorheometry measurements, Soxhlet extraction, differential scanning calorimetry, thermogravimetric analysis, dynamic mechanical thermal analysis, compression, and tensile, and biodegradation test. The author drafted all five manuscripts. Edvinas Skliutas (Laser Research Center, Vilnius University) performed laser direct writing of the selected biobased resins, analyzed printed μ-3D structures, and contributed to drafting the manuscript. Prof. dr. Mangirdas Malinauskas (Laser Research Center, Vilnius University) advised with the μ-3D printing and contributed to the editing of the paper. Vaidas Talačka (AmeraLabs) evaluated printing parameters for acrylated epoxidized soybean oil-based resins and performed digital light processing 3D printing. Andrius Gineika (Kaunas University of Technology) synthesized, characterized calcium silicate hydrate fillers, and contributed to drafting the manuscript. Prof. dr. Kęstutis Baltakys (Kaunas University of Technology) advised with the synthesis of calcium silicate hydrate fillers and contributed to the editing of the paper. Prof. dr. Jolita Ostrauskaitė (Kaunas University of Technology) contributed to conceiving the initial ideas, advising with the synthesis and characterization on acrylated epoxidized soybean oil cross-linked polymers and contributed to the editing of all five papers. Dr. Rathish Rajan and dr. Egidija Rainosalo (Centria University of Applied Sciences, Finland) modelled and performed cradle-to-gate life-cycle assessment of optical 3D printing of bio-based and conventional acrylic resin. Saulius Lileikis and colleagues from JSC 3D Creative performed 3D scanning of medical fittings and produced real-scale objects from bio-based resin by digital light processing 3D printing.

List of scientific publications on the topic of the dissertation

1. <u>Miglė Lebedevaitė</u>, Jolita Ostrauskaitė, Edvinas Skliutas, Mangirdas Malinauskas. Photocross-linked polymers based on plant-derived monomers for potential application in optical 3D printing. *Journal of applied polymer science*. **2020**, *137* (20), 48708. JIF: 3.125.
2. <u>Miglė Lebedevaitė,</u> Jolita Ostrauskaitė, Edvinas Skliutas, Mangirdas Malinauskas. Photoinitiator free resins composed of plant-derived monomers for the optical μ-3D printing of thermosets, *Polymers*. **2019**, *11* (1), 116. JIF: 4.329.
3. <u>Miglė Lebedevaitė,</u> Jolita Ostrauskaitė. Influence of photoinitiator and temperature on photocross-linking kinetics of acrylated epoxidized soybean oil and properties of the resulting polymers. *Industrial crops and products*. **2021**, *161*, 113210. JIF: 5.645.

4. <u>Miglė Lebedevaitė,</u> Vaidas Talačka, Jolita Ostrauskaitė. High biorenewable content acrylate photocurable resins for DLP 3D printing. *Journal of Applied Polymer Science*. **2021**, *138* (16), 50233. JIF: 3.125.
5. <u>Miglė Lebedevaitė,</u> Andrius Gineika, Vaidas Talačka, Kęstutis Baltakys, Jolita Ostrauskaitė. Development and optical 3D printing of acrylated epoxidized soybean oil-based composites with functionalized calcium silicate hydrate filler derived from aluminum fluoride production waste. *Composites Part A: Applied Science and Manufacturing*. **2022**, *157*, 106929. JIF: 7.664.

Scientific conferences

The results of this dissertation have been presented in 17 international scientific conferences, including "6th international Baekeland symposium 2019" Tarragona, Spain; "Poly-Char Venice international polymer characterization forum 2021" Venice, Italy; "IUPAC-MACRO 2020: the 48th world polymer congress", Jeju, Korea. A full list of scientific conferences is presented in section 8. LIST OF PUBLICATIONS.

LITERATURE REVIEW

1.1. Optical 3D printing

In recent years, 3D printing, or additive manufacturing, has become extensively used because of its simplicity, immense creativity, and its relatively low cost. This process allows one to create complex structural objects that cannot be carved, cut, or assembled [9]. Optical 3D printing employs vat photopolymerization, where photo-sensitive liquid resin is layer-by-layer solidified by light. The most popular optical 3D printing techniques are digital light processing (DLP) and stereolithography (SLA). Their working basics are closely related, and the difference is that SLA employs a fast-moving laser beam for photoresin curing, while DLP uses projected light [10] (Figure 1). Less common is laser direct writing (LDW)-based two-photon polymerization technology that uses a laser to create complex 3D structures on the nanoscale [11]. Due to the focused high-energy laser beam, the wider spectrum of materials could be applied in LDW [12]. Compared to bulk materials, micro/nano-structured materials have different properties, thus such feature could be applied in biomedicine, microchip formation and more [13]. Although this complex and rather expensive technology is more popular among researchers [14].
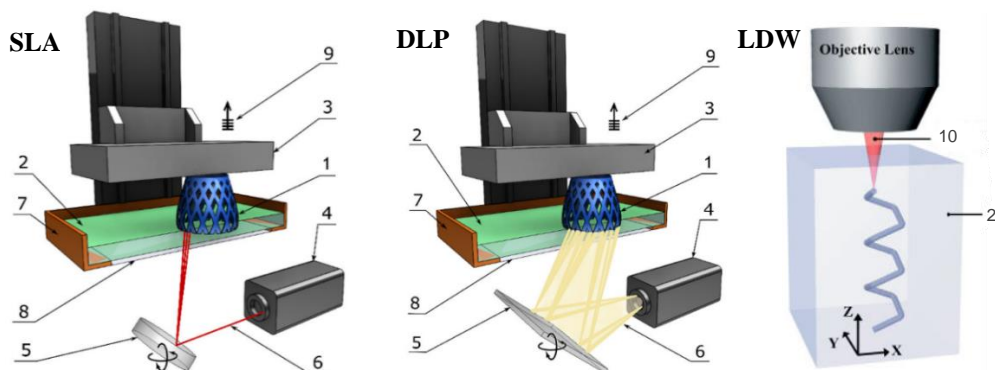
Figure 1. Components of typical SLA (left), DLP (middle), and LDW (right) machines: 1 – printed object, 2 – photoresin, 3 – building platform, 4 – UV laser source (left), UV LED light source (right), 5 – XY scanning mirror (left), digital projector (middle), 6 – light beam, 7 – resin tank, 8 – window, 9 – layer-by-layer elevation, and 10 – tightly focused laser beam [15, 16]

Materials used in conventional optical 3D printing techniques such as SLA and DLP are liquid photoresins. Most photosensitive resins are composed of mono-, di-, tri-, or poli(meth)acrylic monomers and/or oligomers, accompanied with other functionalities such as urethane, epoxy, or other [17]. Depending on the structure and functionality of the monomer/oligomer, the printed object could obtain different tensile, flexural, impact, and thermal properties [15]. Resins containing materials with long aliphatic chains result in elastic and flexible polymers with elongation at break up to 1000% [18, 19, 20], while highly functional low molecular weight (meth)acrylate-containing resins produce rigid and even brittle polymers [21, 22]. Thus, by combining materials with various functionalities, tailored printed polymeric products could be created according to the desired properties.

Although 3D printing is a sustainable manufacturing method due to low raw material usage and low waste accumulation [23], researchers are trying to reduce the environmental impact of 3D printing by using bio-based materials. Gelatin [24, 25], lignin [26, 27, 28], starch [29, 30] and other bio-based materials have been successfully applied in SLA/DLP technology, producing solid, free-standing polymers. Vegetable oils have also attracted a lot of interest from researchers in their application in optical 3D printing due to their high availability and relatively easy functionalization with photocross-linkable groups [31]. Acrylated epoxidized soybean oil is one of the most promising bio-based materials in commercial optical 3D printing application.

1.2. Acrylated epoxidized soybean oil-based polymers in optical 3D printing

Acrylated epoxidized soybean oil (AESO) is a commercially available bio-based material used under the trademark Ebecryl 5848 [32] and is widely used in the coating and plastic industries [33, 34]. AESO is a viscous liquid, produced mainly by the epoxidation of double bonds of soybean oil fatty acids followed by the acrylation of the epoxy ring (Scheme 1) [35]. AESO-based resins could be easily and

quickly photocross-linked under UV light with low energy consumption and inherent biodegradability [36].
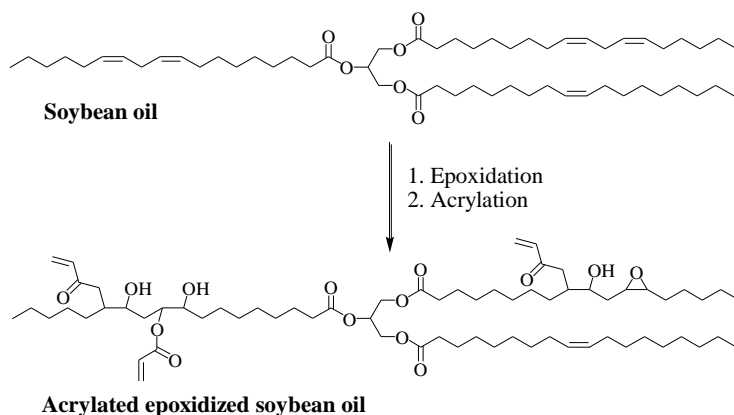
Scheme 1. Synthesis scheme of acrylated epoxidized soybean oil

Since the first attempts to photocross-link AESO in the early 1990s, it was mostly applied in UV-cured coatings. Only in 2016, Miao *et al.* [37] published the first attempt to produce photocross-linked AESO by optical 3D printing. By using self-made SLA 3D printer biomedical scaffolds of AESO and the photoinitiator bis (2,4,6-trimethylbenzoyl)-phenylphosphineoxide (BAPO) were produced with high biocompatibility and shape memory effects. The same team later published several articles on the same AESO polymer optimizing the 3D printing technique and improving shape memory effects [38, 39]. Wu *et al.* [40] also applied the same AESO and BAPO polymer in commercial DLP 3D printing using it as a comparison for photocross-linked acrylated McDonald's waste cooking oil. Photocross-linked AESO was successfully developed and printed by a commercial 3D printer; however, due to the absence of photostabilizer in the AESO polymer, diffraction and spreading of light occurred, leading to overcure, and reduced structural definition compared to that of the developed polymer from waste cooking oil.

A different approach to produce AESO-enriched polymers was published by Rosace *et al.* [41]. They combined AESO with commercial resin to reduce the impact on the environment and simplify the development procedure. The AESO content in the photocross-linked commercial resin varied from 10 to 50 wt%. Even though the addition of AESO resulted in a decrease in both tensile strength and Young's modulus of 3D printed polymer due to the network loosening, the elongation at break improved and mixtures containing 10, 20, and 30 wt% of AESO showed mechanical properties similar to those of other photocross-linked commercial materials. This study showed a simplified development procedure of a petroleum-based polymer with an enrichment of bio-based material that matches the circular economy concept.

By developing AESO-based photocross-linked polymers from raw materials, the viscosity of AESO could be reduced to obtain the necessary viscosity for optical 3D printing by adding reactive diluents (RDs), which, unlike common inert solvents, participate in the photopolymerization reaction and link into the polymer network

[42]. The AESO-based polymers with ethyl lactate or monofunctional urethane acrylate Genomer 112TF [43] and 1,6-hexanediol diacrylate (HDDA) with trimethylolpropane triacrylate (TMPTA) [44, 45] have been successfully produced by DLPA/SLA 3D printing. The printed objects indicated good layer adhesion with smooth surface finishing and high printing accuracy (Figure 2). Also, Skliutas *et al.* [43] developed the same AESO polymer with ethyl lactate or Genomer 112TF by nonlinear laser lithography on a nanoscale without the need for any supportive structures. The researchers demonstrated the way of multiscale manufacturing of a single AESO-based polymer broadening its application in optical 3D printing.
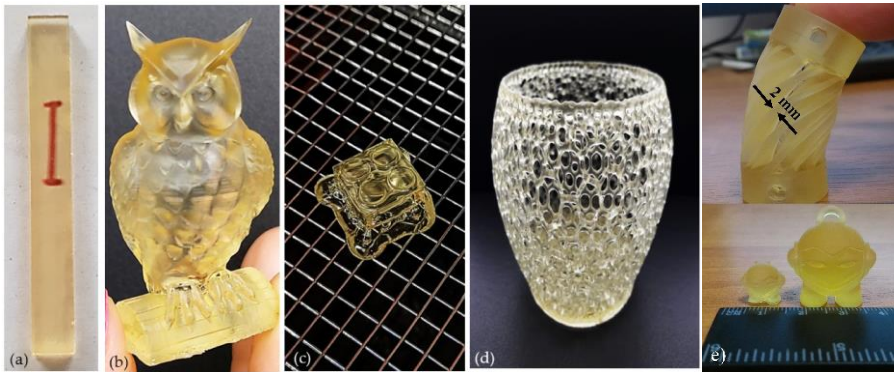
Figure 2. Printed polymers with AESO, HDDA, and TMPTA transparent bar (a), owl (b), a Lego cube (c), and basket-like bowl (d) [45] and printed objects of AESO and Genomer 112TF polymer [43]

As the interest in bio-based materials increases, more bio-based RDs have been synthesized and even commercialized. With increased availability of bio-based RDs, fully bio-based optical 3D printed polymers could be produced. Voet *et al.* [46, 47] have produced photocross-linked polymers only from commercially available bio-based acrylates with a bio-based content ranging from 34 to 67% by commercial SLA apparatus. Sustainable bio-based polymers resulted in highly accurate prototypes with a complex shape and superior surface finishing, similar to commercial synthetic printed objects. Later, the same group of researchers have developed bio-based photopolymers based on modified soybean oil by commercial SLA printers [5]. Polymers with synthesized soybean oil methacrylates with various functionalities and bio-based IBOMA were 3D printed and the developed parts demonstrated complete layer fusion and accurate printing quality. The mechanical performance of the printed bio-based polymer was comparable with that of the commercial counterparts that are competitive with current fossil-based products from commercial manufacturers.

By increasing the application of optically 3D printed parts as operative components rather than conceptual prototypes [48], reinforcements or fillers could be added to photoresin to improve the mechanical, thermal, and other properties of the printed object [31]. There have been several attempts to produce AESO-based composites by optical 3D printing. Mondal *et al.* [49] developed AESO and nano-hydroxyapatite (nHA) composite materials for bone tissue engineering by extrusion-based 3D printing with simultaneous UV curing during layer-by-layer

15

deposition. The printed scaffolds demonstrated controlled morphology with well-dispersed nHA particles within the polymer matrices and were shown to support cell proliferation and osteogenic differentiation after 14 and 21 days of culture. Liu *et al.* [50] also employed UV-assisted direct ink writing to develop AESO and methacrylic anhydride-modified ethylcellulose macromonomer (ECM) composites. The improved thermal and mechanical properties of AESO-ECM composites compared to the pure AESO indicated a good fiber-matrix interface with excellent interfacial adhesion between printed layers. However, no AESO-based composites were developed by conventional 3D printing techniques such as DLP and SLA leaving them without a wider application. Therefore, more research is needed to introduce AESO-based composites as a potential material for commercial use.

2. REVIEW OF ARTICLES

2.1. Investigating the properties of photocross-linked polymer composed of acrylated epoxidized soybean oil, myrcene, and vanillin dimethacrylate

This chapter is based on published work: *M. Lebedevaitė, J. Ostrauskaitė, E. Skliutas, M. Malinauskas. Photocross-linked polymers based on plant-derived monomers for potential application in optical 3D printing. Journal of Applied Polymer Science. 2019, 137 (20), 48708* [51]. *JIF: 3.125.*

AESO was used as the main starting material for the development of bio-based polymeric materials. Photocross-linked polymers of AESO, myrcene (MYR) and vanillin dimethacrylate (VDM) or divinylbenzene (DVB, for comparison) (Figure 3) were developed to evaluate the properties of a fully bio-based resin. To estimate the suitability of AESO-based polymeric materials for potential application in optical 3D printing they were compared with popular commercial petroleum-derived materials Aurodesk Clear PR48 (PR48) and Formlabs Clear FLGPCL02 (FLGPCL02).

MYR   **DVB**   **VDM**
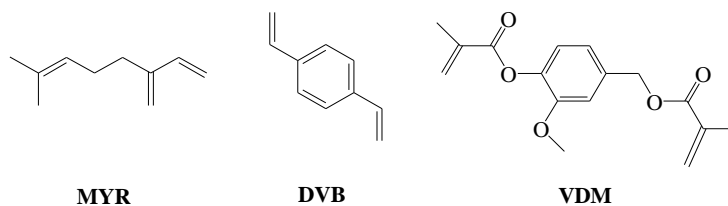
Figure 3. Chemical structure of myrcene (MYR), divinylbenzene (DVB), and vanillin dimethacrylate (VDM)

The compositions of AESO-based polymers were designed to investigate the influence on MYR and VDM or DVB amounts on the photocuring kinetics and properties of resulting polymers. Plant-derived VDM was used as a bio-based aromatic compound for a synthetic DVB replacement. The compositions of the designed formulations are presented in Table 1.

16

Table 1. Compositions of designed formulations

Composition	AESO, mol	MYR, mol	DVB, mol	VDM, mol
C0	1	1	-	-
C1	1	1	1	-
C2	1	3	1	-
C3	1	5	1	-
C4	1	1	-	1
C5	1	3	-	1
C6	1	5	-	1
C7	1	1	3	-
C8	1	1	5	-
C9	1	1	-	3
C10	1	1	-	5

The photorheometry test showed a significant influence of the content of monomers on photocuring kinetics. A higher amount of MYR in the composition led to a prolonged photocuring process and lower values of the storage modulus (G') showing the formation of a softer cross-linked polymer (Table 2). Although the addition of a higher amount of DVB in the formulations slowed the photocuring process, higher G' values were obtained. The higher amount of aromatic compound improved the rigidity of the cross-linked network, leading to higher G' values. Faster photocuring was observed after replacing synthetic DVB with bio-based VDM in compositions (Figure 4a). By comparing the photocuring of synthetic resins PR48 and FLGPCL02 with the composition of C9 (Figure 4b), a similar rate of photocuring and comparable values of G' were obtained, which distinguished the composition of C9 as suitable for application in optical 3D printing.
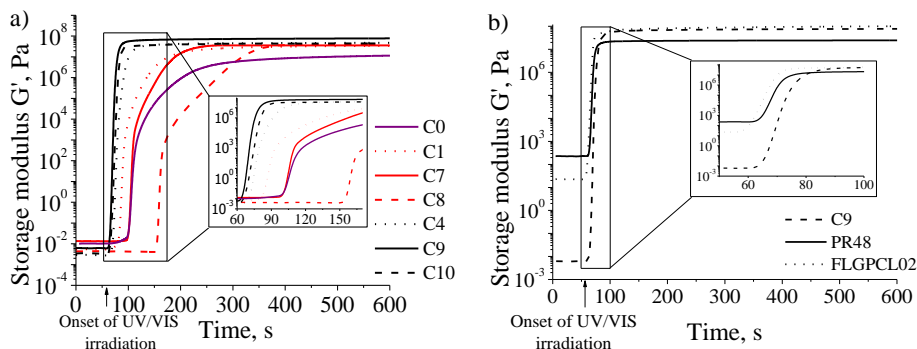
Figure 4. The irradiation time dependency of storage modulus G' of: resins without aromatic compound C0 (purple) and the resins C1, C4 and C7-C10 with different amounts of aromatic compound: VDM (black) and DVB (red) a); resins C9 PR48, and FLGPCL02 b)

The yield of the insoluble fraction (YIF) of polymers after Soxhlet extraction is presented in Table 2. A higher amount of MYR caused lower YIF values as a result of the formation of a higher amount of linear/branched polymer chains during photocuring. AESO-based polymers with VDM showed higher YIF values compared

to those of polymers with DVB. A correlation was observed between YIF and cross-linking density (v_e). Polymers with lower YIF values also had lower v_e values.

Table 2. Characteristics of designed resins and photocross-linked polymers

Composition	t_{gel}[1], s	G'[2], MPa	YIF[3], %	v_e[4], kmol·m^{-3}	E_C[5], MPa
C0	60 ± 1.5	15.52 ± 2.45	-	-	-
C1	35 ± 4.2	34.10 ± 1.25	94	13.83 ± 0.50	9.8 ± 0.2
C2	323 ± 8.7	3.62 ± 1.25	93	1.46 ± 0.50	8.4 ± 0.1
C3	465 ± 11.7	0.14 ± 0.07	53	0.58 ± 0.03	1.1 ± 0.02
C4	18 ± 0.7	47.64 ± 1.25	97	19.23 ± 5.06	18.4 ± 0.2
C5	200 ± 7.9	30.81 ± 6.95	94	12.41 ± 2.81	9.9 ± 0.2
C6	403 ± 12.0	0.63 ± 0.20	58	0.03 ± 0.01	0.5 ± 0.1
C7	48 ± 1.4	35.61 ± 3.48	88	14.40 ± 1.41	7.6 ± 0.4
C8	102 ± 5.5	40.64 ± 1.95	90	16.43 ± 0.79	9.7 ± 0.2
C9	12 ± 0.0	77.83 ± 3.11	96	31.42 ± 1.26	21.2 ± 0.2
C10	15 ± 1.0	44.93 ± 6.09	94	18.14 ± 4.27	15.8 ± 0.2
PR48	13 ± 0.0	25.91 ± 0.99	99	10.52 ± 0.40	16.9 ± 0.3
FLGPCL02	12 ± 1.0	71.22 ± 3.49	99	28.71 ± 7.87	13.1 ± 0.3

[1] gel time, calculated from the onset of UV/VIS irradiation
[2] Storage modulus at 1200s from the beginning of the test
[3] Yield of insoluble fraction after Soxhlet extraction with chloroform for 24 h
[4] Cross-linking density calculated from G' curves
[5] Compressive modulus obtained from the top pressure test

The compressive modulus (E_C) from the top pressure test characterized the mechanical properties of photocross-linked AESO-based polymers. Because of the low density of cross-links, polymers with a higher content of MYR were soft and showed low E_C values. Polymers with VDM showed higher E_C values compared to polymers with DVB and cross-linked petroleum-based resins. The composition C9 of AESO/MYR/VDM, molar ratio 1:1:3, had the highest v_e and E_C values and showed properties resembling commercial products and could potentially be applied in optical 3D printing.

2.2. Investigation of photoinitiator-free acrylated epoxidized soybean oil-based resin photocuring and properties of the resulting polymers

This chapter is based on published work: *M. Lebedevaitė, J. Ostrauskaitė, E. Skliutas, M. Malinauskas. Photoinitiator free resins composed of plant-derived monomers for the optical μ-3D printing of thermosets. Polymers. 2019, 11 (1), 116* [52]. *JIF: 4.329.*

Photocross-linked polymers of AESO and vanillin dimethacrylate (VDM) or vanillin diacrylate (VDA) (Figure 5) have been synthesized without any photoinitiator or solvent and have been applied in laser direct writing lithography. These polymers were investigated in order to develop plant-derived photopolymers without the use of any toxic photoinitiators and other petroleum-derived components.
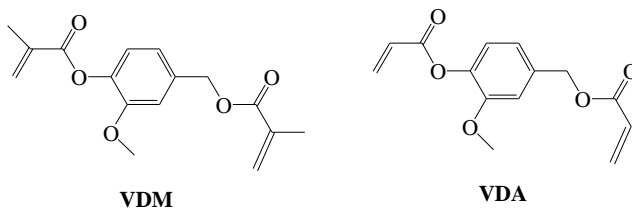
Figure 5. Chemical structure of vanillin dimethacrylate (VDM) and vanillin diacrylate (VDA)

The bio-based resins were composed of AESO and VDM in molar ratios of 1:1 (AESO/VDM1), 1:0.5 (AESO/VDM2), and 1:0.25 (AESO/VDM3). Analogous resins with VDA were also composed. The photocuring kinetics of AESO and the mixture of AESO and VDM or VDA was monitored by real-time photorheometry. The G' was monitored as a function of time, where the increase in the G' values indicated the formation of a three-dimensional polymer network. The irradiation time dependencies of the storage modulus G' of bio-based resins are shown in Figure 6.
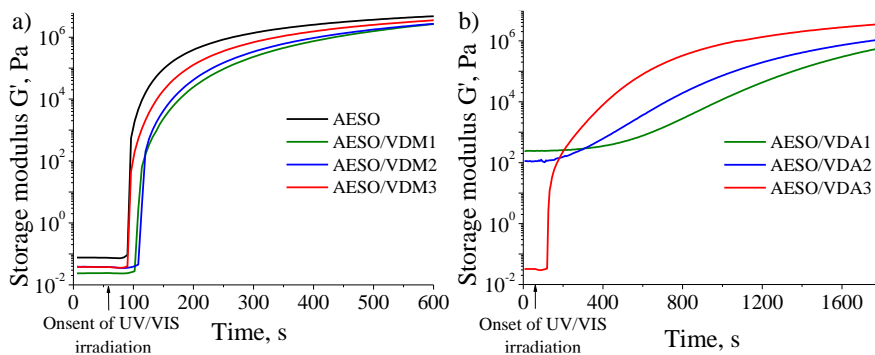
Figure 6. The irradiation time dependency of the storage modulus G' of AESO and resin series AESO/VDM (a) and AESO/VDA (b)

The photorheometry test confirmed the formation of a three-dimensional polymer network of the designed bio-based resins without any photoinitiator. Photocross-linking of photoinitiator-free plant-derived resins was initiated by the cleavage of vinyl double bonds of monomers generating a free radical, which initiated the reaction of the (meth)acrylic groups [53]. When comparing the photocuring kinetics, the easier cleavage of vinyl double bonds of VDM was determined as a faster increase and higher values of G' were observed. It was noticed that a higher amount of bio-based aromatic compound led to slower photocuring and lower G' values, resulting in poorer mechanical properties. Due to this, the series AESO/VDA was not further investigated.

The formation of a cross-linked polymer structure was confirmed by Soxhlet extraction. The pAESO polymer had the highest *YIF* of 88% showing the tendency of AESO to form solid cross-linked polymers without any presence of photoinitiators. The higher amount of VDM in the polymers resulted in a lower amount of *YIF*, which

could be explained by the tendency of VDM to form linear and/or branched polymer chains in the photoinitiator-free system.

Table 3. Yield of insoluble fraction, thermal and mechanical characteristics of the cross-linked polymers

Polymer	YIF^1, %	$T_g{}^2$, °C	$T_{dec-10\%}{}^3$, °C	$E_C{}^4$, MPa
pAESO	88	-4.5	356	0.62 ± 0.1
pAESO/VDM1	31	-2.6	295	0.19 ± 0.03
pAESO/VDM2	48	-2.6	318	0.46 ± 0.13
pAESO/VDM3	63	-1.6	331	0.66 ± 0.13

[1] Yield of insoluble fraction after Soxhlet extraction with chloroform for 24 h
[2] Glass transition temperature estimated by DSC
[3] Temperature at the weight loss of 10% obtained from the TGA curves
[4] Compressive modulus obtained from the top pressure test

The thermal and mechanical properties of the cross-linked polymers (Table 3) were closely related to the *YIF* of the polymers. Photocross-linked polymers with a large amount of VDM resulted in lower *YIF* values, thus lowering the glass transition temperature, thermal stability, and compressive modulus values. This showed that VDM acts as a plasticizer in the photoinitiator-free AESO-based system, deteriorating mechanical and thermal properties of cross-linked polymers.

The 3D microporous woodpile structures obtained via LDW 3D lithography of AESO and AESO/VDM3 were characterized (Figure 7). These bio-based resins were laser polymerized using ultrashort pulses by multiphoton absorption and avalanche-induced cross-linking.
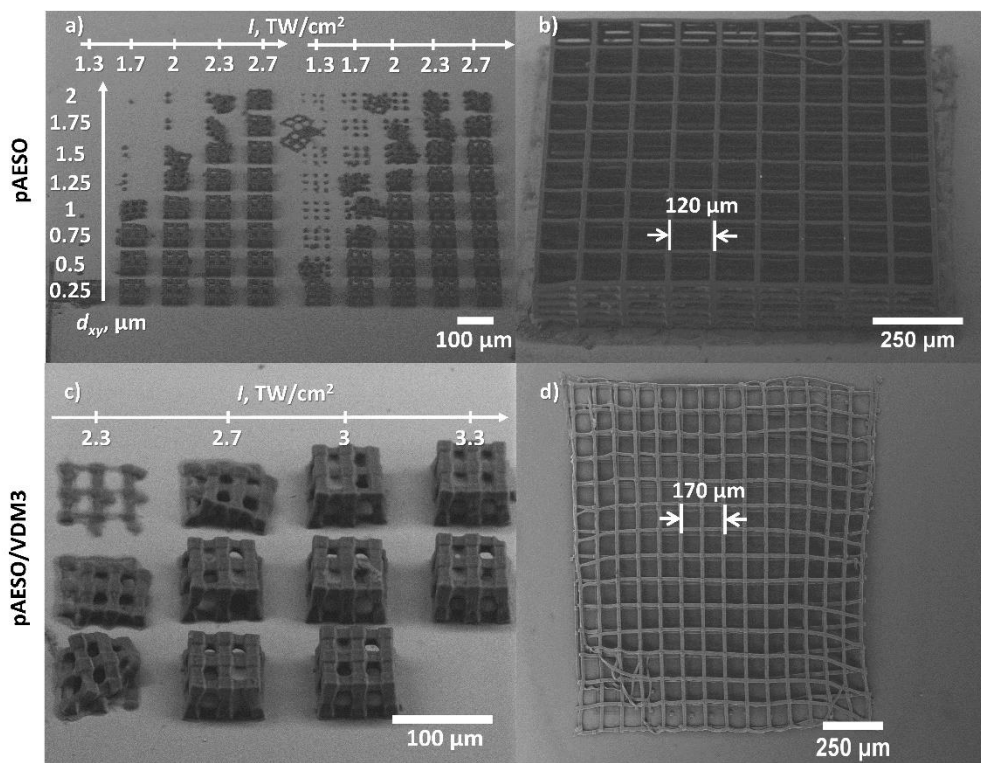
Figure 7. The SEM images of 3D microporous woodpile structures: (a) 75×75 µm^2 woodpile structures of pAESO with 30 µm period, $v = 5$ mm/s. Scale on the left of image shows the distance d_{xy} between neighboring scans; (b) a 1095×1095 µm^2 woodpile of pAESO with 120 µm period, $v = 5$ mm/s, $P = 0.6$ mW (2 TW/cm^2); (c) 75×75 µm^2 woodpile structures of pAESO/VDM3 with a 30 µm period, $v = 5$ mm/s, the scale at the top of the image demonstrates the applied I; (d) a 1065×1065 µm^2 woodpile of pAESO/VDM3 with a 75 µm period, $v = 5$ mm/s, $P = 0.4$ mW (1.3 TW/cm^2);

It was demonstrated that the formed arrays of 75×75 µm^2 woodpiles (Figure 7a and 7c) were formed with v set to 5 mm/s and P varied in the range of 0.4–1 mW (1.3–3.3 TW/cm^2) and with an increased laser power P higher d_{xy} can be used. Fabricated mm scale woodpiles (Figure 7b and 7d) had a 3D architecture, although the woodpiles of pAESO/VDM3 did not sustain themselves due to the low mechanical rigidity.

2.3. Influence of photoinitiator and temperature on photocross-linking kinetics of acrylated epoxidized soybean oil and properties of the resulting polymers

This chapter is based on the published work: *M. Lebedevaitė, J. Ostrauskaitė. Influence of photoinitiator and temperature on photocross-linking kinetics of acrylated epoxidized soybean oil and properties on the resulting polymers. Industrial crops and products. 2021, 161, 113210* [54]. *JIF: 5.645.*

The photocross-linked AESO synthesized without any photoinitiator showed structural stability and thermal stability. Although, compared to commercial petroleum-based 3D printing resins, the mechanical and thermal properties of the cross-linked AESO were poor. Furthermore, the photocuring rate of photoinitiator-free AESO was too slow to apply this system in DLP/SLA 3D printing. To address these issues, the influence of temperature, concentration, and type of photoinitiator on AESO photocuring kinetics was investigated.

Four different commercial photoinitiators were chosen to investigate the influence of temperature, concentration, and type of photoinitiator on the AESO photocuring kinetics by using a photorheometry test. The chosen photoinitiators were as follows: 2,2-dimethoxy-2-phenyl acetophenone (DMPA), phenyl bis(2,4,6-trimethylbenzoyl) phosphine oxide (BAPO), diphenyl (2,4,6-trimethyl benzoyl) phosphine oxide (TPO), and ethyl (2,4,6-thimethylbenzoyl) phenyl phosphinate (TPOL) (Figure 8). The concentrations of 1, 3, and 5 mol% of photoinitiator were used in the resins assigned, respectively (e.g., ADMPA1, ADMPA3, etc.).
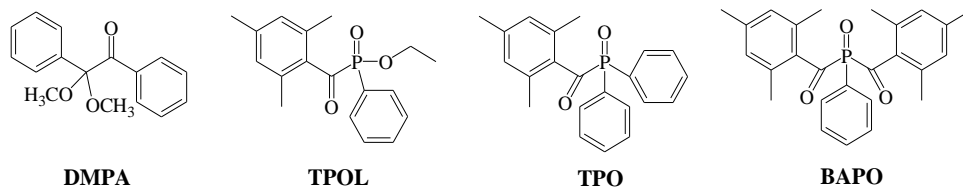
Figure 8. Chemical structure of 2,2-dimethoxy-2-phenyl acetophenone (DMPA), ethyl (2,4,6-thimethylbenzoyl) phenyl phosphinate (TPOL), diphenyl (2,4,6-trimethylbenzoyl) phosphine oxide (TPO), and phenyl bis(2,4,6-trimethylbenzoyl) phosphine oxide (BAPO)

Real-time photorheometry revealed a high reactivity and fast photocross-linking of AESO in the presence of a photoinitiator comparable to other acrylic systems [55, 56, 57]. The G' curves of AESO resins with different concentrations of photoinitiators were compared to determine the influence of photoinitiator on photocuring kinetics. As an example, the irradiation time dependencies of the G' of the resins with (1–5) mol% of TPOL and with 3 mol% of different photoinitiators at 25°C are presented in Figure 5. The photorheometry test revealed that the amount of photoinitiator did not influence the gel time but had an impact on the shape of the G' curves at the beginning of UV/VIS irradiation (Figure 9a). Resin with 3 mol% of TPOL showed the highest photocuring rate reaching the G' plateau 1 s faster than ATPOL5, considering it as the optimum concentration of TPOL. By comparing the photocuring kinetics of the resins with different photoinitiators at a concentration of 3 mol% (Figure 9b), the resin ABAPO3 reached the G' plateau the fastest even though the gel time of all resins was the same. Such a high BAPO reactivity showed its ability to generate free radicals the fastest enabling the rapid photocross-linking of AESO.
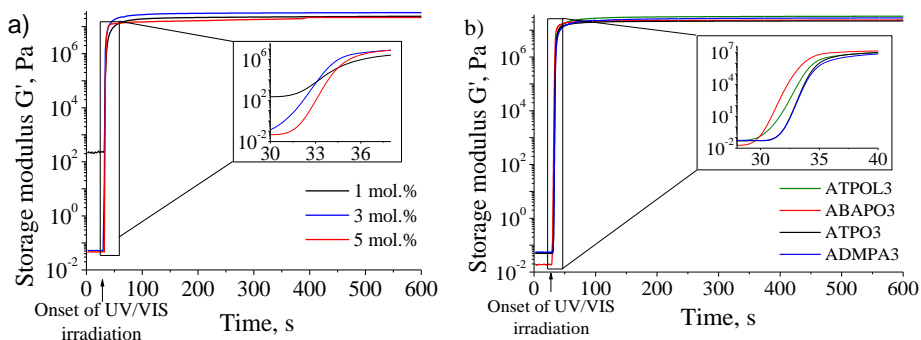
Figure 9. The irradiation time dependencies of the storage modulus *G'* of resins with (1–5) mol% of TPOL (a) and with 3 mol.% of different photoinitiators (b) at 25 °C

The thermal properties of photocross-linked AESO polymers were investigated by using DSC and TGA. TGA showed that all photocross-linked polymers exhibited high thermal stability, obtaining the temperature at a weight loss of 10% ($T_{dec.-10\%}$) in the range of 337°C to 352°C. The highest $T_{dec.-10\%}$ value was determined for ABAPO1 polymer with the smallest amount of BAPO, demonstrating high BAPO efficiency in a smaller amount. DSC confirmed that all synthesized polymers were amorphous materials, indicating only the glass transition (T_g) in the thermograms. The glass transition temperature of the synthesized polymers was (41.1–50.9°C), a notably higher than that of the photocross-linked AESO polymer synthesized without photoinitiator (-4.5°C) (Table 3). This huge difference in the T_g values could be related to the amount of the cross-linked polymer fraction characterized by *YIF*. The photocross-linked initiator-free AESO indicated 88% of *YIF*, whereas AESO polymers with photoinitiator obtained *YIF* in the range of 96.1–97.9%.

Table 4. The yield of insoluble fraction, thermal and mechanical characteristics of the cross-linked polymers

Polymer	YIF[1], %	$T_{dec-10\%}$[2], °C	T_g[3], °C	E_C[4], MPa	E_E[5], MPa	σ[6], MPa
ADMPA1	97.6	338	47.5	323 ± 24	199 ± 7	4.34 ± 0.8
ADMPA3	97.9	342	48.1	335 ± 62	273 ± 11	5.48 ± 0.99
ADMPA5	97.8	340	44.2	359 ± 32	325 ± 7	5.15 ± 0.47
ATPOL1	97.7	337	50.9	318 ± 46	239 ± 30	5.59 ± 0.86
ATPOL3	97.2	337	46.6	384 ± 32	487 ± 11	4.95 ± 1.02
ATPOL5	96.6	348	46.2	350 ± 35	544 ± 12	6.23 ± 0.98
ATPO1	97.5	342	46.4	373 ± 20	135 ± 5	4.23 ± 0.83
ATPO3	96.1	340	41.1	359 ± 20	279 ± 3	5.39 ± 1.01
ATPO5	97.9	337	44.7	350 ± 13	292 ± 15	5.23 ± 0.75
ABAPO1	97.2	352	45.7	392 ± 33	205 ± 8	4.53 ±0.38
ABAPO3	97.4	346	46.1	383 ± 24	240 ± 16	5.56 ± 1.83
ABAPO5	97.1	345	45.7	401 ± 22	490 ± 33	5.42 ± 0.35

[1] Yield of insoluble fraction, after Soxhlet extraction with chloroform for 24 h
[2] Temperature at the weight loss of 10% obtained from the TGA curves

Higher *YIF* values also caused better mechanical properties of the developed AESO polymers compared to the cross-linked AESO polymers synthesized without photoinitiator. The E_C values were improved by at least five hundred times when a photoinitiator was introduced to the AESO resin. It should be noted that different equipment was used in these two cases with certain dissimilarities between the devices. Nevertheless, an obvious improvement of mechanical and thermal properties was observed when a photoinitiator was used in AESO resins.
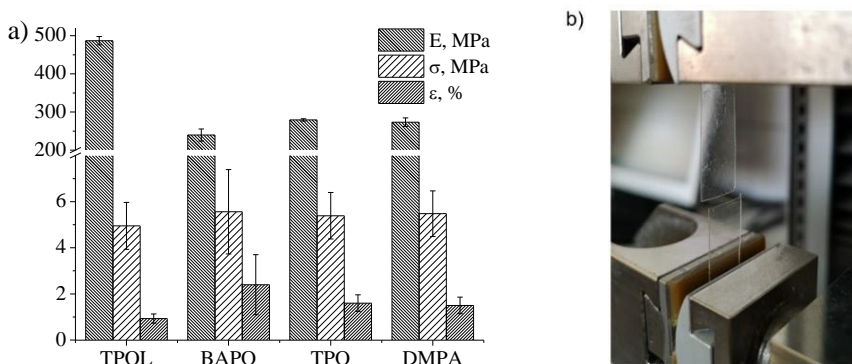
Figure 10. Elastic modulus (E_E), tensile strength (σ) and elongation at brake (ε) of the cross-linked polymers with 3 mol% of photoinitiator (a); a polymer film specimen broken after the tensile test (b)

The tensile test results of photocross-linked AESO polymer films showed a definitive influence on the photoinitiator concentration on the mechanical properties of the synthesized polymers. The tensile characteristics of the AESO polymer films and the picture of the fractured film after the tensile test are presented in Figure 10. The higher amount of photoinitiator led to an increased value of the elastic modulus (E_E) showing the improved rigidity of the photocross-linked polymer. However, increased brittleness and lower elongation at break (ε) values were observed when using a higher amount of photoinitiator. Polymers with TPOL indicated the highest values of E_E in all concentrations used compared to those of other photoinitiators. A significant improvement in E_E values was observed when 3 mol% of TPOL was used, considering it as the most favorable concentration for this photoinitiator. E_E values were improved almost twice when the amount of BAPO was increased from 3 mol% to 5 mol%. This extensive increase in E_E values indicated the efficiency of BAPO in higher amount. Considering that BAPO should be used in a higher amount to achieve better mechanical properties and its incorporation into the resin was more difficult, due to the solid state of BAPO compared to liquid TPOL, 3 mol% of TPOL were chosen as an optimum concentration for AESO resin.

24
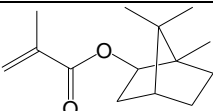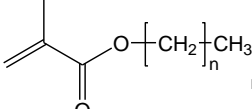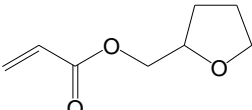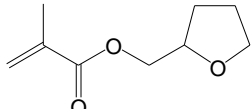
2.4. The properties of acrylated epoxidized soybean oil-based photocross-linked polymers with different bio-based reactive diluents and their suitability for digital light processing 3D printing

This chapter is based on the published work: *M. Lebedevaitė, V. Talačka, J. Ostrauskaitė. High biorenewable content acrylate photocurable resins for DLP 3D printing. Journal of Applied Polymer Science. 2021, 138 (16), 50233* [58]. *JIF: 3.125.*

As the most suitable photoinitiator was chosen and the optimum concentration of it was determined, the AESO resin could be applied in the DLP 3D printing. However, the viscosity of the AESO resin is too high to be used for DLP 3D printing technology. When this issue was addressed, bio-based reactive diluents were introduced to the AESO resin to reduce the resin viscosity and additionally improve the mechanical and thermal properties of cross-linked polymers by inserting them into the polymer network.

Solvent-free resin formulations of bio-based monomers were developed to create novel polymeric materials. Four commercially available bio-based reactive diluents were used, such as isobornyl methacryate (IBOMA), methacrylic ester (ME), tetrahydrofurfuryl acrylate (THFA), and tetrahydrofurfuryl methacrylate (THFMA) with biorenewable carbon content (BRC) of 55–76% (Table 5) to prepare AESO-based polymers with DLP 3D printing. The added amount of TPOL was 3 mol% calculated from the amount of all monomers. Commercial photoresin Monocure3D Rapid Gray (REF) was used for comparison.

Table 5. Characteristics of bio-based reactive diluents [58]

Material	Structural formula	Origin of the material	BRC, %
IBOMA		Pine trees	71
ME		Vegetable oil	76
THFA		Hemicellulose	60
THFMA		Hemicellulose	55

The viscosity of commercial 3D printing resins is usually between 200 and 1,500 mPa·s at 25°C, making them fluid enough to redistribute themselves in the tray during each time the Z-axis moves [59]. Bio-based resins prepared with BRC of 75–

82% obtained viscosity in the range of (557–699) mPa·s (Table 6) making them suitable for application in DLP 3D printing.

Table 6. Composition and characteristics of the prepared resins

Resin	Amount of AESO, wt.%	Amount of RD, wt.%	Amount of TPOL, wt.%	BRC, %	Viscosity, mPa·s
AESO/IBOMA	58.71	39.14	2.15	78.5	699.3 ± 25.7
AESO/ME	68.87	29.52	1.61	81.9	644.3 ± 9.8
AESO/THFA	68.36	29.30	2.34	76.6	557.5 ± 3.1
AESO/THFMA	68.46	29.34	2.20	75.3	634.4 ± 8.5

Photocuring kinetics was determined by the real-time photorheometry test, and high reactivity after irradiation with UV light was observed. Resins AESO/IBOMA and AESO/THFMA underwent the slowest photocross-linking, although indicated the highest G' values (Table 7) showing the most immense rigidity of the composed resins. Also, the correlation between t_{gel} and linear shrinkage (Δd) was determined when faster photopolymerization caused greater shrinkage of the resin during photocross-linking. The shrinkage was caused by the change in length between the intramolecular distance and the newly formed covalent bond distance [60]. This distance change during the photopolymerization reaction depends on polymer network formation time and causes a greater shrinkage due to the higher conversion of functional groups. Therefore, the AESO/THFA resin indicated the lowest t_{gel} and resulted in the highest Δd of all samples.

Table 7. Rheological characteristics, shrinkage of AESO-based resins, *YIF* and thermal properties of cross-linked polymers

Sample	t_{gel}[1], s	G'[2], MPa	Δd[3], %	YIF[4], %	T_g[5], °C	$T_{dec-10\%}$[6], °C	Char[7], %
AESO/IBOMA	2.9 ± 1.0	13.63 ± 6.7	10.0 ± 5.3	98.7	60.8	308	1.5
AESO/ME	2.2 ± 1.2	9.67 ± 0.4	12.7 ± 4.2	96.9	24.3	353	1.6
AESO/THFA	1.9 ± 1.3	10.44 ± 1.8	13.3 ± 2.3	95.4	4.6	345	1.9
AESO/THFMA	3.7 ± 0.02	13.34 ± 2.0	8.0 ± 0	96.3	43.7	351	2.0
REF	-	-	-	99.6	-	386	6.0

[1] Gel time calculated from the onset of UV/VIS irradiation
[2] Storage modulus at 600 s from the beginning of the test
[3] Shrinkage obtained by real-time photorheometry
[4] Yield of insoluble fraction, after Soxhlet extraction with chloroform for 24 h
[5] Glass transition temperature obtained from the DSC curves
[6] Temperature at the weight loss of 10% obtained from the TGA curves
[7] Char yield obtained from TGA curves

AESO-based polymers had *YIF* values in the range of (95.4–98.7%) showing a formation of a high amount of cross-linked structure. Thermal characteristics of photocross-linked bio-based polymers correlated with the determined *YIF*. Polymers with higher *YIF* showed higher T_g and $T_{dec-10\%}$ values, including REF. The exception was the polymer with IBOMA fragments, as the lowest value of $T_{dec-10\%}$ was observed. This low thermal stability was caused by the low thermal stability of the isobornyl fragment through the ester bond scission in the AESO/IBOMA polymer [61]. Due to

26

the low T_g, polymers AESO/ME and AESO/THFA were soft materials holding their solid state on behalf of the cross-linked structure.
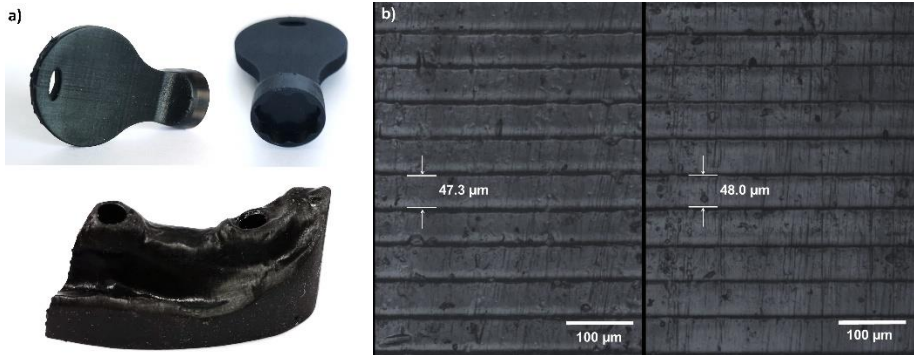
Figure 11. Images of the bolt wrenching tool from polymer AESO/IBOMA (a, top) and image of human lower jaw fragment from polymer AESO/THFMA (a, bottom), both produced by 3DPC; microscope images of the surface of the polymer AESO/ME specimens prepared by 3DWPC (b, left) and by 3DPC (b, right);

All AESO-based polymers designed were successfully produced using DLP 3D printing technology. Bio-based polymer specimens for the tensile test, including the reference material, were prepared in three different ways: by molding (LAB), by DLP 3D printing without post-curing (3DWPC), when unreacted resin was simply washed off of the surface of the specimen, and by DLP 3D printing with post-curing (3DPC) additionally curing the printed specimen under LED light ($\lambda = 400$–405 nm, 50 W) for 2 h at ambient temperature. The complex architecture printed objects prepared by 3DPC (Figure 11a) demonstrated significant printing accuracy with high definition and smooth surface finishing. However, the surface of the 3DWPC-prepared specimen was corrugated due to the unreacted monomer being washed away from the surface of the specimen, while a smoother surface was obtained in the 3DPC-prepared specimens (Figure 11b).
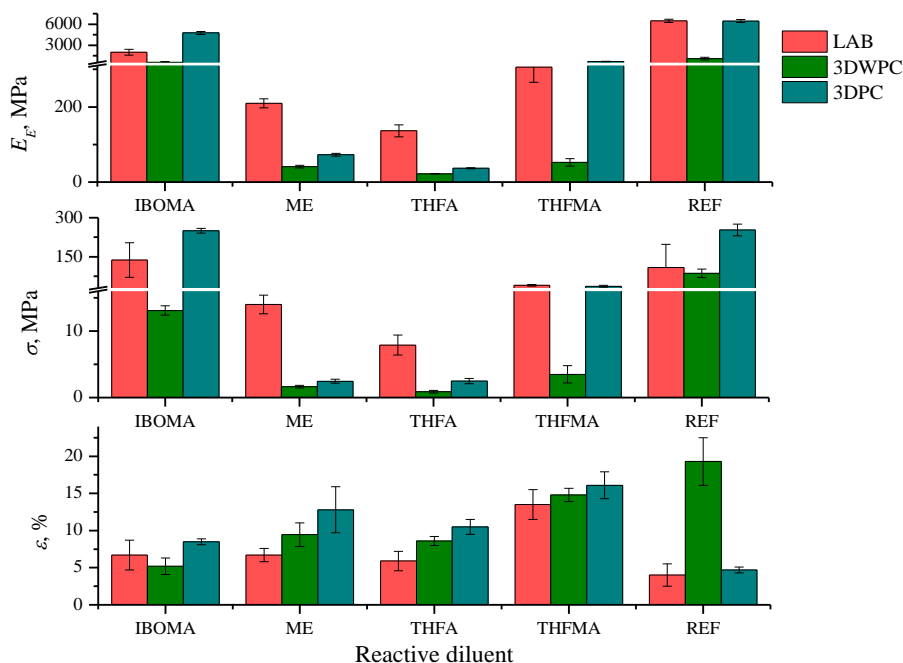
Figure 12. Tensile characteristics of the cross-linked polymer specimens produced by molding (LAB), by using DLP 3D printing without post-curing (3DWPC), and DLP 3D printing with post-curing (3DPC): elastic modulus (E_E), tensile strength (σ), and elongation at break (ε)

The tensile properties of bio-based polymers prepared in three different ways were examined to evaluate the adhesion between the printed layers. Due to the corrugation that occurred in the 3DWPC-prepared specimens, the worst mechanical characteristics were monitored (Figure 12). The polymers AESO/IBOMA and AESO/THFMA showed the highest E_E and σ values of the prepared AESO-based resins. Both polymers also had higher E_E and σ values of the specimens prepared by 3DPC compared to the LAB-prepared polymers, showing a strong adhesion between their printed layers. The tensile properties of the AESO/IBOMA specimen prepared by 3DPC were the most similar to the commercial petroleum-derived resin Monocure3D Rapid Gray considering it as a competitive replacement for commercial resins.

The developed bio-based photoresins/photopolymers AESO/IBOMA and AESO/THFMA have been tested in industrial DLP 3D printer by company AmeraLabs. Also, composition AESO/IBOMA has been tested in the industrial DLP 3D printer Zortrax Inkspire of JSC 3D Creative. The process was validated, and real-scale medical fittings were produced revealing the suitability for the intended use. Trial production acts of both companies are presented in Appendices 10.1 and 10.2.

Tested bio-based photoresin/photopolymer AESO/IBOMA and petroleum-based commercial acrylic resin were evaluated in life-cycle assessment (LCA) by comparing their environmental impact. The dental models printed with

bio-based resin showed reduced impact in 12 out of 16 categories when compared to those made from conventional petroleum-based acrylic resin. The results from this study clearly showed the benefit of using bio-based materials for formulating the UV-curable 3D printing resin. The LCA study is presented in Appendix 10.3.

2.5. Influence of calcium silicate hydrate fillers to photocross-linked acrylated epoxidized soybean oil-based polymer composites, and digital light processing 3D printing of polymeric composites

This chapter is based on the published work: *M. Lebedevaitė, A. Gineika, V. Talačka, K. Baltakys, J. Ostrauskaitė. Development and optical 3D printing of acrylated epoxidized soybean oil-based composites with functionalized calcium silicate hydrate filler derived from aluminum fluoride production waste. Composites Part A: Applied Science and Manufacturing. 2022, 157, 106929.* [62]. *JIF: 7.664.*

Most optically 3D printed polymer products lack toughness and functionality, making them to be still used as conceptual prototypes rather than operative components [48]. Combining the polymer matrix and fillers improved the mechanical, thermal, and other properties which could help overcome this drawback [31]. To improve the mechanical and thermal properties of AESO-based polymers, bio-based composites with functionalized calcium silicate hydrate fillers from aluminum fluoride production waste have been developed and successfully applied in DLP 3D printing.

Table 8. Composition and rheological parameters of the prepared resins

Sample	Monomer ratio AESO: IBOMA (w/w)	Filler	Amount of filler, wt%	Viscosity, mPa·s
AS60/I40/0	60:40	-	0	796
AS60/I40/X1		X	1	1,007
AS60/I40/X3			3	1,262
AS60/I40/X5			5	2,056
AS60/I40/X10			10	2,669
AS40/I60/0	40:60	-	5	157
AS40/I60/X5		X	5	241
AS40/I60/XS5		XS	5	302
AS40/I60/XM5		XM	5	624
AS40/I60/XSM5		XSM	5	266

The fillers for the AESO-based resins were hydrothermally synthesized from calcium oxide and silicagel (X) or SiO_2-rich aluminum fluoride production waste material (XS) in the molar ratio 1:1 at 200°C for 12 h according to [63]. The X filler was mainly composed of tobermorite, xonotlite, and other calcium silicate hydrates, while the XS filler contained tobermorite, cuspidine, katoite, and other calcium silicate hydrates. Later fillers were modified with acryloxypropyltrimethoxysilane (APr) (XM and XSM, respectively). Resins were prepared by mixing AESO with IBOMA in the weight ratio of 60:40 and adding 1 wt% to 10 wt% of X filler or by

mixing AESO with IBOMA in the weight ratio of 40:60 and adding 5 wt% of fillers X, XS, XM and XSM (Table 8, e.g., AS40/I60/XS5 and AS60/I40/X5, where *AS* represents the weight ratio of AESO, *I* represents the weight ratio of IBOMA, and last part stands for the filler used and amount of it). The resins without filler in both monomer ratios (AS60/I40/0 and AS40/I60/0) were also prepared for comparison. The added 3 mol% of TPOL were calculated from the total amount of both monomers.

Table 9. Thermal characteristics of AESO-based photocross-linked composites

Sample	TGA		DMTA	
	$T_{dec\text{-}10\%}$[1], °C	Char[2], %	T_g,[3] °C	v_e[4], mol·m^{-3}
AS60/I40/0	308.5	1.49	99.2	3,655.7
AS60/I40/X1	308.3	2.53	91.6	3,261.8
AS60/I40/X3	320.2	4.09	91.2	3,498.8
AS60/I40/X5	320.2	6.43	91.0	3,999.0
AS60/I40/X10	319.5	11.60	89.4	4,296.9
AS40/I60/0	306.5	1.73	114.8	6,546.0
AS40/I60/X5	320.3	6.88	110.0	8,618.4
AS40/I60/XS5	318.2	5.79	108.5	10,131.3
AS40/I60/XM5	315.9	5.32	106.8	6,727.5
AS40/I60/XSM5	318.8	5.34	111.5	6,872.1

[1] Temperature at the weight loss of 10% obtained from the TGA curves
[2] Char yield obtained from the TGA curves
[3] Glass transition temperature obtained from the DMTA curves
[4] Cross-linking density calculated from the DMTA curves

The TGA revealed that fillers improved the thermal stability of photocross-linked bio-based composites. By adding 3 wt% or more of X filler in AESO-based composite, the $T_{dec.\text{-}10\%}$ was improved from 308.5°C of AS60/I40/0 to 320.2°C of AS60/I40/X5. The reduction of T_g determined by dynamic mechanical thermal analysis (DMTA) was observed when the filler was included in the AESO-based polymer matrix (Table 9). Although the T_g values reduced after the incorporation of filler, v_e increased when at least 5 wt.% of filler was added to the polymer showing improved rigidity of the polymer matrix. It was noticed that polymer composites with XM filler were found to suffer from a reduction of $T_{dec\text{-}10\%}$ and T_g values after filler modification, while the mentioned parameters of the composites with XSM were improved. This showed a betted matrix-filler interaction with filler synthesized from SiO_2-rich aluminum fluoride production waste, leading to better thermal properties of polymer composites.

The mechanical characteristics of the photocross-linked polymer composites prepared in the mold and 3D printed by DLP were determined by tensile test. Stress-strain curves of composites are presented in Figure 13.
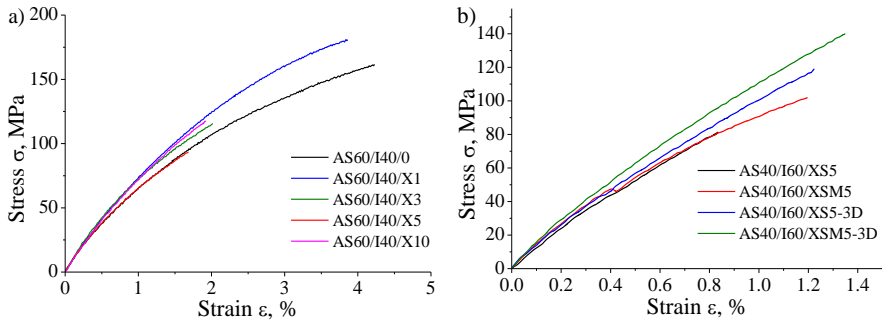
Figure 13. Stress-strain curves of polymer composites AS60/I40/X0-10 (a); stress-strain curves of AS40/I60/XS and AS40/I60/XSM 3D printed specimens and specimens prepared in the mold (b)

An increased amount of inert filler led to reduced values of σ and ε and increased brittleness of the polymer composites (Figure 13a). Photocross-linked polymers with modified filler synthesized from aluminum fluoride production waste showed higher values of σ and ε showing a strong interfacial interaction between the modified filler and the polymer matrix with increased elasticity (Figure 13b). Moreover, a significantly higher values of σ and ε of 3D printed polymer composites AS40/I60/XS5 and AS40/I60/XSM5 indicated a firm adhesion between the printed layers and increased elasticity of the polymer chains.

The resins with XS and XSM fillers were successfully applied in DLP 3D printing. Complex architecture objects were printed with high definition and smooth surface finishing (Figure 14a) demonstrating the suitability of bio-based resins designed for DLP 3D printing. The noticeable surface "whitening" of the printed objects was observed due to the highly exposed enclosed filler when the uncured resin was washed after the 3D printing process as the SEM images confirmed (Figure 14b). The SEM pictures disclosed a desirable matrix-filler interaction because the particles were still embedded in the polymer matrix with noticeable tobermorite and katoite clusters.
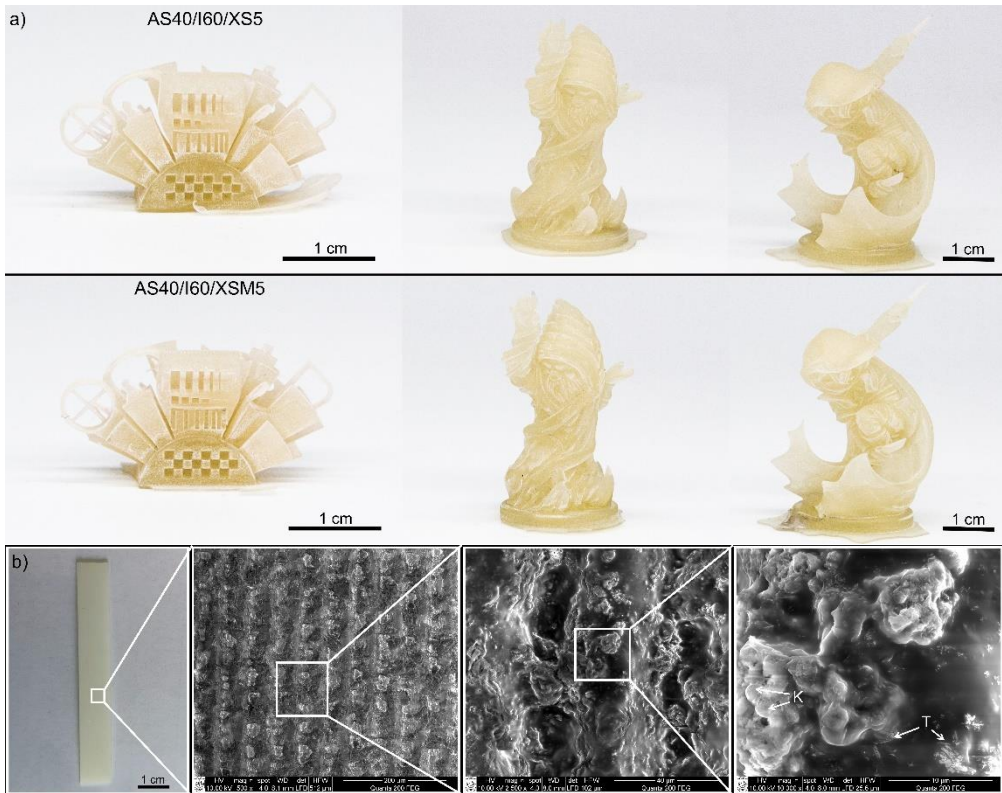
Figure 14. DLP 3D printed objects of AS40/I60/XS5 (top) and AS40/I60/XSM5 (bottom) (a); SEM pictures of DLP 3D printed AS40/I60/XSM5 (b)

The biodegradation of AESO-based polymer composites was determined by measuring oxygen consumption in closed respirometers in an aqueous medium. Photocross-linked polymer composites indicated biodegradation of 0.7–19.6% after 60 days, while the biodegradation of cellulose, used as a reference material, was 54.4% after the same period (Figure 15).
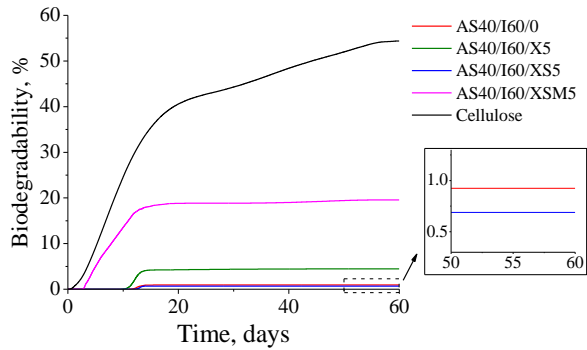
Figure 15. Biodegradation kinetics curves of polymer composites and cellulose as a reference material

The polymer composite AS40/I60/XSM5 with modified filler synthesized from aluminum fluoride production waste showed the highest biodegradability of 19.6%. Due to the decreased v_e of sample AS40/I60/XSM5 compared to AS40/I60/XS5, the penetration of microorganisms or enzymes into the composite sample was increased and biodegradation enhanced [64]. Such notable biodegradability of AS40/I60/XSM5 composite with filler synthesized from aluminum fluoride production waste, as well as improved properties such as elastic modulus, tensile strength, thermal stability, and glass transition make this composite both a sustainable and competitive alternative to aid the rising demand for materials in DLP 3D printing.

The developed bio-based composites AS40/I60/XS5 and AS40/I60/XSM5 have been tested in industrial DLP 3D printer Phrozen Sonic Mini 4K by company AmeraLabs. For the first time, AESO-based composites have been produced by optical 3D printing in industrial 3D printer demonstrating a great practical value of designed biocomposites.

3. CONCLUSIONS

1. Cross-linked polymers based on acrylated epoxidized soybean oil and other plant-derived comonomers can be synthesized by photopolymerization. It was shown that:
   a. higher amounts of myrcene reduced the photocross-linking rate forming 43% lower amount of cross-linked polymer fraction leading to 20 times lower values of Young's modulus from the top pressure test;
   b. the replacement of synthetic divinylbenzene with bio-based vanillin dimethacrylate in synthesized polymers increased cross-linked polymer fraction by 8% and improved Young's modulus values more than twice;
   c. photocross-linked polymer composed of only bio-based monomers showed similar gel point value, but higher storage modulus and compressive modulus values compared to those of commercial petroleum-based photopolymers and is a potential candidate for application in optical 3D printing.
2. Acrylated epoxidized soybean oil-based polymers can be successfully synthesized from the photoinitiator-free systems and applied in laser direct writing lithography. It was determined that:
   a. acrylated epoxidized soybean oil formed solid cross-linked polymers without any presence of photoinitiator;
   b. the addition of plant-derived comonomer vanillin dimethacrylate prolonged the photocross-linking process twice forming up to 57% lower amount of cross-linked polymer fraction leading to lower thermal stability and up to 3 times decreased Young's modulus values;
   c. the 3D microstructures of the acrylated epoxidized soybean oil polymer formed by direct laser writing lithography sustained itself and had a 3D architecture.
3. The photoinitiator and the temperature influence the photocuring kinetics of the acrylated epoxidized soybean oil and the properties of the resulting polymers. The study showed that:
   a. higher temperature caused faster formation of the polymer network of acrylated epoxidized soybean oil;
   b. a higher amount of photoinitiator resulted in more rigid and brittle polymer formation indicated by 3 times decreased elongation at break values;
   c. ethyl (2,4,6-thimethylbenzoyl) phenyl phosphinate was selected as the most suitable photoinitiator, as well as its concentration of 3 mol% was the most suitable for acrylated epoxidized soybean oil-based resins.
4. Cross-linked acrylated epoxidized soybean oil-based polymers with four different bio-based reactive diluents can be synthesized by photopolymerization and successfully applied in digital light processing 3D printing. It was demonstrated that:
   a. depending on the selected reactive diluent (isobornyl methacrylate, methacrylic ester, tetrahydrofurfuryl acrylate or tetrahydrofurfuryl

methacrylate) tunable mechanical and thermal properties of photocross-linked polymer can be obtained;

b. bio-based polymers showed a slower biodegradation process than cellulose at the same experimental conditions, their biodegradability reached up to 7.5% after 60 days;

c. the developed bio-based polymer with isobornyl methacrylate demonstrated tensile properties – elastic modulus 4.75 GPa, tensile strength 250.4 MPa and elongation at break 8.5%, which were to those of commercial petroleum-derived resin Monocure3D Rapid Gray for digital light processing 3D printing.

5. Calcium silicate hydrate fillers have influence on the properties of photocross-linked acrylated epoxidized soybean oil polymer composites which can be successfully applied in digital light processing 3D printing. It was shown that:

a. a higher amount of non-modified filler resulted in reduced storage modulus by nearly 800 MPa at 30°C, a lower glass transition from 99°C to 89°C, lower tensile strength by nearly 80 MPa, and reduced elongation at break from 4.7% to 1.6% of the composite, but improved its thermal stability by up to 12°C;

b. polymer composite with acryloxypropyltrimethoxysilane modified filler synthesized from calcium oxide and silica gel-rich waste material showed improved properties indicating values of elastic modulus 10.7 GPa, tensile strength 97.4 MPa, elongation at break 1.2%, glass transition 111.5°C, and thermal stability 318.8°C at the weight loss of 10%;

c. polymer composite with acryloxypropyltrimethoxysilane modified filler synthesized from calcium oxide and silica gel-rich waste material was produced by digital light processing 3D printing, demonstrating high printing accuracy with strong adhesion between layers and showed biodegradability of 19.6% after 60 days.

4. SANTRAUKA

Pastaraisiais metais 3D spausdinimo technologijos tapo lengvai prieinamos ne tik mokslininkams bei tyrėjams, bet ir įprastiems vartotojams. Naudojant 3D spausdinimo technologijas, galima pagaminti įvairius sudėtingus gaminius, kurių negalima išpjauti ir surinkti neeikvojant papildomai didelio kiekio medžiagų [1]. Gana paprasta ir plačiausiai taikoma 3D spausdinimo technologija yra ekstruduoto lydalo modeliavimas (angl. *fused deposition modelling*, FDM) – išlydant termoplastikų gijas, polimerų lydalo srovę sluoksniuojant ir atvėsinant, suformuojamas norimas gaminys [2]. Atliekant optinį 3D spausdinimą, naudojamos skystos dervos, kurios spinduliuote sluoksnis po sluoksnį yra kietinamos, ir taip gaunamas reikiamas polimerinis objektas [3]. Nors FDM proceso metu gaminiai yra spausdinami greičiau, tačiau optinis 3D spausdinimas pasižymi didesne spausdinimo raiška [4]. Dėl to jis yra tinkamesnis, norint gauti smulkesnius ir tikslesnius gaminius. Dauguma medžiagų, skirtų optiniam 3D spausdinimui, yra gamtoje stabilios sintetinės medžiagos, todėl gamtinės kilmės medžiagos galėtų būti tinkama alternatyva, siekiant sumažinti neigiamą įtaką aplinkai. Parenkant atitinkamas gamtinės kilmės medžiagas, dervos gali būti gautos iš visiškai arba iš dalies gamtinės kilmės medžiagų. Priklausomai nuo parinktų gamtinės kilmės medžiagų struktūros ir funkcionalumo, galima gauti skirtingomis savybėmis pasižyminčius 3D spausdintus objektus [5].

Siekiant gauti geresnių savybių turinčius 3D spausdintus polimerus, į sistemą gali būti pridedama užpildų. Priklausomai nuo dervos sudėties ir užpildo savybių, gali būti gaunami geresnėmis mechaninėmis, terminėmis, elektrinėmis ir kitomis savybėmis pasižymintys polimeriniai kompozitai [6]. Derinant gamtinės kilmės medžiagas, tinkamas optiniam 3D spausdinimui, su atitinkamais užpildais, gauti bioskaidūs 3D spausdinti polimeriniai kompozitai galėtų pakeisti sintetines medžiagas atliekant optinį 3D spausdinimą.

Šiame darbe buvo tiriami akrilinto epoksidinto sojų aliejaus (angl. *acrylated epoxidized soybean oil*, AESO) polimerai ir polimeriniai kompozitai, skirti optiniam 3D spausdinimui. Tyrimams atlikti AESO buvo pasirinkta kaip pagrindinė gamtinės kilmės medžiaga dėl žemos kainos, mažo toksiškumo ir plataus komercinio naudojimo UV kietinamoms dangoms [7]. Disertacijoje nagrinėjamas AESO pritaikymas optiniam 3D spausdinimui, sukuriant panašiomis ar geresnėmis savybėmis pasižyminčius polimerus ar polimerinius kompozitus nei komerciniai sintetiniai produktai. Tyrimų rezultatai publikuoti penkiose publikacijose.

Darbo tikslas – sukurti akrilinto epoksidinto sojų aliejaus ir įvairių komonomerų tinklinius polimerus ir polimerinius kompozitus, kurių gaminius būtų galima gauti atliekant optinį 3D spausdinimą.

Šiam tikslui pasiekti buvo iškelti šie uždaviniai:

1. Sukurti akrilinto epoksidinto sojų aliejaus ir gamtinės kilmės komonomerų kompozicijas, skirtas optiniam 3D spausdinimui, susintetinti tinklinės struktūros polimerus, ištirti jų savybes ir palyginti su komercinėmis medžiagomis.

2. Fototinklinti akrilinto epoksidinto sojų aliejaus polimerus nenaudojant fotoiniciatoriaus ir pritaikyti juos tiesioginio lazerinio rašymo technologijoje.
3. Ištirti keturių fotoiniciatorių ir temperatūros įtaką akrilinto epoksidinto sojų aliejaus fotokietinimo kinetikai ir išanalizuoti gautų polimerų savybes.
4. Sukomponuoti ir susintetinti gamtinės kilmės akrilinto epoksidinto sojų aliejaus polimerus su skirtingais gamtinės kilmės reaktyviaisiais tirpikliais, ištirti jų savybes ir pritaikyti juos skaitmeniniam 3D spausdinimui naudojant šviesą.
5. Nustatyti kalcio hidrosilikatų ($CaO:SiO_2$ molinis santykis 1:1) užpildų įtaką fototinklintų akrilinto epoksidinto sojų aliejaus polimerinių kompozitų savybėms ir juos pritaikyti skaitmeniniam 3D spausdinimui naudojant šviesą.

Mokslinis naujumas

- Pirmą kartą tinkliniai akrilinto epoksidinto sojų aliejaus polimerai buvo gauti nenaudojant fotoiniciatoriaus, išlaikė polimerinių objektų struktūrą ir yra tinkami tiesioginio lazerinio rašymo litografijai.
- Naujos akrilinto epoksidinto sojų aliejaus dervos su augalinės kilmės komonomerais pasižymi dideliu fotojautrumu ir tinklinimosi greičiu, tinkamais optiniam 3D spausdinimui.
- Nauji funkcionalizuoti kalcio hidrosilikato užpildai, susintetinti iš kalcio oksido ir aliuminio fluorido gamybos atliekų, pagerino akrilinto epoksidinto sojų aliejaus polimerinių kompozitų mechanines ir termines savybes, palyginti su polimeriniais kompozitais su užpildais, susintetintais iš kalcio oksido ir silikagelio.

Darbo praktinė vertė

Tinkliniams akrilinto epoksidinto sojų aliejaus polimerams ir polimeriniams kompozitams, tinkamiems optiniam 3D spausdinimui, sukurti buvo naudotos tik komercinės gamtinės kilmės medžiagos. Iš viso iš gamtinės kilmės monomerų buvo sukurtos šešios dervos ir išbandytos komerciniuose skaitmeniniuose 3D spausdintuvuose, naudojančiuose šviesą, įmonėse MB „AmeraLabs" ir UAB „3D Creative". Bendradarbiaujant su Suomijos Centria taikomųjų mokslų universitetu, įmonėje MB „AmeraLabs" buvo atliktas 3D atspausdintų gaminių gyvavimo ciklo vertinimas (angl. *Life Cycle Assessment*, LCA). Palyginus akrilinto epoksidinto sojų aliejaus ir komercinių dervų įtaką aplinkos faktoriams, 12 iš 16 vertintų faktorių buvo nustatytas mažesnis akrilinto epoksidinto sojų aliejaus dervos poveikis aplinkai. Taip buvo pagrįsta komercinių iš naftos gautų produktų pakeitimo gamtinės kilmės produktais nauda atliekant optinį 3D spausdinimą. Visi sukurti gamtinės kilmės polimerai, sėkmingai pritaikyti skaitmeniniam 3D spausdinimui naudojant šviesą, biologiškai skilo, tačiau šis procesas buvo lėtesnis nei celiuliozės tomis pačiomis eksperimentinėmis sąlygomis.

Autorės indėlis rengiant disertaciją

Disertacijos autorė sukomponavo, susintetino ir ištyrė penkias akrilinto epoksidinto sojų aliejaus tinklinių polimerų ir polimerinių kompozitų serijas. Jos pateiktos 4.1–4.5 skyreliuose. Autorė atliko ir išanalizavo fotoreometrijos tyrimą, ekstrakciją Soksleto aparatu, diferencinę skenuojamąją kalorimetriją, termogravimetrinę analizę, dinaminę termomechaninę analizę, gniuždymo ir tempimo testus ir bioskaidumo tyrimą. Disertacijos autorė parengė visus penkis mokslinių straipsnių rankraščius. Edvinas Skliutas (Lazerinių tyrimų centras, Vilniaus universitetas) atliko atrinktų dervų tiesioginį lazerinį rašymą, ištyrė μ-3D struktūras ir prisidėjo rengiant straipsnio rankraštį. Prof. dr. Mangirdas Malinauskas (Lazerinių tyrimų centras, Vilniaus universitetas) konsultavo atliekant tiesioginį lazerinį rašymą ir prisidėjo redaguojant straipsnio rankraštį. Vaidas Talačka (MB „AmeraLabs") nustatė akrilinto epoksidinto sojų aliejaus dervų skaitmeninio 3D spausdinimo naudojant šviesą spausdinimo parametrus ir pagamino gamtinės kilmės dervų 3D spausdintus bandinius. Andrius Gineika (Kauno technologijos universitetas) susintetino ir charakterizavo kalcio hidrosilikatų užpildus ir prisidėjo rengiant straipsnio rankraštį. Prof. dr. Kęstutis Baltakys (Kauno technologijos universitetas) konsultavo atliekant kalcio hidrosilikatų užpildų sintezę ir prisidėjo redaguojant straipsnio rankraštį. Prof. dr. Jolita Ostrauskaitė (Kauno technologijos universitetas) prisidėjo rengiant tyrimų idėjas ir tikslus, konsultavo sintetinant ir charakterizuojant akrilinto epoksidinto sojų aliejaus kompozicijas ir prisidėjo redaguojant visus penkis mokslinių straipsnių rankraščius. Dr. Rathish Rajan ir dr. Egidija Rainosalo (Centria taikomųjų mokslų universitetas, Suomija) sukūrė ir atliko iš gamtinės kilmės ir komercinių akrilinių dervų 3D spausdintų gaminių gyvavimo ciklo vertinimą. Saulius Lileikis su komanda iš UAB „3D Creative" atliko medicininių laikiklių 3D skenavimą ir skaitmeniniu 3D spausdintuvu, naudojančiu šviesą, pagamino spausdintus medicininius laikiklius iš gamtinės kilmės dervos.

Publikacijų sąrašas disertacijos tema

1. <u>Miglė Lebedevaitė</u>, Jolita Ostrauskaitė, Edvinas Skliutas, Mangirdas Malinauskas. Photocross-linked polymers based on plant-derived monomers for potential application in optical 3D printing. *Journal of applied polymer science*. **2020**, *137* (20), 48708. JIF: 3,125.

2. <u>Miglė Lebedevaitė,</u> Jolita Ostrauskaitė, Edvinas Skliutas, Mangirdas Malinauskas. Photoinitiator free resins composed of plant-derived monomers for the optical μ-3D printing of thermosets, *Polymers*. **2019**, *11* (1), 116. JIF: 4,329.

3. <u>Miglė Lebedevaitė,</u> Jolita Ostrauskaitė. Influence of photoinitiator and temperature on photocross-linking kinetics of acrylated epoxidized soybean oil and properties of the resulting polymers. *Industrial crops and products*. **2021**, *161*, 113210. JIF: 5,645.

4. <u>Miglė Lebedevaitė</u>, Vaidas Talačka, Jolita Ostrauskaitė. High biorenewable content acrylate photocurable resins for DLP 3D printing. *Journal of Applied Polymer Science*. **2021**, *138* (16), 50233. JIF: 3.125.

5. <u>Miglė Lebedevaitė</u>, Andrius Gineika, Vaidas Talačka, Kęstutis Baltakys, Jolita Ostrauskaitė. Development and optical 3D printing of acrylated epoxidized soybean oil-based composites with functionalized calcium silicate hydrate filler derived from aluminum fluoride production waste. *Composites Part A: Applied Science and Manufacturing*. **2022**, *157*, 106929. JIF: 7,664.

Mokslinės konferencjos

Disertacijoje pateikti rezultatai buvo pristatyti 17 tarptautinių mokslinių konferencijų, iš kurių: „6th international Baekeland symposium 2019" Taragona, Ispanija, „Poly-Char Venice international polymer characterization forum 2021" Venecija, Italijoje, „IUPAC-MACRO 2020: the 48th world polymer congress", Džedžu, Pietų Korėjoje. Visas mokslinių konferencijų sąrašas pateiktas 8 skyriuje „LIST OF PUBLICATIONS".

4.1. Fototinklintų akrilinto epoksidinto sojų aliejaus polimerų su mirsenu ir vanilinodimetakrilatu savybių tyrimas

Šis skyrius parašytas remiantis publikuotu straipsniu: *M. Lebedevaitė, J. Ostrauskaitė, E. Skliutas, M. Malinauskas. Photocross-linked polymers based on plant-derived monomers for potential application in optical 3D printing. Journal of Applied Polymer Science. 2019, 137 (20), 48708* [51]. *JIF: 3.125.*

AESO buvo pasirinkta kaip pagrindinė gamtinės kilmės medžiaga polimerams, skirtiems optiniam 3D spausdinimui, sukurti. AESO, mirseno (MYR) ir vanilindimetakrilato (VDM) arba divinilbenzeno (DVB, naudoto palyginimui) polimerai buvo sukurti fototinklinimo būdu ir palyginti su komercinėmis sintetinėmis dervomis *Aurodesk Clear PR48 (PR48)* ir *Formlabs Clear FLGPCL02 (FLGPCL02)* potencialiam naudojimui atliekant optinį 3D spausdinimą.
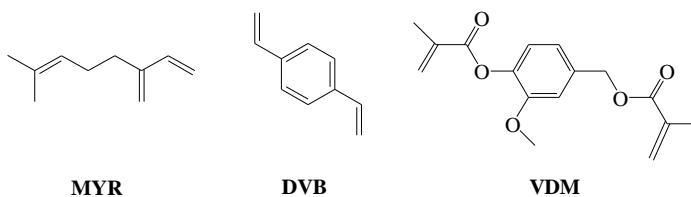
1 pav. Mirseno (MYR), divinilbenzeno (DVB) ir vanilino dimetakrilato (VDM) cheminės struktūros

AESO polimerai buvo sukurti siekiant ištirti MYR, DVB arba VDM kiekio įtaką fotokietinimo kinetikai ir gautų polimerų savybėms. Augalinės kilmės VDM buvo naudotas kaip pakaitalas sintetiniam aromatiniam DVB. Sukurtų polimerų sudėtis pateikta 1 lentelėje.

1 lentelė. Sukurtų dervų sudėtis

| Formuluotė	AESO, mol	MYR, mol	DVB, mol	VDM, mol
C0	1	1	–	–
C1	1	1	1	–
C2	1	3	1	–
C3	1	5	1	–
C4	1	1	–	1
C5	1	3	–	1
C6	1	5	–	1
C7	1	1	3	–
C8	1	1	5	–
C9	1	1	–	3
C10	1	1	–	5

Fotoreometrijos tyrimas parodė stiprią naudotų monomerų kiekio įtaką polimerų fotokietinimo kinetikai. Didesnis MYR kiekis kompozicijose lėmė ilgesnę fototinklinimo reakciją ir mažesnes šlyties tampros modulio (G') vertes, rodančias minkštesnio polimero susiformavimą (2 lentelė). Nors didesnis DVB kiekis kompozicijose sulėtino fotopolimerizacijos procesą, tačiau reakcijos pabaigoje buvo gautos didesnės G' vertės. Didesnis gamtinės kilmės VDM kiekis, juo pakeičiant sintetinį DVB, lėmė greitesnę fototinklinimo reakciją (2 pav., a). Didesnis aromatinio junginio (DVB arba VDM) kiekis pagerino polimerinio tinklo stangrumą, dėl to buvo fiksuotos didesnės G' vertės. Lyginant sintetinių komercinių dervų PR48 ir FLGPCL02 bei formuluotės C9 fotopolimerizaciją (2 pav., b), buvo užfiksuotas panašus fototinklinimo greitis ir G' vertės, rodantys C9 formuluotės tinkamumą potencialiam naudojimui atliekant optinį 3D spausdinimą.
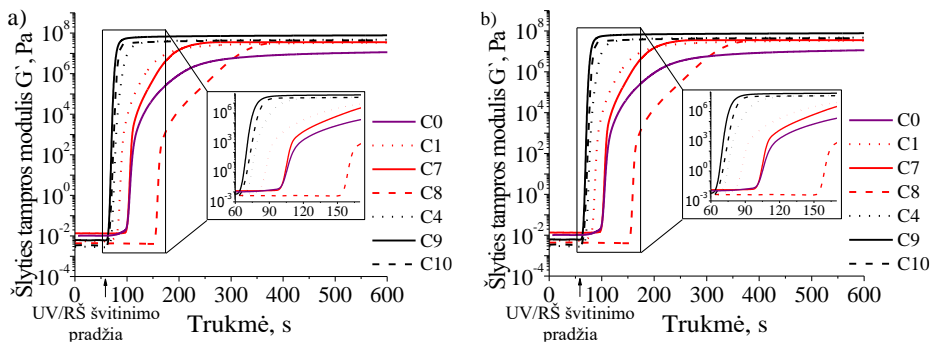
2 pav. Šlyties tampros modulio G' priklausomybė nuo švitinimo trukmės dervų be aromatinio junginio C0 (violetinė) ir dervų C1, C4 ir C7-C10 su skirtingu aromatinio junginio kiekiu: VDM (juoda) ir DVB (raudona) (a); dervų C9, PR48 ir FLGPCL02 (b)

Polimerų netirpios frakcijos kiekis (*YIF*) po ekstrakcijos Soksleto aparatu pateiktas 2 lentelėje. Dėl susidarančio didesnio kiekio linijinių ir (ar) šakotųjų makromolekulių fotopolimerizacijos metu polimeruose, turinčiuose didesnį MYR kiekį, buvo fiksuotos mažesnės *YIF* vertės. Fototinklinti polimerai su VDM

pasižymėjo didesnėmis *YIF* vertėmis nei polimerai su DVB. Taip pat buvo pastebėta priklausomybė tarp *YIF* ir tinklo tankio (v_e) – polimerų, kurių *YIF* vertės buvo mažesnės, v_e vertės taip pat buvo mažesnės.

2 lentelė. AESO dervų ir tinklintų polimerų charakteristikos

Kompozicija	t_{gel}[1], s	G'[2], MPa	YIF[3], %	v_e[4], kmol·m^{-3}	E_C[5], MPa
C0	60 ± 1,5	15,52 ± 2,45	–	–	–
C1	35 ± 4,2	34,10 ± 1,25	94	13,83 ± 0,50	9,8 ± 0,2
C2	323 ± 8,7	3,62 ± 1,25	93	1,46 ± 0,50	8,4 ± 0,1
C3	465 ± 11,7	0,14 ± 0,07	53	0,58 ± 0,03	1,1 ± 0,02
C4	18 ± 0,7	47,64 ± 1,25	97	19,23 ± 5,06	18,4 ± 0,2
C5	200 ± 7,9	30,81 ± 6,95	94	12,41 ± 2,81	9,9 ± 0,2
C6	403 ± 12,0	0,63 ± 0,20	58	0,03 ± 0,01	0,5 ± 0,1
C7	48 ± 1,4	35,61 ± 3,48	88	14,40 ± 1,41	7,6 ± 0,4
C8	102 ± 5,5	40,64 ± 1,95	90	16,43 ± 0,79	9,7 ± 0,2
C9	12 ± 0,0	77,83 ± 3,11	96	31,42 ± 1,26	21,2 ± 0,2
C10	15 ± 1,0	44,93 ± 6,09	94	18,14 ± 4,27	15,8 ± 0,2
PR48	13 ± 0,0	25,91 ± 0,99	99	10,52 ± 0,40	16,9 ± 0,3
FLGPCL02	12 ± 1,0	71,22 ± 3,49	99	28,71 ± 7,87	13,1 ± 0,3

[1] gelio taškas, apskaičiuotas nuo UV/RŠ švitinimo pradžios;
[2] šlyties tampros modulis ties 1200 s nuo testo pradžios;
[3] netirpios frakcijos kiekis po ekstrakcijos Soksleto aparatu 24 h chloroforme;
[4] tinklo tankis, apskaičiuotas pagal *G'* vertes;
[5] Jungo modulis gniuždant.

AESO fototinklintų polimerų mechaninės savybės buvo charakterizuotos Jungo moduliu gniuždant (E_C). Polimerai, turintys didesnį MYR kiekį, buvo minkštesni ir įgijo mažesnes E_C vertes dėl mažesnio polimerų tinklo tankio. AESO polimeruose keičiant sintetinį DVB gamtinės kilmės VDM buvo gautos geresnės mechaninės savybės ir didesnės E_C vertės. Formuluotė C9, sudaryta iš AESO/MYR/VDM moliniu santykiu 1:1:3, pasižymėjo didžiausiomis v_e ir E_C vertėmis, panašiomis į komercinių sintetinių produktų, ir potencialiai gali būti pritaikyta atliekant optinį 3D spausdinimą.

4.2. Akrilinto epoksidinto sojų aliejaus dervų fototinklinimas nenaudojant fotoiniciatoriaus ir gautų polimerų savybių tyrimas

Šis skyrius parašytas remiantis publikuotu straipsniu: *M. Lebedevaitė, J. Ostrauskaitė, E. Skliutas, M. Malinauskas. Photoinitiator free resins composed of plant-derived monomers for the optical μ-3D printing of thermosets. Polymers. 2019, 11 (1), 116* [52]. *JIF: 4.329.*

Fototinklinti AESO ir vanilino dimetakrilato (VDM) arba vanilino diakrilato (VDA) (3 pav.) polimerai buvo gauti nenaudojant fotoiniciatoriaus ar papildomo tirpiklio ir buvo pritaikyti tiesioginio lazerinio rašymo technologijoje arba atliekant optinį μ-3D spausdinimą. Šie polimerai buvo sukurti siekiant gauti augalinės kilmės fototinklintus polimerus nenaudojant papildomų toksiškų fotoiniciatorių ar kitų sintetinių medžiagų.

VDM   **VDA**
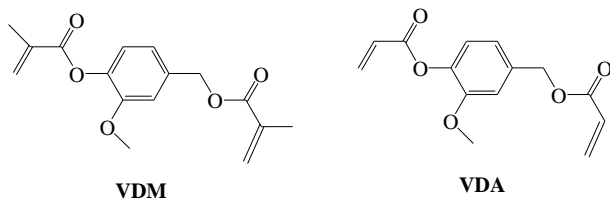
3 pav. Vanilino dimetakrilato (VDM) ir vanilino diakrilato (VDA) cheminės struktūros

Gamtinės kilmės dervos buvo sudarytos iš AESO ir VDM moliniu santykiu 1:1 (AESO/VDM1), 1:0,5 (AESO/VDM2) ir 1:0,25 (AESO/VDM3). Dervos su VDA buvo paruoštos analogiškai. Gryno AESO ir sukurtų gamtinės kilmės dervų fotokietinimo kinetika buvo tirta fotoreometrijos metodu (4 pav.).
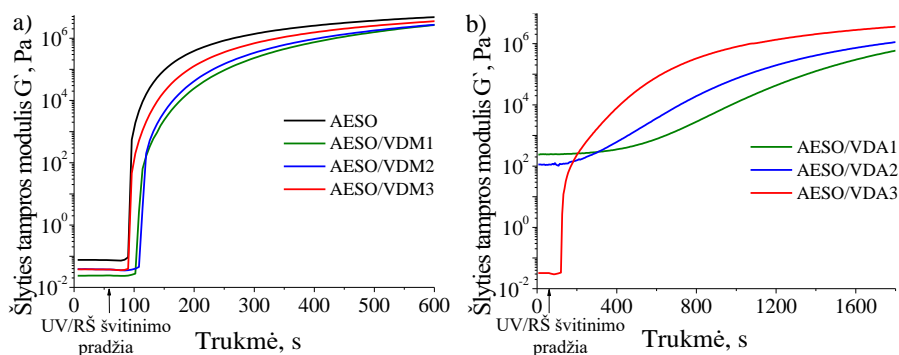
4 pav. Šlyties tampros modulio *G'* priklausomybės nuo eksponavimo trukmės gryno AESO ir dervų AESO/VDM (a) ir AESO/VDA (b)

Fotoreometrijos tyrimu patvirtinta, kad polimerų erdvinis polimerinis tinklas susidarė nenaudojant fotoniciatoriaus. Fotopolimerizacijos reakcija buvo sukelta atskilusių nuo monomerų vinilgrupės dvigubųjų ryšių radikalų, kurie inicijavo (met)akrilgrupės polimerizaciją [53]. Buvo pastebėta, kad didesnis aromatinio junginio kiekis lėmė lėtesnę fotopolimerizacijos reakciją ir mažesnes *G'* vertes. Lyginant dervų su VDM ir VDA fotokietinimo kinetiką, nustatytas greitesnis *G'* kreivės kilimas ir didesnės vertės tyrimo pabaigoje dėl greitesnio VDM vinilgrupės dvigubojo ryšio skilimo. Dėl šios priežasties AESO/VDA formuluotės toliau nebuvo tiriamos.

Tinklinė gamtinės kilmės polimerų struktūra buvo patvirtinta atliekant ekstrakciją Soksleto aparatu. Polimeras pAESO pasižymėjo didžiausiu *YIF* – 88 %, parodant, kad AESO yra linkęs suformuoti tankią polimerinę struktūrą net ir nenaudojant fotoiniciatoriaus. Buvo pastebėta, kad didesnis VDM kiekis polimere lėmė mažesnį *YIF* dėl susidarančio didesnio linijinių ir (ar) šakotųjų polimerų kiekio kompozicijose nenaudojant fotoiniciatoriaus.

3 lentelė. Polimerų netirpios frakcijos kiekis, terminės ir mechaninės charakteristikos.

Polimeras	YIF^1, %	$T_g{}^2$, °C	$T_{dec\text{-}10\%}{}^3$, °C	$E_C{}^4$, MPa
pAESO	88	–4,5	356	$0,62 \pm 0,1$
pAESO/VDM1	31	–2,6	295	$0,19 \pm 0,03$
pAESO/VDM2	48	–2,6	318	$0,46 \pm 0,13$
pAESO/VDM3	63	–1,6	331	$0,66 \pm 0,13$

[1] netirpios frakcijos kiekis po ekstrakcijos Soksleto aparatu 24 h chloroforme;

[2] stiklėjimo temperatūra, nustatyta DSC metodu;

[3] temperatūra, esant 10 % masės nuostoliams, nustatyta iš TGA kreivių;

[4] Jungo modulis gniuždant.

Nustatyta, kad fototinklintų polimerų mechaninės ir terminės savybės yra glaudžiai susijusios su polimerų *YIF* (3 lentelė). Polimerai, turintys didesnį VDM kiekį ir įgiję mažesnes *YIF* vertes, pasižymėjo mažesne stiklėjimo temperatūra, terminiu stabilumu ir žemesnėmis Jungo modulio gniuždant vertėmis. Galima teigti, kad, AESO sistemoje nenaudojant fotoiniciatoriaus, VDM veikia kaip plastifikatorius, prastinantis tinklinio polimero mechanines ir termines savybes.

Mikroakytos 3D struktūros iš AESO ir AESO/VDM3 buvo atspausdintos tiesioginio lazerinio rašymo metodu (4 pav.). Gamtinės kilmės dervos buvo polimerizuotos naudojant ultratrumpaisiais impulsais sužadintą daugiafotonę sugertį arba griūtinę jonizaciją ir taip inicijuojant tinklinimosi reakciją.
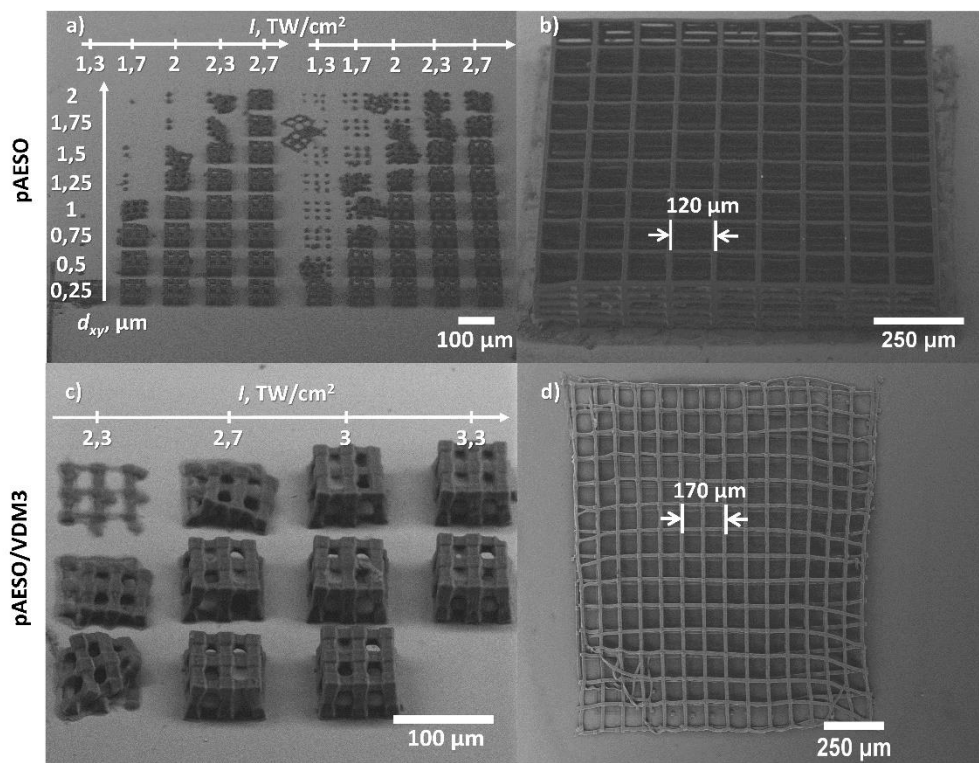
4 pav. Mikroakytų 3D spausdintų struktūrų SEM nuotraukos: (a) 75×75 µm² pAESO erdvinės struktūros esant 30 µm tarpams, v = 5 mm/s; skalė iš kairės į dešinę rodo atstumą d_{xy} tarp gretimų lazeriu eksponuotų vietų; (b) 1095×1095 µm² pAESO erdvinė struktūra esant 120 µm tarpams, v = 5 mm/s, P = 0,6 mW (2 TW/cm²); (c) 75×75 µm² pAESO/VDM3 erdinės struktūros esant 30 µm tarpams, v = 5 mm/s; skalė viršuje rodo energijos intensyvumą I; (d) 1065×1065 µm² pAESO/VDM3 erdvinė struktūra esant 75 µm tarpams, v = 5 mm/s, P = 0,4 mW (1,3 TW/cm²)

Pagaminti 75×75 µm² erdviniai dariniai (4 pav., a ir c) buvo suformuoti esant spausdinimo greičiui v 5 mm/s ir galiai P 0,4–1 mW (1,3–3,3 TW/cm²) ribose. Nustatyta, kad šiose sistemose gaunami struktūriškai stabilesni dariniai, kai naudojamas didesnis lazerinės spinduliuotės intensyvumas I, nes tada vieno skenuojamo taško matmenys yra didesni už atstumą d_{xy}. Atspausdintos gardelės mm skalėje (4 pav., b ir d) pasižymėjo erdvine struktūra, tačiau polimero pAESO/VDM3 struktūra nebuvo patvari dėl didesnio polimero minkštumo.

4.3. Fotoiniciatoriaus ir temperatūros įtaka akrilinto epoksidinto sojų aliejaus fotokietinimo kinetikai ir gautų polimerų savybių tyrimas

Šis skyrius parašytas remiantis publikuotu straipsniu: *M. Lebedevaitė, J. Ostrauskaitė, Influence of photoinitiator and temperature on photocross-linking kinetics of acrylated epoxidized soybean oil and properties of the resulting polymers. Industrial crops and products. 2021, 161, 113210* [54]. *JIF: 5,645.*

Nenaudojant fotoiniciatoriaus fototinklintas AESO pasižymi geru mechaniniu tvirtumu ir terminiu stabilumu, tačiau, palyginti su sintetinėmis komercinėmis dervomis optiniam 3D spausdinimui, polimerinto AESO mechaninės ir terminės savybės yra prastos. Taip pat nustatyta, kad AESO fotokietėjimas nenaudojant fotoiniciatoriaus yra per lėtas, norint AESO pritaikyti DLP/SLA 3D spausdinimui. Siekiant išspręsti šiuos AESO trūkumus, buvo tirta temperatūros, fotoiniciatoriaus tipo ir koncentracijos įtaka AESO fotokietinimo kinetikai.

Siekiant ištirti AESO fotokietinimo kinetiką fotoreometrijos metodu, buvo pasirinkti keturi skirtingi komerciniai fotoiniciatoriai: 2,2-dimetoksi-2-fenilacetofenonas (DMPA), fenil-bis(2,4,6-trimetilbenzoil)fosfino oksidas (BAPO), difenil(2,4,6-trimetilbenzoil)fosfino oksidas (TPO) ir etil(2,4,6-trimetilbenzoil)fenilfosfinatas (TPOL) (5 pav.). Naudota 1, 3 ir 5 mol % fotoinciatoriaus koncentracija dervose, pavadintose pagal naudotą fotoiniciatorių ir jo kiekį (pvz., ADMPA1, ADMPA3 ir t. t.).
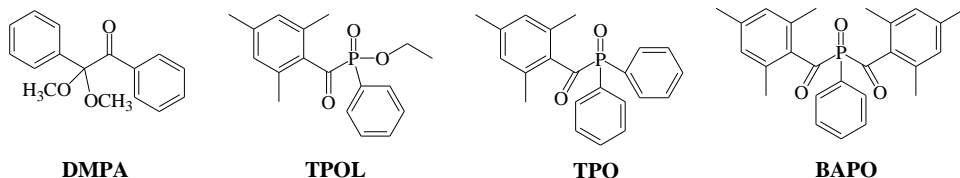
**5 pav.** 2,2-dimetoksi-2-fenilacetofenono (DMPA), fenil-bis(2,4,6-trimetilbenzoil)fosfino oksido (BAPO), difenil(2,4,6-trimetilbenzoil)fosfino oksido (TPO) ir etil(2,4,6-trimetilbenzoil)fenilfosfinato (TPOL) cheminės struktūros

Fotoreometrijos metodu nustatyta, kad sistemoje esant fotoiniciatoriaus AESO fotopolimerizacija vyksta greičiau, palyginti su tioleno ir akrilatų sistemomis, naudojamomis atliekant optinį 3D spausdinimą [55, 56, 57]. Siekiant išsiaiškinti fotoiniciatoriaus įtaką fotokietėjimo kinetikai, buvo lyginamos AESO dervų su skirtingomis fotoiniciatorių koncentracijomis G' kreivės. 6 paveiksle pateikta dervų su 1–5 mol % TPOL ir 3 mol % skirtingų fotoiniciatorių 25 °C temperatūroje G' priklausomybės nuo reakcijos trukmės. Nustatyta, kad fotoiniciatoriaus kiekis neturėjo įtakos gelio taškui ir indukciniam periodui, tačiau lėmė G' kreivės formą UV/RŠ švitinimo pradžioje (6 pav., a). Derva su 3 mol % TPOL pasižymėjo didesniu bandinio kietėjimo greičiu, G' maksimumą pasiekė 1 s greičiau nei derva ATPOL5, todėl priimama, kad 3 mol % TPOL yra optimali koncentracija. Lyginant dervų su skirtingais fotoiniciatoriais fotokietėjimo kinetiką, esant 3 mol % koncentracijai (6 pav., b), pastebėta, kad derva ABAPO3 pasiekė G' maksimumą greičiausiai. Tai rodo didžiausią BAPO jautrumą UV spinduliuotei ir gebėjimą sugeneruoti daugiausia radikalų, iniciuojančių AESO fotopolimerizaciją.
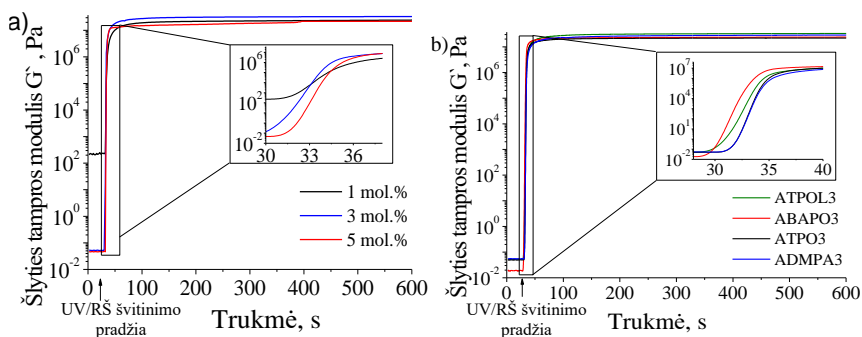
6 pav. Šlyties tampros modulio *G'* priklausomybės nuo eksponavimo trukmės dervų su 1–5 mol % TPOL (a) ir su skirtingais fotoiniciatoriais esant 3 mol % koncentracijai (b) 25 °C temperatūroje

Polimerų terminės savybės buvo ištirtos TGA ir DSC metodais. AESO polimerai pasižymėjo aukštu terminiu stabilumu, o jų temperatūra, esant 10 % masės nuostoliams ($T_{dec-10\%}$), buvo 337–352 °C. DSC patvirtino amorfinę AESO polimerų struktūrą DSC termogramose fiksuojant tik stiklėjimo virsmą. Fototinklintų AESO polimerų stiklėjimo temperatūra (T_g) buvo užfiksuota 41,1–50,9 °C intervale. Palyginti su AESO polimeru, tinklintu nenaudojant fotoiniciatoriaus (–4,5 °C) (3 lentelė), pastebima, kad T_g ryškiai padidėjo, kai dervoje buvo naudojamas fotoiniciatorius. Taip yra todėl, kad naudojant fotoiniciatorių dervoje fotopolimerizacijos metu susidaro daugiau aktyvių centrų ir daugiau tinklinio polimero. Tai galima pastebėti vertinant AESO polimero, tinklinto be fotoiniciatoriaus, *YIF* 88 % ir AESO, tinklinto su fotoiniciatoriumi, *YIF* 96,1–97,9 % intervale.

4 lentelė. Polimerų netirpios frakcijos kiekis, terminės ir mechaninės charakteristikos

Polimeras	YIF^1, %	$T_{dec-10\%}{}^2$, °C	$T_g{}^3$, °C	$E_C{}^4$, MPa	$E_E{}^5$, MPa	σ^6, MPa
ADMPA1	97,6	338	47,5	323 ± 24	199 ± 7	4,34 ± 0,8
ADMPA3	97,9	342	48,1	335 ± 62	273 ± 11	5,48 ± 0,99
ADMPA5	97,8	340	44,2	359 ± 32	325 ± 7	5,15 ± 0,47
ATPOL1	97,7	337	50,9	318 ± 46	239 ± 30	5,59 ± 0,86
ATPOL3	97,2	337	46,6	384 ± 32	487 ± 11	4,95 ± 1,02
ATPOL5	96,6	348	46,2	350 ± 35	544 ± 12	6,23 ± 0,98
ATPO1	97,5	342	46,4	373 ± 20	135 ± 5	4,23 ± 0,83
ATPO3	96,1	340	41,1	359 ± 20	279 ± 3	5,39 ± 1,01
ATPO5	97,9	337	44,7	350 ± 13	292 ± 15	5,23 ± 0,75
ABAPO1	97,2	352	45,7	392 ± 33	205 ± 8	4,53 ±0,38
ABAPO3	97,4	346	46,1	383 ± 24	240 ± 16	5,56 ± 1,83
ABAPO5	97,1	345	45,7	401 ± 22	490 ± 33	5,42 ± 0,35

[1] netirpios frakcijos kiekis po ekstrakcijos Soksleto aparatu 24 h chloroforme;

[2] temperatūra, esant 10 % masės nuostoliams, nustatyta iš TGA kreivių;

[3] stiklėjimo temperatūra, nustatyta DSC metodu;

Jungo modulis gniuždant;
Jungo modulis tempiant;
tempiamasis stipris.

Pastebėta, kad AESO polimerai, tinklinti naudojant fotoiniciatorių, kurių aukštesnės *YIF* vertės, pasižymėjo ir geresnėmis mechaninėmis savybėmis nei AESO polimerai, tinklinti nenaudojant fotoiniciatoriaus. Nustatyta, kad E_C vertės padidėjo bent 500 kartų AESO fotopolimerizuojant su fotoiniciatoriumi. Reikia paminėti, kad AESO polimerams, tinklintiems su fotoiniciatoriumi ir be jo, E_C nustatyti buvo naudota skirtinga aparatūra, o tai galėjo lemti skirtingus rezultatus. Tačiau nepaisant to pastebėta, kad akivaizdžiai pagerėjo mechaninės savybės, kai AESO buvo tinklinamas naudojant fotoiniciatorių.
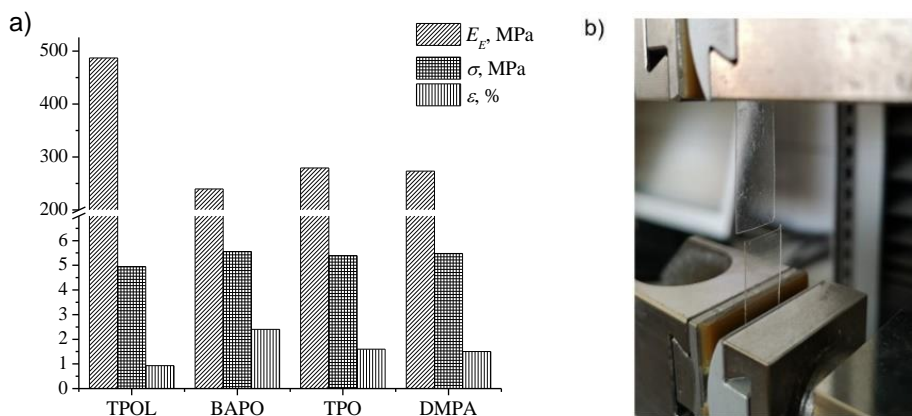
7 pav. AESO polimerų su skirtingais fotoiniciatoriais, esant 3 mol % koncentracijai, Jungo modulis tempiant (E_E), tempiamasis stipris (σ) ir santykinė ištįsa trūkio metu (ε) (a); nutrūkusi AESO polimero plėvelė po tempimo bandymo (b)

Fototinklintų AESO plėvelių tempimo bandymas parodė ryškią fotoiniciatoriaus kiekio įtaką polimero mechaninėms savybėms. AESO polimero plėvelių tempimo bandymo charakteristikos ir trūkusios AESO plėvelės nuotrauka po tempimo bandymo pateikti 7 paveiksle. Nustatyta, kad dėl didesnio fotoiniciatoriaus kiekio padidėjo polimerų Jungo modulis tempiant (E_E), tačiau dėl išaugusio polimero trapumo plėvelių santykinė ištįsa trūkio metu (ε) pastebimai sumažėjo. AESO polimerai su TPOL, ypač polimeras ATPOL3, pasižymėjo didžiausiomis E_E vertėmis, palyginti su kitais fotoiniciatoriais. Nors AESO sistemoje naudojant 5 mol % BAPO vietoje 3 mol %, E_E vertės padidėjo beveik du kartus, tačiau ekonomiškai efektyviau ir patogiau gamybos atžvilgiu naudoti skystą TPOL vietoje kieto BAPO. 3 mol % TPOL buvo pasirinkta kaip optimali koncentracija tolesniems tyrimams atlikti.

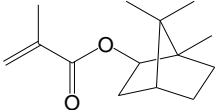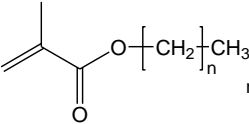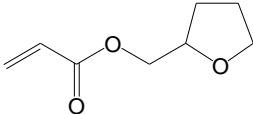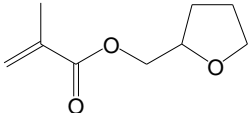### 4.4. Fototinklintų akrilinto epoksidinto sojų aliejaus polimerų su gamtinės kilmės reaktyviaisiais tirpikliais savybių tyrimas ir skaitmeninis 3D spausdinimas naudojant šviesą

Šis skyrius parašytas remiantis publikuotu straipsniu: *M. Lebedevaitė, V. Talačka, J. Ostrauskaitė. High biorenewable content acrylate photocurable resins for DLP 3D printing. Journal of Applied Polymer Science. 2021, 138 (16), 50233* [58]. *JIF: 3.125.*

Parinkus tinkamiausią fotoiniciatorių ir nustačius optimaliausią jo koncentraciją, AESO dervos galėtų būti pritaikomos DLP 3D spausdinimui. Tačiau esant didelei AESO dervos klampai derva negalėtų būti pritaikoma DLP 3D spausdinimui dėl šios technologijos apribojimų klampai. Siekiant išspręsti šią problemą, buvo pasirinkti gamtinės kilmės reaktyvieji tirpikliai AESO klampai mažinti ir tinklinių polimerų mechaninėms ir terminėms savybėms modifikuoti.

Nauji gamtinės kilmės AESO polimerai buvo sukurti parinkus keturis komercinius gamtinės kilmės reaktyviuosius tirpiklius: izobornilmetakrilatą (IBOMA), metakrilo esterį (ME), tetrahidrofurfurilakrilatą (THFA) ir tetrahifrofurfurilmetakrilatą (THFMA). Naudotų reaktyviųjų tirpiklių atsinaujinančios anglies kiekis (BRC) medžiagose kito nuo 55 % iki 76 % (5 lentelė). Naudota 3 mol % fotoiniciatoriaus TPOL nuo visų monomerų kiekio. Palyginimui buvo naudota komercinė derva *Monocure 3D Rapind Gray (REF)*, skirta optiniam 3D spausdinimui.

5 lentelė. Gamtinės kilmės reaktyviųjų tirpikliai [58]

Medžiaga	Struktūrinė formulė	Medžiagos kilmė	BRC, %
IBOMA		Pušų mediena	71
ME		Augalinis aliejus	76
THFA		Hemiceliuliozė	60
THFMA		Hemiceliuliozė	55

Dažniausiai komercinių dervų, skirtų optiniam 3D spausdinimui, klampa yra 200–1500 mPa·s 25 ℃ temperatūroje. Tokia klampa yra reikalinga dervai tolygiai pasklisti spausdintuvo rezervuare spausdinimo metu judant Z ašiai, kad būtų gautas geros kokybės spausdintas gaminys [59]. AESO dervų BRC buvo 75–82 %, o klampa

kito nuo 557 mPa·s iki 699 mPa·s (6 lentelė), todėl jos buvo tinkamos DLP 3D spausdinimui.

6 lentelė. Paruoštų dervų sudėtis ir savybės

Derva	AESO, %	RD, %	TPOL, %	BRC, %	Klampa, mPa·s
AESO/IBOMA	58,71	39,14	2,15	78,5	699,3 ± 25,7
AESO/ME	68,87	29,52	1,61	81,9	644,3 ± 9,8
AESO/THFA	68,36	29,30	2,34	76,6	557,5 ± 3,1
AESO/THFMA	68,46	29,34	2,20	75,3	634,4 ± 8,5

Gamtinės kilmės dervų fotokietinimo kinetika buvo tirta fotoreometrijos metodu. Nustatyta, kad dervų AESO/IBOMA ir AESO/THFMA fotopolimerizacija buvo lėčiausia, tačiau pasižymėjo aukščiausiomis G' vertėmis (7 lentelė), o tai rodo didžiausią polimerinio tinklo tvirtumą. Buvo pastebėta koreliacija tarp t_{gel} ir linijinio susitraukimo (Δd) – tinklinimui vykstant greičiau medžiaga polimerizacijos metu labiau susitraukė. Medžiaga polimerizacijos metu susitraukia dėl neigiamo atstumų pokyčio tarp dervoje esančių molekulių ir naujai susidariusių kovalentinių ryšių ilgio [60]. Atstumo pokytis, vykstantis fotopolimerizacijos metu, priklauso nuo polimerinio ryšio susidarymo trukmės ir dėl didesnės funkcinių grupių konversijos fiksuojamas didesnis medžiagos susitraukimas. Dėl šios priežasties derva AESO/THFMA, pasižymėjusi mažiausiu t_{gel}, fotopolimerizacijos metu iš visų bandinių susitraukė labiausiai.

7 lentelė. Dervų linijinis susitraukimas, reologinės charakteristikos ir tinklintų polimerų *YIF* ir terminės charakteristikos

Kompozicija	t_{gel}[1], s	G'[2], MPa	Δd[3], %	YIF[4], %	T_g[5], °C	$T_{dec-10\%}$[6], °C	Char[7], %
AESO/IBOMA	2,9 ± 1,0	13,63 ± 6,7	10,0 ± 5,3	98,7	60,8	308	1,5
AESO/ME	2,2 ± 1,2	9,67 ± 0,4	12,7 ± 4,2	96,9	24,3	353	1,6
AESO/THFA	1,9 ± 1,3	10,44 ± 1,8	13,3 ± 2,3	95,4	4,6	345	1,9
AESO/THFMA	3,7 ± 0,02	13,34 ± 2,0	8,0 ± 0	96,3	43,7	351	2,0
REF	–	–	–	99,6	–	386	6,0

[1] gelio taškas, apskaičiuotas nuo UV/RŠ švitinimo pradžios;
[2] šlyties tampros modulis ties 1200 s nuo testo pradžios;
[3] linijinis susitraukimas, nustatytas fotoreometrijos metodu;
[4] netirpios frakcijos kiekis po ekstrakcijos Soksleto aparatu 24 val. chloroforme;
[5] stiklėjimo temperatūra, nustatyta DSC metodu;
[6] temperatūra, esant 10 % masės nuostoliams, nustatyta iš TGA kreivių;
[7] medžiagos likutis TGA tyrimo pabaigoje.

AESO polimerai pasižymėjo dideliu tinklinio polimero kiekiu, pademonstruodami aukštas *YIF* vertes 95,4–98,7 % ribose. Nustatyta, kad polimerai, kurių *YIF*, taip pat ir REF buvo aukštesni, pasižymėjo geresnėmis terminėmis savybėmis: aukštesnėmis T_g ir $T_{dec-10\%}$ vertėmis. Išimtis – AESO/IBOMA polimeras, pasižymėjęs žemiausia $T_{dec-10\%}$. Taip nutiko dėl IBOMA struktūroje esančio izobornilfragmento, kuriame esantis esterio ryšys pasižymi žemu terminiu stabilumu [61]. Kambario temperatūroje polimeras AESO/THFA buvo itin minkštas dėl

fiksuotos mažesnės nei 5 °C T_g, , tačiau išlaikė savo formą dėl tinklinės polimero struktūros.
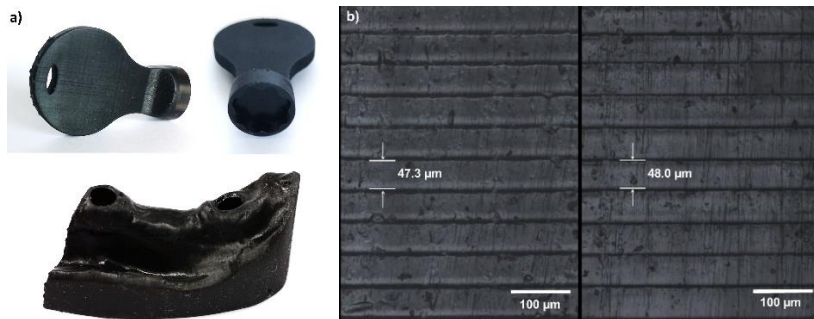
8 pav. 3DPC specialaus varžto raktas iš AESO/IBOMA polimero ((a), viršuje) ir 3DPC žmogaus viršutinio žandikaulio modelio fragmentas iš AESO/TFMA polimero ((a), apačioje); AESO/ME polimero paviršiaus mikroskopo nuotraukos, paruoštos 3DWPC ((b), kairėje) ir 3DPC ((b), dešinėje) būdais

Visi AESO polimerai buvo sėkmingai atspausdinti DLP 3D spausdintuvu. Visos medžiagos, įskaitant ir REF, tempimo bandymui buvo paruoštos trimis skirtingais būdais: teflono formoje (LAB), DLP 3D spausdinimo būdu neatliekant papildomo bandinio apdirbimo po spausdinimo (3DWPC) ir DLP 3D spausdinimo būdu po spausdinimo, izopropanoliu nuplovus nesureagavusią dervą ir papildomai laikant bandinius UV kameroje (3DPC). Sudėtingos struktūros spausdinti bandiniai 3DPC būdu (8 pav., a) pasižymėjo aukštu spausdinimo tikslumu ir lygiu paviršiumi. Dėl išplaunamo didesnio nesureagavusios dervos kiekio bandinių, paruoštų 3DWPC būdu, paviršius buvo su grioveliais ir labiau atskirtais spausdinimo sluoksniais, nei bandinių, paruoštų 3DPC būdu (8 pav., b).

50
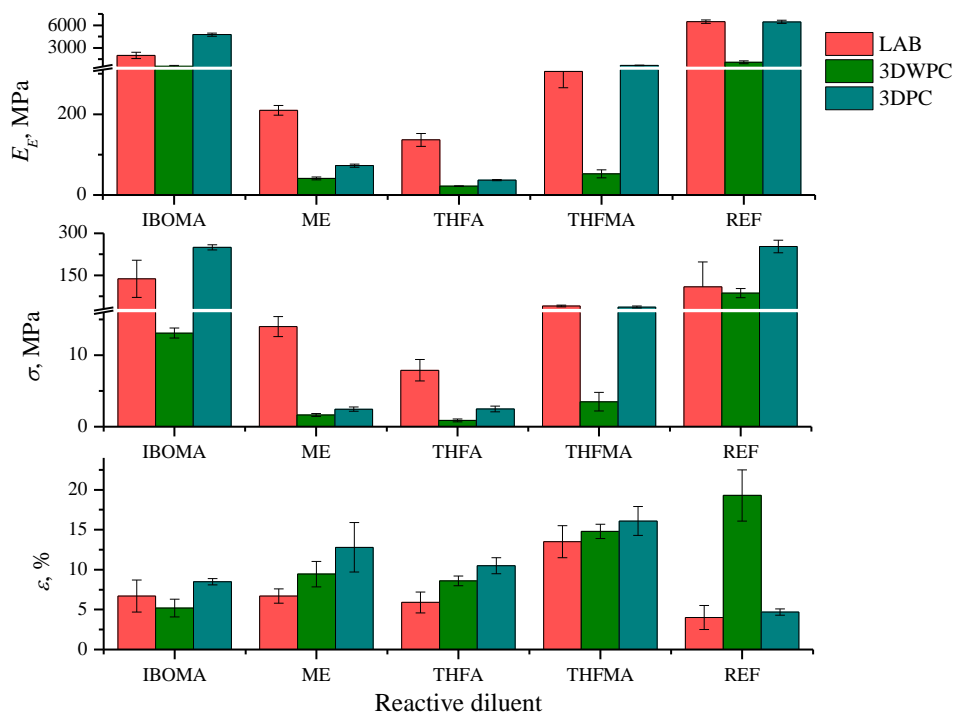
9 pav. Polimerų, paruoštų LAB, 3DWPC ir 3DPC būdais, Jungo modulis tempiant (E_E), tempiamasis stipris (σ) ir santykinė ištįsa trūkio metu (ε)

Gamtinės kilmės polimerų, paruoštų trimis skirtingais būdais, mechaninės savybės buvo tirtos tempiant, siekiant įvertinti adheziją tarp spausdintų sluoksnių. Matavimų rezultatai pateikti 9 paveiksle. Prasčiausios mechaninės savybės fiksuotos 3DWPC būdu paruoštiems polimerams dėl anksčiau nustatytų didelių paviršiaus nelygumų (9 paveikslas). Polimerai AESO/IBOMA ir AESO/THFMA pasižymėjo didžiausiomis E_E ir σ vertėmis iš visų AESO polimerų. Taip pat abiejų šių polimerų bandiniai, paruošti 3DPC būdu, pasižymėjo didesnėmis E_E ir σ vertėmis nei bandiniai, paruošti LAB būdu, o tai rodo stiprią adheziją tarp spausdintų sluoksnių. Polimero AESO/IBOMA, paruošto 3DPC būdu, savybės tempiant buvo artimiausios komercinės sintetinės dervos *Monocure3D Rapid Gray* polimerų savybėms, todėl jis gali būti svarstomas kaip potencialus sintetinių dervų pakaitalas.

4.5. Kalcio hidrosilikato užpildų įtaka fototinklintiems akrilinto epoksidinto sojų aliejaus polimeriniams kompozitams ir skaitmeninis 3D spausdinimas naudojant šviesą

Šis skyrius parašytas remiantis publikuotu straipsniu: *M. Lebedevaitė, A. Gineika, V. Talačka, K. Baltakys, J. Ostrauskaitė. Development and optical 3D printing of acrylated epoxidized soybean oil-based composites with functionalized calcium silicate hydrate filler derived from aluminum fluoride production waste. Composites Part A: Applied Science and Manufacturing. 2022, 106929. [62]. JIF: 7.664.*

Dauguma polimerinių produktų, pagamintų atliekant optinį 3D spausdinimą, nėra pakankamai mechaniškai tvirti, dėl to dažniau yra naudojami tik kaip prototipai, bet ne kaip įprasti komponentai ar detalės [48]. 3D spausdintų gaminių mechaninės, terminės ir kitos savybės gali būti pagerintos įkomponuojant užpildus į polimerinę matricą [31]. Siekiant pagerinti mechanines ir termines AESO polimerų savybes, buvo sukurti gamtinės kilmės kompozitai su funkcionalizuotu kalcio hidrosilikato užpildu, gautu iš aliuminio fluorido gamybos atliekų, ir sėkmingai pritaikyti DLP 3D spausdinimui.

8 lentelė. Paruoštų dervų sudėtis ir klampa

Kompozicija	Monomerų santykis AESO:IBOMA (w/w)	Užpildas	Užpildo kiekis, wt.%	Klampa, mPa·s
AS60/I40/0	60:40	–	0	796
AS60/I40/X1		X	1	1007
AS60/I40/X3			3	1262
AS60/I40/X5			5	2056
AS60/I40/X10			10	2669
AS40/I60/0	40:60	–	5	157
AS40/I60/X5		X	5	241
AS40/I60/XS5		XS	5	302
AS40/I60/XM5		XM	5	624
AS40/I60/XSM5		XSM	5	266

Užpildai buvo ruošiami hidroterminės sintezės būdu iš kalcio oksido ir silikagelio (X) arba didelį kiekį SiO_2 turinčio aliuminio fluorido gamybos atliekų (XS) moliniu santykiu 1:1 200 °C temperatūroje 12 h pagal pateiktą procedūrą [63]. Susintetintame X užpilde vyravo tobermoritas, ksonotlitas ir kiti kalcio hidrosilikatai, o XS užpilde – tobermoritas, kuspidinas, katoitas ir kiti kalcio hidrosilikatai. Vėliau užpildai papildomai modifikuoti akriloksipropiltrimetoksisilanu (APr) (atitinkamai XM ir XSM). Dervos buvo ruošiamos sumaišius AESO ir IBOMA santykiu 60:40 bei pridėjus nuo 1 % iki 10 % užpildo X arba sumaišius AESO ir IBOMA santykiu 40:60 ir pridėjus 5 % užpildo X, XS, XM arba XSM (8 lentelė, pvz., AS40/I60/XS5 ir AS60/I40/X5; čia AS rodo AESO masės santykį, I – IBOMA masės santykį ir paskutinė dalis – naudotą užpildą ir jo kiekį). Palyginimui buvo ruošiamos dervos be užpildo su abiem monomerų santykiais (AS60/I40/0 ir AS40/I60/0). Naudota 3 mol % fotoiniciatoriaus TPOL nuo bendro monomerų kiekio.

9 lentelė. AESO fototinklintų polimerų kompozitų terminės charakteristikos

Kompozitas	TGA		DMTA	
	$T_{dec\cdot10\%}$[1], °C	Char[2], %	T_g,[3] °C	v_e[4], mol·m^{-3}
AS60/I40/0	308,5	1,49	99,2	3655,7
AS60/I40/X1	308,3	2,53	91,6	3261,8
AS60/I40/X3	320,2	4,09	91,2	3498,8
AS60/I40/X5	320,2	6,43	91,0	3999,0

AS60/I40/X10	319,5	11,60	89,4	4296,9
AS40/I60/0	306,5	1,73	114,8	6546,0
AS40/I60/X5	320,3	6,88	110,0	8618,4
AS40/I60/XS5	318,2	5,79	108,5	10131,3
AS40/I60/XM5	315,9	5,32	106,8	6727,5
AS40/I60/XSM5	318,8	5,34	111,5	6872,1

[1] temperatūra, esant 10 % masės nuostoliams, nustatyta iš TGA kreivių;

[2] medžiagos likutis TGA tyrimo pabaigoje;

[3] stiklėjimo temperatūra, nustatyta iš DMTA *tanδ* kreivių;

[4] tinklo tankis, apskaičiuotas iš DMTA *E'* kreivių.

TGA tyrimas parodė, kad užpildas pagerino fototinklintų AESO polimerų kompozitų terminį stabilumą. Nustatyta, kad į kompozicijas įdėjus bent 3 % X užpildo, AESO polimerų kompozitų $T_{dec-10\%}$ padidėja nuo 308,5 °C kompozito AS60/I40/0 iki 320,2 °C kompozito AS30/I40/X5 (9 lentelė). Pastebėta, kad užpildai mažina kompozitų T_g, nustatytą dinaminės mechaninės terminės analizės metodu (DMTA). Nors įkomponavus užpildus T_g sumažėjo AS40/I60 serijoje, tačiau padidėjo kompozitų v_e, rodantis tvirtesnį polimerinį tinklą kartu su užpildo dalelėmis. Lyginant modifikuotus užpildus XM ir XSM, buvo pastebėta, kad kompozitas AS40/I60/XSM5 įgijo didesnes $T_{dec-10\%}$, T_g ir v_e vertes nei AS40/I60/XM5. Galima teigti, kad XSM užpildas, gautas iš aliuminio fluorido gamybos atliekų, pasižymėjo geresne sąveika su polimeriniu tinklu, todėl pagerėjo kompozitų terminės savybės.

Teflono formoje paruoštų ir 3D spausdintų fototinklintų AESO polimerų kompozitų mechaninės savybės buvo tirtos atliekant tempimo bandymą. Kompozitų tempimo įtempio ir deformacijos kreivės pateiktos 10 paveiksle.
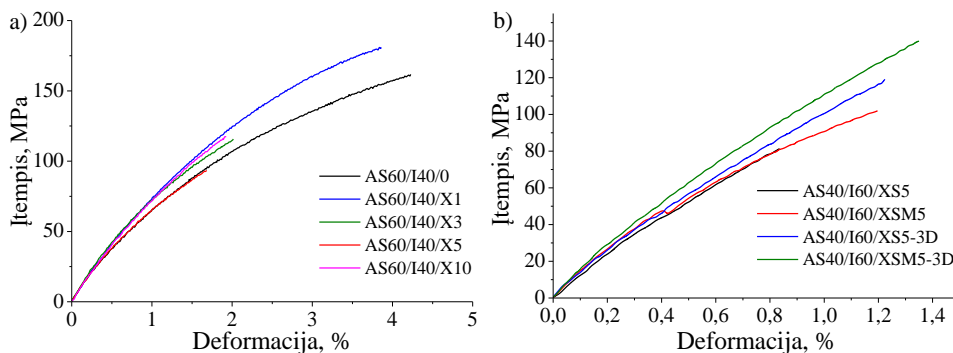
10 pav. Kompozitų AS60/I40/X0-10 tempimo įtempio ir deformacijos kreivės (a); kompozitų AS40/I60/XS ir AS40/I60/XSM, paruoštų teflono formoje ir 3D spausdintų, tempimo įtempio-deformacijos kreivės (b)

Nustatyta, kad, didinant inertinio X užpildo kiekį, dėl didėjančio bandinio trapumo mažėja kompozitų σ ir ε vertės (10 pav., a). Fototinklintų AESO polimerų kompozitai su užpildu iš aliuminio fluorido gamybos atliekų pasižymėjo aukštomis σ ir ε vertėmis, rodančiomis stiprią tarpfazinę sąveiką tarp užpildo ir polimerinio tinklo (10 pav., b). Nustatytos gerokai didesnės 3D spausdintų kompozitų AS40/I60/XS5 ir

AS40/I60/XSM5 σ ir ε vertės parodė tvirtą adheziją tarp spausdintų sluoksnių ir geresnį polimerinio tinklo elastingumą.

Dervos su XS ir XSM užpildais buvo sėkmingai pritaikytos DLP 3D spausdinimui. Tikslios architektūros spausdinti objektai pasižymėjo dideliu smulkių detalių tikslumu ir lygiu paviršiumi (11 pav., a), o tai rodo, kad sukurtos gamtinės kilmės dervos tinkamos DLP 3D spausdinimui. Po 3D spausdinimo proceso nuplovus nesureagavusios dervos perteklių, buvo nustatytas pastebimas kompozitų paviršiaus baltumas dėl atsidengusio didesnio kiekio polimere įkapsuliuotų užpildo dalelių. Kompozito AS40/I60/XSM5 SEM nuotraukose (11 pav., b) su pastebimais tobermorito ir katoito dariniais matyti AESO polimero tinklo ir užpildo dalelių sąveika paviršiuje.
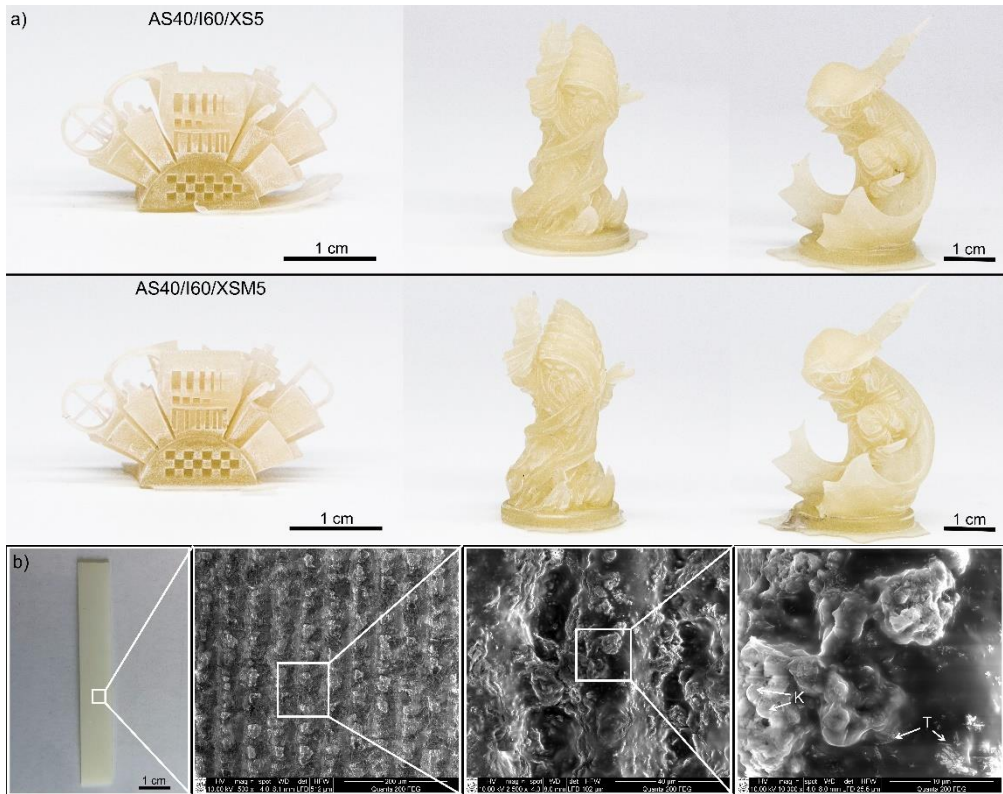
11 pav. DLP 3D spausdinti AS40/I60/XS5 kompozito (viršuje) ir AS40/I60/XSM5 kompozito (apačioje) objektai (a); DLP 3D spausdinto AS40/I60/XSM5 kompozito SEM nuotraukos (b)

AESO polimerų kompozitų bioskaidumas buvo nustatytas matuojant deguonies suvartojimą uždarame respirometre vandeninėje terpėje. Fototinklintų polimerų kompozitų bioskaidumas po 60 dienų buvo 0,7–19,6 %, o celiuliozės, naudotos palyginimui, bioskaidumas po to paties laiko siekė 54,4 % (12 pav.).
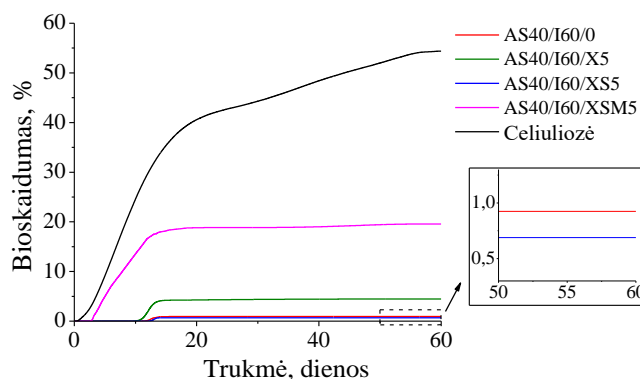
12 pav. AESO polimerų kompozitų ir celiuliozės bioskaidumo kinetikos kreivės

Kompozitas AS40/I30/XSM5 su modifikuotu užpildu, gautu iš aliuminio fluorido gamybos atliekų, pasižymėjo didžiausiu bioskaidumu – 19,6 %. Kompozito AS40/I30/XSM5 tinklo tankis buvo mažesnis nei kompozito AS40/I30/XS5, dėl to mikroorganizmai galėjo lengviau patekti į kompozitų vidų, kas lėmė ir didesnį bioskaidumą [64]. Dėl pastebimai didesnio kompozito AS40/I60/XSM5 bioskaidumo ir geresnių kompozito savybių, tokių kaip Jungo modulis tempiant, tempiamasis stipris, terminis stabilumas ir stiklėjimo temperatūra, šis kompozitas tampa tvaria ir konkurencinga komercinių iš naftos produktų gautų produktų alternatyva DLP 3D spausdinimui.

5. IŠVADOS

1. Akrilinto epoksidinto sojų aliejaus ir kitų gamtinės kilmės komonomerų tinklinius polimerus galima gauti fotopolimerizacijos būdu. Buvo nustatyta, kad:
   a. didesnis mirseno kiekis kompozicijose sulėtino fotopolimerizaciją ir susidarė iki 43 % mažesnis tinklinio polimero netirpios frakcijos kiekis, o tai lėmė 20 kartų mažesnes polimerų gniuždymo modulio vertes;
   b. keičiant sintetinį divinilbenzeną gamtinės kilmės vanilino dimetakrilatu, gauti polimerai, turintys iki 8 % didesnį tinklinio polimero netirpios frakcijos kiekį ir daugiau nei dvigubai didesnes gniuždymo modulio vertes;
   c. fototinklinių polimerų, sudarytų tik iš gamtinės kilmės monomerų, gelio taško, šlyties tampros modulio ir gniuždymo modulio vertės buvo panašios, palyginti su iš komercinių dervų gautais polimerais, todėl potencialiai gali būti pritaikyti optiniam 3D spausdinimui.

2. Akrilinto epoksidinto sojų aliejaus polimerus galima fototinklinti nenaudojant fotoiniciatoriaus ir pritaikyti tiesioginio lazerinio rašymo technologijoje. Atlikus tyrimus nustatyta, kad:
   a. akrilintas epoksidintas sojų aliejus suformavo kietus tinklinius polimerus, nenaudojant jokio fotoiniciatoriaus ir tirpiklio;
   b. vanilino dimetakrilatas dvigubai pailgino akrilinto epoksidinto sojų aliejaus dervų fotopolimerizacijos trukmę ir susidarė iki 57 % mažesnis tinklinio polimero kiekis, kas lėmė mažesnį gautų polimerų terminį stabilumą ir iki 3 kartų mažesnes gniuždymo modulio vertes;
   c. tiesioginio lazerinio rašymo technologija atspausdinti akrilinto epoksidinto sojų aliejaus polimero objektai buvo stabilūs ir išlaikė savo struktūrą.

3. Fotoiniciatoriaus ir temperatūros turi įtakos akrilinto epoksidinto sojų aliejaus fotopolimerazijos kinetikai ir gautų polimerų savybėms. Buvo patvirtinta, kad:
   a. esant aukštesnei temperatūrai, akrilinto epoksidinto sojų aliejaus tinklinis polimeras formuojasi greičiau;
   b. dėl didesnio fotoiniciatoriaus kiekio susiformavo stangresnis ir trapesnis polimeras, kurio santykinė ištįsa trūkio metu sumažėjo iki 3 kartų;
   c. etil(2,4,6-trimetilbenzoil)fenilfosfinatas yra tinkamiausias fotoiniciatorius ir 3 mol % yra optimali koncentracija akrilinto epoksidinto sojų aliejui fototinklinti.

4. Tinklinius gamtinės kilmės akrilinto epokidinto sojų aliejaus polimerus su keturiais gamtinės kilmės reaktyviaisiais tirpikliais galima gauti fotopolimerizacijos būdu ir pritaikyti skaitmeniniam 3D spausdinimui naudojant šviesą. Nustatyta, kad:

    a. keičiant gamtinės kilmės reaktyviuosius tirpiklius (izobornilmetakrilatą, metakrilesterį, tetrahidrofurfurilakrilatą ar tetrahidrofurfurilmetakrilatą), galima gauti mechaninėmis ir terminėmis savybėmis besiskiriančius akrilinto epoksidinto sojų aliejaus tinklinius polimerus;

    b. gamtinės kilmės polimerų bioskilimas buvo lėtesnis už celiuliozės tomis pačiomis eksperimento sąlygomis ir po 60 dienų siekė iki 7,5 %;

    c. akrilinto epoksidinto sojų aliejaus ir izobornilmetakrilato polimerų, atspausdintų skaitmeniniu 3D spausdintuvu, naudojančiu šviesą, parametrai: Jungo modulis tempiant 4,75 GPa, stipris tempiant 250,4 MPa, santykinė ištįsa trūkio metu 8,5 %, buvopanašūs į polimerų bandinių, atspausdintų iš komercinės dervos *Monocure3D Rapid Gray*, skirtos skaitmeniniam 3D spausdinimui naudojant šviesą, parametrus.

5. Kalcio hidrosilikato užpildai turi įtaką tinkliniams akrilinto epoksidinto sojų aliejaus polimeriniams kompozitams, kurie gali būti pritaikyti skaitmeniniam 3D spausdinimui naudojant šviesą. Buvo nustatyta, kad:

    a. didesnis inertinio užpildo kiekis lėmė 800 MPa mažesnes šlyties tampros modulio vertes 30 °C temperatūroje, žemesnę stiklėjimo temperatūrą nuo 99 °C iki 89 °C, 80 MPa mažesnį tempiamąjį stiprį ir ištįsą trūkio metu nuo 4,7 % iki 1,6 %, tačiau pagerino polimerų kompozitų terminį stabilumą 12 °C temperatūroje;

    b. gauti geresni šie kompozitų su akriloksipropiltrimetoksisilanu modifikuotu užpildu, gautu iš kalcio oksido ir aliuminio fluorido gamybos atliekų, parametrai: Jungo modulis tempiant 10,7 GPa, tempiamasis stipris 97,4 MPa, santykinės ištįsa trūkio metu 1,2 %, terminis stabilumas 318,8 °C, esant 10 % masės nuostoliams, ir stiklėjimo temperatūra 111,5 °C;

    c. akrilinto epoksidinto sojų aliejaus polimerų kompozitai su akriloksipropiltrimetoksisilanu modifikuotu užpildu, gautu iš kalcio oksido ir aliuminio fluorido gamybos atliekų, atspausdinti skaitmeniniu 3D spausdintuvu naudojant šviesą, buvo itin tikslūs bei detalūs, pasižymėjo nustatyta stipria adhezija tarp spausdintų sluoksnių, o jų bioskaidumas po 60 dienų siekė 19,6 %.

6. REFERENCES

1. PENG, X., et al. Integrating Digital Light Processing with Direct Ink Writing for Hybrid 3D Printing of Functional Structures and Devices. *Additive Manufacturing*, 2021, vol. 40. pp. 101911.
2. BHAGIA, S., et al. Critical Review of FDM 3D Printing of PLA Biocomposites Filled with Biomass Resources, Characterization, Biodegradability, Upcycling and Opportunities for Biorefineries. *Applied Materials Today*, 2021, vol. 24. pp. 101078.
3. DELLA BONA, A., et al. 3D Printing Restorative Materials using a Stereolithographic Technique: A Systematic Review. *Dental Materials*, 2021.
4. KAFLE, A., et al. 3D/4D Printing of Polymers: Fused Deposition Modelling (FDM), Selective Laser Sintering (SLS), and Stereolithography (SLA). *Polymers*, 2021, vol. 13, no. 18. pp. 3101.
5. GUIT, J., et al. Photopolymer Resins with Biobased Methacrylates Based on Soybean Oil for Stereolithography. *ACS Applied Polymer Materials*, 2020, vol. 2, no. 2. pp. 949-957.
6. ZHANG, Y., XU, Y., SIMON-MASSERON, A. and LALEVÉE, J. Radical Photoinitiation with LEDs and Applications in the 3D Printing of Composites. *Chemical Society Reviews*, 2021.
7. YANG, X., et al. Highly Transparent Acrylate Epoxidized Soybean Oil Based UV–curable Silicone–modified Coatings with Good Thermal Stability and Flame Retardancy. *Progress in Organic Coatings*, 2022, vol. 165. pp. 106769.
8. RAJAN, R., et al. Life Cycle Assessment, Optical 3D Printing of Dental Models using Acrylic Resin Based on Soybean Oils, 2022.
9. SACHYANI KENETH, E., et al. 3D Printing Materials for Soft Robotics. *Advanced Materials*, 2021, vol. 33, no. 19. pp. 2003387.
10. ZHAO, J., LI, Q., JIN, F. and HE, N. Digital Light Processing 3D Printing Kevlar Composites Based on Dual Curing Resin. *Additive Manufacturing*, 2021, vol. 41. pp. 101962.
11. MILLES, S., SOLDERA, M., KUNTZE, T. and LASAGNI, A.F. Characterization of Self-Cleaning Properties on Superhydrophobic Aluminum Surfaces Fabricated by Direct Laser Writing and Direct Laser Interference Patterning. *Applied Surface Science*, 2020, vol. 525. pp. 146518.
12. SKLIUTAS, E., et al. Polymerization Mechanisms Initiated by Spatio-Temporally Confined Light. *Nanophotonics*, 2021.
13. YANG, L., et al. The Fabrication of Micro/Nano Structures by Laser Machining. *Nanomaterials*, 2019, vol. 9, no. 12. pp. 1789.
14. WALLER, E.H., et al. Functional Metallic Microcomponents Via Liquid-Phase Multiphoton Direct Laser Writing: A Review. *Micromachines*, 2019, vol. 10, no. 12. pp. 827.
15. PAGAC, M., et al. A Review of Vat Photopolymerization Technology: Materials, Applications, Challenges, and Future Trends of 3d Printing. *Polymers*, 2021, vol. 13, no. 4. pp. 598.
16. SEET, K.K., et al. Three-dimensional Spiral-architecture Photonic Crystals obtained by Direct Laser Writing. *Advanced Materials*, 2005, vol. 17, no. 5. pp. 541-545.
17. MONDSCHEIN, R.J., et al. Polymer Structure-Property Requirements for Stereolithographic 3D Printing of Soft Tissue Engineering Scaffolds. *Biomaterials*, 2017, vol. 140. pp. 170-188.

18. JI, Z., et al. 3D Printing of Photocuring Elastomers with Excellent Mechanical Strength and Resilience. *Macromolecular Rapid Communications*, 2019, vol. 40, no. 8. pp. 1800873.

19. DU, K., et al. Digital Light Processing 3D Printing of PDMS-Based Soft and Elastic Materials with Tunable Mechanical Properties. *ACS Applied Polymer Materials*, 2021.

20. PATEL, D.K., et al. Highly Stretchable and UV Curable Elastomers for Digital Light Processing Based 3D Printing. *Advanced Materials*, 2017, vol. 29, no. 15. pp. 1606000.

21. BAGHERI, A. and JIN, J. Photopolymerization in 3D Printing. *ACS Applied Polymer Materials*, 2019, vol. 1, no. 4. pp. 593-611.

22. ZHANG, J. and XIAO, P. 3D Printing of Photopolymers. *Polymer Chemistry*, 2018, vol. 9, no. 13. pp. 1530-1540.

23. MATURI, M., et al. Phosphorescent Bio-Based Resin for Digital Light Processing (DLP) 3D-Printing. *Green Chemistry*, 2020, vol. 22, no. 18. pp. 6212-6224.

24. LI, Y., et al. Theoretical Prediction and Experimental Validation of the Digital Light Processing (DLP) Working Curve for Photocurable Materials. *Additive Manufacturing*, 2020. pp. 101716.

25. KRISHNAMOORTHY, S., et al. Investigation of Gelatin Methacrylate Working Curves in Dynamic Optical Projection Stereolithography of Vascular-Like Constructs. *European Polymer Journal*, 2020, vol. 124. pp. 109487.

26. DING, R., et al. Sustainable Near UV-Curable Acrylates Based on Natural Phenolics for Stereolithography 3D Printing. *Polymer Chemistry*, 2019, vol. 10, no. 9. pp. 1067-1077.

27. BASSETT, A.W., et al. Vanillin-Based Resin for Additive Manufacturing. *ACS Sustainable Chemistry & Engineering*, 2020, vol. 8, no. 14. pp. 5626-5635.

28. SUTTON, J.T., RAJAN, K., HARPER, D.P. and CHMELY, S.C. Lignin-Containing Photoactive Resins for 3D Printing by Stereolithography. *ACS Applied Materials & Interfaces*, 2018, vol. 10, no. 42. pp. 36456-36463.

29. NOÈ, C., et al. Light Processable Starch Hydrogels. *Polymers*, 2020, vol. 12, no. 6. pp. 1359.

30. ROPPOLO, I. and CHIAPPONE, A. 3D Printing with LightDe Gruyter, 2021 *Functional Dyes in Light-Induced 3D Printing*, pp. 107-134.

31. VOET, V.S., GUIT, J. and LOOS, K. Sustainable Photopolymers in 3d Printing: A Review on Biobased, Biodegradable, and Recyclable Alternatives. *Macromolecular Rapid Communications*, 2021, vol. 42, no. 3. pp. 2000475.

32. HUBMANN, M., VON GUNTEN, K., ALESSI, D.S. and CURTIS, J.M. Epoxidized Linseed Lipids as a Durable and Fast-Curing Alternative to Drying Oils. *Progress in Organic Coatings*, 2021, vol. 159. pp. 106406.

33. DING, L., et al. Preparation of the Flexible Soybean Oil-based Material Via [2 2] Cycloaddition Photo-polymerization. *Journal of Applied Polymer Science*, 2021, vol. 138, no. 9. pp. 49925.

34. ZYCH, A., et al. Biobased, Biodegradable, Self-Healing Boronic Ester Vitrimers from Epoxidized Soybean Oil Acrylate. *ACS Applied Polymer Materials*, 2020, vol. 3, no. 2. pp. 1135-1144.

35. BEN CHEIKH, F., et al. Honeycomb Organization of Chitin Nanocrystals (ChNCs) in Nanocomposite Films of UV-Cured Waterborne Acrylated Epoxidized Soybean Oil Emulsified with ChNCs. *Biomacromolecules*, 2021.

36. TANG, Q., et al. Development of an Innovative Biobased UV Coating Synthesized from Acrylated Epoxidized Soybean Oil and Poly (Octamethylene Maleate

(Anhydride) Citrate). *Industrial & Engineering Chemistry Research*, 2021, vol. 60, no. 27. pp. 9797-9806.

37. MIAO, S., et al. 4D Printing Smart Biomedical Scaffolds with Novel Soybean Oil Epoxidized Acrylate. *Scientific Reports*, 2016, vol. 6. pp. 27226.

38. MIAO, S., et al. Stereolithographic 4D Bioprinting of Multiresponsive Architectures for Neural Engineering. *Advanced Biosystems*, 2018, vol. 2, no. 9. pp. 1800101.

39. MIAO, S., et al. Photolithographic-Stereolithographic-Tandem Fabrication of 4D Smart Scaffolds for Improved Stem Cell Cardiomyogenic Differentiation. *Biofabrication*, 2018, vol. 10, no. 3. pp. 035007.

40. WU, B., et al. Direct Conversion of McDonald's Waste Cooking Oil into a Biodegradable High Resolution 3D Printing Resin. *ACS Sustainable Chemistry & Engineering*, 2019.

41. ROSACE, G., PALUCCI ROSA, R., ARRIGO, R. and MALUCELLI, G. Photosensitive Acrylates Containing Bio-based Epoxy-acrylate Soybean Oil for 3D Printing Application. *Journal of Applied Polymer Science*, 2021, vol. 138, no. 44. pp. 51292.

42. HU, Y., et al. Bio-Based Reactive Diluent Derived from Cardanol and its Application in Polyurethane Acrylate (PUA) Coatings with High Performance. *Journal of Coatings Technology and Research*, 2019, vol. 16, no. 2. pp. 499-509.

43. SKLIUTAS, E., et al. A Bio-Based Resin for a Multi-Scale Optical 3d Printing. *Scientific Reports*, 2020, vol. 10, no. 1. pp. 1-9.

44. BARKANE, A., PLATNIEKS, O., JURINOVS, M. and GAIDUKOVS, S. Thermal Stability of UV-Cured Vegetable Oil Epoxidized Acrylate-Based Polymer System for 3D Printing Application. *Polymer Degradation and Stability*, 2020, vol. 181. pp. 109347.

45. BARKANE, A., et al. UV-Light Curing of 3D Printing Inks from Vegetable Oils for Stereolithography. *Polymers*, 2021, vol. 13, no. 8. pp. 1195.

46. VOET, V.S., et al. Biobased Acrylate Photocurable Resin Formulation for Stereolithography 3D Printing. *ACS Omega*, 2018, vol. 3, no. 2. pp. 1403-1408.

47. VOET, V.S., et al. Stereolithographic 3D Printing with Renewable Acrylates. *JoVE (Journal of Visualized Experiments)*, 2018, no. 139. pp. e58177.

48. WANG, X., et al. 3D Printing of Polymer Matrix Composites: A Review and Prospective. *Composites Part B: Engineering*, 2017, vol. 110. pp. 442-458.

49. MONDAL, D., et al. Acrylated Epoxidized Soybean Oil/Hydroxyapatite-Based Nanocomposite Scaffolds Prepared by Additive Manufacturing for Bone Tissue Engineering. *Materials Science and Engineering: C*, 2021, vol. 118. pp. 111400.

50. LIU, Z., et al. 3D Printing Acrylated Epoxidized Soybean Oil Reinforced with Functionalized Cellulose by UV Curing. *Journal of Applied Polymer Science*, 2021. pp. 51561.

51. LEBEDEVAITE, M., OSTRAUSKAITE, J., SKLIUTAS, E. and MALINAUSKAS, M. Photocross-linked Polymers Based on Plant-derived Monomers for Potential Application in Optical 3D Printing. *Journal of Applied Polymer Science*, 2020, vol. 137, no. 20. pp. 48708.

52. LEBEDEVAITE, M., OSTRAUSKAITE, J., SKLIUTAS, E. and MALINAUSKAS, M. Photoinitiator Free Resins Composed of Plant-Derived Monomers for the Optical M-3d Printing of Thermosets. *Polymers*, 2019, vol. 11, no. 1. pp. 116.

53. PARKATZIDIS, K., et al. Initiator-Free, Multiphoton Polymerization of Gelatin Methacrylamide. *Macromolecular Materials and Engineering*, 2018, vol. 303, no. 12. pp. 1800458.

54. LEBEDEVAITE, M. and OSTRAUSKAITE, J. Influence of Photoinitiator and Temperature on Photocross-Linking Kinetics of Acrylated Epoxidized Soybean Oil and Properties of the Resulting Polymers. *Industrial Crops and Products*, 2021, vol. 161. pp. 113210.

55. DING, R., et al. Sustainable Near UV-Curable Acrylates Based on Natural Phenolics for Stereolithography 3D Printing. *Polymer Chemistry*, 2019, vol. 10, no. 9. pp. 1067-1077.

56. ZHANG, C., et al. Photopolymerizable Thiol-Acrylate Maleiated Hyaluronic Acid/Thiol-Terminated Poly (Ethylene Glycol) Hydrogels as Potential in-Situ Formable Scaffolds. *International Journal of Biological Macromolecules*, 2018, vol. 119. pp. 270-277.

57. JIANG, L., et al. Performance Comparison of Acrylic and Thiol-Acrylic Resins in Two-Photon Polymerization. *Optics Express*, 2016, vol. 24, no. 12. pp. 13687-13701.

58. LEBEDEVAITE, M., TALACKA, V. and OSTRAUSKAITE, J. High Biorenewable Content Acrylate Photocurable Resins for DLP 3D Printing. *Journal of Applied Polymer Science*, 2021, vol. 138, no. 16. pp. 50233.

59. PUGH, R.J. and BERGSTROM, L. *Surface and Colloid Chemistry in Advanced Ceramics Processing.* CRC Press, 2017.

60. HE, Y., YAO, M. and NIE, J. Protective CoatingsSpringer, 2017 *Shrinkage in UV-Curable Coatings*, pp. 195-223 ISBN 978-3-319-51625-7.

61. JAILLET, F., et al. Synthesis and Characterization of Novel Vinylester Prepolymers from Cardanol. *European Journal of Lipid Science and Technology*, 2014, vol. 116, no. 7. pp. 928-939.

62. LEBEDEVAITE, M., et al. Development and Optical 3D Printing of Acrylated Epoxidized Soybean Oil-Based Composites with Functionalized Calcium Silicate Hydrate Filler Derived from Aluminium Fluoride Production Waste. *Composites Part A: Applied Science and Manufacturing*, 2022. pp. 106929.

63. GINEIKA, A., DAMBRAUSKAS, T. and BALTAKYS, K. Synthesis and Characterisation of Wollastonite with Aluminium and Fluoride Ions. *Ceramics International*, 2021, vol. 47, no. 16. pp. 22900-22910.

64. CALABIA, B.P., et al. Biodegradable Poly (Butylene Succinate) Composites Reinforced by Cotton Fiber with Silane Coupling Agent. *Polymers*, 2013, vol. 5, no. 1. pp. 128-141.

7. CURRICULUM VITAE

Personal information

Name, Surname	Miglė Žamoit
Date of Birth	September 20, 1993
Nationality	Lithuanian
email	migle.zamoit@gmail.com

Education

2018 – 2022	Kaunas University of technology PhD studies, Chemical Engineering
2016 – 2018	Kaunas University of technology Master of Chemical Engineering
2012 – 2016	Kaunas University of Technology Bachelor of Chemistry
2004 – 2012	Panevėžys gymnasium No. 5 Secondary school

Work experience

2021.12 – till now	JSC "VEIKA" Researcher
2019.04 – 2021.10	Kaunas University of Technology Junior researcher
2017.06 – 2019.04	Kaunas University of Technology Laboratory technician
2016.06 – 2018.12	JSC "Baltic NanoTechnologies" Chemical technologist

Scientific work

2020.10 – 2020.12	Project "SLA 3D printing and commercialisation of photopolymeric materials with antistatic effect" funded by the Agency for Science, Innovation and Technology
2020.03 – 2021.10	Project "Click dual-cured plant-derived polymers for laser 3D meso-scale structuring" (CDCmeso3D) funded by the Research Council of Lithuania
2019.04 – 2021.10	Project "Network of service providers for eco-innovations in manufacturing SMEs" (ECOLABNET), funded by European Regional Development Fund under the Interreg Baltic Sea Region Programme
2017.06 – 2018.12	Project "Optical bioplastics micro- and nanoformation", funded by Research Council of Lithuania

Languages

Lithuanian	Native speaker
English	Level C1
Russian	Level A2

Scholarships

2020 – 2022	Lithuanian Research Council PhD student scholarship for the academic achievements – 2 times
2019 – 2021	KTU most active PhD scholarship – 2 times
2017 – 2018	KTU Talent scholarship – 3 times

8. LIST OF PUBLICATIONS

List of publications on the subject of thesis:

1. <u>Lebedevaite, Migle</u>; Gineika, Andrius; Talacka, Vaidas; Baltakys, Kestutis; Ostrauskaite, Jolita. Development and optical 3D printing of acrylated epoxidized soybean oil-based composites with functionalized calcium silicate hydrate filler derived from aluminium fluoride production waste // Composites Part A: Applied science and manufacturing. Oxford : Elsevier. ISSN 1359-835X. eISSN 1878-5840. 2022, vol. 157, art. no. 106929, p. 1-12. DOI: 10.1016/j.compositesa.2022.106929. IF: 9,463

2. <u>Lebedevaite, Migle</u>; Talacka, Vaidas; Ostrauskaite, Jolita. High biorenewable content acrylate photocurable resins for DLP 3D printing // Journal of applied polymer science. Hoboken, NJ : Wiley. ISSN 0021-8995. eISSN 1097-4628. 2021, vol. 138, iss. 16, art. no. e50233, p. 1-13. DOI: 10.1002/app.50233. IF: 3,057

3. <u>Lebedevaite, Migle</u>; Ostrauskaite, Jolita. Influence of photoinitiator and temperature on photocross-linking kinetics of acrylated epoxidized soybean oil and properties of the resulting polymers // Industrial crops and products. Amsterdam : Elsevier. ISSN 0926-6690. eISSN 1872-633X. 2021, vol. 161, art. no. 113210, p. 1-8. DOI: 10.1016/j.indcrop.2020.113210. IF: 6,449

4. <u>Lebedevaite, Migle</u>; Ostrauskaite, Jolita; Skliutas, Edvinas; Malinauskas, Mangirdas. Photocross-linked polymers based on plant-derived monomers for potential application in optical 3D printing // Journal of applied polymer science. Hoboken, NJ : John Wiley & Sons. ISSN 0021-8995. eISSN 1097-4628. 2020, vol. 137, iss. 20, art. no. 48708, p. 1-8. DOI: 10.1002/app.48708. IF: 3,125

5. <u>Lebedevaite, Migle</u>; Ostrauskaite, Jolita; Skliutas, Edvinas; Malinauskas, Mangirdas. Photoinitiator free resins composed of plant-derived monomers for the optical μ-3D printing of thermosets // Polymers. Basel : MDPI. ISSN 2073-4360. 2019, vol. 11, iss. 1, art. no. 116, p. 1-14. DOI: 10.3390/polym11010116. IF: 3,426

List of other publications:

1. Rajan, Ratish; Rainosalo, Egidija; Lebedevaite, Migle; Ostrauskaite, Jolita; Talacka, Vaidas. Optical 3D printing of dental models using acrylic resin based on soybean oils: life cycle assessment. Kokkola : Centria university of applied sciences, 2022. 19 p. (Centria reports, ISSN 2814-8924 ; 1). ISBN 9789527173657

2. Goździuk, Magdalena; Kavetskyy, Taras; Roquero, Daniel Massana; Smutok, Oleh; Gonchar, Mykhailo; Královič, David P.; Švajdlenková, Helena; Šauša, Ondrej; Kalinay, Pavol; Nosrati, Hamed; <u>Lebedevaite, Migle</u>; Grauzeliene, Sigita; Ostrauskaite, Jolita; Kiv, Arnold;

Zgardzińska, Bożena. UV-cured green polymers for biosensorics: correlation of operational parameters of highly sensitive biosensors with nanovolumes and adsorption properties // Materials. Basel : MDPI. ISSN 1996-1944. 2022, vol. 15, iss. 19, art. no. 6607, p. 1-23. DOI: 10.3390/ma15196607. IF: 3,748

3. Goździuk, M.; Zgardzińska, B.; Kavetskyy, T.; Zubrytska, K.; Smutok, O.; Šauša, O.; Lebedevaite, M.; Ostrauskaite, J.; Kiv, A. Nanostructure research and amperometric testing to determine detection capabilities of biopolymer matrices based on acrylated epoxidized soybean oil // Acta physica Polonica A. Warsaw : Polish academy of sciences. ISSN 0587-4246. eISSN 1898-794X. 2021, vol. 139, iss. 4, p. 432-437. DOI: 10.12693/APhysPolA.139.432. IF: 0,725

4. Skliutas, Edvinas; Lebedevaite, Migle; Kabouraki, Elmina; Baldacchini, Tommaso; Ostrauskaite, Jolita; Vamvakaki, Maria; Farsari, Maria; Juodkazis, Saulius; Malinauskas, Mangirdas. Polymerization mechanisms initiated by spatio-temporally confined light // Nanophotonics. Berlin : De Gruyter. ISSN 2192-8606. eISSN 2192-8614. 2021, vol. 10, iss. 4, p. 1211-1242. DOI: 10.1515/nanoph-2020-0551. IF: 7,923

5. Skliutas, Edvinas; Lebedevaite, Miglė; Kasetaite, Sigita; Rekštytė, Sima; Lileikis, Saulius; Ostrauskaite, Jolita; Malinauskas, Mangirdas. A bio-based resin for a multi-scale optical 3D printing // Scientific reports. London : Nature. ISSN 2045-2322. 2020, vol. 10, art. no. 9758, p. 1-9. DOI: 10.1038/s41598-020-66618-1. IF: 4,380

List of conferences

1. Lebedevaite, Migle; Motiekaityte, Greta; Pabricaite, Ausrine; Talacka, Vaidas; Ostrauskaite, Jolita. Soybean oil-based acrylate photocurable resins for dlp 3D printing // VESPS2021: 6th virtual European symposium of photopolymer science, dedicated to Ewa Andrzejewska: online, June 15 – 17, 2021. Gumpoldskirchen : ChemIT e.U., 2021, PT-6. ISBN 9783950480931. p. 168.

2. Lebedevaitė, Miglė; Skliutas, Edvinas; Lileikis, Saulius; Malinauskas, Mangirdas; Ostrauskaitė, Jolita. Eco-innovative optical 3D printed medical fittings made of bioresins // Technorama 2021: from vision to innovation. Kaunas : KTU. 2021, p. 134-135.

3. Navaruckiene, Aukse; Lebedevaite, Migle; Ostrauskaite, Jolita. Real-time photorheometrical study of plant–derived monomer resins // IUPAC-MACRO 2020: the 48th world polymer congress, May 16-20, 2021, Jeju, Korea. [S.l.] : IUPAC. 2021, 4OS8-24, p. 491.

4. Lebedevaite, Migle; Navaruckiene, Aukse; Ostrauskaite, Jolita. Photocross-linked polymers based on plant-derived monomers for optical 3D printing // Poly-Char Venice international polymer characterization forum, April 12-14, 2021, Zoom platform: book of

abstracts. [Venezia] : [International Union of Pure and Applied Chemistry (IUPAC) Polymer Division]. 2021, 13-F-O01, p. 58.

5. Lebedevaite, Migle; Ostrauskaite, Jolita. Investigation of photocross-linking kinetics of acrylated soybean oil with different photoinitiators and properties of the resulting polymers // Open readings 2021: 64th international conference for students of physics and natural sciences, March 16-19, Vilnius, LIthuania: abstract book / editors: Š. Mickus, R. Platakytė, S. Pūkienė. Vilnius : Vilnius University Press, 2021, P6-30. ISBN 9786090705902. p. 398.

6. Lebedevaitė, Miglė; Talačka, Vaidas; Ostrauskaitė, Jolita. Bio-based resins for optical 3D printing // Technorama 2020: from vision to innovation. Kaunas : KTU. 2020, p. 54-55.

7. Lebedevaite, Migle; Ostrauskaite, Jolita. Photocross-linked bio-based polymers for potential application in optical 3D printing // CGPM 2020: First international conference on "green" polymer materials, 05-25 November 2020, online. Basel : MDPI. 2020, p. 1. DOI: 10.3390/CGPM2020-07192.

8. Klimaitis, Vidmantas; Lebedevaite, Migle; Ostrauskaite, Jolita. Synthesis and investigation of polymers composed of biobased methacrylates // Open readings 2020: 63rd international conference for students of physics and natural sciences, March 17-20, Vilnius, Lithuania: abstract book. Vilnius : Vilnius University, 2020, P2-11. ISBN 9786090703779. p. 224.

9. Lebedevaite, M.; Ostrauskaite, J.; Skliutas, E.; Malinauskas, M. Photoinitiator free resins composed of plant-derives monomers for the opticas μ-3D printing of thermosets // 6th international Baekeland symposium, October 15-18, 2019, Tarragona, Spain: book of abstracts. [Tarragona] : Universitat Rovira i Virgili. 2019, P-30, p. 153-154.

10. Lebedevaitė, M.; Ostrauskaite, J. Investigation of UV-cured acrylated epoxidized soybean oil films with different photoinitiators : poster presentation // Baltic polymer symposium 2019, Vilnius, Lithuania, September 18-20, 2019: programme and proceedings. [Vilnius] : [s.n.]. 2019, p. 67.

11. Skliutas, Edvinas; Lebedevaitė, Miglė; Ostrauskaitė, Jolita; Malinauskas, Mangirdas. Three-dimensional direct laser writing of acrylated epoxidized soybean oil // LiM 2019 : Lasers in manufacturing conference, June 20-24, 2019, Munich, Germany : programme and book of abstracts. Munich : [s.n.]. 2019, p. 73.

12. Lebedevaitė, Miglė; Skliutas, Edvinas; Ostrauskaitė, Jolita; Malinauskas, Mangirdas; Lileikis, Saulius; Matukaitis, Matas. Printing the oils – soybean oil-based resin for optical 3D printing // Technorama 2019: from vision to innovation! : [2019 m. gegužės 9 d.]: innovation catalogue. [Kaunas] : KTU. 2019, project no. 56, p. 65.

13. Navaruckiene, A.; Lebedevaite, M.; Ostrauskaite, J. Photosensitive resins composed of plant-derived monomers for optical 3d printing //

4th Green and sustainable chemistry conference, 5-8 May 2019, Dresden, Germany. [S.l.] : [s.n.]. 2019, P1.54, p. [1].

14. Lebedevaitė, Miglė; Ostrauskaitė, Jolita; Skliutas, Edvinas; Malinauskas, Mangirdas. Photoinitiator-free plant-derived resins for the optical 3D μ-printing : poster // Open readings 2019: 62nd international conference for students of physics and natural sciences, March 19-22, Vilnius, Lithuania: abstract book. Vilnius : Vilnius University, 2019, P3-30. ISBN 9786090701379. p. 306.

15. Skliutas, Edvinas; Lebedevaitė, Miglė; Ostrauskaitė, Jolita; Malinauskas, Mangirdas. Three-dimensional photostructuring of acrylated epoxidized soybean oil : poster // Open readings 2019: 62nd international conference for students of physics and natural sciences, March 19-22, Vilnius, Lithuania: abstract book. Vilnius : Vilnius University, 2019, P3-8. ISBN 9786090701379. p. 284.

16. Skliutas, Edvinas; Kašėtaitė, Sigita; Jonušauskas, Linas; Lebedevaitė, Miglė; Ostrauskaitė, Jolita; Malinauskas, Mangirdas. Photosensitive naturally derived resins toward optical 3D printing // 11th International conference on photo-excited processes and applications – ICPEPA 11, September 10-14, 2018, Vilnius, Lithuania: programme book of abstracts. Vilnius : [s.n.], 2018, P36. ISBN 9786099551159. p. 147.

17. Lebedevaite, M.; Kasetaite, S.; Ostrauskaite, J.; Skliutas, E.; Malinauskas, M. Soybean oil-based photosensitive resin for optical 3d printing // Baltic polymer symposium 2018, Jurmala, Latvia, September 12-14: programme and proceedings / organised by Institute of Polymer Materials Riga Technical University, ... [et al.]. [Riga] : [s.n.]. 2018, p. 57.

Photocross-linked polymers based on plant-derived monomers for potential application in optical 3D printing

Migle Lebedevaite,[1] Jolita Ostrauskaite ©,[1] Edvinas Skliutas,[2] Mangirdas Malinauskas[2]

[1]Department of Polymer Chemistry and Technology, Kaunas University of Technology, Radvilenu Road 19, Kaunas LT-50254, Lithuania

[2]Laser Research Center, Vilnius University, Sauletekio Avenue 10, Vilnius LT-10223, Lithuania

Correspondence to: J. Ostrauskaite (E-mail: jolita.ostrauskaite@ktu.lt)

ABSTRACT: Photocross linking of the resins composed of plant-derived monomers, acrylated epoxidized soybean oil (AESO), myrcene (MYR) and vanillin dimethacrylate (VDM) or divinylbenzene (DVB, for comparison), was performed using 2,2-dimethoxy-2-phenylacetophenone as photoinitiator. Photocross-linking rate and properties of the crosslinked polymers depended on the resin compositions. The higher amount of MYR caused not only the better homogenization and lower viscosity of the resin but also the reduction of polymerization rate and the worse mechanical and thermal properties of the resulting polymers. The higher amount of aromatic component (VDM or DVB) improved mechanical and thermal properties of polymers. Moreover, the use of VDM instead of DVB in the system led to the higher photocross-linking rate and higher yield of insoluble fraction. The resin composed of only plant-derived monomers AESO/MYR/VDM, molar ratio 1:1:3, showed characteristics comparable to those of commercial petroleum-derived photoresins and was selected as a potential renewable photoresin for application in optical 3D printing. © 2019 Wiley Periodicals, Inc. J. Appl. Polym. Sci. 2020, *137*, 48708.

INTRODUCTION

In recent years, stereolitography or optical three-dimensional (3D) printing, one of the additive manufacturing technologies, attained a lot of interest due to the high printing accuracy and speed, simplicity, and low raw material usage technology.[1] It is a photopolymerization method, where photosensitive resin is polymerized layer by layer using UV/Vis light. Synthetic acrylates are the most common choice in optical 3D printing because of their relatively low cost and high light sensitivity.[2]

Among other renewable raw materials, soybean oil is one of the most promising starting materials for polymer synthesis which could replace petroleum-derived monomers. It contains a high amount of unsaturated bonds which can be transformed into more reactive functional groups.[3] Acrylated epoxidized soybean oil (AESO), containing high amount of various functional groups such as acrylic, epoxy, and hydroxy groups, is commercially available under Ebecryl 860 trademark.[4] Usually, AESO can be crosslinked by UV/Vis light using appropriate photoinitiator and various comonomers improving solvent resistance, mechanical, and thermal properties of resulted polymers.[5–8]

Various petroleum-derived aromatic comonomers such as styrene, divinylbenzene (DVB), dicyclopentadiene acrylonitrile, and others were used to improve the poor mechanical properties of AESO polymers predetermined by fatty acid long aliphatic chains.[9,10] Vanillin dimethacrylate (VDM) or methacrylated vanillin alcohol, which can be produced from lignin, is a considerable candidate to replace petroleum-derived aromatic compounds because of its high reactivity.[11] The polymerization of pure VDM[12] and VDM with maleinated AESO[13] by thermal polymerization at 90–130 °C has been reported. However, a considerable period of time of at least 2 h was consumed to achieve the good mechanical and thermal properties of resulted polymers. Photopolymerization could be an alternative method to shorten the polymerization time of such thermosets. Photoinitiator-free photopolymerization of VDM and AESO was carried out.[14] Even though the polymerization rate was in order of minutes, the mechanical properties of obtained polymers were insufficient due to the low yield of insoluble fraction.

Reactive diluents such as petroleum-derived bi- or triacrylates were added to reduce the high viscosity (19000–31 000 cP·mPa^{-1}·s^{-1}) of AESO.[15] They not only efficiently reduced AESO viscosity but

68

also were inserted into polymer network during photopolymerization. Natural compound myrcene (MYR) could replace the petroleum-derived reactive diluents due to the very low viscosity[16] and possession of three reactive double bonds, which one is conjugated. MYR, 7-methyl-3-methylene-1,6-actadien, is a monoterpene and a significant component of the essential oils of several plants, including bay, cannabis, ylang-ylang, mango, wild thyme, parsley, cardamom, and hops.[17]

In this study, the resins composed of commercially available AESO, DVB, and MYR were photocross linked in various ratios, and plant-derived VDM was used as a replacement of DVB (Figure 1). The investigation of photocross-linking kinetics of the resins composed of aforementioned monomers was carried out by the real-time photorheometry for the first time. The dependency of photocross-linking rate and properties of the crosslinked polymers on the resin compositions was determined. The resin composed of only plant-derived monomers, AESO, MYR, and VDM, molar ratio 1:1:3, showed characteristics comparable to those of commercial petroleum-derived photoresins Autodesk Clear PR48 and Formlabs Clear FLGPCL02 and was selected as a potential renewable photoresin for application in optical 3D printing.

EXPERIMENTAL

Materials
AESO (an average number of acryloyl groups per molecule calculated from ^{1}H-NMR spectrum is 2.7 and 0.3 of epoxy groups), MYR, DVB, and 2,2-dimethoxy-2-phenylacetophenone (DMPA) were purchased from Sigma-Aldrich. Chloroform was purchased from Chempur. VDM was purchased from Specific Polymers. Commercial photosensitive resins Autodesk Clear PR48 (PR48) and Formlabs Clear FLGPCL02 (FLGPCL02) were purchased from original supplier. All materials were used without further purification.

Preparation of Crosslinked Polymers
Curing formulations were prepared by mixing adequate amounts (see Table I) of AESO, MYR, and aromatic compound (DVB or VDM) at 40 °C temperature with magnetic stirrer. 3 mol% of photoinitiator DMPA was added. Prepared resins were poured

Table I. Compositions of Photoresins

Resin	AESO (mol)	MYR (mol)	DVB (mol)	VDM (mol)
C0	1	1	-	-
C1	1	1	1	-
C2	1	3	1	-
C3	1	5	1	-
C4	1	1	-	1
C5	1	3	-	1
C6	1	5	-	1
C7	1	1	3	-
C8	1	1	5	-
C9	1	1	-	3
C10	1	1	-	5

into a tablet-shaped (ø 15 mm, h 3 mm) Teflon mold and irradiated with Helios Italquartz, model GR.E 500 W lamp, wavelength range was (250–450) nm, intensity was 310 mW·cm^{-2} at the distance of 15 cm, until hard polymer tablets were formed.

Chemical Structure Analysis
Chemical structure of photocross-linked polymers was confirmed by Fourier transform infrared (FTIR) spectroscopy with Perkin Elmer Spectrum BX II FTIR spectrometer. The spectra were acquired from 10 scans. The range of wavenumber was 400–4000 cm^{-1}.

Soxhlet Extraction
The amount of insoluble polymer fraction was determined by Soxhlet extraction. Samples of prepared polymers were wrapped into a filter package and put in a Soxhlet apparatus. Extraction was performed with chloroform for 24 h. Extracted polymer specimens were dried under vacuum to constant weight. The amount of insoluble fraction was calculated as the difference of the sample weight before and after extraction.
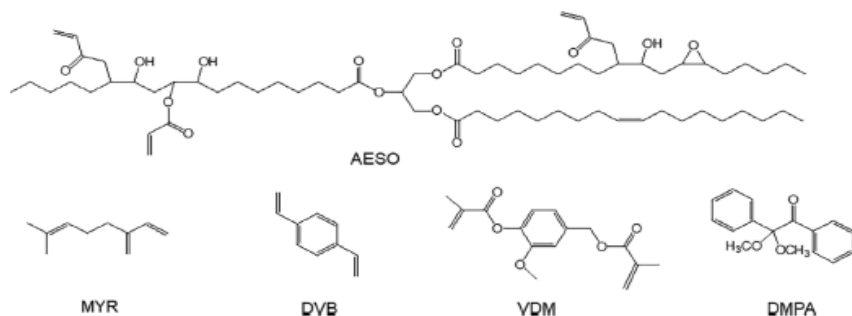

Figure 1. Chemical structure of acrylated epoxidized soybean oil (AESO), myrcene (MYR), divinylbenzene (DVB), vanillin dimethacrylate (VDM), and 2,2-dimethoxy-2-phenylacetophenone.

69

Kinetics of Photocross Linking

The investigation of photocross-linking kinetics was carried out with MCR302 rheometer from Anton Paar equipped with plate/plate measuring system. Peltier-controlled temperature chamber with the top plate PP08 (diameter of 8 mm) and the glass plate (diameter of 38 mm) was used. Measuring gap was set to 0.3 mm. The samples were irradiated at ambient temperature by UV/Vis radiation in a wavelength range of 250–450 nm through the glass plate of the temperature chamber using UV/Vis spot curing system OmniCure S2000, Lumen Dynamics Group Inc. Irradiation intensity was 9.3 W cm^{-2} (high pressure 200 W mercury vapor short arc). Shear mode with the frequency of 10 Hz and strain of 0.3% was used. Storage modulus G', loss modulus G'', loss factor tanδ (tan$\delta = G''/G'$), and complex viscosity $\eta*$ were recorded as a function of irradiation time. The mean values of two to five samples of each resin were calculated. The onset of UV/VIS irradiation was at 60 s after experiment start for all samples.

Crosslinking density was calculated according to the theory of rubber elasticity using the following equation:

$$G' = \nu RT \qquad (1)$$

where ν is a crosslinking density (mol·m^{-3}); G' is the steady-state value of storage modulus taken from the real-time photoreometry measurement curve after 1200 s (Pa); R is the universal gas constant (8.314 J·mol^{-1}·K^{-1}); and T is the temperature (K).[18]

Differential Scanning Calorimetry

Glass transition temperature (T_g) of the photocross-linked polymers was estimated by differential scanning calorimetry (DSC). The measurements were performed on a Perkin Elmer DSC 8500 apparatus with heating–cooling–heating rate of 10 °C·min^{-1} under nitrogen atmosphere (nitrogen flow rate 50 mL·min^{-1}). The T_g value was taken as the middle point in the heat capacity step of the glass transition.

Thermogravimetric Analysis

Thermogravimetric analysis (TGA) measurements of prepared polymers were performed on a Perkin Elmer TGA 4000 apparatus in the temperature range from room temperature to 800 °C at a heating rate of 20 °C·min^{-1} under nitrogen atmosphere (nitrogen flow rate 100 mL·min^{-1}).

Mechanical Testing

Mechanical properties of the photocross-linked polymer tablets were estimated by compression test on a BDO-FB0.5TH (Zwick/Roell) testing machine at room temperature. The crosslinked polymer specimen of 15 mm diameter and 3 mm thickness was placed in a Teflon mold of the same size in order to avoid the expansion of the specimen to the sides during the test. A cylindrical steel rod with a flat end of 8 mm diameter was pressed to the polymer specimen. The speed of the rod movement was 5 mm·min^{-1}. The specimen pressure was stopped when the upper force limit of 100 N was reached. The compressive modulus was calculated by the following equation:

$$E_c = \frac{F l_0}{S \Delta l} \qquad (2)$$

where E_c is a compressive modulus (N·mm^{-2}); F is a force (N); S is a surface area of the specimen that interacts with the steel rod flat end (mm^2); l_0 is an initial thickness of specimen (mm); and Δl is the difference of an initial thickness of specimen and the thickness of a loaded specimen (mm).

The mean values of 10 samples of each resin were calculated. Results with variation below 5% within group were taken.

RESULTS AND DISCUSSION

Real-Time Photorheometry

In this study, AESO was used as the main component which is easily UV/Vis-curable, plant-derived, and biodegradable material.[19] Synthetic, cheap, and effective crosslinking agent DVB[20] was used to improve mechanical properties of the polymer. As an alternative for DVB, plant-derived bifunctional VDM was used.[21] MYR was used to control mixture viscosity and dissolve solid components. Due to three double bonds, MYR acts as a reactive diluent which connects into polymer network.[22]

DMPA was used as photoinitiator. It absorbs full range of UV light and decomposes according to Norrish I mechanism. DMPA molecule generates two reactive free radicals which initiate radical polymerization.[23] It was determined earlier, that 3 mol% was an optimum concentration of DMPA to initiate the photopolymerization of acrylates.[24]

Ten different resins C1–C10 (Table I) were designed to investigate the influence of their composition to the reaction rate and properties of the resulting polymers. The resin without aromatic component (C0) and two commercially available resins PR48 and FLGPCL02 were investigated for comparison.

The kinetics of photocross linking of the resins C0–C10 was monitored by the real-time photorheometry. In photorheometry test, the photosensitive resin values of storage modulus G', loss modulus G'', loss factor tanδ, and complex viscosity $\eta*$ were measured. During the UV/Vis irradiation of the resins, the values of G', G'', and $\eta*$ started to rise indicating the formation of 3D polymer network. The viscous liquid transformed into a hard, elastic polymer when the value of G' increased faster and exceeded the values of G''. At the gel point (t_{gd}) (when $G' = G''$) loss factor tanδ, defined as G''/G', started to decrease,[25] then values of G' and G'' increased continuously until the final degree of crosslinking was reached.[26,27] As an example, the dependencies of G', G'', tanδ, and $\eta*$ on irradiation time of the resin C9 are presented in Figure 2.

The values of G', G'', $\eta*$, and t_{gel} of the resins C0–C10, PR48, and FLGPCL02 are presented in Table II. It was determined that all components of photopolymerizable compositions have an impact to the kinetics of photocross linking. The dependence of the photocross-linking kinetics on the amount of MYR is shown in Figure 3. It was determined that the higher amount of MYR was used in the resin, the longer induction period was observed. The induction period was determined as a period of time, when G', G'', and $\eta*$ started to increase rapidly from the onset of irradiation. Moreover, with the increment of MYR in resins, the values of G' reached their plateau much slower, what indicated
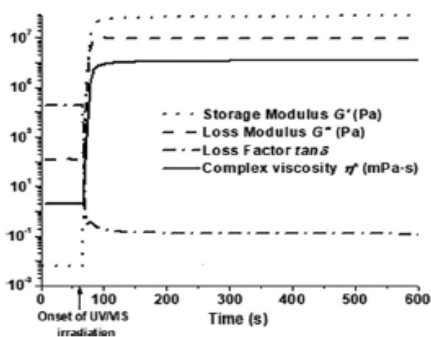
70

Figure 2. Dependencies of storage modulus G', loss modulus G'', loss factor $\tan\delta$, and complex viscosity η^* of the resin C9 on irradiation time.

the reduction of the photocross-linking rate and the sluggish formation of polymer network.[28]

The reduction of the G' values with an increase of MYR amount in resin was observed. High G' values indicated better mechanical properties of polymers determined by the high density of cross-links.[29] The polymers with the higher amount of MYR had the rarer 3D polymer network and the worse mechanical properties, thus MYR was used mostly in small amounts as comonomer to adjust elastomeric properties as a soft block.[30]

It was determined that the resins C4–C6 containing plant-derived VDM had the higher photocross-linking rate than the resins containing petroleum-derived DVB C1–C3, which was determined by the shorter induction period and t_{gel} of C4–C6. Moreover, the resins with VDM had the higher G' values than the resins with DVB which indicated better mechanical properties of the formed polymers.

Time dependencies of storage modulus G' of the resins C1, C4, and C7–C10 with different amounts of aromatic compounds are

shown in Figure 4. Aromatic component (DVB or VDM) of the resins caused the higher rigidity of the formed polymers, as it was observed comparing the maximal G' values of the resins C1, C4, and C7–C10 with aromatic compounds and that of the resin C0 without aromatic compound. C0 showed G' values lower from 2 to 5 times in comparison to other resins with aromatic compounds (Table II). Also, the addition of aromatic compound shortened the induction period and t_{gel}, but this tendency was not valid for polymers with higher amount of DVB (C7, C8). It was noticed that, when amount of DVB was increased from 1 to 5 mol, the gel time was prolonged by 67 s, but G' values were increased by 6.55×10^6 Pa (C1, C7, and C8). It confirmed that DVB was not only an effective comonomer improving mechanical properties of the polymer[31] but it also highly prolonged the photopolymerization time.

It was determined that VDM was more efficient aromatic compound comparing to DVB, because the addition of it improved t_{gel} and G' values.[13] Short gel time of the resins with VDM showed the high photosensitivity of the compound, which is one of the most important features for optical 3D printing.[32] The resin with 3 mol of VDM (C9) showed the best results of t_{gel} (12 s) and G' (7.78×10^7 Pa). The higher concentrations of photoinitiator caused the high levels of surface crosslinking which did not allow UV/Vis radiation to penetrate into the lower layers of the resin effectively and harden them properly.

The different rate of photocross linking of the resins with DVB and VDM can be explained referring to their structure. Even though both compounds are bifunctional, DVB has two vinyl groups and VDM has two methacryl groups. Lee et al.[33] investigated the conversion of acrylic and vinyl groups and determined that only after ~85% conversion of acrylate double bonds was reached, did vinyl double bonds began to react and form a highly crosslinked network. Thus, due to the high reactivity, acrylates are one of the most common materials in optical 3D printing.[34]

Time dependencies of storage modulus G' of the resins C9, PR48, and FLGPCL02 are shown in Figure 5. Since the resin C9 showed

Table II. Storage Modulus (G'), Loss Modulus (G''), and Complex Viscosity (η^*) at 1200 s and Gel Time (t_{gel}) of the Resins C0–C10, PR48, and FLGPCL02

Resin	G' (MPa)	G'' (MPa)	η^* (kPa·s)	t_{gel}[a] (s)
C0	15.52 ± 2.45	5.13 ± 2.23	2.61 ± 0.05	60 ± 1.5
C1	34.10 ± 1.25	7.97 ± 2.83	5.57 ± 3.81	35 ± 4.2
C2	3.62 ± 1.25	1.02 ± 0.63	0.60 ± 0.01	323 ± 8.7
C3	0.14 ± 0.07	0.01 ± 0.002	0.02 ± 0.001	465 ± 11.7
C4	47.64 ± 1.25	5.58 ± 3.63	7.62 ± 2.06	18 ± 0.7
C5	30.81 ± 6.95	8.87 ± 2.86	5.09 ± 2.63	200 ± 7.9
C6	0.63 ± 0.20	0.07 ± 0.01	0.10 ± 0.02	403 ± 12.0
C7	35.61 ± 3.48	17.23 ± 1.35	5.91 ± 1.17	48 ± 1.4
C8	40.64 ± 1.95	10.93 ± 4.05	6.69 ± 5.93	102 ± 5.5
C9	77.83 ± 3.11	9.43 ± 1.02	12.51 ± 3.27	12 ± 0.0
C10	44.93 ± 6.09	17.91 ± 4.20	7.69 ± 1.59	15 ± 1.0
PR48	25.91 ± 0.99	8.37 ± 0.88	4.33 ± 0.10	13 ± 0.0
FLGPCL02	71.22 ± 3.49	10.40 ± 3.08	11.39 ± 0.53	12 ± 1.0

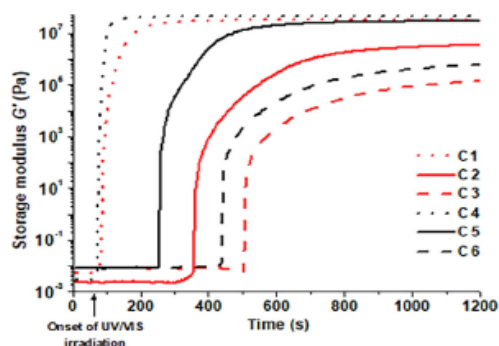[a] Gel time was calculated from the onset of UV/VIS irradiation.

71

Figure 3. Time dependencies of storage modulus G' of the resins C1–C6 with different concentrations of MYR and different aromatic compounds: VDM (black) and DVB (red). [Color figure can be viewed at wileyonlinelibrary.com]

Figure 5. Time dependencies of storage modulus G' of the resins C9, PR48, and FLGPCL02.

the best results of all newly composed resins C0–C10 (Table II), it was compared with commercial resins PR48 and FLGPCL02. The induction period of the resins C9 and PR48 was very close, 6 and 5 s, respectively. However, the commercial resin FLGPCL02 had no induction period, its photocross linking started at the same time as the UV/VIS lamp was switched on (Figure 5). All three resins C9, PR48, and FLGPCL02 had very similar values of the gel time in the range of 12–13 s. PR48 showed the lowest G' values (25.91 ± 0.99 MPa), while G' values of C9 and FLGPCL02 were very close, 77.83 ± 3.11 and 71.22 ± 3.49, respectively.

Characterization of Photocross-Linked Polymer Structure

The crosslinked materials were studied by FTIR, which spectra showed the typical absorption bands of the polymers C0–C10 and the reduction of acrylic group absorption signal at 1637 cm^{-1}. As an example, FTIR spectra of AESO, MYR, DVB,
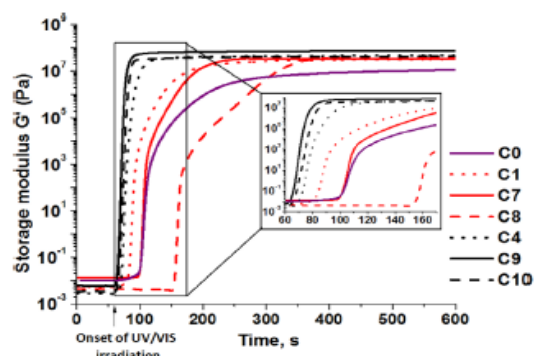

Figure 4. Time dependencies of storage modulus G' of the resin without aromatic compound C0 (purple) and the resins C1, C4, and C7–C10 with different amounts of aromatic compound: VDM (black) and DVB (red). [Color figure can be viewed at wileyonlinelibrary.com]
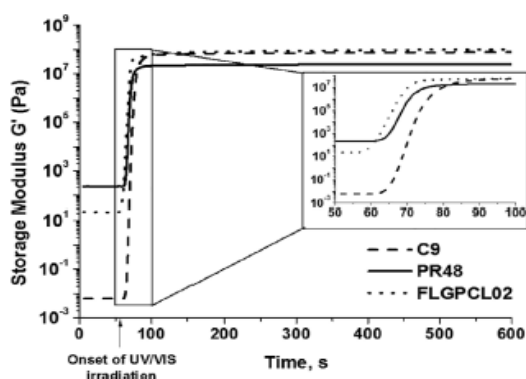
VDM, and crosslinked polymers C1 and C4 are presented in Figure 6.

All polymers with DVB showed new absorption signals of aryl alkyl ether groups C—O—C at 1267 and 1295 cm^{-1}. Also, the reduction of the absorption signals of AESO acrylic group C=C at 1630 cm^{-1} and DVB vinyl group =C—H at 897 cm^{-1} was observed which confirmed the formation of polymer network from AESO and DVB molecules.

Strong absorption signals of AESO aliphatic C—H groups at 2927 and 2855 cm^{-1} and alkyl ether group C—O—C at 1160 cm^{-1} were observed in FTIR spectra of all polymers with VDM. Also, the reduction of the absorption signals of AESO and VDM acrylic group C=C at 1630 cm^{-1} and vinyl group —C—H of MYR at 890 cm^{-1} was determined which confirmed the formation of the crosslinked polymer structure from all three monomers.

Formation of polymer crosslinked structure was confirmed by Soxhlet extraction. The yields of insoluble fraction of the crosslinked polymers obtained after Soxhlet extraction with chloroform for 24 h were in the range of 53–99% (Table III). It was determined that the higher amount of MYR was added to the reaction mixture, the lower yield of insoluble fraction of polymer was observed. This confirmed the tendency of MYR to form linear and/or branched polymer chains.[35] Also, the FTIR spectra showed the increment of methyl and methylene groups C—H signals at 1459 and 1407 cm^{-1} which corresponds to —CH$_2$ and —CH$_3$ bending vibrations of polymers C5–C6 and C9–C10, respectively.[36] The photocross-linked polymers with VDM fragments indicated the higher values of the yield of insoluble fraction values than those of the polymers with DVB fragments. The crosslinked polymers with VDM fragments as well as PR48 and FLGPCL02 indicated the highest values of the yield of insoluble fraction which defined the acrylate ability to exhibit high reaction rate and high density of crosslinks.[37] However, no significant influence of the amount of aromatic component to the yield of insoluble fraction of the synthesized polymers was observed.
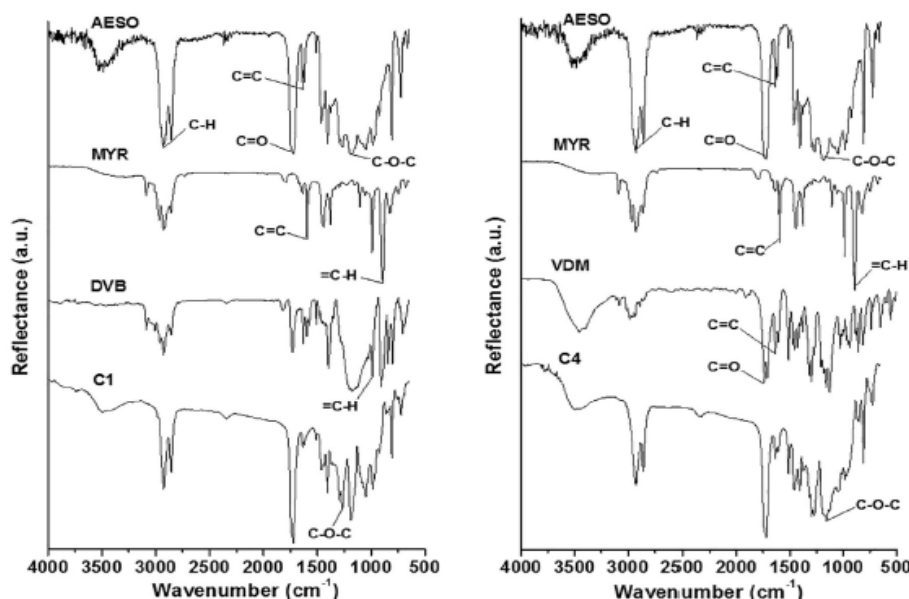
Figure 6. FTIR spectra of AESO, MYR, DVB, and the crosslinked polymer C1 (a) and AESO, MYR, VDM, and the crosslinked polymer C4 (b).

Thermal Properties

DSC confirmed that all synthesized photocross-linked polymers were amorphous materials. Only the glass transition was observed in the thermograms of all polymers synthesized. The values of the T_g of all polymers were very low (from −10.6 to −7 °C) even the polymers were solid materials at room temperature (Table III). Such low T_g values were determined by the flexible chains of AESO and MYR. The crosslinked structure of

Table III. Yield of Insoluble Fraction, Thermal, and Mechanical Analysis Data of the Crosslinked Polymers

Polymer	Yield of insoluble fraction[a] (%)	Density of crosslinks[b] (kmol·m^{-3})	$T_g{}^c$ (°C)	$T_{dec-10\%}{}^d$ (°C)	E^e (MPa)
C1	94	13.83 ± 0.50	−9.7	360	9.8 ± 0.20
C2	93	1.46 ± 0.50	−8.0	350	8.4 ± 0.06
C3	53	0.58 ± 0.03	−7.0	350	1.1 ± 0.02
C4	97	19.23 ± 5.06	−8.7	340	18.4 ± 0.2
C5	94	12.41 ± 2.81	−9.0	350	9.9 ± 0.2
C6	58	0.03 ± 0.01	−10.0	355	0.5 ± 0.14
C7	88	14.40 ± 1.41	−7.5	360	7.6 ± 0.35
C8	90	16.43 ± 0.79	−10.6	360	9.7 ± 0.20
C9	96	31.42 ± 1.26	−8.8	350	21.2 ± 0.2
C10	94	18.14 ± 4.27	−9.4	365	15.8 ± 0.2
PR48	99	10.52 ± 0.40	n[f]	n	16.9 ± 0.3
FLGPCL02	99	28.71 ± 7.87	n	n	13.1 ± 0.3

[a] After Soxhlet extraction with chloroform for 24 h.
[b] Density of crosslinks calculated according to the theory of rubber elasticity.
[c] Glass transition temperature estimated by DSC.
[d] Temperature at the weight loss of 10% obtained from TGA curve.
[e] Young's modulus from the top pressure test.
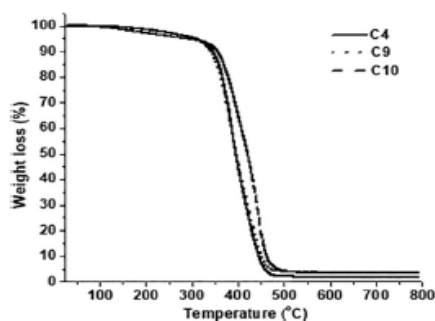[f] not measured.

73

Figure 7. Thermogravimetric curves of the polymers C4, C9, and C10.

polymers caused their solid state at room temperature. These features of the natural oil-based crosslinked polymers were observed in earlier studies.[38,39] No clear dependency of the amount of MYR, VDM, or DVB on the T_g values of the synthesized polymers was observed.

TGA confirmed that the photocross-linked polymers exhibited high thermal stability. Thermal decomposition of all polymers occurred in one step. As an example, TGA curves of the crosslinked polymers C4, C9, and C10 are presented in Figure 7. The 10% weight loss temperatures ($T_{dec-10\%}$) of all photocross-linked polymers were very similar and ranged from 340 to 365 °C (Table III). No clear dependency of the used aromatic compound and amount of MYR on the $T_{dec-10\%}$ values of the crosslinked polymers was observed.

Mechanical Properties

The mechanical properties of the synthesized crosslinked polymer samples were investigated by the compression test. No visible cracks were observed after the testing of all polymer specimens. The dependency of Young's modulus of polymers with different aromatic compounds on molar amount of MYR is shown in Figure 8. It was observed that the value of Young's modulus
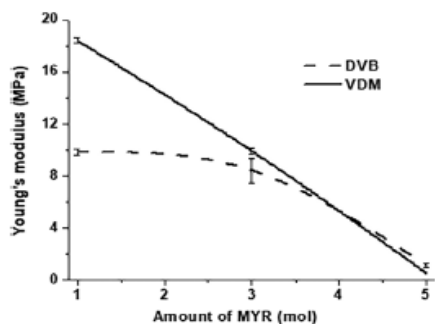

Figure 8. Dependency of Young's modulus of the polymers with 1 mol of different aromatic compounds on molar amount of MYR.

decreased when the higher amount of MYR was present in the resin. It could be explained by the formation of MYR soft and flexible chains and by lower crosslinking density in such cases leading to the loss of polymer stiffness.[40]

The higher yield of insoluble fraction of the crosslinked polymer was observed when the higher value of Young's modulus was reached (Table III). It was observed that the higher values of Young's modulus of the photocross-linked polymers with VDM fragments were reached comparing to the polymers with DVB fragments. However, no significant influence of the amount of aromatic component to Young's modulus of the synthesized polymers was observed.

CONCLUSIONS

The novel crosslinked polymers were synthesized from AESO, MYR, and VDM or DVB by UV/Vis photopolymerization. It was observed that MYR significantly reduced not only the viscosity of resin but also the rate of photocross linking, and impaired mechanical properties of polymers. The replacement of the petroleum-derived aromatic component DVB by plant-derived VDM led to the higher rate of photocross linking, better mechanical, and thermal properties of polymers. The resin composed of only plant-derived monomers, AESO, MYR, and VDM, molar ratio 1:1:3, showed characteristics comparable to those of commercial petroleum-derived photoresins and was selected as a potential renewable photoresin for application in optical 3D printing.

REFERENCES

1. Juskova, P.; Ollitrault, A.; Serra, M.; Viovy, J.; Malaquin, L. *Anal Chim. Acta.* **2018**, *1000*, 239.

2. Patil, D. M.; Phalak, G. A.; Mhaske, S. *Des. Monomers Polym.* **2017**, *20*, 269.

3. Quiles-Carrillo, L.; Duart, S.; Montanes, N.; Torres-Giner, S.; Balart, R. *Mater. Des.* **2018**, *140*, 54.

4. Zareanshahraki, F.; Mannari, V. *Int. J. Cosmetic Sci.* **2018**, *40*, 555.

5. Kim, H.; Kim, H.; Kim, B. S. *J. Polym. Environ.* **2010**, *18*, 291.

6. Wu, J. F.; Fernando, S.; Jagodzinski, K.; Weerasinghe, D.; Chen, Z. *Polym. Int.* **2011**, *60*, 571.

7. Yang, X.; Li, S.; Xia, J.; Song, J.; Huang, K.; Li, M. *Bioresources.* **2015**, *10*, 2130.

8. Miezinyte, G.; Ostrauskaite, J.; Rainosalo, E.; Skliutas, E.; Malinauskas, M. *Rapid Prototyp. J.* **2018**, *25*, 378.

9. Ferreira, G. R.; Braquehais, J. R.; da Silva, W. N.; Machado, F. *Ind. Crops Prod.* **2015**, *65*, 14.

74

10. Liu, K.; Madbouly, S. A.; Kessler, M. R. *Eur. Polym. J.* **2015**, *69*, 16.

11. Fache, M.; Boutevin, B.; Caillol, S. *ACS Sustain. Chem. Eng.* **2015**, *4*, 35.

12. Kessler, M. R.; Zhang, C. U.S. Pat. 15/742 (**2018**).

13. Zhang, Y.; Thakur, V. K.; Li, Y.; Garrison, T. F.; Gao, Z.; Gu, J.; Kessler, M. R. *Macromol. Mater. Eng.* **2018**, *303*, 1700278.

14. Lebedevaite, M.; Ostrauskaite, J.; Skliutas, E.; Malinauskas, M. *Polymers.* **2019**, *11*, 116.

15. Allnex Belgium SA., Ebecryl 860 Technical Data Sheet, http://www.palmerholland.com/Assets/User/Documents/Product/40754/4912/MITM00452.pdf (accessed July 11, 2019).

16. Behr, A.; Johnen, L. *ChemSusChem.* **2009**, *2*, 1072.

17. Zheng, H.; Li, C.; Chen, J.; Chen, J.; Zhao, S.; Wang, Y. *J. Anal. Appl. Pyrolysis.* **2017**, *123*, 99.

18. Flory, P. Principles of Polymer Chemistry; Cornell University Press: Ithaca, New York, **1953**.

19. Miao, S.; Zhu, W.; Castro, N. J.; Nowicki, M.; Zhou, X.; Cui, H.; Fisher, J. P.; Zhang, L. G. *Sci. Rep.* **2016**, *6*, 27226.

20. Li, F.; Larock, R. C. *J Polym Sci B.* **2000**, *38*, 2721.

21. Firdaus, M.; Meier, M. A. *Eur. Polym. J.* **2013**, *49*, 156.

22. Tomeckova, V.; Norton, S. J.; Love, B. J.; Halloran, J. W. *J. Eur. Ceram. Soc.* **2013**, *33*, 699.

23. Mouquinho, A. I.; Petrova, K.; Barros, M. T.; Sotomayor, J. New polymer networks for PDLC films application. In New Polymers for Special Applications, IntechOpen: London, **2012**. https://doi.org/10.5772/48203.

24. Mucci, V.; Vallo, C. *J. Appl. Polym. Sci.* **2012**, *123*, 418.

25. Kasetaite, S.; Ostrauskaite, J.; Grazuleviciene, V.; Bridziuviene, D.; Budreckiene, R.; Rainosalo, E. *React. Funct. Polym.* **2018**, *122*, 42.

26. Borges, A.; Bourban, P.; Pioletti, D.; Manson, J. *Compos. Sci. Technol.* **2010**, *70*, 1847.

27. Sarmento, V.; Frigerio, M.; Dahmouche, K.; Pulcinelli, S. H.; Santilli, C. V. *J. Sol-Gel Sci. Technol.* **2006**, *37*, 179.

28. Kreutzer, J.; Qin, X.; Gorsche, C.; Peterlik, H.; Liska, R.; Schubert, U. *Mater. Today Commun.* **2015**, *5*, 10.

29. Zhang, C.; Madbouly, S. A.; Kessler, M. R. *Macromol. Chem. Phys.* **2015**, *216*, 1816.

30. Zhou, C.; Wei, Z.; Jin, C.; Wang, Y.; Yu, Y.; Leng, X.; Li, Y. *Polymer.* **2018**, *138*, 57.

31. Ronda, J. C.; Lligadas, G.; Galia, M.; Cadiz, V. *React. Funct. Polym.* **2013**, *73*, 381.

32. Skliutas, E.; Kasetaite, S.; Jonusauskas, L.; Ostrauskaite, J.; Malinauskas, M. *Opt. Eng.* **2018**, *57*, 041412.

33. Lee, T. Y.; Roper, T. M.; Jonsson, E. S.; Kudyakov, I.; Viswanathan, K.; Nason, C.; Guymon, C. A.; Hoyle, C. E. *Polymer.* **2003**, *44*, 2859.

34. Voet, V. S. D.; Strating, T.; Schnelting, G. H. M.; Dijkstra, P.; Tietema, M.; Xu, J.; Woortman, A. J. J.; Loos, K.; Jager, J.; Folkersma, R. *ACS Omega.* **2018**, *3*, 1403.

35. Liu, B.; Li, L.; Sun, G.; Liu, D.; Li, S.; Cui, D. *Chem. Commun.* **2015**, *51*, 1039.

36. Sarkar, P.; Bhowmick, A. K. *RSC Adv.* **2014**, *4*, 61343.

37. Ge, X.; Ye, Q.; Song, L.; Misra, A.; Spencer, P. *Macromol. Chem. Phys.* **2015**, *216*, 856.

38. Kasetaite, S.; De la Flor, S.; Serra, A.; Ostrauskaite, J. *Polymers.* **2018**, *439*, 1.

39. Kasetaite, S.; Ostrauskaite, J.; Grazuleviciene, V.; Svediene, J.; Bridziuviene, D. *J. Appl. Polym. Sci.* **2014**, *131*, 40683.

40. Zhang, J.; Schneiderman, D. K.; Li, T.; Hillmyer, M. A.; Bates, F. S. *Macromolecules.* **2016**, *49*, 9108.

75

Article

Photoinitiator Free Resins Composed of Plant-Derived Monomers for the Optical μ-3D Printing of Thermosets

Migle Lebedevaite [1], Jolita Ostrauskaite [1,*], Edvinas Skliutas [2] and Mangirdas Malinauskas [2]

[1]   Department of Polymer Chemistry and Technology, Kaunas University of Technology, Radvilenu Rd. 19, 50254 Kaunas, Lithuania; migle.lebedeveaite@ktu.lt
[2]   Laser Research Center, Vilnius University, Sauletekis Ave. 10, 10223 Vilnius, Lithuania; edvinas.skliutas@ff.vu.lt (E.S.); mangirdas.malinauskas@ff.vu.lt (M.M.)
*   Correspondence: jolita.ostrauskaite@ktu.lt; Tel.: +370-37-300192

Abstract: In this study, acrylated epoxidized soybean oil (AESO) and mixtures of AESO and vanillin dimethacrylate (VDM) or vanillin diacrylate (VDA) were investigated as photosensitive resins for optical 3D printing without any photoinitiator and solvent. The study of photocross-linking kinetics by real-time photorheometry revealed the higher rate of photocross-linking of pure AESO than that of AESO with VDM or VDA. Through the higher yield of the insoluble fraction, better thermal and mechanical properties were obtained for the pure AESO polymer. Here, for the first time, we validate that pure AESO and mixtures of AESO and VDM can be used for 3D microstructuring by employing direct laser writing lithography technique. The smallest achieved spatial features are 1 μm with a throughput in 6900 voxels per second is obtained. The plant-derived resins were laser polymerized using ultrashort pulses by multiphoton absorption and avalanche induced cross-linking without the usage of any photoinitiator. This advances the light-based additive manufacturing towards the 3D processing of pure cross-linkable renewable materials.

Keywords: acrylated epoxidized soybean oil; vanillin dimethacrylate; vanillin diacrylate; photocross-linking; direct laser writing; nanolithography; optical 3D printing; two-photon polymerization (2PP); multi-photon processing

---

1. Introduction

In recent years, 3D printing or rapid prototyping as a flexible additive manufacturing technique became very popular because of its simplicity, relatively low cost, and unlimited creativity. This process enables the creation of complex three-dimensional objects which cannot be cut, assembled or carved. It is possible because of Computer-Aided Design (CAD) modeling, where various objects are generated and files are transmitted for the printing of 3D items [1]. Stereolithography (SLA) is a process which obtains a high printing accuracy and speed, simple and low raw material usage technology [2]. It is a layer by layer photopolymerization method, where the photosensitive resin is polymerized by UV/VIS light.

Epoxy and acrylic resins are the most popular materials in optical 3D printing. Printed epoxy polymers have low shrinkage and high structural stability, while acrylates have high light sensitivity, low critical energy and viscosity, controllable mechanical properties and relatively high dependence on temperature and humidity changes [3]. While epoxides have higher structural stability, acrylates possess higher photosensitivity due to which they are more popular in the SLA process.

Most of the photosensitive resins for optical 3D printing are made from acrylic oligomers, acrylic monomers and/or reactive diluents, photoinitiator and UV stabilizators/blockers [4].

Photopolymerized acrylates are in an irregular molecular structure because of high curing speed. Petroleum-derived acrylic resins such as polyesters, polyether oligomers or diglicidylether bisphenol A acrylates are those that are mostly used for optical 3D printing [5]. Due to decreasing petroleum recourses, it became crucial to search for alternative materials such as renewable resources [6]. Natural oils are one of the best alternatives for petroleum-derived resins [7–9]. Due to their richness in double bonds which can be polymerized or converted to other functional groups, biodegradability and renewability, natural oils became a popular target of researchers [10,11].

Soybean oil is one of the most promising materials to replace petroleum-derived resins. It contains a high amount of unsaturated fatty acids such as monounsaturated oleic acid (C-18:1, ~23%), polyunsaturated α-linoleic acid (C-18:3, 7–10%), and linoleic acid (C-18:2, ~51%) [12,13]. Carbon-carbon double bonds of fatty acids can be oxidized [14], polymerized [15,16] or converted to various reactive groups [17–19].

Acrylated epoxidized soybean oil (AESO) is produced by the epoxidation of fatty acid double bonds followed by epoxy ring acrylation [20–23]. Due to the high amount of various functional groups such as the acrylic, epoxy and hydroxy groups, AESO is widely used in industry and is commercially available under Ebecryl 860 trademark [24]. AESO can be polymerized by UV/VIS light using appropriate photoinitiators and can form a cross-linked polymer network. AESO is already photopolymerized with polycaprolactone diacrylate and polyethylenglycol diacrylate [25], tetrahydrophurphuryl acrylate [26,27], myrcene [28], and various thiols [29,30]. The addition of comonomers improved the mechanical and thermal properties as well as solvent resistance of the resulted polymers. Due to AESO fatty acid long aliphatic chains, cross-linked polymers are soft and mechanically resistless. To improve the polymer mechanical properties, aromatic comonomers are added. Such compounds such as styrene [31,32], divinylbenzene (DVB) [33,34], dicyclopentadiene [35] and acrylepoxymethylester [36] were used as stiffening agents for AESO polymers. But these materials are petroleum-derived and harmful to health [37–39]. Initially, we selected the plant-derived vanillin acrylates to replace the petroleum-derived aromatic compounds because of their aromatic structure, renewability and reactivity [40].

Vanillin dimethacrylate (VDM) or methacrylated vanillin alcohol is produced from lignin, one of the most abundant natural polymers [41]. The bio-based thermosets made from VDM and maleinated AESO showed high glass transition temperatures (63–79 °C) and high Young's modulus values (570–855 MPa), but a high viscosity of the mixture and very long reaction time (about 8 h) was also observed [42]. Vanillin diacrylate (VDA) is a bifunctional aromatic compound which can also be produced from lignin. It has two acrylic groups which can be polymerized via free-radical polymerization, yet no data was found of its usage in polymerization.

In this study, the plant-derived AESO, VDM and VDA (Scheme 1) were used as photosensitive monomers for the optical 3D printing of thermosets. The monitoring of photocross-linking kinetics was carried out by real-time photorheometry which provides a wide range of information on typical rheological properties such as viscosity and shear modulus while the material is irradiated with UV/VIS light. It enables us to track the occurrence of structural phenomena, such as gelation and vitrification [43], indicating the moment, when the structural changes have started [44]. The chemical structure of the polymers was investigated by FTIR spectroscopy. The formation of polymer cross-linked structure was confirmed by Soxhlet extraction. The thermal properties of cross-linked polymers were investigated by differential scanning spectroscopy and thermogravimetric analysis. The compressive modulus was determined from the top pressure test. The plant-derived resins AESO and AESO/VDM were laser polymerized using ultrashort pulses by multiphoton absorption and avalanche induced cross-linking without a photoinitiator.
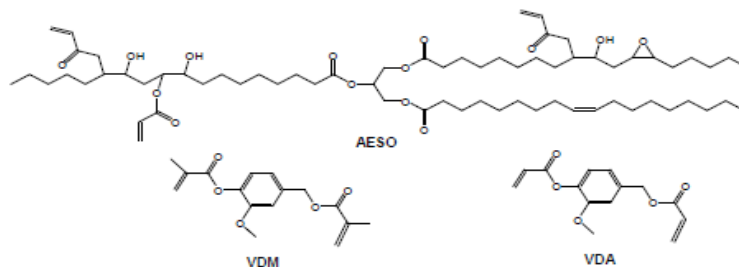
Scheme 1. The chemical structure of acrylated epoxidized soybean oil (AESO), vanillin dimethacrylate (VDM) and vanillin diacrylate (VDA).

2. Materials and Methods

2.1. Materials

Acrylated epoxidized soybean oil (AESO, an average number of acryloyl groups per molecule calculated from the ^{1}H-NMR spectrum is 2.7 and 0.3 of epoxide groups) was purchased from Sigma-Aldrich (Darmstadt, Germany). Vanillin dimethacrylate (VDM) and vanillin diacrylate (VDA) were purchased from Specific Polymers. Chloroform was purchased from Chempur (Karlsruhe, Germany). All materials were used without further purification.

2.2. Real-Time Photorheometry

UV/VIS curing tests of pure AESO and two resin series, AESO/VDM and AESO/VDA (Table 1), without any photoinitiator and solvent were carried out with an MCR302 rheometer from Anton Paar (Graz, Austria) equipped with plate/plate measuring system. A Peltier-controlled temperature chamber with the glass plate (diameter of 38 mm) and the top plate PP08 (diameter of 8 mm) was used. The measuring gap was set to 0.3 mm. The samples were irradiated at room temperature by UV/VIS radiation in a wavelength range of (250–450) nm through the glass plate of the temperature chamber using a UV/VIS spot curing system OmniCure S2000, Lumen Dynamics Group Inc (Mississauga, Ontario, Canada). The intensity of the irradiation was 9.3 W·cm^{-2} (high pressure 200 W mercury vapor short arc). Shear mode with a frequency of 10 Hz and a strain of 0.3% was used. Storage modulus G′, loss modulus G″, loss factor tanδ (tanδ = G″/G′), and complex viscosity η* were recorded as a function of irradiation time. The onset of UV/VIS irradiation was at 60 s after the experiment start for all samples.

2.3. Preparation of Cross-Linked Polymers

The homopolymer pAESO was synthesized from pure AESO and the copolymer series pAESO/VDM was synthesized from the mixtures of AESO and VDM without a photoinitiator and any solvent. The mixtures of AESO and VDM (Table 1) were stirred at 40 °C for 24 h. Resins were poured into a tablet-shaped (Ø 15 mm, h 3 mm) Teflon mold and irradiated with Helios Italquartz, model GR.E 500 W lamp with an intensity of 310 mW·cm^{-2} at the distance of 15 cm until hard polymer tablets were formed.

2.4. Chemical Structure Analysis

Fourier Transform Infrared Spectroscopy (FT-IR) measurements of photocross-linked polymer samples were performed on a Spectrum BX II FT-IR spectrometer (Perkin Elmer, Llantrisant, UK). The spectra were acquired from 10 scans. The range of the wavenumber was (400–4000) cm^{-1}.

2.5. Soxhlet Extraction

The amount of the insoluble fraction was determined by Soxhlet extraction. Samples of photocross-linked polymers were put into a filter package and placed in a Soxhlet apparatus (Sigma-Aldrich, Darmstadt, Germany). Extraction was performed with chloroform for 24 h. Insoluble fractions were dried under vacuum to a constant weight. The amount of insoluble fraction was calculated as the difference of the sample weight before and after extraction.

2.6. Differential Scanning Calorimetry

The glass transition temperature (T_g) of the photocross-linked polymers were estimated by differential scanning calorimetry (DSC). The measurements were performed on a DSC 8500 apparatus (Perkin Elmer, Llantrisant, UK) with a heating-cooling-heating rate of $10\ °C·min^{-1}$ under a nitrogen atmosphere (nitrogen flow rate $50\ mL·min^{-1}$). The T_g value was taken as the middle point in the heat capacity step of the glass transition.

2.7. Thermogravimetric Analysis

The thermal stability of prepared polymers was determined by thermogravimetric analysis (TGA). The measurements were performed on a TGA 4000 apparatus (Perkin Elmer, Llantrisant, UK) in a temperature range from room temperature to $800\ °C$ at a heating rate of $20\ °C·min^{-1}$ under a nitrogen atmosphere (nitrogen flow rate $100\ mL·min^{-1}$).

2.8. Mechanical Testing

The mechanical properties of the photocross-linked polymer tablets were estimated by a compression test on a BDO-FB0.5TH (Zwick/Roell, Kennesaw, Georgia, USA) testing machine at room temperature. The cross-linked polymer specimen with a 15 mm diameter and 3 mm thickness was placed in a Teflon mold of the same size in order to avoid the expansion of specimen to the sides during the test. The specimen was pressed with a cylindrical steel rod with a flat end diameter of 8 mm. The speed of the rod movement was 5 mm/min. The specimen pressure was stopped when the upper force limit of 100 N was reached. The compressive modulus was calculated by the following equation:

$$E_c = \frac{F \cdot l_0}{S \cdot \Delta l} \tag{1}$$

where E_c is a compressive modulus (N/mm^2); F is a force (N); S is a surface area of the specimen that interacts with the steel rod flat end (mm^2); l_0 is an initial thickness of the specimen (mm); Δl is the difference of the initial thickness of the specimen and the thickness of a loaded specimen (mm).

The mean values of the ten samples of each polymer were calculated. Results with a within-group variation below 5% were taken.

2.9. Direct Laser Writing 3D Lithography

Direct laser writing (DLW) 3D lithography experiments were conducted employing a Pharos laser (515 nm, 300 fs, 200 kHz, Light Conversion Ltd, Vilnius, Lithuania), 20 × NA = 0.8 objective and the combined movement of the linear stages and Galvano-scanners. A detailed description of the experimental setup can be found in a previous publication [45]. The goal was to figure out if AESO and VDM monomer based resins can be suitable for ultra-fast laser pulses initiated by 3D polymerization in a confined space. An investigation test to assess the optimal fabrication parameters was performed. A 3D model of so-called resolution bridges (RB) was programmed accordingly. It consisted of five rectangle-shaped columns which were 15 µm wide, 60 µm long and 15 µm high. Gaps between the columns varied from 5 µm to 20 µm every 5 µm. The five straight lines perpendicular to the columnar long edges formed in the gaps. Such a structure corresponds to the RB suspended between the columns. Each line was polymerized from a single laser beam scan. RB were obtained with different longitudinal and lateral sizes by varying the laser power (P), which corresponded to the light intensity (I) at the

sample and the scanning velocity (v). It enabled the evaluation of the smallest features and their dependence on the applied I which could be formed in AESO and VDM based resins. The capability to form 3D microporous woodpile structures was demonstrated. They consisted out of two layers separated via vertical 20 µm height columns. The layers were made of a 15 µm wide and 75 µm long log pattern with a 15 µm gap between the logs, resulting in a 30 µm period. Each log was made from multiple scans whose number depended from the distance d_{xy} between scans. d_{xy} was 0.25–2 µm every 0.25 µm. During the fabrication, the resin was placed between two glass slides, as shown in Figure 1. After the exposure the samples were developed in 4-methyl-2-pentanone for 15 min, removing the uncured resin and leaving only the formed structures on the substrate. The fabricated structures were characterized using a scanning electron microscope (SEM, Hitachi TM-1000, Tokyo, Japan).
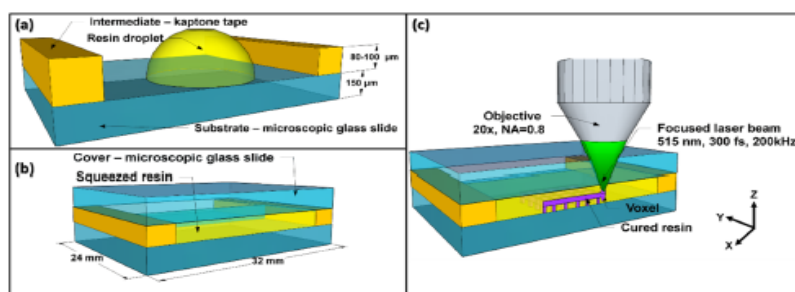

Figure 1. The explanatory scheme of a sample preparation and Direct Laser Writing (DLW) 3D lithography: (a) Kapton tape attached to the glass slide and working as an intermediate, resin's droplet drop cast on such a substrate; (b) another glass slide used as a cover to squeeze the droplet and spread it uniformly through the substrate; (c) laser beam focused through the cover glass into the resin and initiating the 3D confined polymerization reaction.

3. Results

3.1. Kinetics of Photocross-Linking

In this study, the photocross-linking of AESO and the mixtures of AESO and VDM or AESO and VDA was performed without any photoinitiator and solvent. The composition of resins is presented in Table 1. Different ratios of AESO and VDM or VDA were used in the resin series AESO/VDM and AESO/VDA. The resin AESO/VDM1 contains the maximum amount of VDM possible to dissolve in AESO without any solvent at 40 °C. The same amounts of VDA and VDM were taken in the resin series AESO/VDA and AESO/VDM for comparison.

Table 1. The composition of resins.

Resin	Ratio of Functional Groups [1]	Ratio of Monomers, mol	Amount of Monomers, g
AESO	-	1	1.5
AESO/VDM1	1.5:1	1:1	1.5/0.375
AESO/VDM2	3:1	1:0.5	1.5/0.187
AESO/VDM3	6:1	1:0.25	1.5/0.094
AESO/VDA1	1.5:1	1:1	1.5/0.339
AESO/VDA2	3:1	1:0.5	1.5/0.170
AESO/VDA3	6:1	1:0.25	1.5/0.085

[1] Ratio of AESO acrylic groups and VDM or VDA acrylic groups.

The kinetics of photocross-linking was monitored by real-time photorheometry. In the photorheometry test, when the photosensitive resin is being irradiated with UV/VIS light, the values of storage modulus G', loss modulus G", and complex viscosity η* start to increase. This increment indicates the formation of a three-dimensional polymer network. During the process, the values of G' increase faster and exceed the values of G" showing the high viscosity Newton liquid transforms into a hard elastic polymer. In this transformation, the point where G' = G" is commonly used to define the gel point (t_{gel}) [46]. At this point, the loss factor tanδ, the ratio of the viscous and the elastic portion of the viscoelastic deformation behavior (G"/G') starts to decrease. Then, the values of G' and G" increase continuously and the tanδ value decreases until the final degree of cross-linking is reached [47,48]. As an example, the dependencies of G', G", tanδ and η* on the irradiation time of the photocross-linking of AESO are presented in Figure 2.

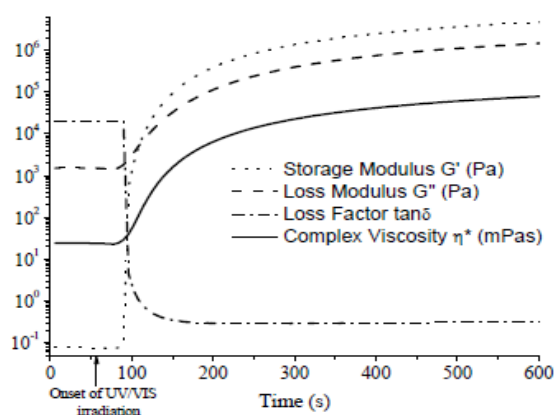**Figure 2.** The dependencies of storage modulus G', loss modulus G", loss factor tanδ and complex viscosity η* of AESO on irradiation time.

The values of G', G", η*, and t_{gel} of AESO, the resin series AESO/VDM and AESO/VDA are presented in Table 2. It was determined that the rate of photocross-linking of resins containing AESO and VDM or VDA was lower than that of pure AESO. The addition of VDM or VDA to the resins caused a longer induction period and the higher t_{gel} values. The values of t_{gel} of the resin series AESO/VDA were much higher than those of AESO or the resin series AESO/VDM. Moreover, the G' values of AESO were higher than those of the resin series AESO/VDM and AESO/VDA, indicating the lower rigidity of the latter polymers (Figures 3 and 4).

Table 2. The storage modulus (G'), loss modulus (G"), complex viscosity (η*), and gel time (t_{gel}) of all resins.

Resin	G' [1], Pa	G" [1], Pa	η* [1], mPa·s	t_{gel}, s [2]
AESO	4.76×10^6	1.47×10^6	7.93×10^4	49
AESO/VDM1	2.65×10^6	1.01×10^6	4.51×10^4	98
AESO/VDM2	2.70×10^6	9.31×10^5	4.55×10^4	91
AESO/VDM3	3.51×10^6	1.18×10^6	5.89×10^4	66
AESO/VDA1	5.89×10^5	2.27×10^5	1.01×10^4	782
AESO/VDA2	1.11×10^6	3.74×10^5	1.87×10^4	531
AESO/VDA3	3.56×10^6	1.17×10^6	5.96×10^4	290

[1] at an irradiation time of 600 s for AESO and AESO/VDM, and 1800 s for AESO/VDA. [2] calculated from the onset of UV/VIS irradiation.

81

It is known that the acrylic group is more reactive than methacrylic [49]. This explains the increase of the induction period and t_{gel} value during the photocross-linking of the resin series AESO/VDM in comparison to AESO. Additionally, the slope of the G′ curve of AESO was steeper than that of the resin series AESO/VDM indicating the quicker formation of the polymer network [50]. High G′ values indicate better mechanical properties of polymers caused by the high density of cross-links [41]. Thus, the higher G′ values of AESO indicate the higher density of cross-links in this polymer (pAESO).
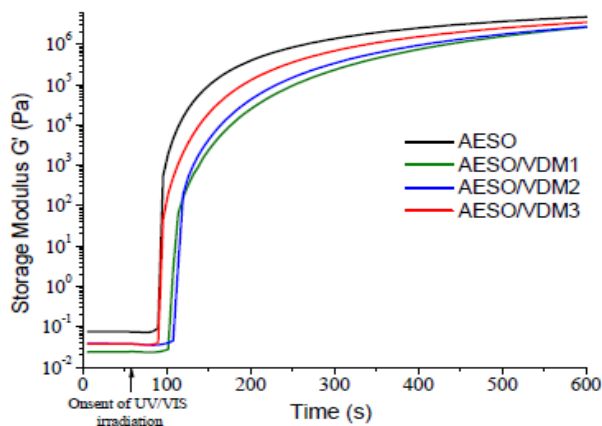

Figure 3. The irradiation time dependencies of the storage modulus G′ of AESO and the resin series AESO/VDM.
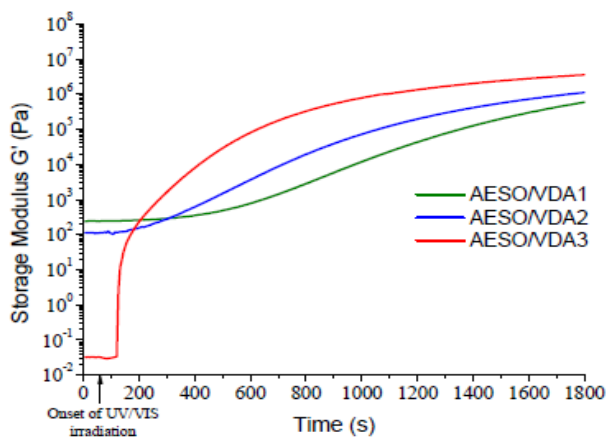

Figure 4. The irradiation time dependencies of the storage modulus G′ of the resin series AESO/VDA.

The irradiation time dependencies of the storage modulus of the resin series AESO/VDA are shown in Figure 4. The photocross-linking kinetics of this resin series strongly depends on the VDA concentration. The higher the amount of VDA was used, the higher the values of t_{gel} obtained (Table 1). The increase of the VDA amount caused the lower G' values obtained to show a lower density of cross-links in these polymers. The induction period of AESO/VDA was longer and the G' values were lower compared to those of the resin series AESO/VDM. Due to these data, especially due to the very high t_{gel} values of the resin series AESO/VDA, further experiments were performed only with AESO and the resin series AESO/VDM.

3.2. Characterization of Photocross-Linked Polymer Structure

The chemical structure of the polymer pAESO and the polymer series pAESO/VDM was investigated by FTIR spectroscopy (Figure 5). The reduction of the acrylic group signal at 1637 cm^{-1} was observed in the FTIR spectra of photocross-linked polymers pAESO and all the polymers pAESO/VDM in comparison to that of the FTIR spectra of AESO and VDM showing that most of the acrylic groups were reacted. The more intensive signal of acrylic group C=C at 1630 cm^{-1} in FTIR spectra of pAESO/VDM could be assigned to the free VDM methacrylic groups. The strong peak at 1513 cm^{-1} is assigned to VDM aromatic ring C=C vibrations.
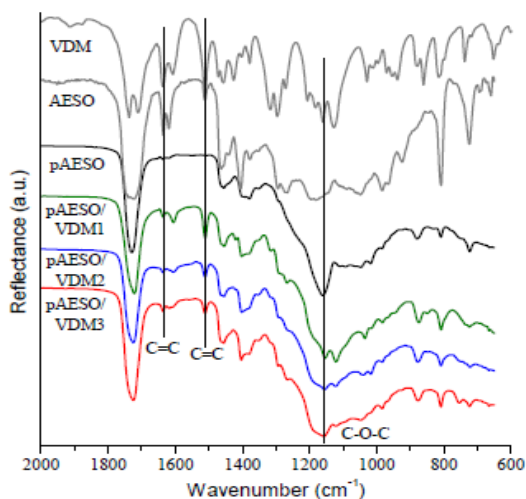
Figure 5. The FT-IR spectra of AESO, VDM, homopolymer pAESO and copolymer series pAESO/VDM.

The formation of polymer cross-linked structure was confirmed by Soxhlet extraction. The yield of insoluble fraction of pAESO was much higher (88%) than that of the cross-linked polymers pAESO/VDM (31–63%) (Table 2). This showed that AESO tends to form densely cross-linked polymers even without photoinitiators. Sucha low yield of insoluble fraction of the polymer series pAESO/VDM could be explained by the tendency of VDM to form linear and/or branched polymers. This statement is confirmed by the increase of the yield of an insoluble fraction with the reduction of VDM amount.

83

3.3. Thermal Properties

DSC confirmed that all synthesized photocross-linked polymers are amorphous materials. Only the glass transitions were observed in the thermograms of all the polymers prepared. The values of the glass transition temperatures (T_g) were very low and varied from $-4.5\,°C$ to $-1.6\,°C$ (Table 3) even though these polymers were solid materials at room temperature. Such low T_g values were determined by the flexible chains of AESO. The lower T_g value of the polymers pAESO/VDM1 and pAESO/VDM2 than pAVDM3 could be explained by their lower yield of insoluble fraction. A huge amount of linear and/or branched macromolecules was formed in these polymers probably due to the different activities of the functional group affected the T_g value of these copolymers [51]. The cross-linked structure of polymers caused their solid state at room temperature. Such a feature of the natural oil-based cross-linked polymers was observed in earlier studies [30,52].

Table 3. The yield of the insoluble fraction and the thermal and mechanical characteristics of the cross-linked polymers.

Polymer	Yield of Insoluble Fraction [1] (%)	T_g [2] (°C)	$T_{dec-10\%}$ [3] (°C)	E_c [4] (Pa)
pAESO	88	−4.5	356	0.62 ± 0.1
pAESO/VDM1	31	−2.6	295	0.19 ± 0.03
pAESO/VDM2	48	−2.6	318	0.46 ± 0.13
pAESO/VDM3	63	−1.6	331	0.66 ± 0.13

[1] After Soxhlet extraction with chloroform for 24 h.; [2] Glass transition temperature estimated by DSC; [3] Temperature at the weight loss of 10 % obtained from TGA curves; [4] Compressive modulus from the top pressure test.

TGA confirmed that the photocross-linked polymers exhibited high thermal stability. TGA curves of the cross-linked polymers are presented in Figure 6. The 10% weight loss temperatures ($T_{dec-10\%}$) of pAESO and the polymer series pAESO/VDM range from 295 °C to 356 °C (Table 3). It was noticed, that the higher the amount of VDM was used, the lower the $T_{dec-10\%}$ value indicated. Lower $T_{dec-10\%}$ values and a two- or even three-step thermal decomposition of the polymers containing VDM fragments could be due to the higher rate of linear and/or branched macromolecules while higher thermal stability is related to the high density of the cross-links [53].
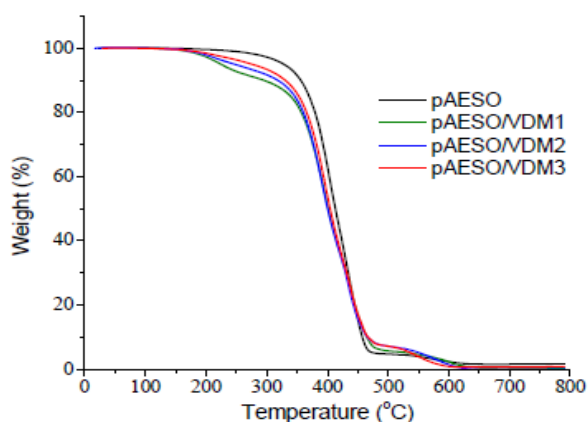

Figure 6. The thermogravimetric curves of the polymers pAESO and the polymer series pAESO/VDM.

3.4. Compressive Modulus

The compressive modulus of the synthesized cross-linked polymer samples was determined from the top pressure test. No visible cracks were observed after the testing of all polymer samples. The higher value of the compressive modulus was observed for the polymer pAESO in comparison to that of the polymers pAESO/VDM1 and pAESO/VDM2, and similar to that of the polymer pAESO/VDM3 (see Table 2). This shows the correlation of the compressive modulus and insoluble fraction of cross-linked polymers. The higher yield of the insoluble fraction caused the higher value of the compressive modulus. The tendency of the increase of the compressive modulus with the reduction of the VDM amount in the resin was also observed.

3.5. Characterization of DLW 3D Lithography Produced Structures

RB and 3D microporous woodpile structures obtained via DLW 3D lithography out of AESO and ASEO/VDM1 were characterized. These plant-derived resins were laser polymerized using ultrashort pulses by multiphoton absorption and avalanche induced cross-linking [54,55]. Scanning Electron Microscopy (SEM) images are shown in Figure 7. Figure 7a demonstrates RB—five columns with five straight lines perpendicular to the column long edges. Figure 7b shows a close up view of RB from the top. P was set to 0.6 mW (2 TW/cm^2) for the lines and each line was scanned with a different velocity v, varying from 2 mm/s to 6 mm/s. It can be seen that each line has a slightly different width: the higher the v, the narrower the line. Further 3D microporous woodpile structures were formed. Arrays of 75×75 μm^2 woodpiles are demonstrated in Figure 7c,e. In both cases, v was set to 5 mm/s and P was varied in the range of 0.4–1 mW (1.3–3.3 TW/cm^2). It can be seen that an increased laser power P higher than d_{xy} can be used. Finally, the mm scale woodpiles were fabricated. Figure 7d shows a 1065×1065 μm^2 woodpile with a 75 μm period and 4 layers, $v = 5$ mm/s, $P = 0.4$ mW (1.3 TW/cm^2). However, it did not sustain itself due to the low mechanical rigidity. Figure 7f demonstrates a 1095×1095 μm^2 woodpile with a 120 μm period and 6 layers, $v = 5$ mm/s, $P = 0.6$ mW (2 TW/cm^2). The structure sustained itself and had a 3D architecture. To sum up, AESO and the resin AESO/VDM1 can be the great candidates as new renewable materials for DLW 3D lithography technology [56]. It has a wide working window ranging P from 0.1 mW to 1 mW (dynamic fabrication window aspect ratio 10 times). Spatial features of 1 μm and a 6900 voxels/second throughput was achieved as a method for the evaluation of normalized μ-3D fabrication throughput [57]. We note that the possibility to the photostructure without the use of photoinitiators is not limited to serial direct write (DLW/SLA), but also can be extended to projection DLP lithography (SLM/DMD based) if the peak exposure intensity is sustained (for current case of employed material and light source the ranging within $\approx$ 1–3 TW/cm^2).

It is envisaged that the photostructuring without the photoinitiators is beneficial for the fields of biomedicine, micro-optics and nanophotonics. The avoidance of toxic photoinitiators increases the integrity of biodegradable cell-growth scaffolds and reduces the auto-fluorescence while performing microscopy in vitro or in vivo. The absorbing materials are detrimental for the use in micro-optics and nanophotonics due to their reduced optical resilience and induced signal losses [58]. Moreover, the use of plant-derived materials in such technologies would benefit greatly due to their low toxicity, high biodegradability, and improved recycling options. Finally, it would reduce the dependency on limited and increasingly expensive fossil resources as well as greenhouse gas emission, which are the targets of the European Commission initiated "Europe 2020" strategy.
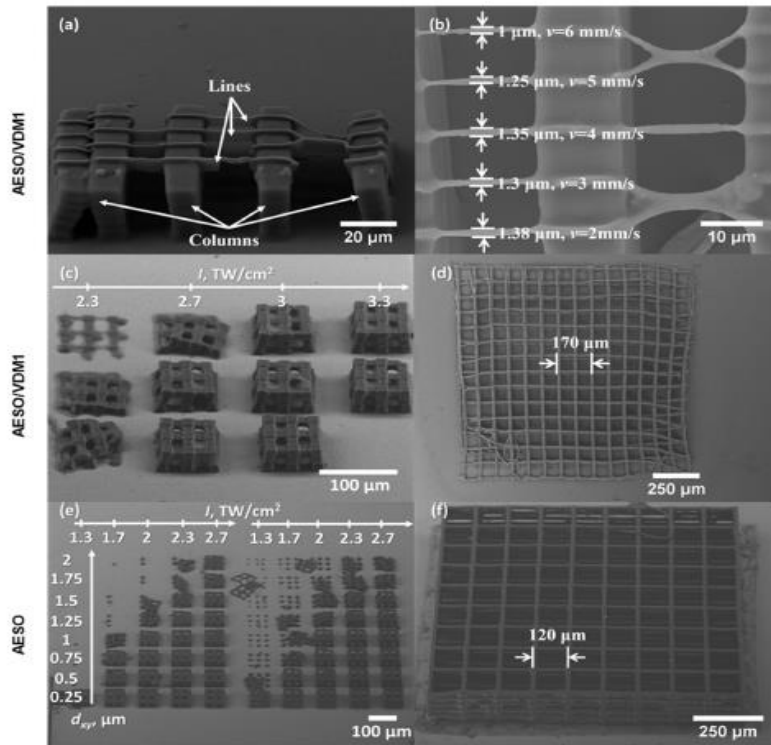
85

Figure 7. The SEM images of RB and 3D microporous woodpile structures: (**a**) a side view of RB at the angle of 45 degrees and 1800 magnification. The applied power P to produce bridges was 0.6 mW (2 TW/cm^2), scan velocity v varied from 0.1 mm/s to 0.5 mm/s every 0.1 mm/s; (**b**) a top view of the other RB at 4000 magnification. $P = 0.6$ mW (2 TW/cm^2), $v = 2$–6 mm/s every 1 mm/s; (**c**) 75 × 75 μm^2 woodpile structures with a 30 μm period, $v = 5$ mm/s, the scale at the top of the image demonstrates the applied I; (**d**) a 1065 × 1065 μm^2 woodpile with a 75 μm period, $v = 5$ mm/s, $P = 0.4$ mW (1.3 TW/cm^2). (**a–d**) The structures were fabricated out of the resin AESO/VDM1; (**e**) 75 × 75 μm^2 woodpile structures with a 30 μm period, $v = 5$ mm/s. Scale on the left of image shows the distance d_{xy} between neighboring scans; (**f**) a 1095 × 1095 μm^2 woodpile with 120 μm period, $v = 5$ mm/s, $P = 0.6$ mW (2 TW/cm^2). (**e,f**) structures were fabricated out of AESO.

4. Conclusions

The real-time photorheometry study revealed the higher rate of photocross-linking of pure acrylated epoxidized soybean oil than that of its mixture with vanillin dimethacrylate or vanillin diacrylate without a photoinitiator and solvent. Novel plant-derived photocross-linked polymers were synthesized from acrylated epoxidized soybean oil and its mixtures with vanillin dimethacrylate. It was determined that the addition of vanillin dimethacrylate reduced the rate of photocross-linking and the values of the glass transition temperature, thermal decomposition temperature and compressive modulus. The formation of more linear and/or branched macromolecules considered the vanillin dimethacrylate effect as a plasticizer for acrylated epoxidized soybean oil in photocross-linking without

a photoinitiator. It was experimentally demonstrated that the homopolymer of acrylated epoxidized soybean oil and the copolymer of acrylated epoxidized soybean oil and vanillin dimethacrylate are suitable materials for rapid 3D microstructuring by the direct laser writing lithography technique. Spatial features of 1 µm and a 6900 voxels/second throughput was achieved. Since the 3D cross-linking of the plant-derived materials was initiated using ultrafast laser inducing multiphoton absorption and avalanche ionization, it does not require the usage of any photoinitiator and opens a new pathway for green 3D µ-printing as a flexible tool for rapid prototyping or advanced additive manufacturing.

References

1. Rengier, F.; Mehndiratta, A.; Von Tengg-Kobligk, H.; Zechmann, C.M.; Unterhinninghofen, R.; Kauczor, H.; Giesel, F.L. 3D Printing Based on Imaging Data: Review of Medical Applications. *Int. J. Comput. Assist. Radiol. Surg.* **2010**, *5*, 335–341. [CrossRef] [PubMed]

2. Cooke, M.N.; Fisher, J.P.; Dean, D.; Rimnac, C.; Mikos, A.G. Use of Stereolithography to Manufacture Critical-sized 3D Biodegradable Scaffolds for Bone Ingrowth. *J. Biomed. Mater. Res. Part B: Appl. Biomater.* **2003**, *64*, 65–69. [CrossRef] [PubMed]

3. Corbel, S.; Dufaud, O.; Roques-Carmes, T. Materials for stereolithography. In *Stereolithography*; Springer: Boston, MA, USA, 2011; pp. 141–159.

4. Skliutas, E.; Kasetaite, S.; Jonušauskas, L.; Ostrauskaite, J.; Malinauskas, M. Photosensitive Naturally Derived Resins toward Optical 3-D Printing. *Opt. Eng.* **2018**, *57*, 041412. [CrossRef]

5. Ligon-Auer, S.C.; Schwentenwein, M.; Gorsche, C.; Stampfl, J.; Liska, R. Toughening of Photo-Curable Polymer Networks: A Review. *Polym. Chem.* **2016**, *7*, 257–286. [CrossRef]

6. Reddy, M.M.; Vivekanandhan, S.; Misra, M.; Bhatia, S.K.; Mohanty, A.K. Biobased Plastics and Bionanocomposites: Current Status and Future Opportunities. *Prog. Polym. Sci.* **2013**, *38*, 1653–1689. [CrossRef]

7. Güner, F.S.; Yağcı, Y.; Erciyes, A.T. Polymers from Triglyceride Oils. *Prog. Polym. Sci.* **2006**, *31*, 633–670. [CrossRef]

8. Lligadas, G.; Ronda, J.C.; Galia, M.; Cádiz, V. Plant Oils as Platform Chemicals for Polyurethane Synthesis: Current State-of-the-Art. *Biomacromolecules* **2010**, *11*, 2825–2835. [CrossRef]

9. Pelletier, H.; Gandini, A. Preparation of Acrylated and Urethanated Triacylglycerols. *Eur. J. Lipid Sci. Technol.* **2006**, *108*, 411–420. [CrossRef]

10. Pelletier, H.; Belgacem, N.; Gandini, A. Acrylated Vegetable Oils as Photocrosslinkable Materials. *J. Appl. Polym. Sci.* **2006**, *99*, 3218–3221. [CrossRef]

11. Wool, R.; Sun, X.S. *Bio-Based Polymers and Composites*; Elsevier: Burlington, MA, USA, 2011.

12. Ivanov, D.S.; Lević, J.D.; Sredanović, S.A. Fatty Acid Composition of various Soybean Products. *Food Feed Res.* **2010**, *37*, 65–70.

13. Haun, W.; Coffman, A.; Clasen, B.M.; Demorest, Z.L.; Lowy, A.; Ray, E.; Retterath, A.; Stoddard, T.; Juillerat, A.; Cedrone, F. Improved Soybean Oil Quality by Targeted Mutagenesis of the Fatty Acid Desaturase 2 Gene Family. *Plant Biotechnol. J.* **2014**, *12*, 934–940. [CrossRef] [PubMed]

14. Lowe, A.B. Thiol–ene "click" Reactions and Recent Applications in Polymer and Materials Synthesis: A First Update. *Polym. Chem.* **2014**, *5*, 4820–4870. [CrossRef]

15. Huang, X.; Liu, H.; Shang, S.; Rao, X.; Song, J. Preparation and Characterization of Polymeric Surfactants Based on Epoxidized Soybean Oil Grafted Hydroxyethyl Cellulose. *J. Agric. Food Chem.* **2015**, *63*, 9062–9068. [CrossRef]

16. Liu, Z.; Doll, K.M.; Holser, R.A. Boron Trifluoride Catalyzed Ring-Opening Polymerization of Epoxidized Soybean Oil in Liquid Carbon Dioxide. *Green Chem.* **2009**, *11*, 1774–1780. [CrossRef]

17. Fu, L.; Yang, L.; Dai, C.; Zhao, C.; Ma, L. Thermal and Mechanical Properties of Acrylated Expoxidized-soybean Oil-based Thermosets. *J. Appl. Polym. Sci.* **2010**, *117*, 2220–2225. [CrossRef]

18. De Espinosa, L.M.; Meier, M.A. Plant Oils: The Perfect Renewable Resource for Polymer Science?! *Eur. Polym. J.* **2011**, *47*, 837–852. [CrossRef]

19. Sacristán, M.; Ronda, J.C.; Galià, M.; Cádiz, V. Synthesis and Properties of Boron-Containing Soybean Oil Based Thermosetting Copolymers. *Polymer* **2010**, *51*, 6099–6106. [CrossRef]

20. Del Rio, E.; Lligadas, G.; Ronda, J.; Galia, M.; Cadiz, V. Biobased Polyurethanes from Polyether Polyols obtained by Ionic-coordinative Polymerization of Epoxidized Methyl Oleate. *J. Polym. Sci. Part A Polym. Chem.* **2010**, *48*, 5009–5017. [CrossRef]

21. Del Rio, E.; Galia, M.; Cadiz, V.; Lligadas, G.; Ronda, J. Polymerization of Epoxidized Vegetable Oil Derivatives: Ionic-coordinative Polymerization of Methylepoxyoleate. *J. Polym. Sci. Part A Polym. Chem.* **2010**, *48*, 4995–5008. [CrossRef]

22. Yang, Y.; Shen, M.; Huang, X.; Zhang, H.; Shang, S.; Song, J. Synthesis and Performance of a Thermosetting Resin: Acrylated Epoxidized Soybean Oil Curing with a Rosin-based Acrylamide. *J. Appl. Polym. Sci.* **2017**, *134*. [CrossRef]

23. Demengeot, E.; Baliutaviciene, I.; Ostrauskaite, J.; Augulis, L.; Grazuleviciene, V.; Rageliene, L.; Grazulevicius, J.V. Crosslinking of Epoxidized Natural Oils with Diepoxy Reactive Diluents. *J. Appl. Polym. Sci.* **2010**, *115*, 2028–2038. [CrossRef]

24. Yadav, S.K.; Schmalbach, K.M.; Kinaci, E.; Stanzione, J.F.; Palmese, G.R. Recent Advances in Plant-Based Vinyl Ester Resins and Reactive Diluents. *Eur. Polym. J.* **2018**, *98*, 199–215. [CrossRef]

25. Kim, H.M.; Kim, H.R.; Kim, B.S. Soybean Oil-Based Photo-Crosslinked Polymer Networks. *J. Polym. Environ.* **2010**, *18*, 291–297. [CrossRef]

26. Chen, Z.; Wu, J.F.; Fernando, S.; Jagodzinski, K. Soy-Based, High Biorenewable Content UV Curable Coatings. *Prog. Org. Coat.* **2011**, *71*, 98–109. [CrossRef]

27. Wu, J.F.; Fernando, S.; Jagodzinski, K.; Weerasinghe, D.; Chen, Z. Effect of Hyperbranched Acrylates on UV-curable Soy-based Biorenewable Coatings. *Polym. Int.* **2011**, *60*, 571–577. [CrossRef]

28. Yang, X.; Li, S.; Xia, J.; Song, J.; Huang, K.; Li, M. Renewable Myrcene-Based UV-Curable Monomer and Its Copolymers with Acrylated Epoxidized Soybean Oil: Design, Preparation, and Characterization. *BioResources* **2015**, *10*, 2130–2142. [CrossRef]

29. Chen, Z.; Chisholm, B.J.; Patani, R.; Wu, J.F.; Fernando, S.; Jogodzinski, K.; Webster, D.C. Soy-Based UV-Curable Thiol–ene Coatings. *J. Coat. Technol. Res.* **2010**, *7*, 603–613. [CrossRef]

30. Kašėtaitė, S.; De la Flor, S.; Serra, A.; Ostrauskaitė, J. Effect of Selected Thiols on Cross-Linking of Acrylated Epoxidized Soybean Oil and Properties of Resulting Polymers. *Polymers* **2018**, *10*, 439. [CrossRef]

31. Can, E.; Wool, R.; Küsefoğlu, S. Soybean-and Castor-oil-based Thermosetting Polymers: Mechanical Properties. *J. Appl. Polym. Sci.* **2006**, *102*, 1497–1504. [CrossRef]

32. Lu, J.; Khot, S.; Wool, R.P. New Sheet Molding Compound Resins from Soybean Oil. I. Synthesis and Characterization. *Polymer* **2005**, *46*, 71–80. [CrossRef]

33. Lu, Y.; Larock, R.C. Corn Oil-based Composites Reinforced with Continuous Glass Fibers: Fabrication and Properties. *J. Appl. Polym. Sci.* **2006**, *102*, 3345–3353. [CrossRef]

34. Lu, Y.; Larock, R.C. Novel Biobased Nanocomposites from Soybean Oil and Functionalized Organoclay. *Biomacromolecules* **2006**, *7*, 2692–2700. [CrossRef] [PubMed]

35. Andjelkovic, D.D.; Larock, R.C. Novel Rubbers from Cationic Copolymerization of Soybean Oils and Dicyclopentadiene. 1. Synthesis and Characterization. *Biomacromolecules* **2006**, *7*, 927–936. [CrossRef] [PubMed]

36. Campanella, A.; Scala, J.J.L.; Wool, R. Fatty Acid-based Comonomers as Styrene Replacements in Soybean and Castor Oil-based Thermosetting Polymers. *J. Appl. Polym. Sci.* **2011**, *119*, 1000–1010. [CrossRef]

37. National Toxicology Program. Toxicology and Carcinogenesis Studies of Divinylbenzene-HP (Cas no. 1321-74-0) in F344/N Rats and B6C3F1 Mice (Inhalation Studies). *Natl. Toxicol. Program. Tech. Rep. Ser.* **2006**, *534*, 1–290.

38. Roe, F.J. Styrene: Toxicity Studies—What do they show? *Crit. Rev. Toxicol.* **1994**, *24*, s117–s125. [CrossRef]

39. Kinkead, E.; Pozzani, U.; Geary, D.; Carpenter, C. The Mammalian Toxicity of Dicyclopentadiene. *Toxicol. Appl. Pharmacol.* **1971**, *20*, 552–561. [CrossRef]

40. Fache, M.; Boutevin, B.; Caillol, S. Vanillin Production from Lignin and its use as a Renewable Chemical. *ACS Sustain. Chem. Eng.* **2015**, *4*, 35–46. [CrossRef]

41. Zhang, C.; Madbouly, S.A.; Kessler, M.R. Renewable Polymers Prepared from Vanillin and Its Derivatives. *Macromol. Chem. Phys.* **2015**, *216*, 1816–1822. [CrossRef]

42. Zhang, Y.; Thakur, V.K.; Li, Y.; Garrison, T.F.; Gao, Z.; Gu, J.; Kessler, M.R. Soybean-Oil-Based Thermosetting Resins with Methacrylated Vanillyl Alcohol as Bio-Based, Low-Viscosity Comonomer. *Macromol. Mater. Eng.* **2018**, *303*, 1700278. [CrossRef]

43. Schmidt, L.E.; Leterrier, Y.; Vesin, J.; Wilhelm, M.; Mânson, J.E. Photorheology of Fast UV-Curing Multifunctional Acrylates. *Macromol. Mater. Eng.* **2005**, *290*, 1115–1124. [CrossRef]

44. Schmidt, L.E.; Schmäh, D.; Leterrier, Y.; Mânson, J.E. Time-Intensity Transformation and Internal Stress in UV-Curable Hyperbranched Acrylates. *Rheol. Acta* **2007**, *46*, 693–701. [CrossRef]

45. Rekštytė, S.; Jonavičius, T.; Malinauskas, M. Direct Laser Writing of Microstructures on Optically Opaque and Reflective Surfaces. *Opt. Lasers Eng.* **2014**, *53*, 90–97. [CrossRef]

46. Kasetaite, S.; Ostrauskaite, J.; Grazuleviciene, V.; Bridziuviene, D.; Budreckiene, R.; Rainosalo, E. Biodegradable Photocross-Linked Polymers of Glycerol Diglycidyl Ether and Structurally Different Alcohols. *React. Funct. Polym.* **2018**, *122*, 42–50. [CrossRef]

47. Borges, A.; Bourban, P.; Pioletti, D.; Mânson, J. Curing Kinetics and Mechanical Properties of a Composite Hydrogel for the Replacement of the Nucleus Pulposus. *Compos. Sci. Technol.* **2010**, *70*, 1847–1853. [CrossRef]

48. Sarmento, V.; Frigerio, M.; Dahmouche, K.; Pulcinelli, S.H.; Santilli, C.V. Evolution of Rheological Properties and Local Structure during Gelation of Siloxane-Polymethylmethacrylate Hybrid Materials. *J. Sol. Gel. Sci. Technol.* **2006**, *37*, 179–184. [CrossRef]

49. Anseth, K.S.; Wang, C.M.; Bowman, C.N. Reaction Behaviour and Kinetic Constants for Photopolymerizations of Multi (Meth) Acrylate Monomers. *Polymer* **1994**, *35*, 3243–3250. [CrossRef]

50. Kreutzer, J.; Qin, X.; Gorsche, C.; Peterlik, H.; Liska, R.; Schubert, U. Variation of the Crosslinking Density in Cluster-Reinforced Polymers. *Mater. Today Commun.* **2015**, *5*, 10–17. [CrossRef]

51. Beyler, C.L.; Hirschler, M.M. Thermal Decomposition of Polymers. *SFPE Handb. Fire Prot. Eng.* **2002**, *2*, 111–131.

52. Kasetaite, S.; Ostrauskaite, J.; Grazuleviciene, V.; Svediene, J.; Bridziuviene, D. Camelina Oil-and Linseed Oil-based Polymers with Bisphosphonate Crosslinks. *J. Appl. Polym. Sci.* **2014**, *131*. [CrossRef]

53. Nagai, A.; Kamei, Y.; Wang, X.; Omura, M.; Sudo, A.; Nishida, H.; Kawamoto, E.; Endo, T. Synthesis and Crosslinking Behavior of a Novel Linear Polymer Bearing 1, 2, 3-triazol and Benzoxazine Groups in the Main Chain by a Step-growth Click-coupling Reaction. *J. Polym. Sci. Part A Polym. Chem.* **2008**, *46*, 2316–2325. [CrossRef]

54. Malinauskas, M.; Žukauskas, A.; Bičkauskaitė, G.; Gadonas, R.; Juodkazis, S. Mechanisms of Three-Dimensional Structuring of Photo-Polymers by Tightly Focussed Femtosecond Laser Pulses. *Opt. Express* **2010**, *18*, 10209–10221. [CrossRef] [PubMed]

55. Parkatzidis, K.; Kabouraki, E.; Selimis, A.; Kaliva, M.; Ranella, A.; Farsari, M.; Vamvakaki, M. Initiator-Free, Multiphoton Polymerization of Gelatin Methacrylamide. *Macromol. Mater. Eng.* **2018**, *303*, 1800458. [CrossRef]

56. Malinauskas, M.; Žukauskas, A.; Hasegawa, S.; Hayasaki, Y.; Mizeikis, V.; Buividas, R.; Juodkazis, S. Ultrafast Laser Processing of Materials: From Science to Industry. *Light Sci. Appl.* **2016**, *5*, e16133. [CrossRef] [PubMed]

57. Jonušauskas, L.; Gailevičius, D.; Rekštytė, S.; Baldacchini, T.; Juodkazis, S.; Malinauskas, M. Mesoscale Laser 3D Printing. *Preprints* **2018**, 2018100384. [CrossRef]

58. Jonušauskas, L.; Gailevičius, D.; Mikoliūnaitė, L.; Sakalauskas, D.; Šakirzanovas, S.; Juodkazis, S.; Malinauskas, M. Optically Clear and Resilient Free-Form μ-Optics 3D-Printed via Ultrafast Laser Lithography. *Materials* **2017**, *10*, 12. [CrossRef] [PubMed]

Influence of photoinitiator and temperature on photocross-linking kinetics of acrylated epoxidized soybean oil and properties of the resulting polymers

Migle Lebedevaite, Jolita Ostrauskaite *

Department of Polymer Chemistry and Technology, Kaunas University of Technology, Radvilenu Rd. 19, Kaunas, LT-50254, Lithuania

ABSTRACT

Acrylated epoxidized soybean oil is a very attractive photocurable starting material for synthesis of high bio-renewable content polymers with a wide range of applications, however its UV/VIS-curing kinetics studies is still lacking. A detailed investigation of photocross-linking kinetics of acrylated epoxidized soybean oil using four different photoinitiators was performed at various temperatures by real-time photorheometry for the first time. It was determined that the amount and type of photoinitiator did not affect the gel time, but influenced the final values of storage modulus (G'), which plateau values were in the range of $(1.3-3.6) \cdot 10^7$ Pa. Photocross-linking at 50 °C resulted in the faster growth of the G' values, though their plateau values were lower due to the increased oxygen inhibition by phosphine oxides. Obtained highly photocross-linked polymers exhibited high thermal stability with the thermal decomposition temperature at the weight loss of 10 % in the range of (337–352) °C and the glass transition temperature in the range of (41.1–50.9) °C. Higher amount of the used photoinitiators increased the values of elastic modulus and tensile strength of the resulting polymers, though the values of elongation at break were decreased. Phenyl bis(2,4,6-trimethylbenzoyl) phosphine oxide was the most efficient photoinitiator in smaller amount forming a highly cross-linked polymer, though ethyl (2,4,6-thimethylbenzoyl) phenyl phosphinate, as the liquid photoinitiator, facilitated its incorporation into the resin. This work could help integrate modified soybean oil into UV/VIS curing systems using the most appropriate photoinitiator and temperature, thereby reducing their environmental impact.

1. Introduction

The UV-curing of photopolymerizable systems, containing monomer/oligomer, photoinitiator and additives, has found an industrial application, mainly in coatings, varnishes, adhesives, and microelectronics (Liu et al., 2015a). These systems undergo prompt conversion from liquid monomer/oligomer into solid polymer easily by exposure to UV irradiation in the presence of photoinitiators (Sangermano et al., 2014). In recent years, more and more petroleum-derived materials are replaced by biobased compounds in UV-curing systems reducing environmental impact and even improving properties of cured products (Huang et al., 2018; Fernandes et al., 2018). The most common process for commercial, as well as biobased, acrylate and methacrylate oligomer applications is a free radical polymerization (Zhou et al., 2018). In approach to replace petroleum-based (meth)acrylates with biobased materials, investigation of the photocuring kinetics determining reaction propagation and termination mechanisms or understanding the influence of various process parameters (i.e. light intensity,

concentration and type of photoinitiator, or temperature) is crucial (Kousaalya et al., 2019; Jiang et al., 2016). Moreover, a detailed investigation of the performance of biobased materials in UV-curing systems enables their wider and easier application in various areas.

Photoinitiator is well known key factor influencing the curing speed and the throughout cure of the final layer. The effectiveness of photo-initiator in UV-curable system can be investigated employing various techniques, such as photo-differential scanning calorimetery (DSC), real-time Fourier transform infrared (RT-FTIR) or real-time photo-rheometry (Bastani and Mohseni, 2015).

Photo-DSC is the oldest (Tryson and Shultz, 1979) and extensively used evaluation method of the kinetics of UV-curing systems. Photo-DSC is used to monitor the cure kinetics by measuring the change of enthalpy during the curing (Bail et al., 2016), it is effectively suited to compare various curing conditions (Kim et al., 2017; Saenz-Dominguez et al., 2018) and different photoinitiators (Li et al., 2018; Radebner et al., 2017; Xu et al., 2018). Although, the theoretical value of the reaction enthalpy is needed for the reaction process investigation, it is not always
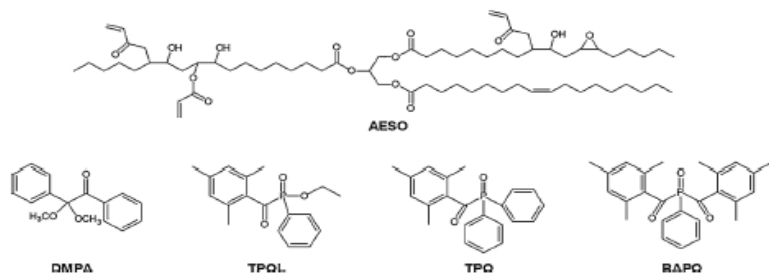
Fig. 1. Chemical structure of acrylated epoxidized soybean oil (AESO), 2,2-dimethoxy-2-phenyl acetophenone (DMPA), ethyl (2,4,6-thimethylbenzoyl) phenyl phosphinate (TPOL), diphenyl (2,4,6-trimethylbenzoyl) phosphine oxide (TPO), and phenyl bis(2,4,6-trimethylbenzoyl) phosphone oxide (BAPO).

accessible for novel and complicated systems containing a mixture of various materials (Castell et al., 2007). RT-FTIR is a likewise spread technique used for the monitoring of UV-curing reactions due to its relatively simple execution and ability to monitor prompt reactions occurring in a short time scale (Kasisomayajula et al., 2016). RT-FTIR is used to measure the conversion of the selected functional groups during the UV irradiation, in case of (meth)acrylates, the change of acrylic C=C group signal at 1637 cm^{-1} is monitored (Meereis et al., 2016). This method offers a rapid and quantitative determination of the functional groups, though poor temperature control (Kerbouc'h et al., 2004) and inaccessible monitoring of functional group conversion in deeper layers (Rusu et al., 2012) confine this method. Real-time photorheometry is a relatively new technique for the investigation of the UV-curing reaction kinetics compared to photo-DSC and RT-FTIR. Real-time photorheometry is used to monitor rheological parameters such as storage modulus (G'), loss modulus (G''), and complex viscosity (η*) defining the material mechanical properties and determining the gel point (Kasetaite et al., 2018). At the gel point the microgels, groups of highly intra-crosslinked chains, are formed and the viscosity rapidly increases defining the material transition from liquid to solid (Bassett et al., 2020; Mohammad Raei Nayini et al., 2018). By this method the influence of temperature, light intensity, concentration and type of photoinitiator to the photocross-linking process parameters, formation of the cross-linked structure, rheological and mechanical characteristics of the photocross-linked polymer can be determined.

Acrylated epoxidized soybean oil (AESO) is a bio-based material, easily cross-linked via UV-induced free radical polymerization, resulting into a highly dense polymer. It has brought a lot of researcher's attention as a replacement for synthetic (meth)acrylates in UV-curable coatings, varnishes, and even in optical 3D printing (Miao et al., 2016; Wu et al., 2019). Even though it has a wide spectrum of applications, the investigation of AESO UV-curing kinetics is still lacking. Kousaalya et al. (Kousaalya et al., 2019) performed a photocalorimetry-based kinetics study of AESO in the presence of two different photoinitiators, 2,2-dimethoxy phenylacetophenone and 1-hydroxycyclohexyl phenyl ketone. The effect of varying photoinitiator concentration, temperature, and light intensity on the extent of crosslinking were examined presenting a vast and detailed data of AESO photocuring kinetics, though thermal or mechanical properties were not examined. Studies of photocuring kinetics of initiator-free AESO-based resins (Lebedevaite et al., 2019b), three component plant-based resins (Lebedevaite et al., 2019a), and AESO with aromatic dithiols (Miezinyte et al., 2019) by real-time photorheometry have been reported by our group earlier. Although an investigation of AESO-based pressure sensitive adhesive systems by real-time photorheometry has been reported (Lee et al., 2019), however, a detailed study of AESO photocross-linking kinetics in bulk using various photoinitiators by real-time photorheometry has not yet been performed.

In this work, a detailed investigation of pure AESO photocross-linking kinetics using four different photoinitiators was performed by real-time photorheometry for the first time. The photocross-linking of AESO using the most popular near-UV photoinitiator DMPA and phosphine oxides BAPO, TPO, and TPOL was compared (Fig. 1). The influence of photoinitiator type and concentration on AESO photocross-linking rate and rheological characteristics was investigated. In order to determine the influence of temperature to the photocross-linking kinetics and rheometrical properties, the real-time photorheometry tests at different temperatures were performed. Thermal and mechanical properties of the synthesized AESO polymers were investigated and compared.

2. Experimental section

2.1. Materials

Acrylated epoxidized soybean oil (AESO, an average number of acryloyl groups per molecule calculated from the ^{1}H-NMR spectrum is 2.7 and 0.3 of epoxide groups) and 2,2-dimethoxy-2-phenyl acetophenone (DMPA) were purchased from Sigma-Aldrich. Phenyl bis(2,4,6-trimethylbenzoyl) phosphine oxide (BAPO) and diphenyl (2,4,6-trimethyl benzoyl) phosphine oxide (TPO) were purchased from Tokyo Chemical Industry. Ethyl (2,4,6-thimethylbenzoyl) phenyl phosphinate (TPOL) was purchased from Fluorochem. Chloroform and acetone were purchased from Chempur. All materials were used without further purification.

2.2. Ultraviolet–visible spectroscopy

Ultraviolet–visible (UV/VIS) spectra of photoinitiators were recorded using Lambda 35 UV/VIS spectrometer. The solutions of 0.05 % of each photoinitiator in acetone were measured in the wavelength range of (200–600) nm.

2.3. Real-time photorheometry

UV/VIS curing tests of AESO with four different photoinitiators were carried out using MCR302 rheometer from Anton Paar equipped with plate/plate measuring system. A Peltier-controlled temperature chamber with the top plate PP08 (diameter of 15 mm) and the glass plate (diameter of 38 mm) were used. The measuring gap was set to 0.3 mm. The samples were irradiated by UV/VIS radiation of (250–450) nm through the glass plate of the temperature chamber at (25–50) °C using a UV/VIS spot curing system OmniCure S2000, Lumen Dynamics Group Inc. The intensity of irradiation was 9.3 W·cm^{-2} (high pressure 200 W mercury vapor short arc). Shear mode with a frequency of 10 Hz and a strain of 0.3 % was used. Storage modulus G', loss modulus G'', loss factor $\tan\delta$ ($\tan\delta = G''/G'$), and complex viscosity η^* were recorded as a function of irradiation time (Navaruckiene et al., 2020). The onset of

91

UV/VIS irradiation was at 30 s after the experiment start for all samples.

2.4. Preparation of the cross-linked polymer specimens

The AESO was photocross-linked with four different photoinitiators: DMPA, BAPO, TPO, and TPOL. Three different concentrations, 1, 3 and 5 mol percent (mol.%), of photoinitiator were used in the resins assigned respectively (e.g. ADMPA1, ADMPA3, and etc.). The solutions of 5 mol. % of solid photoinitiators such as DMPA, BAPO and TPO were prepared in acetone, blended with AESO, and placed in a vacuum dryer to evaporate acetone. Polymer tablets were prepared by pouring the resins into the tablet-shape Teflon mold ($\varnothing$ = 15 mm, h = 3 mm) and irradiated with Helios Italquartz, model GR.E 500 W lamp with an intensity of 310 mW·cm^{-2} at the distance of 15 cm until hard polymer tablets were formed. Polymer films were prepared by pouring the resins on a polyamide film sheet using the layer forming frame with the gap of 400 μm and irradiating at the same conditions as for polymer tablets.

2.5. Chemical structure analysis

Fourier Transform Infrared Spectroscopy (FTIR) measurements of the photocross-linked polymer samples were performed on a Spectrum BX II FT-IR spectrometer. The spectra were acquired from 10 scans. The range of the wavenumber was (400–4000) cm^{-1}.

Synthesized polymers FTIR (film): υ = 3464–3469 (O–H), 2924–2885 (C–H), 1724–1733 (C = O), 1456–1378 (C–H), 1160–1186 (C–O–C), 809–813 (C–H), 724 (C–H) cm^{-1}.

2.6. Soxhlet extraction

The yield of insoluble fraction was determined by Soxhlet extraction. Samples of the photocross-linked polymers were wrapped into a filter paper package and placed into a Soxhlet apparatus. Extraction was performed with chloroform for 24 h. Insoluble fractions were dried under vacuum to a constant weight. The yield of insoluble fraction was calculated as the difference of the sample weight before and after extraction and drying.

2.7. Thermogravimetric analysis

The thermal stability of the prepared polymers was determined by thermogravimetric analysis (TGA). The measurements were performed on a TGA 4000 apparatus in a temperature range from room temperature to 800 °C at a heating rate of 20 °C min^{-1} under a nitrogen atmosphere (nitrogen flow rate was 100 mL·min^{-1}).

2.8. Differential scanning calorimetry

The glass transition temperature (T_g) of the photocross-linked polymers was estimated by differential scanning calorimetry (DSC). The measurements were performed on a Perkin Elmer DSC 8500 apparatus with a heating-cooling-heating rate of 10 °C min^{-1} under a nitrogen atmosphere (nitrogen flow rate was 50 mL·min^{-1}). The T_g value was taken as a middle point of the glass transition heat capacity step.

2.9. Mechanical testing

The mechanical properties of the photocross-linked polymer films were estimated by a tensile test (ISO 527–3) on a BDO-FB0.5TH Zwick/Roell testing machine at room temperature. Test specimens with the dimensions of (70 × 10 × 0.2) mm were cut and placed between the grips at the distance of 50 mm. Test was performed at the speed of 50 mm/min until the break of the film. Elastic modulus (E_g), tensile strength (σ) and elongation at break (ε) were determined. The mean values of the five samples of each polymer film were calculated.

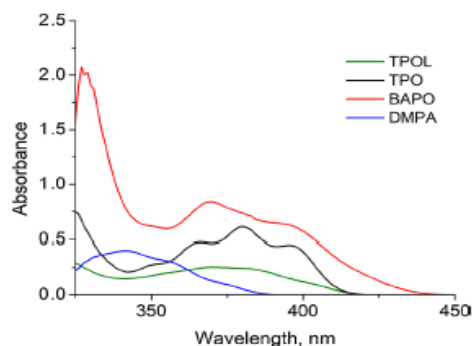The mechanical properties of the photocross-linked polymer tablets

Fig. 2. UV/VIS spectra of photoinitiators: TPOL, TPO, BAPO, and DMPA.

Table 1
Storage modulus (G') and gel time (t_{gel}) of all resins at (25-50) °C.

Resin	t_{gel} [s][a]	Storage modulus [Pa][b]			
		G'$_{25}$	G'$_{30}$	G'$_{30}$	G'$_{50}$
		Temperature			
		25 °C	30 °C	40 °C	50 °C
ADMPA1	3	3.17·10^7	2.10·10^7	2.37·10^7	2.19·10^7
ADMPA3	3	2.86·10^7	4.07·10^7	3.49·10^7	2.40·10^7
ADMPA5	3	3.61·10^7	3.84·10^7	2.88·10^7	2.37·10^7
ATPOL1	3	2.43·10^7	2.43·10^7	1.71·10^7	1.78·10^7
ATPOL3	3	3.31·10^7	2.13·10^7	1.33·10^7	2.08·10^7
ATPOL5	3	2.19·10^7	2.75·10^7	1.31·10^7	1.96·10^7
ATPO1	3	2.78·10^7	2.36·10^7	2.12·10^7	1.52·10^7
ATPO3	3	2.21·10^7	2.94·10^7	2.42·10^7	2.20·10^7
ATPO5	3	2.29·10^7	3.14·10^7	2.62·10^7	1.84·10^7
ABAPO1	3	3.19·10^7	2.46·10^7	2.27·10^7	1.44·10^7
ABAPO3	3	2.39·10^7	2.28·10^7	2.07·10^7	1.96·10^7
ABAPO5	3	1.51·10^7	2.10·10^7	1.77·10^7	1.41·10^7

[a] From the onset of UV/VIS irradiation at 25 °C.
[b] After 600 s from the beginning of the test.

were estimated by a compression test (ISO 604) on a M500–50CT Testometric apparatus. The cross-linked polymer specimen of a 15 mm diameter and 3 mm thickness was placed between circular compression platens and compressed at the speed of 5 mm/min until the specimen fracture. The mean values of the compressive modulus (E_C) of the three tablets of each polymer were calculated.

3. Results and discussion

The UV/VIS spectra of BAPO, TPO, TPOL, and DMPA were measured in the wavelength range of (325–450) nm for the purpose to evaluate and compare the absorbance intensity of each photoinitiator (Fig. 2). The irradiation absorbance of DMPA was registered below 390 nm indicating the photo-stability of this photoinitiator in the visible light region. All phosphine oxides (TPO, BAPO, and TPOL) absorbed irradiation not only in UV region but also above 400 nm, indicating the possibility of the resins with these photoinitiators to photocross-link under the visible light. This is an advantage which prevents the health issues caused by short-wavelength UV irradiation and eliminates expensive equipment, however, the handling and storing of prepared resins becomes more complicated (Ikemura and Endo, 2010). It was determined that liquid TPOL absorbed light in the same wavelength range as the solid TPO, however, the absorption was less intensive. BAPO showed the most intensive absorbance covering the widest wavelength range what indicated the highest photosensitivity allowing
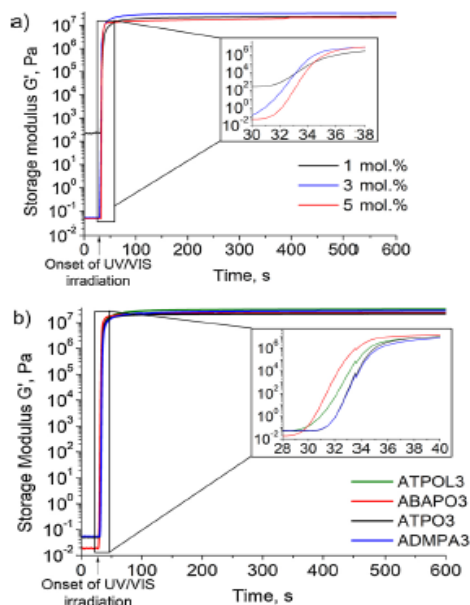
92

Fig. 3. The irradiation time dependencies of the storage modulus G' of resins with (1 -5) mol.% of TPOL (a) and with 3 mol.% of different photoinitiators (b) at 25 °C.

it to be used in smaller quantities.

Real-time photorheometry test was performed in order to investigate the photocross-linking kinetics of AESO resins. The storage modulus (G'), a measure of the deformation energy stored by the sample during the shear process and representing the elastic behavior of the material, was analyzed (Mezger, 2014). The maximal values of G' of all resins varied in the range of $(1.3–3.6) \cdot 10^7$ Pa (Table 1) indicating the formation of a hard, highly cross-linked polymers (Liu et al., 2015b). A clear dependence of the G' values on the photoinitiator concentration was observed only for the resins with BAPO at 25 °C, 30 °C and 40 °C. The irregularities of G' values of the resins with BAPO at 50 °C could have been obtained due to the increased oxygen inhibition at higher temperature leading to the formation of less cross-linked polymer. The G' values decreased with an increase of the amount of BAPO which could be explained by the competition between the reactions of primary radicals and double bonds during the initiation stage due to the higher concentration of active species, i.e. radicals (Macarie and Ilia, 2005). This shows that an optimum concentration of TPOL, DMPA and TPO was 3 mol.% and 1 mol.% of BAPO, indicating that BAPO was more efficient in smaller concentration at (25–40) °C.

The comparison of the G' curves of the resins with different concentrations of photoinitiators was carried out to determine the influence of photoinitiator to photocross-linking kinetics. As an example, the irradiation time dependencies of storage modulus G' of the resins with (1–5) mol.% of TPOL and with 3 mol.% of different photoinitiators at 25 °C are presented in Fig. 3. The gel point of all AESO resins was at 3 s after the onset of UV/VIS irradiation (Table 1), reaching the G' plateau after approximately 200 s from the onset of UV/VIS irradiation. This indicated a very high reactivity and a fast photocross-linking rate of AESO resin comparable to those of thiol-ene and acrylic systems (Ding et al., 2019; Ha, 2016; Tachi and Suyama, 2016; Zhang et al., 2018a) and
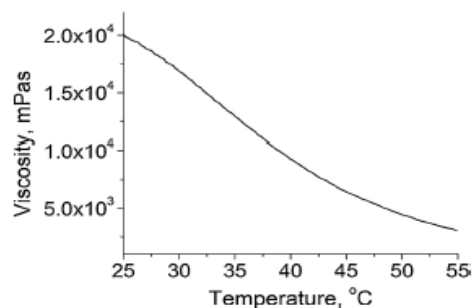
Fig. 4. Temperature dependence of AESO viscosity.

made it a considerable candidate for replacing synthetic acrylates (Neves et al., 2018). It was observed, that the concentration of photo-initiator did not influence the gel time (Table 1), but had an impact to the shape of the G' curves at the beginning of UV/VIS irradiation (Fig. 3a). The resin with 3 mol.% of TPOL (ATPOL3) reached G' plateau 1 s faster than the resin ABAPO5, considering it as an optimum concentration of TPOL (Fig. 3a). The resin ATPOL5 reached G' plateau the second, it was followed by the resin ATPOL1 with the lowest concentration of free radicals and presumably the smallest amount of active centers. Several reports claimed that the curing rate and the degree of polymerization of resin will at first rise with the increased concentration
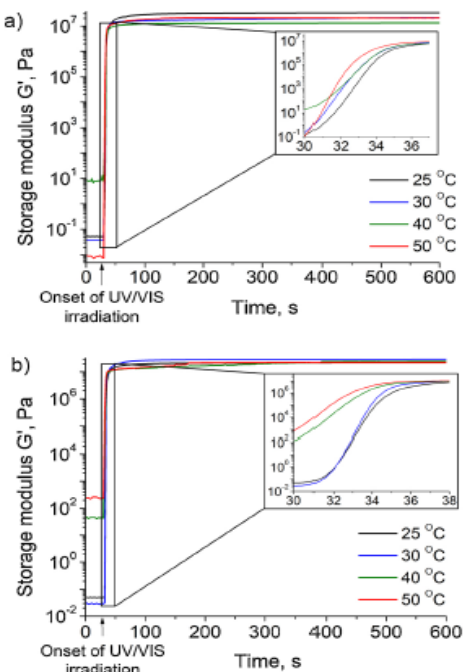
Fig. 5. The irradiation time dependencies of the storage modulus G' of resin with 3 mol.% of TPOL (a) and TPO (b) at (25–50) °C.

of photoinitiator, and after passing through a maximum or an optimum concentration, the effect will rapidly decline (Doğruyol et al., 2010). At higher photoinitiator concentrations, a higher concentration of free radicals at the surface are generated, which block the sufficient energy from penetrating, leading to the decreased rate of polymerization (Doğruyol et al., 2012). This phenomenon could be seen in the cases of the resins (ATPOL5, ATPO3, ABAPO5) with the highest concentration of photoinitiator which did not reach the highest G' values. Comparing the photocross-linking kinetics of AESO resins with different photo-initiators, the plateau of the G' values was reached in the distinctive time (Fig. 3b) even the gel time did not change. This showed the higher reactivity of BAPO and its ability to generate free radicals the fastest, which enabled the rapid photocross-linking of AESO.

AESO contains acryl and hydroxyl functionalities which participate in hydrogen bonding formation between the triglyceride molecules and increase the viscosity of AESO (Liu et al., 2015c), which is around 20,000 mPa·s (Zhang et al., 2018b). AESO could be diluted with various reactive or inert diluents, but mechanical and thermal properties of the cross-linked polymer could be changed in such case.

Viscosity could also be controlled by a temperature change, which facilitates the AESO processability due to the improved mobility of polymer chains at higher temperatures (Liu et al., 2016). The dependency of AESO viscosity at (25–55) °C is presented in Fig. 4. The AESO viscosity dropped from 20,000 mPa·s at 25 °C to 3000 mPa·s at 55 °C exponentially with an increase of temperature, which can be fitted with the Arrhenius equation (Campanella et al., 2009; Khan et al., 2018). This 17,000 mPa·s viscosity descent in the mentioned temperature range enables the improvement of AESO processability (Palmer Holland, 2018).

The dependencies of AESO photocross-linking rate and rheological characteristics on the reaction temperature and AESO viscosity were investigated by the real-time photorheometry. The irradiation time dependencies of the storage modulus G' of ATPOL3 and ATPO3 at (25–50) °C are presented in Fig. 5. It was observed that the temperature did not have any influence to the gel point (Table 1), even though the slight changes in storage modulus curves were observed, the crossover point of G' and G'' did not changed. It was noticed, that the higher temperature was, the more vertical G' curve, after the start of the UV irradiation, was registered. It demonstrated the faster formation of the AESO photocross-linked polymer network at higher temperature which was due to the increased Brownian motion at higher temperature enabling the faster free radical migration and leading to the more rapid active center occurrence and the higher cross-linking rate (Steyrer et al., 2018). Although, the reduction of the G' plateau values at higher temperature was observed due to the formation of more lineal or branched chains in the polymer network or due to the increased thermal motions. This phenomenon was also observed during photocross-linking of AESO with other photoinitiators. Comparing the photocross-linking kinetics of the resins with TPOL and TPO (Fig. 5), the higher reactivity of TPO at higher temperature could be seen. The G' plateau of the resin ATPO3 at 40 °C and 50 °C was reached 1 s faster than that at lower temperatures. This showed that TPO was more reactive at higher temperatures and faster cleaved into free radicals than the liquid TPOL indicating the faster photocross-linking. Such temperature influence on the degree of conversion was also reported by Kousaalya et al (Kousaalya et al., 2019), where the effect of type and concentration of photoinitiator, DMPA or 1-hydroxycyclohexyl phenyl ketone, light intensity, and temperature on the extent of cross-linking was calculated from the ratio of experimentally measured reaction enthalpy and the theoretical enthalpy of reaction by photo-DSC method.

UV-curing at higher temperature enables better resin processability because the descent of viscosity and the increased curing depth is observed. However, oxygen inhibition in films increases with an increase of temperature due to the faster diffusion of oxygen (Studer et al., 2003). This phenomenon was also noticed when AESO resin was cured at 50 °C. The irradiation time dependencies of the storage modulus G' of
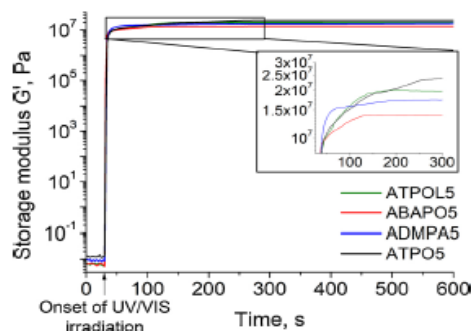
Fig. 6. The irradiation time dependencies of the storage modulus G' of resin with 5 mol.% of photoinitiator at 50 °C.

Table 2
The yield of insoluble fraction, thermal and mechanical characteristics of the cross-linked polymers.

Polymer	YIF [%][a]	$T_{dec-10\%}$ [°C][b]	T_g [°C][c]	E_C [MPa][d]	E_E [MPa][e]	δ [MPa][f]	ε [%][g]
ADMPA1	97.6	338	47.5	323 ± 24	199 ± 7	4.34 ± 0.8	1.67 ± 0.32
ADMPA3	97.9	342	48.1	335 ± 62	273 ± 11	5.48 ± 0.99	1.5 ± 0.36
ADMPA5	97.8	340	44.2	359 ± 32	325 ± 7	5.15 ± 0.47	0.47 ± 0.12
ATPOL1	97.7	337	50.9	318 ± 46	239 ± 30	5.59 ± 0.86	2.48 ± 0.42
ATPOL3	97.2	337	46.6	384 ± 32	487 ± 11	4.95 ± 1.02	0.93 ± 0.2
ATPOL5	96.6	348	46.2	350 ± 35	544 ± 12	6.23 ± 0.98	1.07 ± 0.22
ATPO1	97.5	342	46.4	373 ± 20	135 ± 5	4.23 ± 0.83	3.02 ± 1.05
ATPO3	96.1	340	41.1	359 ± 20	279 ± 3	5.39 ± 1.01	1.6 ± 0.36
ATPO5	97.9	337	44.7	350 ± 13	292 ± 15	5.23 ± 0.75	1.3 ± 0.19
ABAPO1	97.2	352	45.7	392 ± 33	205 ± 8	4.53 ± 0.38	1.9 ± 0.17
ABAPO3	97.4	346	46.1	383 ± 24	240 ± 16	5.56 ± 1.83	2.4 ± 1.3
ABAPO5	97.1	345	45.7	401 ± 22	490 ± 33	5.42 ± 0.35	0.93 ± 0.07

[a] Yield of insoluble fraction (YIF) after the Soxhlet extraction with chloroform for 24 h.
[b] Temperature at the weight loss of 10 % obtained from TGA curves.
[c] Glass transition temperature obtained from DSC curves.
[d] Compressive modulus from the polymer tablet compression test.
[e] Elastic modulus from the polymer film tensile test.
[f] Tensile strength from the polymer film tensile test.
[g] Elongation at break from the polymer film tensile test.

the AESO resin with 5 mol.% of photoinitiator at 50 °C are shown in Fig. 6. It was observed, that G' plateau was reached slower at higher temperature than that at room temperature. Furthermore, the highest sensitivity to oxygen of investigated phosphine oxides was observed due to the very high sensitivity of phosphonyl radical to oxygen (Green,

Fig. 7. Thermogravimetric curves of polymers with 5 mol.% of photoinitiator.

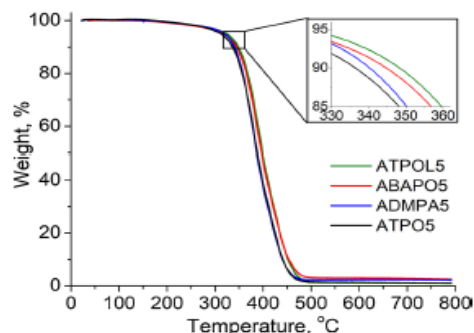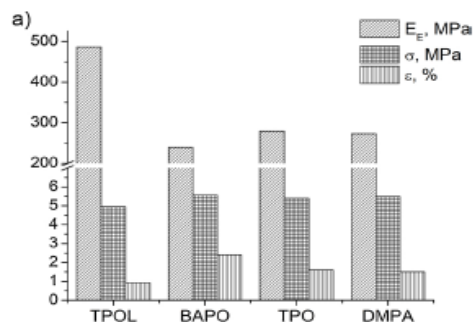Fig. 8. Elastic modulus (E_E), tensile strength (σ) and elongation at brake (ε) of cross-linked polymers with 3 mol. % of photoinitiator (a); a broken polymer film specimen after the tensile test (b).

2010). Although, DMPA did not suffer from the oxygen inhibition, which makes it a suitable photoinitiator in the UV-curing systems at higher temperature. It was noticed that the resin ATPO5 G' plateau was reached the latest, indicating the highest sensitivity to oxygen from all photoinitiators used in this study. Though resins ATPOL5 and ABAPO5 reached G' plateau at the similar time, the G' values of the resin ATPOL5 was higher, indicating not just the more cross-linked polymer formation, but also an immense advantage of liquid photoinitiator.

Thermal properties of the synthesized AESO polymers were investigated by DSC and TGA. DSC confirmed that all synthesized polymers were amorphous materials. Only the glass transition (T_g) was observed in the thermograms of the cross-linked polymers. The glass transition temperature of the photocross-linked polymers was in the range of (41.1–50.9) °C (Table 2) and was higher than those of the photocross-linked initiator-free AESO polymers (-4.5 °C) (Lebedevaite et al., 2019b). This immense differences between T_g values could occure due to the divergence in the yield of insoluble fraction. The yield of insoluble fraction of AESO polymers synthesized with photoinitiators was higher, thus the higher T_g values were observed. The relation between the yield of insoluble fraction and the T_g was clearly observed in the case of the polymer ATPO3 when the lowest values of the yield of insoluble fraction (96.1 %) and the T_g (41.1 °C) were obtained. This tendency correlated with that of other synthesized polymers in this study. It was observed, that the highest T_g value was not reached by any polymer with 5 mol.% of the used photoinitiators, indicating the excess amount of photoinitiator. Although, the T_g of 65 °C of the AESO polymer photocross-linked with nearly 5 wt.% of DMPA was reported (Rengasamy and Mannari, 2013). This difference of T_g values could be explained by the used amount of DMPA which was higher nearly five times than that used in this study, also, this could happen due to the different measuring parameters, system or the measuring conditions (Pelletier et al., 2006).

TGA confirmed that all photocross-linked polymers exhibited high thermal stability. TGA curves of the polymers with 5 mol.% of photoinitiator are presented in Fig. 7. It was observed that the polymer ATPOL5 showed the highest temperature at the weight loss of 10 % (T_{dec}.10 %) from this group of polymers, indicating the highest thermal stability which was determined by the higher density of the cross-linked network (Ma et al., 2014). Although, when 1 mol.% of photoinitiator was used, the T_{dec}.10 % of ABPO1 was the highest, demonstrating the highly cross-linked network, which implied the highest BAPO efficiency in smaller amount. The T_{dec}.10 % of the synthesized polymers varied from 337 °C to 352 °C (Table 2).

The mechanical properties of the photocross-linked AESO polymers were evaluated by the tensile and compression tests. Mechanical characteristics of the photocross-linked AESO polymer films and the photo of
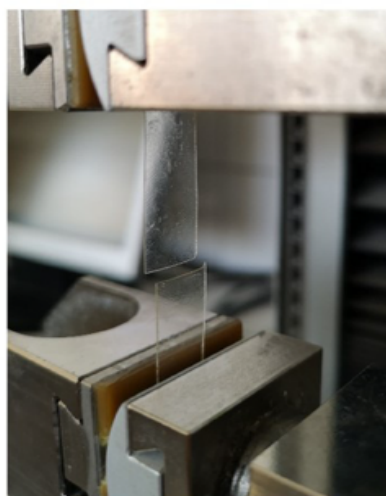
the broken specimen after the tensile test are shown in Fig. 8. Though the tensile strength values varied in the narrow range of (4.95–5.56) MPa, the immense higher E_E values of the polymer ATPOL3 indicated a significant efficiency of TPOL. An increment of the elastic modulus (E_E) and the decline of the elongation at break (ε) were observed when higher amount of photoinitiator was used (Table 2). This showed, that when 5 mol.% of photoinitiator was used, the stronger and stiffer photocross-linked AESO polymer films were formed. The UV-cured AESO polymer films with 3 wt.% of DMPA and specimen dimensions of 80 mm x 8 mm x 0.5 mm showed about 40 MPa of E_E and nearly 13 % of ε (Ma et al., 2014), while the polymer films with 2 wt.% of DMPA and specimen dimensions of 45 mm x 5 mm x 0.17 mm indicated nearly 20 % of ε (Kim et al., 2010). In both papers higher ε values of AESO films were reported, although more narrow and thinner specimens were used in tensile test, which could be the main reason indicating the differences in the ε values.

Most of the reported studies of the structural changes of polymers caused by deformation were performed in a tensile mode. From a
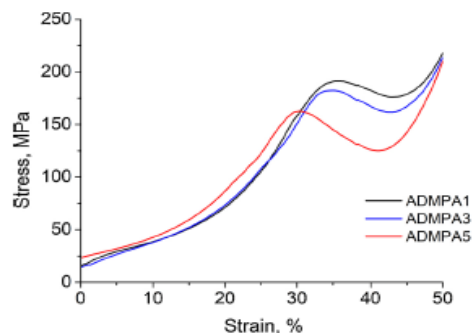
Fig. 9. Stress-strain curves of polymer tablets with DMPA.

fundamental point of view, deformation by compression is more important because of its great advantage that the deformation is nearly a homogenous process, and occurs without any significant deformation instabilities, such as neck formation observed in the tensile test (Galeski, 2003). The stress-strain curves of the AESO polymer tablets obtained using DMPA are presented in Fig. 9. The similar shape of the curves was observed for other AESO polymers as well. At the beginning, the usual elastic response was observed (up to 30 % of strain) followed by the sudden drop of the stress showing a sample fracturing. This is a typical compression stress-strain curve of a brittle amorphous polymer, such as polymethylmethacrylate, indicating its structural similarities to AESO polymers (Swallowe and Lee, 2006). The compressive modulus (E_C) values of the photocross-linked polymer tablets varied in the range of (318–401) MPa (Table 2). It was observed, that E_C values were increased alongside with the amount of DMPA used, although nearly the lowest values of E_C were obtained compared to the other polymers in this study. However, no clear dependency of the photoinitiator concentration on E_C of the polymers synthesized with BAPO, TPOL and TPO was observed. This irregularity of the data collected from polymers synthesized with different amount of photoinitiator can be explained by the close E_C values that overlap within the standard deviation range. The highest values of E_C were indicated for the photocross-linked polymers with BAPO. These differences between E_C of the polymers synthesized with different photoinitiators could be explained by the highest absorbance and sensitivity to the visible light of BAPO in comparison to the all used photoinitiators, while DMPA absorbed UV irradiation only in lower intensity.

4. Conclusions

The real-time photorheometry study revealed the high cross-linking rate of AESO with all investigated photoinitiators. Photocross-linking at higher temperature indicated the faster polymer network formation though the increased oxygen inhibition occurred and the smaller values of storage modulus were obtained. Formed highly cross-linked AESO polymers exhibited high thermal stability with the thermal decomposition temperature at the weight loss of 10 % in the range of (337–352) °C and the glass transition temperature in the range of (41.1–50.9) °C. Higher amount of photoinitiator in the AESO resins caused the higher values of elastic modulus and tensile strength of the photocross-linked polymers, but the lower values of elongation at break. 3 mol.% of photoinitiator was considered as an optimum concentration leading to the most favorable thermal and mechanical properties of the polymer without an excess of photoinitiator. This work could help integrate modified soybean oil into UV/VIS curing systems using the most appropriate photoinitiator and temperature, thereby reducing their

environmental impact.

Credit author statement

M.L. and J.O. conceived and designed the experiments, analyzed the data.

M.L. performed all experiments and characterizations.

M.L. and J.O. contributed to writing the manuscript.

Declaration of Competing Interest

The authors declare that they have no known competing financial interests or personal relationships that could have appeared to influence the work reported in this paper.

Acknowledgements

References

Bail, R., Hong, J.Y., Chin, B.D., 2016. Effect of a red-shifted benzotriazole UV absorber on curing depth and kinetics in visible light initiated photopolymer resins for 3D printing. J. Ind. Eng. Chem. 38, 141–145.

Bassett, A.W., Honnig, A.E., Breyta, C.M., Dunn, I.C., La Scala, J.J., Stanzione, I., Joseph, F., 2020. Vanillin-based resin for additive manufacturing. ACS Sustain. Chem. Eng.

Bastani, S., Mohseni, M., 2015. UV-curable nanocomposite coatings and materials. Anonymous Handbook of Nanoceramic and Nanocomposite Coatings and Materials. Elsevier, pp. 155–182.

Campanella, A., La Scala, J.J., Wool, R.P., 2009. The use of acrylated fatty acid methyl esters as styrene replacements in triglyceride-based thermosetting polymers. Polym. Eng. Sci. 49, 2384–2392.

Castell, P., Wouters, M., Fischer, H., 2007. Kinetic studies of a UV-curable powder coating using photo-DSC, real-time FTIR and rheology. J. Coat. Technol. Res. 4, 411–423.

Ding, R., Du, Y., Goncalves, R.B., Francis, L.F., Reineke, T.M., 2019. Sustainable near UV-curable acrylates based on natural phenolics for stereolithography 3D printing. Polym. Chem. 10, 1067–1077.

Doğruyol, Z., Karasu, F., Temel, G., Balta, D., Aydın, M., Keskin, S., Pekcan, Ö, Arsu, N., 2010. Basics and Applications of Photopolymerization Reactions, Chapter XI. Research Signpost, Kerala, India.

Doğruyol, Z., Arsu, N., Doğruyol, S.K., Pekcan, Ö, 2012. Producing critical exponents from gelation for various photoinitiator concentrations; a photo differential scanning calorimetric study. Prog. Org. Coat. 74, 181–185.

Fernandes, F.C., Kirwan, K., Wilson, P.R., Coles, S.R., 2018. Optimisation of waste vegetable oil-based thermoset polymers. Green Mater. 6 (1), 38–46.

Galeski, A., 2003. Strength and toughness of crystalline polymer systems. Prog. Polym. Sci. 28, 1643–1699.

Green, W.A., 2010. Industrial Photoinitiators: A Technical Guide. CRC Press.

Ha, K., 2016. A study on radial spreading of a resin droplet with varying viscosity under UV curing process. J. Mech. Sci. Technol. 30, 1649–1658.

Huang, J., Yuan, T., Ye, X., Man, L., Zhou, C., Hu, Y., Zhang, C., Yang, Z., 2018. Study on the UV curing behavior of tung oil: mechanism, curing activity and film-forming property. Ind. Crops Prod. 112, 61–69.

Ikemura, K., Endo, T., 2010. A review of the development of radical photopolymerization initiators used for designing light-curing dental adhesives and resin composites. Dent. Mater. J. 1009140075-1009140075.

Jiang, L., Xiong, W., Zhou, Y., Liu, Y., Huang, X., Li, D., Baldacchini, T., Jiang, L., Lu, Y., 2016. Performance comparison of acrylic and thiol-acrylic resins in two-photon polymerisation. Opt. Express 24 (12), 13687–13701.

Kasetaite, S., Ostrauskaite, J., Grazuleviciene, V., Bridziuviene, D., Budreckiene, R., Rainosalo, E., 2018. Biodegradable photocross-linked polymers of glycerol diglycidyl ether and structurally different alcohols. React. Funct. Polym. 122. Amsterdam: Elsevier, 2018.

Kasisomayajula, S., Jadhav, N., Gelling, V.J., 2016. Conductive polypyrrole and acrylate nanocomposite coatings: mechanistic study on simultaneous photopolymerization. Prog. Org. Coat. 101, 440–454.

Kerbouc'h, P., Lebaudy, P., Lecamp, L., Bunel, C., 2004. Numerical simulation to correlate photopolymerization kinetics monitoring by RT-NIR spectroscopy and photocalorimetry. Thermochim. Acta 410, 73–78.

Khan, M.I., Qayyum, S., Hayat, T., Waqas, M., Khan, M.I., Alsaedi, A., 2018. Entropy generation minimization and binary chemical reaction with Arrhenius activation energy in MHD radiative flow of nanomaterial. J. Mol. Liq. 259, 274–283.

Kim, H., Kim, H., Kim, B.S., 2010. Soybean oil-based photo-crosslinked polymer networks. J. Polym. Environ. 18, 291–297.

Kim, Y.C., Hong, S., Sun, H., Kim, M.G., Choi, K., Cho, J., Choi, H.R., Koo, J.C., Moon, H., Byun, D., 2017. UV-curing kinetics and performance development of in situ curable 3D printing materials. Eur. Polym. J. 93, 140–147.

Kousaalya, A.B., Ayalew, B., Pilla, S., 2019. Photopolymerization of acrylated epoxidized soybean oil: a photocalorimetry-based kinetic study. ACS Omega.

Lebedevaite, M., Ostrauskaite, J., Skliutas, E., Malinauskas, M., 2019a. Photocross-linked polymers based on plant-derived monomers for potential application in optical 3D printing. J. Appl. Polym. Sci. 48708.

Lebedevaite, M., Ostrauskaite, J., Skliutas, E., Malinauskas, M., 2019b. Photoinitiator free resins composed of plant-derived monomers for the optical μ-3D printing of thermosets. Polymers 11, 116.

Lee, T.H., Park, Y.I., Lee, S., Shin, J., Noh, S.M., Kim, J.C., 2019. A crack repair patch based on acrylated epoxidized soybean oil. Appl. Surf. Sci. 476, 276–282.

Li, T., Su, Z., Xu, H., Jiang, X., Ma, X., Yin, J., 2018. Hyperbranched poly (ether amine) (hPEA) as novel backbone for amphiphilic one-component type-II polymeric photoinitiators. Chin. Chem. Lett. 29, 451–455.

Liu, F., Wang, Y., Xue, X., Yang, H., 2015a. UV curable EA-Si hybrid coatings prepared by combination of radical and cationic photopolymerization. Prog. Org. Coat. 85, 46–51.

Liu, K., Madbouly, S.A., Kessler, M.R., 2015b. Biorenewable thermosetting copolymer based on soybean oil and eugenol. Eur. Polym. J. 69, 16–28.

Liu, Q., Li, M., Gu, Y., Wang, S., Zhang, Y., Li, Q., Gao, L., Zhang, Z., 2015c. Interlocked CNT networks with high damping and storage modulus. Carbon 86, 46–53.

Liu, W., Xie, T., Qiu, R., 2016. Biobased thermosets prepared from rigid isosorbide and flexible soybean oil derivatives. ACS Sustain. Chem. Eng. 5, 774–783.

Ma, S., Jiang, Y., Liu, X., Fan, L., Zhu, J., 2014. Bio-based tetrafunctional crosslink agent from gallic acid and its enhanced soybean oil-based UV-cured coatings with high performance. RSC Adv. 4, 23036–23042.

Macarie, L., Ilia, G., 2005. The influence of temperature and photoinitiator concentration on photoinitiated polymerization of diacrylate monomer. Open Chem. 3, 721–730.

Meereis, C.T., Leal, F.B., Ogliari, F.A., 2016. Stability of initiation systems in acidic photopolymerizable dental material. Dent. Mater. 32, 889–898.

Mezger, T.G., 2014. The Rheology Handbook: For Users of Rotational and Oscillatory Rheometers, 4th ed. Vincentz Network, GmbH & Co KG, Hanover, Germany.

Miao, S., Zhu, W., Castro, N.J., Nowicki, M., Zhou, X., Cui, H., Fisher, J.P., Zhang, L.G., 2016. 4D printing smart biomedical scaffolds with novel soybean oil epoxidized acrylate. Sci. Rep. 6, 27226.

Miezinyte, G., Ostrauskaite, J., Rainosalo, E., Skliutas, E., Malinauskas, M., 2019. Photoresins based on acrylated epoxidized soybean oil and benzenedithiols for optical 3D printing. Rapid Prototyp. J.

Mohammad Raei Nayini, M., Bastani, S., Moradian, S., Croutxé-Barghorn, C., Allonas, X., 2018. Manipulating the surface structure of hybrid UV curable coatings through photopolymerization-induced phase separation: influence of inorganic portion and photoinitiator content. Macromol. Chem. Phys. 219, 1700377.

Navaruckiene, A., Skliutas, E., Kasetaite, S., Rekštytė, S., Raudoniene, V., Bridžiuviene, D., Malinauskas, M., Ostrauskaite, J., 2020. Vanillin acrylate-based resins for optical 3D printing. Polymers 12, 397.

Neves, J., Valadares, L., Machado, F., 2018. Tailoring acrylated soybean oil-containing terpolymers through emulsion polymerization. Colloids Interfaces 2, 46.

Palmer Holland, 2018. Allnex Ebecryl 860 Technical Data Sheet.

Pelletier, H., Belgacem, N., Gandini, A., 2006. Acrylated vegetable oils as photocrosslinkable materials. J. Appl. Polym. Sci. 99, 3218–3221.

Radebner, J., Eibel, A., Leypold, M., Gorsche, C., Schuh, L., Fischer, R., Torvisco, A., Neshchadin, D., Geier, R., Moszner, N., 2017. Tetraacylgermanes: highly efficient photoinitiators for visible-light-induced free-radical polymerization. Angew. Chemie Int. Ed. 56, 3103–3107.

Rengasamy, S., Mannari, V., 2013. Development of soy-based UV-curable acrylate oligomers and study of their film properties. Prog. Org. Coat. 76, 78–85.

Rusu, M.C., Block, C., Van Assche, G., Van Mele, B., 2012. Influence of temperature and UV intensity on photo-polymerization reaction studied by photo-DSC. J. Therm. Anal. Calorim. 110, 287–294.

Saenz-Dominguez, I., Tena, I., Sarrionandia, M., Torre, J., Aurrekoetxea, J., 2018. Effect of ultraviolet curing kinetics on the mechanical properties of out of die pultruded vinyl ester composites. Compos. Part A Appl. Sci. Manuf. 109, 280–289.

Sangermano, M., Razza, N., Crivello, J.V., 2014. Cationic UV-curing: technology and applications. Macromol. Mater. Eng. 299, 775–793.

Steyrer, B., Busetti, B., Harakály, G., Liska, R., Stampfl, J., 2018. Hot Lithography vs. Room temperature DLP 3D-printing of a dimethacrylate. Addit. Manuf. 21, 209–214.

Studer, K., Decker, C., Beck, E., Schwalm, R., 2003. Overcoming oxygen inhibition in UV-curing of acrylate coatings by carbon dioxide inerting, Part I. Prog. Org. Coat. 48, 92–100.

Swallowe, G., Lee, S., 2006. Quasi-static and dynamic compressive behaviour of poly (methyl methacrylate) and polystyrene at temperatures from 293 K to 363 K. J. Mater. Sci. 41, 6280–6289.

Tachi, H., Suyama, K., 2016. Photo-induced polymerization and degradation of formulations containing photolabile crosslinkers monitored in a rheometer. J. Photopolym. Sci. Technol. 29, 139–142.

Tryson, G., Shultz, A., 1979. A calorimetric study of acrylate photopolymerization. J. Polym. Sci. Polym. Phys. Ed. 17, 2059–2075.

Wu, B., Sufi, A., Ghosh Biswas, R., Hisatsune, A., Moxley-Paquette, V., Ning, P., Soong, R., Dicks, A.P., Simpson, A.J., 2019. Direct conversion of McDonald's waste cooking oil into a biodegradable high resolution 3D printing resin. ACS Sustain. Chem. Eng.

Xu, J., Jiang, Y., Zhang, T., Dai, Y., Yang, D., Qiu, F., Yu, Z., Yang, P., 2018. Synthesis of UV-curing waterborne polyurethane-acrylate coating and its photopolymerization kinetics using FT-IR and photo-DSC methods. Prog. Org. Coat. 122, 10–18.

Zhang, C., Dong, Q., Liang, K., Zhou, D., Yang, H., Liu, X., Xu, W., Zhou, Y., Xiao, P., 2018a. Photopolymerizable thiol-acrylate maleiated hyaluronic acid/thiol-terminated poly (ethylene glycol) hydrogels as potential in-situ formable scaffolds. Int. J. Biol. Macromol. 119, 270–277.

Zhang, Y., Thakur, V.K., Li, Y., Garrison, T.F., Gao, Z., Gu, J., Kessler, M.R., 2018b. Soybean-oil-Based thermosetting resins with methacrylated vanillyl alcohol as bio-based, low-viscosity comonomer. Macromol. Mater. Eng. 303, 1700278.

Zhou, J., Allonas, X., Liu, X., 2018. Fluorinated organozirconiums: enhancement of overcoming oxygen inhibition in the UV-curing film. Prog. Org. Coat. 120, 228–233.

97

ARTICLE

High biorenewable content acrylate photocurable resins for DLP 3D printing

Migle Lebedevaite[1] | Vaidas Talacka[2] | Jolita Ostrauskaite[1]

[1]Department of Polymer Chemistry and Technology, Kaunas University of Technology, Kaunas, Lithuania

[2]AmeraLabs, Kaunas, Lithuania

Correspondence
Jolita Ostrauskaite, Department of Polymer Chemistry and Technology, Kaunas University of Technology, Radvilenu Rd. 19, 50254 Kaunas, Lithuania.
Email: jolita.ostrauskaite@ktu.lt

Funding information
Interreg, Grant/Award Number: R077

Abstract

Green chemistry and green engineering concepts have been combined to develop novel sustainable polymeric materials. Solvent free photocurable acrylate resins with biorenewable carbon content of 75%–82% suitable for application in DLP 3D printing technology were composed by commercially available bio-based materials, acrylated epoxidized soybean oil (AESO), isobornyl methacrylate (IBOMA), methacrylic ester (ME), tetrahydrofurfuryl acrylate (THFA), and tetrahydrofurfuryl methacrylate (THFMA). They demonstrated high printing accuracy and good adhesion between layers. The monitoring of photocross-linking kinetics of high biorenewable content acrylate photoresins by the real-time photorheometry and analysis of their rheological parameters was carried out. Synthesized polymers exhibited high yield of insoluble fraction and thermal decomposition temperature at the weight loss of 10% above 300°C. Polymers AESO/IBOMA and AESO/THFMA showed the highest values of tensile modulus and tensile strength. Biodegradability of the synthesized polymers AESO/ME, AESO/THFA, and AESO/THFMA was investigated by measuring oxygen consumption in a closed respirometer. Such AESO-based polymers can be a competitive solution to replace petroleum-derived polymeric materials in additive manufacturing and reduce the environmental impact.

KEYWORDS

applications, biopolymers and renewable polymers, cross-linking, photopolymerization, thermosets

1 | INTRODUCTION

Additive manufacturing, usually known as 3D printing, is a technique brought in a few decades ago to manufacture objects, mainly for prototyping. 3D printing is a group of methods, which could apply processes as extrusion, direct energy deposition, powder solidification, sheet lamination, and photopolymerization.[1] Digital light processing (DLP) is an optical 3D printing technology employing vat photopolymerization for construction of complex shapes and high design flexibility.[2] DLP uses high-resolution light engines which can precisely polymerize a thin layer of a photocurable resin reaching a precision of tens micrometers in X-, Y-, and Z-axes.[3] Another advantage of DLP process is the low consumption of raw materials[4] along with achieving high-resolution products by green engineering principles. In such technology, the replacement of petroleum-derived materials by materials derived from renewable resources will give the ecological and economic benefits due to their low toxicity and high biodegradability, improved recovery and

recycling options, and reduce greenhouse gas emission.[5]

In the past decade, optical 3D printing of bio-based materials has emerged employing epoxidized linseed oil,[3] modified gelatin,[6] vanillin,[7–9] camphene,[1,10] isosorbibe derivatives,[11] and others. Ding et al.[12] successfully printed a bio-based resin consisting of guaiacyl methacrylate, eugenol acrylate, and vanillyl alcohol dimethacrylate, ratio 60:20:20 mol% with 2 wt% of TPO as photoinitiator using a commercial desktop stereolithographic 3D printer with 405 nm violet laser source. Printed objects formed from softwood lignin exhibited glass transition temperature up to 130°C, tensile modulus, tensile strength, and thermal stability suitable for high performance optical 3D printing.

Soybean oil derivatives have brought a huge interest in prototyping of bio-based materials. The advantage of using soybean oil is that it is biocompatible and possesses reactive unsaturated double bonds, which make it easier to functionalize than PCL and PLA.[13] Soybean oil is a common feedstock for bio-based-vinyl ester resins because it is comparatively inexpensive and easily available.[14] Due to a high number of unsaturated sites in triglyceride, acrylate, or methacrylate groups can be introduced to soybean oil through hydroxy and epoxy functionalities resulting in its higher reactivity in photocross-linking reactions. Acrylated epoxidized soybean oil (AESO) available under trademark Ebecryl 860 is being widely used in plastics and coating industry exhibiting good flow and leveling, and improving flexibility.[15]

A microstructuring of initiator-free AESO[16] and a larger scale prototyping of AESO with commercial photoinitiator Irgacure 819 have been reported.[17–19] Although printed parts were free-standing solid polymeric materials, the prototyping of pure AESO had been challenging and time-consuming process due to the high viscosity of AESO. The AESO viscosity could be reduced by adding reactive diluents (RD) which participate in cross-linking reaction without deterioration of mechanical properties. Petroleum-based RDs, such as isobornyl acrylate,[20] trimethylolpropane trimethacrylate[21–23] tripropylene glycol diacrylate with dipropylene glycol diacrylate,[24] styrene[25] have been extensively used for the synthesis of novel AESO-based UV-cured coatings and composites, controlling AESO viscosity and improving mechanical properties of cured polymers. As the demand of bio-based material grows, researchers are focusing on the synthesis of bio-based RDs, such as acrylated sucrose,[26] mycene derivative,[27] itaconic acid derivative,[28] eugenol-based acrylates,[29,30] vanillin dimethacrylate[31] tetrahydrofurfuryl acrylate (THFA),[32] and fatty acid-based acrylates,[33] for AESO-based UV-cured coatings. Ma

et al.[34] synthesized gallic acid-based cross-linking agent (GACA) and copolymerized it with AESO under UV radiation. It resulted in the higher gel content, cross-linking density, tensile strength, and modulus, as well as much better coating properties of GACA cross-linked AESO networks than those of synthetic triallyl isocyanurate (TAIC) cross-linked AESO networks. It was proved that bio-based GACA could replace petroleum-based cross-linking agents and the high-performance AESO-based UV-cured coatings with the high bio-based carbon content could be achieved.

Optical 3D printing of AESO-based resins with bio-renewable carbon content of 77%–80% has been performed by Guit et al.[35] Synthesized soybean oil (meth) acrylates with different functionality were photocross-linked with bio-based monofunctional RDs isobornyl methacrylate (IBOMA) and tetrahydrofurfuryl methacrylate (THFMA). Manufactured parts demonstrated complete layer fusion and accurate print quality with competitive thermal and mechanical properties employing bio-based materials, which can reduce the usage of petroleum-derived materials in additive manufacturing and thus the negative environmental impact of this technology. Although the mechanical and thermal properties of 3D printed parts were investigated, the biodegradability of fully bio-based 3D printed parts was not examined.

Biodegradability of soybean oil-based polymers could be predicted due to biodegradable triglyceride moieties,[36] through various RDs, cross-linkers, and additives change the structure and density of cross-links and affect biodegradability of polymers. About 15%–16% of thermally cross-linked AESO and vanillin dimethacrylate thermosets degraded after a 3-month soil burial test.[37] About 25% of 50% AESO blends with polyurethane acrylate biodegraded in the presence of the soft-rot fungus *Chaetomium globosum* after 130 days of exposure,[38] while only about 6% of poly(ethylene glycol) diacrylate photocross-linked with the same amount of AESO degraded in 24 days in phosphate buffer solution.[39] These moderate differences in the biodegradability of AESO-based polymers indicate not only the huge effect of comonomer, but also the type of the test used for determination of biodegradability on the obtained results.

In this study, bio-based starting materials, solvent free formulations of resins, and photocuring process, corresponding to the concepts of green chemistry, exploring ways of preparing materials in more environment-friendly conditions from renewable resources, and green engineering, focusing on the optimization of processes and systems to maximize mass, energy, space, and time efficiency,[40] were used to develop novel sustainable polymeric materials. A series of AESO mixtures with bio-

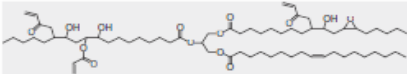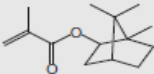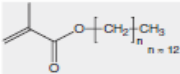**TABLE 1** Characteristics of bio-based materials used in this study
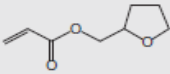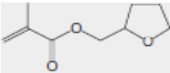
Material	Structural formula	Origin of material	BRC, %
AESO		Soybean	86
IBOMA		Pine trees	71
ME		Vegetable oil	76
THFA		Hemicellulose	60
THFMA		Hemicellulose	55

TABLE 2 Composition and characteristics of the prepared resins

Resin	Amount of AESO, wt.%	Amount of RD, wt.%	Amount of TPOL, wt.%	BRC[a], %	η, pa s
AESO/IBOMA	58.71	39.14	2.15	78.5	0.70 ± 0.03
AESO/ME	68.87	29.52	1.61	81.9	0.64 ± 0.01
AESO/THFA	68.36	29.30	2.34	76.6	0.56 ± 0.003
AESO/THFMA	68.46	29.34	2.20	75.3	0.63 ± 0.01

[a]Biorenewable carbon content calculated according to the Equation (1).

based commercially available RDs, such as IBOMA, methacrylic ester (ME), THFA, and THFMA, with biorenewable carbon content of 75%–82% were investigated as solvent free photocurable resins for DLP 3D printing technology. The monitoring of photocrosslinking kinetics of fully bio-based photoresins composed of above listed (meth)acrylates by the real-time photorheometry and analysis of their rheological parameters was carried out. Additionally, thermal properties of resulting photocross-linked polymers were investigated by differential scanning spectroscopy and thermogravimetric analysis. AESO-based polymer specimens prepared by molding and by DLP 3D printing with and without postcuring were mechanically tested and compared. The biodegradability of the synthesized photocross-linked polymers was determined by measuring the oxygen consumption in a closed respirometer in an aqueous medium.

2 | EXPERIMENTAL

2.1 | Materials

Acrylated epoxidized soybean oil (AESO, MV = 1160 g/mol, an average number of acryloyl groups per molecule calculated from 1H-NMR spectrum is 2.7 and 0.3 of epoxide groups) was purchased from Merck. Isobornyl methacrylate (IBOMA, MV = 222.3 g/mol) and methacrylic ester C13-MA (ME, MW = 268.0 g/mol) were kindly donated by Evonik Industries. Tetrahydrofurfuryl acrylate (SA5100, THFA, MV = 156.2 g/mol) and tetrahydrofurfuryl methacrylate (SA6100, THFMA, MV = 170.2 g/mol) were supplied by Sartomer. Photoinitiator ethyl(2,4,6-thimethylbenzoyl) phenyl phosphinate (TPOL, MV = 316.3 g/mol) was purchased from Fluorochem. Chloroform and acetone were purchased from Chempur. Commercial photosensitive resin

FIGURE 1 Tension load direction [Color figure can be viewed at wileyonlinelibrary.com]

Monocure3D Rapid Gray (REF) was purchased from Monocure3D. All materials were used without further purification.

Characteristics of bio-based materials are presented in Table 1, where biorenewable carbon (BRC) content was calculated according to the equation:

$$BRC, \% = \frac{Bio\ Sourced\ Carbon}{Bio\ Sourced\ Carbon + Fossil\ Carbon} \times 100. \tag{1}$$

2.2 | Preparation of cross-linked polymer specimens

The resins were prepared by mixing AESO with bio-based RDs in the ratio 60:40 (AESO:IBOMA) and 70:30 (AESO: ME/THFA/THFMA) to achieve the required resin viscosity of 500–800 mPa s for DLP 3D printing technology. The added amount of TPOL was 3 mol% calculated from amount of all monomers. Table 2 displays an overview of all resin formulations.

Test specimens were prepared by molding and by DLP 3D printing as described below.

The first group of rectangular $(70 \times 10 \times 1\ mm)$ photocross-linked polymer specimens (LAB) was prepared in Teflon mold by irradiation of AESO resins with Helios Italquartz, model GR.E 500 W lamp with an intensity of 310 mW cm^{-2} at the distance of 15 cm until hard specimens were formed in 5–8 min.

The second group of specimens was prepared by DLP 3D printing without postcuring (3DWPC). Specimens were printed using Ameralabs custom made DLP 3D printer. The printer was equipped with an Acer H6518BD projector 400–600 nm with XY resolution of 37.4 μm and had a building volume of $71.8 \times 40.4 \times 230\ mm$. Layer thickness was 50 μm with an exposure time of 6 s. 0.3% of carbon black pigment was added in all resins before the printing process to absorb light and control layer thickness. After printing, specimens were removed from the printing head and soaked in isopropanol for 15 min to remove any unreacted compounds.
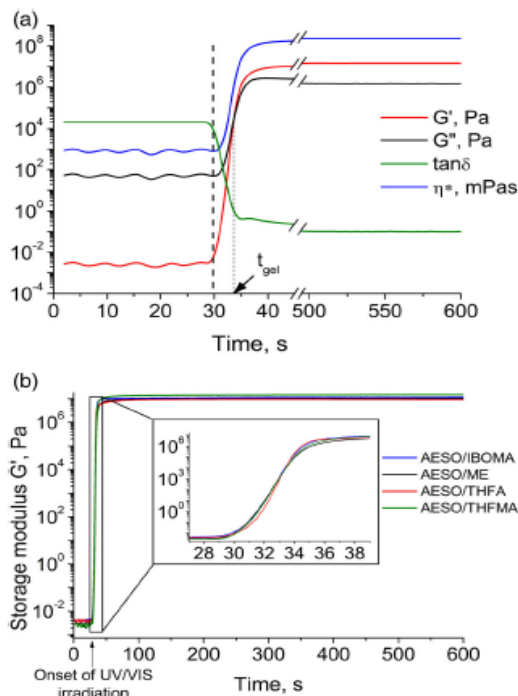
FIGURE 2 The dependencies of storage modulus G', loss modulus G'', loss factor tanδ, and complex viscosity η^* of resin AESO/THFA on irradiation time. The onset of irradiation (30 s) is marked with black vertical dashed line (a); the irradiation time dependencies of storage modulus G' of AESO-based resins with different reactive diluents (b) [Color figure can be viewed at wileyonlinelibrary.com]

The third group of specimens was prepared by DLP 3D printing with postcuring (3DPC). After printing and soaking in isopropanol, specimens were post-cured under LED light $(\lambda = 400\text{–}405\ nm,\ 50\ W)$ for 2 h at ambient temperature.

2.3 | Characterization

UV/VIS curing tests were carried out with a MCR302 rheometer from Anton Paar equipped with a plate/plate measuring system. A Peltier-controlled temperature chamber with the glass plate (diameter of 38 mm) and the top plate PP08 (diameter of 15 mm) was used. The measuring gap was set to 50 μm to simulate the 3D

101

TABLE 3   Rheological characteristics and shrinkage of AESO-based resins

Resin	t_{gel}[a], s	G'[b], MPa	G''[c], MPa	Tanδ[d]	η^*[e], pa s	Shrinkage, %
AESO/IBOMA	2.9 ± 1.0	13.63 ± 6.7	1.64 ± 1.3	0.109 ± 0.03	218.5 ± 108.7	10.0 ± 5.3
AESO/ME	2.2 ± 1.2	9.67 ± 0.4	1.49 ± 0.3	0.154 ± 0.03	155.7 ± 7.1	12.7 ± 4.2
AESO/THFA	1.9 ± 1.3	10.44 ± 1.8	2.51 ± 0.6	0.243 ± 0.07	171.1 ± 27.6	13.3 ± 2.3
AESO/THFMA	3.7 ± 0.02	13.34 ± 2.0	1.71 ± 0.3	0.131 ± 0.04	214.2 ± 31.2	8.0 ± 0

[a]Gel time calculated from the onset of UV/VIS irradiation.
[b]Storage modulus.
[c]Loss modulus.
[d]Loss factor.
[e]Complex viscosity. G', G'', tanδ, and η^* were calculated at an irradiation time of 600 s.

printing process conditions. The samples were irradiated at room temperature by UV/VIS radiation in a wavelength range of 250–450 nm through the glass plate of the temperature chamber using a UV/VIS spot curing system OmniCure S2000, Lumen Dynamics Group Inc. The intensity of the irradiation was 9.3 W cm^{-2} (high pressure 200 W mercury vapor short arc). Shear mode with a frequency of 10 Hz and a strain of 0.3% was used. A normal force of 0 N was set for the upper geometry that moved during the test. When the material shrank during the photopolymerization process, the upper geometry shifted downward to maintain a normal force of 0 N. Storage modulus G', loss modulus G'', loss factor tanδ (tanδ = G''/G'), complex viscosity η^*, and the gap change between the parallel plates were recorded as a function of time. Material linear shrinkage during the photocrosslinking reaction was determined from the ratio between the actual gap and the gap before the reaction. The mean values of three measurements of each resin were calculated.

The viscosity of AESO resins with bio-based reactive diluents IBOMA, ME, THFA, and THFMA (Table 2) were measured with a MCR302 rheometer from Anton Paar equipped with a steel parallel plate (top plate diameter of 15 mm) measuring system at room temperature (25°C). The measuring gap was set to 0.3 mm.

Fourier Transform Infrared Spectroscopy (FT-IR) measurements were performed on a Spectrum BX II FT-IR spectrometer (Perkin Elmer). The reflection spectra were acquired from 10 scans. The wavenumber range was 400–4000 cm^{-1}.

The yield of insoluble fraction (YIF) was determined by Soxhlet extraction. Samples of photocross-linked polymers were wrapped into a filter package, placed in a Soxhlet apparatus and extracted with chloroform for 24 h. Insoluble fractions were dried under vacuum to a constant weight. The yield of insoluble fraction was calculated as a difference of the sample weight before and after extraction and drying.

The glass transition temperature (T_g) of the photocross-linked polymers was estimated by differential scanning calorimetry (DSC). The measurements were performed on a DSC 8500 apparatus (Perkin Elmer) with a heating–cooling–heating rate of 10°C min^{-1} under nitrogen atmosphere (nitrogen flow rate 50 ml min^{-1}). The T_g value was taken as a middle point in the heat capacity step of the glass transition.

The thermogravimetric analysis (TGA) was performed on a TGA 4000 apparatus (Perkin Elmer) in a temperature range from room temperature to 800°C at a heating rate of 20°C min^{-1} under nitrogen atmosphere (nitrogen flow rate 100 ml min^{-1}).

The mechanical properties of the synthesized polymers were estimated by a tensile test according to the standard ISO 527-3 with some modifications. The tensile test was performed on a Testometric M500-50CT testing machine with flat faced grips HDFF100 at the room temperature. Test specimens with the dimensions of 70 × 10 × 1 mm prepared by molding and by DLP 3D printing were placed between the grips at the distance of 30 mm. Tension load direction was perpendicular to the printed layers as shown in Figure 1. Test was performed at the speed of 5 mm/min until the break of the specimen. Elastic modulus (E_E), tensile strength (σ), and elongation at break (ε) were determined. The mean values of three specimens of each polymer were calculated.

3D printed specimens were examined using a microscope Olympus BX41 at ×50 magnification.

2.4 | Biodegradability test

The biodegradation of synthesized materials was determined under aerobic conditions in closed respirometers (OxiTop Control, WTW GmbH) by measuring oxygen consumption according to the standard ISO 14851:1999.[41] An aqueous standard test medium prepared as described

102

in the standard ISO 14851 was inoculated with the activated sludge, prepared from compost purchased from a local store. Samples and blanks (inoculated media without test sample) were stirred at $(28 \pm 2)°C$ for 60 days. The biodegradability (BD) was determined by comparing the biochemical oxygen demand (BOD) with the theoretical oxygen demand (ThOD) and defined as follows:

$$BD, \% = \frac{BOD_{test} - BOD_{blank}}{ThOD \cdot C_{test}} \times 100, \qquad (2)$$

where BD is a biodegradability (%), BOD_{test} (mg/l) is BOD of the sample in a test bottle, BOD_{blank} (mg/l) is BOD of the activated sludge, C_{test} (g/l) is the concentration of the sample in aqueous test medium, and ThOD (mg/g) is BOD of the sample calculated theoretically by assuming that the polymer completely degraded into CO_2 and H_2O. The mean values of two parallel measurements of each sample were calculated.

3 | RESULTS AND DISCUSSION

3.1 | Kinetics of photocross-linking

In this study, bio-based resins were prepared from AESO and bio-based RDs in appropriate amounts (Table 2) to achieve necessary viscosity (η) of 0.50–0.80 Pa s for DLP 3D printing technology. The viscosity values of prepared resins measured by rheometer were in the range of 0.56–0.70 Pa s. Resin AESO/IBOMA possessed the highest viscosity even though the highest amount of bio-based RD was used in it. This could be due to the poor dilution ability of IBOMA.[42]

Real-time photorheometry test was performed to investigate photocross-linking kinetics and linear shrinkage of bio-based resins. During the measurement, storage modulus (G'), loss modulus (G''), complex viscosity (η^*), and loss factor (tanδ) were recorded as a function of irradiation time. The shape of all resin curves was similar, so, as an example, the dependencies of G', G'', tanδ, and η^* of resin AESO/THFA on irradiation time are presented in Figure 2a. All measured parameters were constant or nearly constant values before the onset of UV/VIS irradiation, indicating the stability of the material over that time. As the UV/VIS irradiation of bio-based resins had started, the values of G', G'', and η^* started to rise with time and later reached the intersection of the G' and G'' curves which indicated a sol/gel transition point (gel point t_{gel}) where $G' = G''$, corresponding to the transition from liquid resin to solid polymer.[43] Finally, all curves reached asymptotically constant values showing $G' > G''$.[44]

The irradiation time dependencies of G' of AESO-based resins with different RDs are presented in Figure 2b. The real-time photorheometry measurements confirmed the high cross-linking rate of all resins. The rapid growth of G' values immediately after the onset of UV/VIS irradiation was obtained. The values of t_{gel} varied in the range of 1.9–3.7 s (Table 3). This rapid increase of the G' values indicated the prompt formation of photocross-linked polymer network yielding to a solid polymer after irradiation. Since G' correlates directly with the cross-linking density,[45] the high G' values of the measured resins ranging from 9.67 to 13.63 MPa, as well as the plateau values of G', G'', and η^* reached at the end of photocross-linking process showed the formation of highly cross-linked polymers.

Tanδ, the ratio of G' and G'', determines the mechanical properties of the cross-linked polymers in photorheometry: when tan$\delta > 1$, the loss (viscous) modulus G'' dominates and the cross-linked material is soft and rubbery; when tan$\delta < 1$, the storage (elastic) modulus G' overcome G'' indicating the formation of highly cross-linked polymer.[46] It was observed that resin AESO/IBOMA showed the highest G' values and the lowest tanδ values indicating the robust polymer formed. Resin AESO/THFMA showed the similar G' values, although the tanδ values were significantly different. The higher tanδ values of resin AESO/THFMA imply a considerable liquid-state behavior of the sample dissipating the energy, expressed as the higher values of G''. This G' and tanδ values irregularity was also observed in resins AESO/ME and AESO/THFA. Resin AESO/THFA showed the higher values of G' and tanδ than those of resin AESO/ME. Although parameters G' and tanδ contradict each other comparing these two resins. However, tanδ really determines the mechanical properties of cross-linked polymer. Tanδ indicates where liquid (tan$\delta > 1$) and solid (tan$\delta < 1$) regions predominate evaluating the G'' values, which highly affect mechanical properties of photocross-linked polymer.[47] The highest tanδ values and thus the highest values of G'' of resin AESO/THFA indicated the formation of soft rubbery polymer.

Resin AESO/THFA with the only acrylate RD used in this study underwent the fastest photocross-linking process at the beginning and reached the gel point the fastest. However, the resins with slower reacting methacrylate RDs, AESO/IBOMA and AESO/THFMA, showed the higher G' values at the end of the process and thus more rigid polymers were formed in these cases. This observation correlates with previously determined the higher conversion of methacrylate groups in comparison to acrylate groups resulting in polymers with better mechanical properties.[48] Moreover, it was observed that the rate of cross-linking was associated with the material

103

shrinkage during the photopolymerization.[49,50] The shrinkage is caused by the transformation of intermolecular distances ~3–5 Å linked via weak Van der Waals force into the typical C—C strong covalent bond distance ~1.54 Å.[51] This change of distance during the
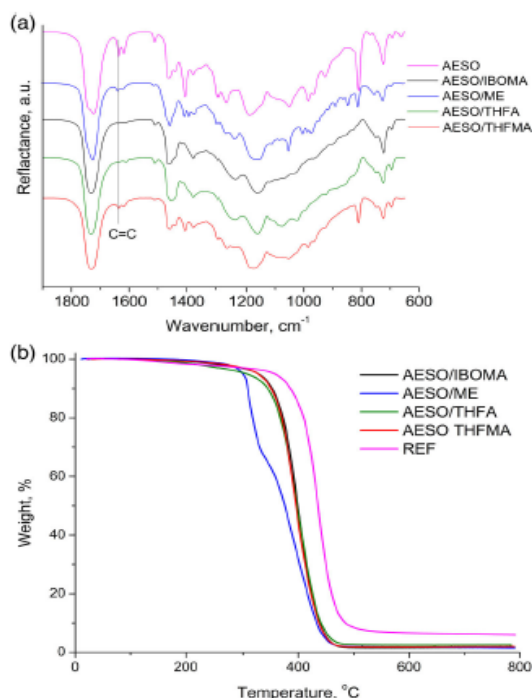

FIGURE 3 The FT-IR spectra of AESO and copolymers AESO/IBOMA, AESO/ME, AESO/THFA, and AESO/THFMA (a); TGA curves of synthesized polymers (b) [Color figure can be viewed at wileyonlinelibrary.com]

photocross-linking reaction is time dependent and causing a higher shrinkage at the higher conversion of functional groups. Resins AESO/THFA and AESO/ME showed the lowest t_{gel} due to the prompt photocross-linking, which resulted in the highest shrinkage of the samples.

3.2 | Characterization of photocross-linked polymer structure

Chemical structure of the synthesized polymers was investigated by FTIR spectroscopy. The reduction of C=C stretching signal at 1637 cm^{-1} was observed in the FTIR spectra of all photocross-linked polymers (Figure 3a) indicating the formation of polymer which most of (meth)acrylic groups were reacted. Due to aliphatic structure of bio-based reactive diluents, all the characteristic peaks of these materials were in the fingerprint region and overlapped with AESO characteristic peaks in this region. Due to this overlap, the confirmation of the reactive diluent incorporation into the photocross-linked polymer network could not be made by FTIR spectra. Therefore, the formation of photocross-linked copolymers of AESO and bio-based RDs was confirmed by Soxhlet extraction (Table 4).

The yield of insoluble fraction (YIF) of the photocross-linked polymers varied in the range of 95.4%–98.7%. Polymer AESO/IBOMA showed the highest YIF value indicating its highest amount of the cross-linked structure of bio-based polymers, whereas the lowest values of YIF of polymer AESO/THFA indicated the lowest amount of the cross-linked structure and increased formation of linear and/or branched macromolecules during photopolymerization, which was also confirmed by the highest value of tanδ. The highest initial photocross-linking rate of polymer AESO/THFA confirmed by the lowest t_{gel} value could cause the reduced extent of its final double bond conversion[52] and thus led

TABLE 4 Yield of insoluble fraction and thermal characteristics of the cross-linked polymers

Polymer	YIF, %[a]	T_g, °C[b]	$T_{dec-10\%}$, °C[c]	Char yield, %[d]
AESO/IBOMA	98.7	60.8	308	1.5
AESO/ME	96.9	24.3	353	1.6
AESO/THFA	95.4	4.6	345	1.9
AESO/THFMA	96.3	43.7	351	2.0
REF	99.6	n[e]	386	6.0

[a]Yield of insoluble fraction after Soxhlet extraction with chloroform for 24 h.
[b]Glass transition temperature determined by DSC.
[c]Temperature at the weight loss of 10% obtained from TGA curves.
[d]Char yield obtained from TGA curves.
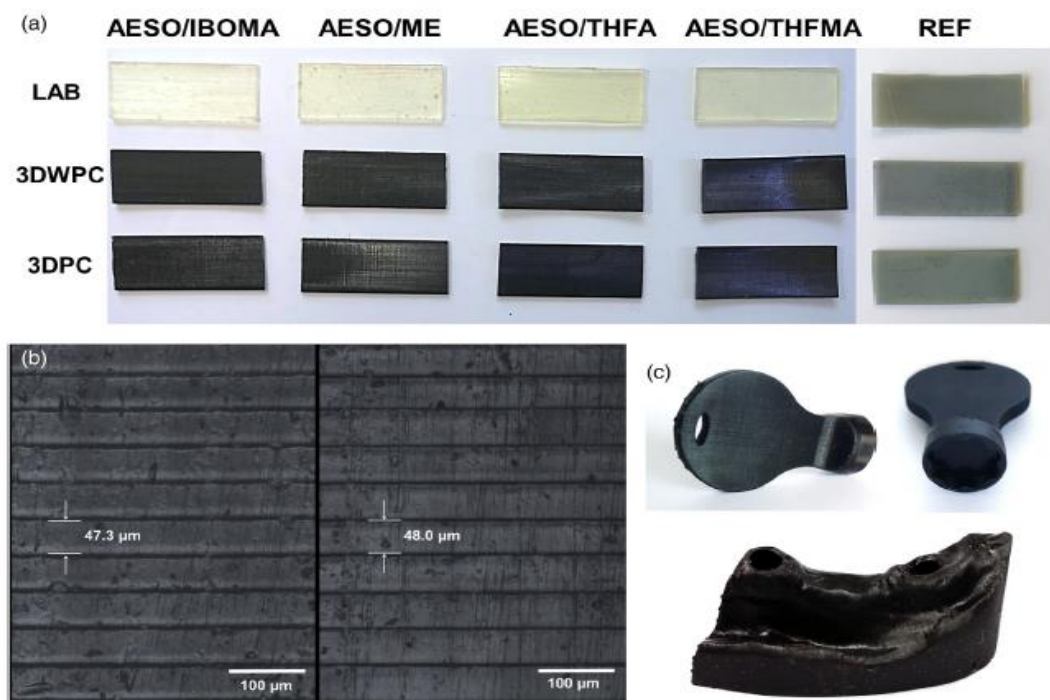[e]Could not be determined by DSC.

FIGURE 4 Images of the AESO-based polymer specimens and the commercial 3D printing resin (REF) specimens prepared by three different methods: by molding (LAB), by DLP without post-curing (3DWPC), and by DLP with post-curing (3DPC) (a); microscope images of the surface of the polymer AESO/MA specimens prepared by 3DWPC (b, left) and by 3DPC (b, right); images of the bolt wrenching tool formed from polymer AESO/IBOMA (c, top) and image of the human lower jaw fragment formed from polymer AESO/THFMA (c, bottom), both produced by 3DPC [Color figure can be viewed at wileyonlinelibrary.com]

to the lower YIF value compared to that of polymer AESO/THFMA.

3.3 | Thermal properties

DSC and TGA were used to study the thermal properties of the photocross-linked AESO-based polymers. The glass transition temperature (T_g) values of the photocross-linked polymers determined by DSC varied in the range of 4.6–60.8°C (Table 4). It was determined that T_g values strongly depended on the used RD. The T_g values of the polymers with methacrylate fragments were much higher than that of the polymer AESO/THFA with acrylate fragments which YIF was the lowest as well. The highest T_g of 60.8°C was obtained for polymer AESO/IBOMA which yield of insoluble fraction was also the highest.

The thermal degradation behavior of the cross-linked polymers AESO/RD was investigated using TGA under nitrogen atmosphere. All unpigmented polymers AESO/RD showed the thermal decomposition temperature at the weight loss of 10% above 300°C, however these values were lower by 33–78°C than that of REF (Table 4). The TGA curves of polymers AESO/ME, AESO/THFA, and AESO/THFMA (Figure 3b) showed a single stage degradation characteristic to cross-linked networks with a similar bond thermal stability. The two-stage degradation of polymer AESO/IBOMA was caused by the loss of isobornyl fragment through ester bond scission which thermal stability was lower than that of carbon–carbon bonds formed during photopolymerization.[53] Due to the low thermal stability of isobornyl fragment, the char yield 1.5% of polymer AESO/IBOMA was the lowest. Polymers AESO/THFA and AESO/THFMA indicated the highest char yield values, 1.9% and 2.0% respectively, which were caused by the thermally stable furan ring moieties.[54] REF exhibited not only the highest thermal stability, but also the highest char yield, which was caused by the presence of pigments.

105

TABLE 5 Mechanical characteristics of polymer specimens prepared by different methods

Polymer	Type of processing	Pigmentation	E_E, MPa[a]	δ, MPa[b]	ε, %[c]
AESO/IBOMA	LAB	Unpigmented	4852.3 ± 226.0	257.2 ± 36.9	5.3 ± 1.0
		Pigmented	1986.2 ± 424.6	137.5 ± 66.3	6.7 ± 2.0
	3DWPC	Pigmented	554.3 ± 101.4	13.1 ± 0.7	15.6 ± 2.4
	3DPC	Pigmented	4749.9 ± 204.3	250.4 ± 9.2	8.5 ± 0.4
AESO/ME	LAB	Unpigmented	289.7 ± 21.7	19.0 ± 1.6	6.6 ± 0.6
		Pigmented	209.4 ± 12.1	14.0 ± 1.4	6.7 ± 0.9
	3DWPC	Pigmented	40.9 ± 3.7	1.7 ± 0.2	9.5 ± 1.6
	3DPC	Pigmented	72.9 ± 3.9	3.3 ± 0.7	12.8 ± 3.1
AESO/THFA	LAB	Unpigmented	176.0 ± 14.3	24.4 ± 2.0	14.0 ± 2.1
		Pigmented	136.4 ± 15.7	7.9 ± 1.5	5.9 ± 1.3
	3DWPC	Pigmented	22.0 ± 1.0	0.9 ± 0.2	8.6 ± 0.6
	3DPC	Pigmented	36.6 ± 1.4	2.5 ± 0.4	10.5 ± 1.0
AESO/THFMA	LAB	Unpigmented	794.8 ± 188.2	110.2 ± 30.0	14.3 ± 3.4
		Pigmented	306.1 ± 40.2	40.7 ± 2.7	13.5 ± 2.0
	3DWPC	Pigmented	52.4 ± 10.1	3.5 ± 1.1	14.8 ± 0.9
	3DPC	Pigmented	664.0 ± 33.8	37.2 ± 3.4	16.1 ± 1.8
REF	LAB	Pigmented	6479.7 ± 216.0	108.8 ± 89.32	4.0 ± 1.5
	3DWPC	Pigmented	1089.8 ± 179.9	87.1 ± 16.3	19.3 ± 3.2
	3DPC	Pigmented	6451.9 ± 205.9	252.7 ± 22.3	4.7 ± 0.4

[a]Elastic modulus.
[b]Tensile strength.
[c]Elongation at break.

FIGURE 5 Tensile characteristics of the cross-linked polymer specimens produced by molding (LAB), by DLP 3D printing without postcuring (3DWPC) (a), and by 3DPC: Elastic modulus (E_E), tensile strength (δ), and elongation at break (ε) (b) [Color figure can be viewed at wileyonlinelibrary.com]

106
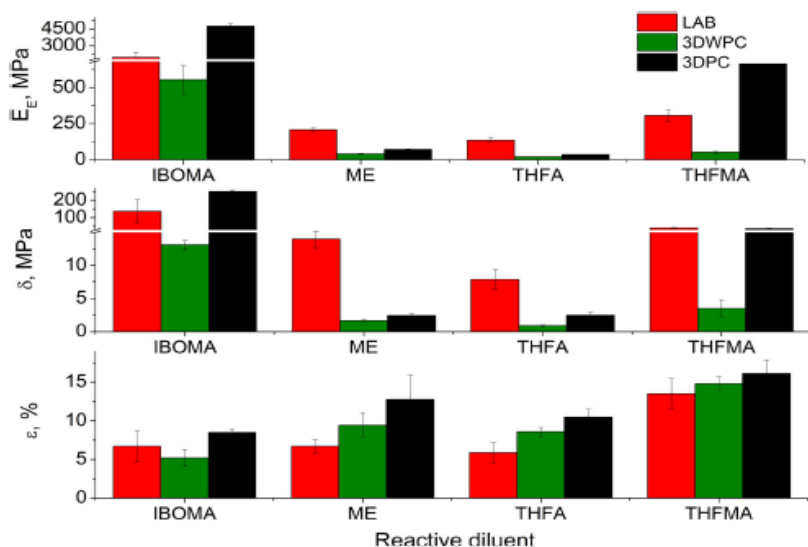
3.4 | DLP 3D printing and tensile test

All prepared bio-based resins were successfully applied in DLP 3D printing technology. The images of the AESO-based polymer specimens as well as a reference specimens prepared by three different ways: by molding (LAB), by DLP without post-curing (3DWPC), and by DLP with post-curing (3DPC), are presented in Figure 4a. 3D printed parts demonstrated high printing accuracy with smooth surface finishing after the post-curing. However, a corrugation at the surface of the specimens prepared by 3DWPC occurred due to the washing away of the unreacted monomer from the specimen surface, while a smoother surface was obtained after post-curing process (Figure 4b). The complex architecture of the fragment of human lower jaw printed from resin AESO/THFMA with high definition (Figure 4c) confirmed the suitability of the prepared bio-based resins for DLP 3D printing technology.

Tensile testing was conducted to determine the effects of RDs on mechanical properties of polymers. Since only pigmented resins could be 3D printed on the used printing equipment, pigmented and unpigmented specimens were prepared by LAB to determine the influence of pigmentation to the tensile properties of bio-based polymers. The considerable reduction of the tensile parameter values of pigmented photocross-linked polymers was observed (Table 5). The carbon black pigment is often employed to control the cured layer thickness in DLP 3D printing, as the light penetration is suppressed in deeper layers and the resin could not be fully cured. This led to the decreased values of E_E and δ of pigmented specimens prepared by LAB.

The tensile test was performed for pigmented samples prepared by three different ways: LAB, 3DWPC, and 3DPC, when moving axis was perpendicular to printed layers. Due to the different methods of specimen preparation, the adhesion between different layers during the 3D printing process has been evaluated. The worst mechanical properties were obtained when specimens were prepared by DLP 3D printing without post-curing (Table 5). Post-curing after photocross-linking generally involves the removal of unreacted compounds using solvent (e.g., ethanol, isopropanol) followed by UV-curing and/or thermal curing to improve the conversion of functional groups and increase the cross-linking density.[55] The specimens prepared by 3DWPC showed poor mechanical properties because of an inevitable presence of unreacted functional groups caused by the conversion gradient in each layer.[56]

Polymer AESO/IBOMA showed the highest values of elastic modulus (E_E) and tensile strength (δ) (Figure 5). Due to the bulky and rigid isobornyl bis-cyclic group,
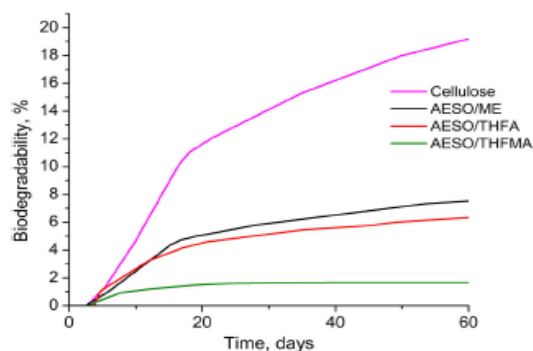

FIGURE 6 Biodegradation kinetics curves of synthesized polymers and cellulose as a reference material [Color figure can be viewed at wileyonlinelibrary.com]

photocross-linked polymer AESO/IBOMA was stiff and inflexible[57] with the lowest elongation at break (ε) values. IBOMA, as a bulk-toughening agent in AESO-based polymers, improved the mechanical properties of the synthesized polymer. Comparing tensile parameters of polymer AESO/IBOMA prepared by 3DPC and unpigmented LAB, the values of E_E and ε were nearly identical, indicating the highly rigid specimens with a very high adhesion between the printed layers. The huge differences of tensile properties between pigmented specimens prepared by LAB and 3DPC could be explained by the cure depth caused by the carbon black pigment. Since the layer thickness in DLP 3D printing was 50 µm, the layer fully cured during the light irradiation, while preparing pigmented samples by LAB there was a single layer of 1 mm thickness, which could not be fully cured due to the restrained light penetration.

Polymers AESO/ME and AESO/THFA showed the lowest values of E_E and δ indicating poor mechanical properties and formation of soft rubbery polymers. The specimens of these two polymers prepared by 3DPC showed significantly lower E_E values than those of specimens prepared by LAB. As these two resins (AESO/ME and AESO/THFA) showed the highest shrinkage, this huge reduction of tensile parameters of printed samples could be explained by the layer shrinkage during the DLP 3D printing process, which could led to the weak adhesion between the printed layers.

Higher YIF and T_g values of polymer AESO/THFMA led to the better mechanical properties compared to those of polymer AESO/THFA. This was caused by the replacement of methyl group in THFMA by hydrogen in THFA followed by increased chain flexibility.[58] Moreover, methyl group in THFMA caused the lower shrinkage during photocross-linking. Although both polymer

AESO/THFA and AESO/THFMA specimens showed considerably high ε values when were prepared by LAB, compared to the specimens prepared by 3DPC. Polymer AESO/THFA showed a significant reduction of ε values, what confirmed the poor adhesion between layers during DLP 3D printing.

In general, all AESO-based polymers demonstrated the tunable properties varying from soft to rigid. Polymers AESO/IBOMA and AESO/THFMA exhibited the highest values of elastic modulus. Tensile properties of AESO/IBOMA specimen prepared by 3DPC were the closest to those of the commercial petroleum-derived resin REF. The highest E_E and δ values of REF and AESO/IBOMA prepared by 3DPC indicated the formation of highly cross-linked hard polymers. Although nearly two times higher ε values of AESO/IBOMA compared to REF prepared by 3DPC, showed the higher flexibility of AESO/IBOMA polymer due to the long fatty acid chains in AESO molecule. The comparison of the tensile properties of AESO-based polymers with those of REF shows that they could be considered as a competitive substitute for commercial ones.

3.5 | Biodegradation of photocross-linked polymers

The biodegradation of photocross-linked polymers was determined by measuring oxygen consumption in the closed respirometers in an aqueous medium under laboratory conditions with an inoculum from compost. The synthesized polymers (0%–7.5%) AESO/RD were biodegraded after 60 days while biodegradation of cellulose, used as a reference material, was 19.1% after the same period (Figure 6). Polymer AESO/IBOMA sample did not consumed oxygen during the test and showed no biodegradation due to the highly cross-linked polymer network and non-biodegradable isobornyl moieties.[59,60] It was observed that cellulose did not reach the plateau of BOD after 60 days indicating the continuing biodegradation process. Massardier–Nageotte et al.[61] investigated cellulose biodegradability by measuring BOD and reported a biodegradation of 17.3% after 28 days confirming the slow biodegradation process of cellulose.

Since all synthesized photocross-linked polymers were AESO-based, they all consisted of glycerol esterified three fatty acids moieties. During aerobic degradation, hydrolyzed fatty acids degraded via β-oxidation mechanism by which saturated fatty acids were converted to shorter fatty acid fragments by the repeated cleavage of two-carbon molecules acetyl-CoA. Acetyl-CoA can then enter the tricarboxylic acid cycle where it is further

oxidized to CO_2.[62] However, nondegradable linkages are formed during cross-linking reactions and the biodegradability of triglycerides significantly decreases.[63] Due to the formed cross-links or branches in fatty acid portion of the triacylglycerol network, binding and activity of lipases, which cleave the glycerol ester bonds is inhibited. As the cross-linking of triglyceride increases some glycerol ester bonds are cleaved but further metabolism of fatty acids is blocked by the branch points leading to decreased biodegradability.

It was noticed that polymers AESO/ME and AESO/THFA with low YIF and poor mechanical properties showed the highest biodegradability. ME is obtained from vegetable oils and is of the same origin as AESO forming a complex network of cross-linked fatty acids which are targeted by microorganisms and easily biodegradable. Glycerol ester groups and furan ring in polymers AESO/THFA and AESO/THFMA were triggered by microorganisms and participated in biodegradation process. Furan ring moieties cleave in the place of oxygen heteroatom forming various levulinic acid or 2-furoic acid derivatives, which further cleave into smaller molecules.[64,65] Due to this degradation mechanism, all furan derivatives are biodegradable, although the rate of biodegradation is irregular as it was observed for polymers AESO/THFA and AESO/THFMA. The rate of biodegradation of these polymers differs due to the different density of cross-links. The higher YIF led to the lower biodegradability of polymer AESO/THFMA.

4 | CONCLUSIONS

In this study, bio-based photocurable resins were composed of commercially available materials and applied in DLP 3D printing technology. Acrylated epoxidized soybean oil was mixed with bio-based monofunctional (meth)acrylates to obtain the required resin viscosity for DLP 3D printing of 557.5–699.3 mPa s. Bio-based resins with biorenewable carbon content of 75%–82% indicated high photocross-linking rate, yield of insoluble fraction, and thermal decomposition temperature at the weight loss of 10% above 300°C. DLP 3D printing of developed resins resulted in smooth surface finishing and good layer adhesion. Photocross-linked soybean oil–based polymers with methacrylic ester, tetrahydrofurfuryl acrylate, and tetrahydrofurfuryl methacrylate fragments indicated slow biodegradation process with a biodegradability up to 7.5% after 60 days showing their suitability for production of the long-term usage products. Investigated bio-based resins can reduce the petroleum-based carbon footprint in additive manufacturing and reduce the environmental impact.

ORCID

Jolita Ostrauskaite https://orcid.org/0000-0001-8600-7040

REFERENCES

[1] V. S. Voet, G. H. Schnelting, J. Xu, K. Loos, R. Folkersma, J. J. V. E. Jager, *J. Vis. Exp.* **2018**, *139*, e58177.

[2] Y. Lee, J. Lee, W. Maeng, Y. Koh, H. Kim, *J. Eur. Ceram. Soc.* **2019**, *39*, 4358.

[3] E. Skliutas, S. Kasetaite, L. Jonušauskas, J. Ostrauskaite, M. Malinauskas, *Opt. Eng.* **2018**, *57*, 041412.

[4] C. J. Thrasher, J. J. Schwartz, A. J. Boydston, ACS Appl. Mater. Interfaces. **2017**, *9*, 39708.

[5] Y. Zhu, C. Romain, C. K. Williams, *Nature* **2016**, *540*, 354.

[6] T. Billiet, E. Gevaert, T. De Schryver, M. Cornelissen, P. Dubruel, *Biomaterials* **2014**, *35*, 49.

[7] A. Navaruckiene, E. Skliutas, S. Kasetaite, S. Rekštytė, V. Raudoniene, D. Bridziuviene, M. Malinauskas, J. Ostrauskaite, *Polymers* **2020**, *12*, 397.

[8] J. T. Sutton, K. Rajan, D. P. Harper, S. C. Chmely, *ACS Appl. Mater. Interfaces* **2018**, *10*, 36456.

[9] A. Navaruckiene, S. Kasetaite, J. Ostrauskaite, *Rapid Prototyp. J.* **2019**, *26*, 402.

[10] V. S. Voet, T. Strating, G. H. Schnelting, P. Dijkstra, M. Tietema, J. Xu, A. J. Woortman, K. Loos, J. Jager, R. Folkersma, *ACS Omega* **2018**, *3*, 1403.

[11] A. Champion, X. Allonas, C. Croutxé-Barghorn, A. Schuller, C. Delaite, *Prog. Org. Coat.* **2019**, *131*, 240.

[12] R. Ding, Y. Du, R. B. Goncalves, L. F. Francis, T. M. Reineke, *Polym. Chem.* **2019**, *10*, 1067.

[13] J. Z. Manapat, Q. Chen, P. Ye, R. C. Advincula, *Macromol. Mater. Eng.* **2017**, *302*, 1600553.

[14] S. K. Yadav, K. M. Schmalbach, E. Kinaci, J. F. Stanzione III., G. R. Palmese, *Eur. Polym. J.* **2018**, *98*, 199.

[15] S. A. Allnex Belgium, Allnex Ebecryl 860 Technical Data Sheet. https://www.palmerholland.com/getmedia/9e536241-07e2-4874-b44e-01ae01f430e7/MITM00452_1 (accessed October 29, 2020).

[16] M. Lebedevaite, J. Ostrauskaite, E. Skliutas, M. Malinauskas, *Polymers* **2019**, *11*, 116.

[17] S. Miao, W. Zhu, N. J. Castro, M. Nowicki, X. Zhou, H. Cui, J. P. Fisher, L. G. Zhang, *Sci. Rep.* **2016**, *6*, 27226.

[18] B. Wu, A. Sufi, R. Ghosh Biswas, A. Hisatsune, V. Moxley-Paquette, P. Ning, R. Soong, A. P. Dicks, A. J. Simpson, *ACS Sustain. Chem. Eng.* **2019**, *8*, 1171.

[19] S. Miao, H. Cui, M. Nowicki, S. Lee, J. Almeida, X. Zhou, W. Zhu, X. Yao, F. Masood, M. W. Plesniak, *Biofabrication* **2018**, *10*, 035007.

[20] K. Tan, R. Liu, J. Luo, Y. Zhu, W. Wei, X. Liu, *Prog. Org. Coat.* **2019**, *130*, 214.

[21] F. Habib, M. Bajpai, *Chem. Chem. Technol.* **2011**, *5*, 317.

[22] Y. Hu, P. Jia, Q. Shang, M. Zhang, G. Feng, C. Liu, Y. Zhou, *J. Biores. Bioprod.* **2019**, *4*, 183.

[23] H. Liu, W. Lu, S. Liu, *J. Appl. Polym. Sci.* **2018**, *135*, 45698.

[24] S. Rengasamy, V. Mannari, *Prog. Org. Coat.* **2013**, *76*, 78.

[25] Y. Hong, K. Zhang, M. Zhao, N. Wang, *J. Hubei Univ.* **2018**, *1*, 9.

[26] Z. Chen, J. F. Wu, S. Fernando, K. Jagodzinski, *Prog. Org. Coat.* **2011**, *71*, 98.

[27] X. Yang, S. Li, J. Xia, J. Song, K. Huang, M. Li, *BioResources* **2015**, *10*, 2130.

[28] J. Dai, X. Liu, S. Ma, J. Wang, X. Shen, S. You, J. Zhu, *Prog. Org. Coat.* **2016**, *97*, 210.

[29] J. Dai, Y. Jiang, X. Liu, J. Wang, J. Zhu, *RSC Adv.* **2016**, *6*, 17857.

[30] Y. Zhang, Y. Li, V. K. Thakur, L. Wang, J. Gu, Z. Gao, B. Fan, Q. Wu, M. R. Kessler, *RSC Adv.* **2018**, *8*, 13780.

[31] M. Lebedevaite, J. Ostrauskaite, E. Skliutas, M. Malinauskas, *J. Appl. Polym. Sci.* **2019**, *137*, 48708.

[32] J. F. Wu, S. Fernando, K. Jagodzinski, D. Weerasinghe, Z. Chen, *Polym. Int.* **2011**, *60*, 571.

[33] P. Liu, X. Zhang, R. Liu, X. Liu, J. Liu, *Prog. Org. Coat.* **2019**, *134*, 342.

[34] S. Ma, Y. Jiang, X. Liu, L. Pan, J. Zhu, *Rsc Adv.* **2014**, *4*, 23036.

[35] J. Guit, M. B. Tavares, J. Hul, C. Ye, K. Loos, J. Jager, R. Folkersma, V. S. Voet, *ACS Appl. Polym. Mater.* **2020**, *2*, 949.

[36] S. Oprea, *Polym. Plast. Technol. Eng.* **2015**, *54*, 342.

[37] J. Chen, H. Liu, W. Zhang, L. Lv, Z. Liu, *J. Appl. Polym. Sci.* **2020**, *137*, 48827.

[38] S. Oprea, F. Doroftei, *Int. Biodeterior. Biodegrad.* **2011**, *65*, 533.

[39] H. Kim, H. Kim, B. S. Kim, *J. Polym. Environ.* **2010**, *18*, 291.

[40] M. Lancaster, *Green Chemistry: An Introductory Text*, 3rd ed., Royal Society of Chemistry, Cambridge **2016**.

[41] ISO ISO 14851: 1999. Determination of the ultimate aerobic biodegradability of plastic materials in an aqueous medium—Method by measuring the oxygen demand in a closed respirometer, **1999**.

[42] G. Wei, H. Xu, L. Chen, Z. Li, R. Liu, *Prog. Org. Coat.* **2019**, *126*, 162.

[43] C. Gorsche, R. Harikrishna, S. Baudis, P. Knaack, B. Husar, J. Laeuger, H. Hoffmann, R. Liska, *Anal. Chem.* **2017**, *89*, 4958.

[44] T. G. Mezger, *The Rheology Handbook: For Users of Rotational and Oscillatory Rheometers*, Vincentz Network GmbH & Co KG, Hannover, Germany **2006**.

[45] Y. Hao, H. Shih, Z. Muñoz, A. Kemp, C. Lin, *Acta Biomater.* **2014**, *10*, 104.

[46] B. Ziółkowski, Z. Ates, S. Gallagher, R. Byrne, A. Heise, K. J. Fraser, D. Diamond, *Macromol. Chem. Phys.* **2013**, *214*, 787.

[47] G. Wicaksono, I. Djordjevic, A. H. Shah, T. W. J. Steele, *Polym. Test.* **2019**, *80*, 106099.

[48] R. Ghorpade, S. Bhosle, S. Ponrathnam, C. Rajan, N. Chavan, R. Harikrishna, *J. Polym. Res.* **2012**, *19*, 9811.

[49] S. Ye, N. B. Cramer, I. R. Smith, K. R. Voigt, C. N. Bowman, *Macromolecules* **2011**, *44*, 9084.

[50] M. Dewaele, D. Truffier-Boutry, J. Devaux, G. Leloup, *Dent. Mater.* **2006**, *22*, 359.

[51] Y. He, M. Yao, J. Nie, *Protective Coatings, Anonymous*, Springer, Berlin **2017**, p. 195.

[52] E. Andrzejewska, in *In Three-Dimensional Microfabrication Using Two-Photon Polymerization*, 2nd ed. (Ed: T.

Baldacchini), William Andrew Publishing, Elsevier, Norwich, New York **2019**, p. 77.

[53] F. Jaillet, H. Nouailhas, R. Auvergne, A. Ratsimihety, B. Boutevin, S. Caillol, *Eur. J. Lipid Sci. Technol.* **2014**, *116*, 928.

[54] W. Liu, T. Xie, R. Qiu, *ACS Sustain. Chem. Eng.* **2017**, *5*, 774.

[55] J. S. Oakdale, J. Ye, W. L. Smith, J. Biener, *Opt. Express* **2016**, *24*, 27077.

[56] A. C. Uzcategui, A. Muralidharan, V. L. Ferguson, S. J. Bryant, R. R. McLeod, *Adv. Eng. Mater.* **2018**, *20*, 1800876.

[57] F. Jaillet, E. Darroman, B. Boutevin, S. Caillol, *OCL* **2016**, *23*, D511.

[58] A. Zioga, N. Ekizoglou, E. Siakali-Kioulafa, N. Hadjichristidis, *J. Polym. Sci.* **1997**, *35*, 1589.

[59] J. Huang, J. Sun, R. Zhang, R. Zou, X. Liu, Z. Yang, T. Yuan, *Prog. Org. Coat.* **2016**, *95*, 20.

[60] J. Favarão, D. C. R. S. d. Oliveira, M. G. Rocha, M. M. Zanini, G. F. Abuna, M. J. Mendonça, M. A. C. Sinhoreti, *Braz. Dent. J.* **2019**, *30*, 272.

[61] V. Massardier-Nageotte, C. Pestre, T. Cruard-Pradet, R. Bayard, *Polym. Degrad. Stab.* **2006**, *91*, 620.

[62] D. A. Salam, N. Naik, M. T. Suidan, A. D. Venosa, *Environ. Sci. Technol.* **2012**, *46*, 2352.

[63] R. L. Shogren, Z. Petrovic, Z. Liu, S. Z. Erhan, *J. Polym. Environ.* **2004**, *12*, 173.

[64] R. Kumar, D. Rashmi, *World J. Microbiol. Biotechnol.* **2018**, *34*, 2.

[65] P. Singh, R. Kumar, *J. Polym. Environ.* **2019**, *27*, 901.

Development and optical 3D printing of acrylated epoxidized soybean oil-based composites with functionalized calcium silicate hydrate filler derived from aluminium fluoride production waste

Migle Lebedevaite [a], Andrius Gineika [b], Vaidas Talacka [c], Kestutis Baltakys [b], Jolita Ostrauskaite [a,*]

[a] Department of Polymer Chemistry and Technology, Kaunas University of Technology, Radvilenu Rd. 19, Kaunas LT-50254, Lithuania
[b] Department of Silicate Technology, Kaunas University of Technology, Radvilenu Rd. 19, Kaunas LT–50299, Lithuania
[c] AmeraLabs, Kestucio str. 6A, Kaunas LT-44320, Lithuania

ABSTRACT

In this study, novel photocurable biobased and biodegradable composites with functionalized fillers from industrial inorganic waste have been developed and applied in optical 3D printing technology. Hydrothermally synthesized calcium silicate hydrates from aluminium fluoride production waste were used as fillers in photoresins based on acrylated epoxidized soybean oil-based. The use of fillers synthesized from industrial waste led to an improvement in the mechanical properties of polymer composites compared to filler synthesized from impurity-free material. The high 3D printing accuracy, perfect layer adhesion, and smooth surface finishing of 3D objects printed with a commercial digital light processing (DLP) 3D printer were shown by the developed composites. The biodegradability of photocured polymer composites reached 19.6% in 60 days. The developed composites have the great potential to be a competitive alternative to conventional petroleum-derived ones and reduce the environmental impact.

1. Introduction

Optical 3D printing (O3DP) technologies, such as digital light processing (DLP) or stereolithography (SLA), in which liquid resins are layer-by-layer photocross-linked under UV or visible light [1], have gained a lot of interest due to high printing accuracy, low raw material usage, and the ability to create objects that cannot be cut, carved, or assembled [2]. However, since O3DP polymer products lack strength and functionality, they are still used as conceptual prototypes instead as operative constituents [3]. Due to this, the industrial application of O3DP polymers is still limited. The use of composite materials could help overcome this drawback, as improved mechanical, thermal, and other properties can be achieved by the combination of a polymer matrix and reinforcements or fillers [4,5].

Filler reinforcements are widely used to enhance the polymer properties of the matrix in O3DP due to their low price and simple incorporation into liquid photoresins. Fillers such as aluminum oxide (Al_2O_3) [6], diamond microparticles [7], carbon nanotubes [8,9], graphene oxide [10], titanium dioxide [11,12], and montmorillonite nanoclay [13] have been used in photosensitive resins and improved thermal, mechanical and electrical properties of O3DP objects. Although an enhancement of the composite properties was observed, the incorporated fillers were inert particles connected to the polymer matrix only via weak intermolecular interaction. Due to this, the addition of fillers is limited to a certain value, called the threshold point, beyond which the filler particles begin to form clusters and increase the accumulation of voids, leading to deterioration of the mechanical properties [14,15]. This problem could be solved by adding modified fillers with functional groups that react with the polymer matrix and promote a more efficient bonding to the polymer matrix. [16]. Silane-treated Al_2O_3 [17], graphene oxide [18], SiO_2 [19], barium titanate [20] and β-carboxyethyl acrylate treated boehmite [21] were incorporated into photoresins and significantly improved the mechanical properties of O3DP composites. Furthermore, waste materials could be used to produce fillers for composite materials: calcium silicate hydrates could be synthesized from aluminium fluoride production waste, an alternative source of silicon dioxide [22]. Although this waste is contaminated with aluminum and fluoride ions, these ions could be bound to chemically inert compounds

* Corresponding author.
E-mail address: jolita.ostrauskaite@ktu.lt (J. Ostrauskaite).

111

such as katoite and cuspidine during hydrothermal treatment [23]. In this way, the consumption of waste material and the conversion of it into the added value product would be combined. Calcium silicate hydrates of various compositions are the primary binding phases in concrete, based on Portland cement, and the main products of the calcium oxide-silica-water system under hydrothermal conditions with hydrolytic decomposition at low pH [24–28]. Crystalline calcium silicate hydrate compounds such as gyrolite (CaO and SiO2 molar ratio (C/S) = 4/6) and 1.1 nm tobermorite (C/S = 5/6) exhibit a lamellar (2D) nanoscale structure [29,30] , while xonotlite (C/S = 1) tends to form needle-shaped nanofibers (1D structure) [31], which makes these minerals suitable for use as structural fillers in polymer composites [32]. Calcium silicate hydrates can be modified with silanes to improve the interaction between the hydrophilic filler and the hydrophobic polymer matrix in composite materials. Such fillers synthesized from waste materials could provide an added value to polymeric materials by improving their mechanical and thermal properties [33]. However, its application for polymer composites for O3DP has not been sufficiently investigated.

Most O3DP materials are petroleum-derived, non-biodegradable (meth)acrylates, which have a significant negative impact on the environment [16]. AESO is a commercial biobased material that could be photocross-linked by free radical polymerization producing a solid, biodegradable polymer [34,35]. AESO is suitable not only for UV-cured coatings, but also for O3DP [36–40]. UV-cured AESO compounds with modified montmorillonite nanoclay of alkylamine [41], functionalized graphene or graphene oxide [42], modified cellulose nanocrystals [43], acryloyl group functionalized graphene [44], and carbon nanotubes functionalized with tannic acid [45] have been prepared. The reported modified fillers improved the mechanical and thermal properties of AESO-based polymers at a concentration of 1 wt%. Wu et al. [46] have produced vinyl palm oil-based biocomposites with methacrylic anhydride modified micro-scale bamboo fibers by SLA 3D printing. Introduced modified fibers to the bio-based matrix not only improved the mechanical and thermal properties of the biocomposite but could also be recycled after mild degradation of the composite matrix. AESO-based biocomposites with nanohydroxyapatite for bone tissue engineering were produced by extrusion-based 3D printing with simultaneous UV curing during layer-by-layer deposition by Mondal et al. [47]. Liu et al. [48] employed the same method to produce AESO and methacrylic anhydride-modified ethylcellulose macromonomer (ECM) composites with ECM weight contents of up to 30 wt%. Improved mechanical properties such as elongation at break, tensile strength, and elastic modulus as well as glass transition with higher loading of ECM showed excellent fiber-matrix interaction of printed composites with modified filler. AESO biocomposites with improved properties have a huge potential for use in optical 3D printing, yet their application in conventional 3D printing such as SLA and DLP is insufficient and needs to be further investigated for a broader commercial use.

The aim of this work was to develop novel AESO-based composites with functionalized calcium silicate hydrate-based fillers from waste material and apply them in optical 3D printing. Calcium silicate hydrate fillers were hydrothermally synthesized from the CaO and SiO2-rich aluminium fluoride production waste while the remaining hazardous aluminium and fluoride ions have been bound into chemically inert compounds. The performance of the filler synthesized from production waste was evaluated by comparing it with the filler synthesized from impurity-free SiO2. The interaction between the filler and the AESO-based polymer matrix was improved by modifying the fillers with acrylic groups containing silane. Complex and precise 3D objects have been produced by DLP 3D printing from AESO-based polymer composites and their mechanical, thermal properties and biodegradability were investigated.

2. Materials and methods

2.1. Materials

Acrylated epoxidized soybean oil (AESO) and UV blocker 2,5-bis(5-tert-butylbenzoxazol-2-yl) thiophene were purchased from Merck (Taufkirchen, Germany). Biobased isobornyl methacrylate (IBOMA) was kindly donated by Evonik Industries (Essen, Germany). Ethyl (2,4,6-thimethylbenzoyl) phenyl phosphinate (TPOL) was purchased from Fluorochem (Hadfield, England).

The material used to synthesize the fillers: silica gel waste, a by-product of the aluminium fluoride manufacturing process, was kindly donated by Lifosa (Kedainiai, Lithuania). The dried waste material (at room temperature until a constant mass) was milled using a Fritsch Pulverisette 9 planetary mill (Idar-Oberstein, Germany) (950 rpm, 2.5 min), S_a = 1540 m^2/kg (by Cilas LD 1090 granulometer (Orleans, France)), ρ = 2350 kg/m^3 (by Quantachrome Instruments Ultrapyc 1200e gas pycnometer (Boynton Beach, Florida, USA)). The detailed composition of the silica gel waste is available in refs [53,54]. CaO (obtained by calcining Ca(OH)$_2$ for 1 h at 550 °C, ≥96%) was purchased from Honeywell (Seelze, Germany). Calcium oxide was milled (950 rpm, 30 s), free CaO – 94%, ρ = 2840 kg/m3, S_a = 2080 m^2/kgHydrated amorphous silica – SiO$_2$·nH$_2$O was purchased from Reaktiv (Saint-Petersburg, Russia). Hydrated silica was milled (850 rpm, 2.5 min), loss of ignition (LOI) – 11.79 wt%, ρ = 2390 kg/m^3, S_a = 1430 m^2/kg [49]. For modification of the fillers, acryloxypropyltrimethoxysilane (APTMS) was purchased from Alfa Aesar (Kandel, Germany).

2.2. Synthesis and functionalisation of calcium silicate hydrates

Two types of unmodified fillers, calcium silicate hydrates, were synthesized by hydrothermal treatment at 200 °C for 12 h according to Ref. [49]: filler X, where amorphous hydrated silica (SiO$_2$·nH$_2$O) was used as the source of SiO$_2$ (CaO and SiO$_2$ molar ratio was 1:1). Filler XS, where aluminium fluoride production waste, AlF$_3$-rich silica gel was used, (CaO and (SiO$_2$ + Al$_2$O$_3$ + F$^-$) molar ratio was 1:1). The initial mixtures were homogenized using a WAB Turbula Type T2F homogenizer (Muttenz, Switzerland) at 49 rpm for 1 h. Subsequently, the homogeneous initial mixtures were combined with water (distilled) to prepare 400 mL suspensions with a liquid to solid ratio (by weight) equal to 20 in a Parr Instrument 4560 autoclave (Moline, Illinois, USA), where they were hydrothermally treated with stirring at 50 rpm for 12 h at 200 °C. Subsequently, the suspensions were filtered and the fillers obtained were treated with acetone and dried at 105 ± 0.3 °C until a constant mass. The composition of the obtained unmodified fillers is given in Table 1 [49].

The functionalization of hydrothermally synthesized calcium silicate hydrate fillers was carried out as follows. APTMS (10 wt% of the unmodified filler weight) was added to the distilled water, which was acidified with acetic acid (0.1 mol L^{-1}) to reach a pH of 3–4 at 70 °C. The APTMS was left to hydrolyze for 30 min under stirring and then the fillers were added to the solution to prepare a suspension where w/s = 10 (by weight). Functionalization was carried out in stirred suspensions for 5 h at 70 °C and then dried at 70 °C until a constant mass. The dried fillers were rinsed with isopropanol to remove weakly attached silane molecules and homocondensate of APTMS, and then dried again at 70 °C until a constant mass. The functionalized X and XS fillers were named, respectively, XM and XSM. The composition of functionalized fillers is given in Table 2.

Equations (1)–(4) show the main chemical reactions that occurred during the silanization process [50],[52].

Hydrolysis and condensation of APTMS:
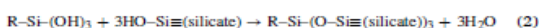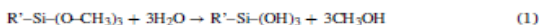
$$R'\!-\!Si\!-\!(O\!-\!CH_3)_3 + 3H_2O \rightarrow R'\!-\!Si\!-\!(OH)_3 + 3CH_3OH \qquad (1)$$

$$R\!-\!Si\!-\!(OH)_3 + 3HO\!-\!Si\!\equiv\!(silicate) \rightarrow R\!-\!Si\!-\!(O\!-\!Si\!\equiv\!(silicate))_3 + 3H_2O \qquad (2)$$

2

Table 1
Composition and characteristics of unmodified fillers [49]

| Unmodified fillers	SiO₂ source	Chemical composition, %	Mineral composition	Tapped density ρ_T, g/ml	Density ρ[a], g/ml
X	Amorphous hydrated silica ($SiO_2 \cdot nH_2O$)	44.04 % CaO, 47.18 % SiO₂, 8.78 % LOI ($CO_2 + H_2O$)	Tobermorite, xonotlite, C-S-H(I), calcite (traces)	0.070	3.1063
XS	Aluminium fluoride production waste	41.23 wt% CaO, 35.87 wt% SiO₂, 4.26 wt% Al₂O₃, 3.67 wt% F⁻ 14.97 % LOI ($CO_2 + H_2O$)	Tobermorite, cuspidine, katoite, C-S-H(I), calcite (traces)	0.0958	3.4094

[a] measured by gas pycnometer

Table 2
Composition of calcium silicate hydrate fillers from the STA data.

Filler	Mass loss at − 340–620 °C, %	Amount, % Acryloxypropyl C₆H₉O₂ group	Organic carbon C	Organic hydrogen H	Organic oxygen O	Silane silicon Si	Silane coating
X	1.75	–	–	–	–	–	–
XS	3.79	–	–	–	–	–	–
XM	3.96	2.21	1.46	0.19	0.56	0.49	2.70
XSM	5.49	1.70	1.12	0.15	0.43	0.37	2.07

The sum reaction:

$$R–Si–(O–CH_3)_3 + 3HO–Si\equiv(silicate)\ 3R–Si–(O–Si–(silicate))_3 + 3CH_3OH \quad (3)$$
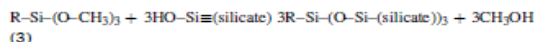
The hydrolyzed silane may also undergo homocondensation and produce silicone:

$$nR–Si–(OH)_3 \rightarrow (R–Si–(O–)_3)_n + 3nH_2O \quad (4)$$
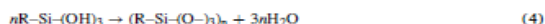
2.3. Characterisation of functionalised calcium silicate hydrate fillers

Simultaneous thermal analysis (STA) was used to quantify the silane coating on the modified fillers. STA was performed on a Linseis PT 1000 (Selb, Geramany) apparatus as in Ref. [23].

The Perkin Elmer Spectrum BX II FT-IR spectrometer (Llantrisant, UK) was used to perform Fourier transform infrared spectroscopy (FT-IR) as in Ref. [25].

Tapped density of the inorganic fillers was measured using a capped graduated cylinder (250 mL, readable to 2 mL) and a manual mechanic tapping device (VTV, Moscow, Russia). The sample was weighted to 0.0001 g, placed in a cylinder, and then tapped ∼ 250 times until the tapped volume was constant. The obtained tapped volume V_T was used to calculate the tapped density ρ_T:

$$\rho_T = \frac{m}{V_T}$$

2.4. Preparation of photocurable resins

The resins were produced by combining AESO with IBOMA in the weight ratio of 60:40 and adding from 1 wt% to 10 wt% of X filler or by combining AESO with IBOMA in the weight ratio of 40:60 and adding 5 wt% of fillers X, XS, XM and XSM (e.g. AS40/I60/XS5 and AS60/I40/X5, where AS shows weight ratio of AESO, I shows weight ratio of IBOMA, and the last part of the filler resin code stands for the filler used and amount of it). Resins without both monomer ratios (AS60/I40/0 and AS40/I60/0). The 3 mol.% of TPOL added was calculated from the total amount of both monomers. The appropriate amount of filler was mixed with the resin using an IKA T25 digital ULTRA TURRAX (Staufen, Germany) disperser at a speed of 15000 rpm at room temperature for 2 min. The composition of the prepared resins is presented in Table 3.

The viscosity of the resins was measured using a rotational Fungilab SMART L viscosimeter (Barcelona, Spain) with L2 geometry under 20 RPM at 25 °C.

2.5. Investigation of photocuring kinetics

The kinetics of photocuring and linear shrinkage (Δd) were investigated with an Anton Paar MCR302 rheometer (Graz, Austria) as reported in previous studies [37]. Average values were calculated from three measurements of each resin.

2.6. Preparation of polymer composite specimens in Teflon molds

Bio-based resins were photocross-linked in a rectangular Teflon mold $(70 \times 10 \times 1) \pm 0.08$ mm under the Helios Italquartz model GR.E 500 W

Table 3
Composition and rheological parameters of the prepared resins.

Sample	Monomer ratio AESO: IBOMA (wt./wt.)	Filler	Amount of filler, wt.%	Viscosity, mPa•s	G'[a], MPa	Δd, %	t_{gel}[b], s
AS60/I40/0	60:40	–	0	796	20.5 ± 2.5	8 ± 3.5	1.8
AS60/I40/X1		X	1	1007	9.7 ± 3.2	9.3 ± 3.1	1.0
AS60/I40/X3			3	1262	10.8 ± 2.9	8.7 ± 1.2	1.1
AS60/I40/X5			5	2056	13.1 ± 6.5	10.7 ± 3.1	1.4
AS60/I40/X10			10	2669	17.4 ± 3.0	9.3 ± 2.3	1.7
AS40/I60/0	40:60	–	5	157	15.5 ± 1.3	8 ± 2	4
AS40/I60/X5		X	5	241	10.2 ± 1.7	8.7 ± 1.2	3.5
AS40/I60/XS5		XS	5	302	8.1 ± 2.9	8.7 ± 1.2	3.3
AS40/I60/XM5		XM	5	624	11.2 ± 1.3	9.3 ± 2.3	3.7
AS40/I60/XSM5		XSM	5	266	11.4 ± 2.1	8.7 ± 2.3	3.8

[a] – G' after 600 s of irradiation
[b] – t_{gel} determined from the beginning of UV/VIS illumination.

lamp (Cambiago, Italy), intensity 310 mW cm^{-2}, at a gap of 15 cm for 5 min until solid polymer was formed.

2.7. DLP 3D printing of polymer composite specimens

A Phrozen Sonic Mini 4 K 3D printer (desktop LCD/LED, Hsinchu, Taiwan) was used for DLP 3D printing of polymer composite specimens. The printer was equipped with a LED array ($\lambda = 405$ nm) arranged throughout the build area and a monochrome LCD screen as a mask to selectively filter LED light and thus project each layer of an object to be printed. The actual building volume was ($69 \times 121 \times 132$) mm. The XY (lateral) resolution of the printer was 35 µm (6.1″ 4 K Monochrome LCD screen was used). 50 µm of layer thickness was chosen with set exposure for 12 s. Rectangular bars of ($70 \times 10 \times 1$) ± 0.01 mm were printed for the tensile test and complex shape city models. All DLP 3D printed specimens were cleaned with fresh isopropyl alcohol for 20 min and post-cured in UV chamber (LED light source: $\lambda = 365$ nm (45 W), $\lambda = 380$ nm (25 W), $\lambda = 395$ nm (70 W)) for 60 min.

2.8. Characterisation of photocross-linked polymer composites

The yield of the insoluble fraction (*YIF*) was obtained by Soxhlet extraction as previously reported [37].

Thermogravimetric analysis (TGA) was performed on a TGA 4000 apparatus (Perkin Elmer, Llantrisant, UK) according to the procedure reported [37].

Dynamic mechanical thermal analysis (DMTA) was carried out with an TA Instruments RSA-G2 (New Castle, USA) equipped with 3-point bending fixtures at a frequency of 1 Hz with a strain of 0.01 % and an axial force of 0.1 N. The test was performed from 25 °C to 200 °C at a heating rate of 3 °C/min. The storage modulus (*E′*), loss modulus (*E″*), and damping factor (*tanδ*) were monitored as a function of temperature. The glass transition temperature (*T$_g$*) was established by the peak maximum of *tanδ*. The cross-link density (*ν$_e$*) was determined according to Ref. [36].

The mechanical properties of the synthesized polymer composites were determined by a tensile test followed by the ISO 527–3 standard according to the procedure reported earlier [37] with the use of PWG50 grips.

The morphology of the fillers and composite materials was investigated with FEI Quanta FEG 200 scanning electron microscopy (SEM) (Hillsboro, USA) with a magnification of 500 to 20,000. The acceleration voltage was 10 kV.

DLP 3D printed specimens of polymer composites were analyzed using an Olympus BX41 microscope (Shinjuku, Japan) at a magnification of 50 times.

2.9. Biodegradability test of photocross-linked polymer composites

The biodegradation of polymer composites was determined according to the standard ISO 14851:1999 [52] under aerobic conditions in a closed respirometers OxiTop® Control (WTW, Weilheim, Germany) as previously reported [37].

3. Results and discussion

3.1. Functionalisation of calcium silicate hydrate fillers

The FT-IR spectrum of acryloxypropyltrimethoxysilane (APTMS) (Fig. 1a, curve 1) shows a distinctive peak at 1724 cm−1, which refers to the stretching vibrations of the C = O bond in the acrylate fragment of APTMS. Other important peaks were the following: symmetric and antisymmetric stretching of the C–H bond in the methylene CH$_2$ and methyl CH$_3$ groups at 2842–2945 cm^{-1}, as well as scissor-type stretching at 1466, 1408, 1185 and 775 cm^{-1}, axial deformation of the C = C bond at 1636 cm^{-1}, stretching and bending of the Si–O–C bond at 1076 and 810 cm^{-1} [53,54].

The main peaks in the unmodified fillers X (Fig. 1a, curve 2) and XS (Fig. 1a, curve 4) were the vibration of the stretching of the O–H bond of the silanol groups in the range of 2900–3800 cm^{-1}, the vibration of the bending of the H$_2$O molecules at 1640 cm^{-1}, the asymmetric stretching of the C–O$_3$$^{2-}$ bond in the carbonate anion at ~ 1440 cm^{-1} and 876 cm^{-1}. The distinctive peaks of the silicate structure were the following: the asymmetric stretching vibration of the Si–O bond in the SiO$_4$ silicate tetrahedra at ~ 971 cm^{-1}, the bending of the O–Si–O and Si–O–Si bonds were characterized by peaks at and ~ 450 and ~ 670 cm^{-1} respectively [25,55].

The FT-IR spectra of the functionalized fillers XM (Fig. 1a, curve 3) and XSM (Fig. 1a, curve 5) contain a peak at 1724 cm^{-1} that indicated acrylate fragments (acrylic C = O bond); therefore, it could be stated that APTMS had reacted with the filler successfully. Other segments of the spectra differed slightly from the unmodified filler and raw materials: a peak at ~ 3615 cm^{-1} was better revealed, which is common to CaO–H bonds of Al-substituted tobermorite and xonotlite [56] together with a decreased peak in the range of 2900–3800 cm^{-1} possibly due to the decrease in the amount of free silanol groups, and the broadening of
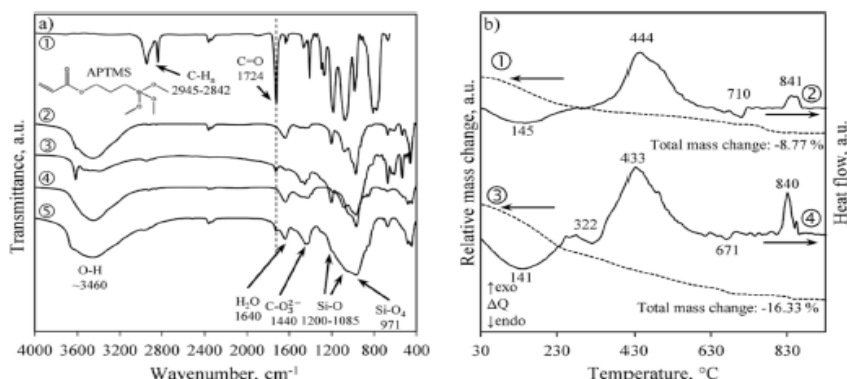

Fig. 1. a) FT-IR curves of: 1 –APTMS, 2 – filler X, 3 – filler XM, 4 – filler XS, 5 – filler XSM; b) STA curves: 1 – TG and 2 – DSC of filler XM, 3 – TG and 4 – DSC of filler XSM.

4

114

the peaks in the range of ~ 700–1400 cm^{-1} which could be caused by the increase of different types of Si–O bonds.

The STA data of the functionalized fillers XM (Fig. 1b, curves 1(TG) and 2(DSC)) and XSM (Fig. 1b, curves 3(TG) and 4(DSC)) differ from the curves of the raw materials, as they contain an exothermal peak in the range ~ 340–620 °C which refers to the oxidation and decomposition of silane residues. The mass loss in the unmodified fillers in the afore-mentioned temperature range was 1.75 % for filler X and 3.79 % for filler XS, while in the functionalized fillers: XM – 3.96 % and XSM – 5.49 %. The difference in mass loss due to the presence of silane coating was 2.21 wt% and 1.70 wt%, respectively, which corresponds to the decomposition of the carbon chain part (acryloxypropyl group) of the silane coating connected to the filler. The calculated amount of coating and its elemental composition in the filler are given in Table 2.

The other thermal effects from the STA curves are as follows: 141–145 °C – decomposition and dehydration of calcium silicate hydrates, 322 °C (XS filler only) – decomposition of katoite, 671–710 °C – decomposition of calcite, ~ 840 °C - recrystallization of semiamorphous calcium silicate hydrate phases into wollastonite [49].

SEM images of the unmodified filler XS (Fig. 2 a) and the function-alized XSM (Fig. 2 b) showed the presence of semiamorphous C–S–H(I) which could be distinguished by large agglomerates of needle-shaped particles [25], tobermorite could be recognized by its translucent plate-shaped particles [29]. Small dense round-shaped particles could be attributed to katoite [57] or calcite [25], as the filler contained traces of the latter mineral identified by STA [49]. The CSH(I) agglomerates underwent some disintegration during the coating process, but the particle shape and size of other minerals remained unchanged. The changes in the surfaces were not visible as a result of the low concentration of APTMS.

3.2. Resin characterisation and photocuring kinetics

The viscosity of conventional 3D printing resins at 25 °C is usually in the range of (200 – 1500) mPa·s, enabling them to redistribute themselves in the resin tank during the movements of the Z axis [58]. Fillers added to resin greatly influence viscosity in two aspects, the particle-solvent and particle-particle interactions [59]. The higher amount of filler from the AS60/I40 resin series significantly increased resin viscosity, influencing the stability of the prepared resins (Fig. 3). The higher amount of X filler in the AS60/I40 sample series tremendously enhanced the viscosity of the resin due to the increased particle-particle interactions [60] and improved the stability of the resin showing no sedimentation after 60 days with 10 wt% of X filler. The higher amount of X filler in the AS60/I40 sample series tremendously increased the viscosity of the resin due to the increase in particle-particle interactions

[60] and improved the stability of the resin showing no sedimentation after 60 days with 10 wt% of X filler. Such AS60/I40/X10 resin stability was monitored due to increased viscosity [61] and decreased sedimentation velocity as the concentration of X filler increased [62]. As the density of the X and XS particles was greater than 3 g/ml (Table 1) and higher than that of the fluid, the mixture is influenced by the gravitational force that leads to sedimentation. The XS filler showed a higher tapped and real density compared to the X filler showing a denser packing of heavier XS particles, resulting in increased sedimentation. Furthermore, due to the fiber-like X filler structure, the sedimentation is qualitatively different from the sedimentation of spheres, leading to slower fiber orientation distribution-dependent sedimentation [63].

The resin should be stable and homogeneous for the maximum period of time and remain uniform throughout the 3D printing process. Resin AS40/I60 with added fillers showed a suitable viscosity for O3DP in the range of (241–624) mPa·s. As the SEM images did not show obvious structural changes in the XSM filler after functionalization, the resins AS40/I60/XS5 and AS40/I60/XSM5 had relatively similar viscosity values (Table 3) and demonstrated similar resin stability (Fig. 3b). The resin AS40/I60/XM5 showed the highest viscosity of 624 mPa s, which could be affected by the steric hindrance of the XM filler with a higher amount of APTMS coupled to the filler particles.

The photocuring kinetics of biobased resins and the influence of the filler on the rheological parameters of the resins were studied by real-time photorheometry. It was determined that the fillers reduced the final values of the storage modulus (G') of all the resins investigated (Table 3). In the AS60/I40 series, 1 % of filler X significantly reduced the final values of G' compared to the same resin AS60/I40/0 without filler (Fig. 4a). The addition of a larger amount of filler increased the final value of G' and thus improved the rigidity of the composite. However, the AS60/I40/X10 resin with the highest amount of filler did not have the same final G' values as the AS60/I40/0 resin without filler, showing that the inert filler acted as a physical barrier for the formation of the polymer network and thus deteriorated the rigidity of the composite. When comparing the slope of the G' curves of AS60/I40 resins, no significant differences were observed, showing that the amount of filler had no significant influence on the photocuring rate. The addition of filler to the resin led to decreased values of the gel point (t_{gel}) (Table 3) due to the increased photocross-linking reaction. During the photopolymerization reaction, the mobility of the radical species is restricted by the formed polymer network, leading to the diffusion-controlled termination step, which leads to an increased concentration of the free radical and therefore to the polymerization rate [1]. The effect of the inorganic filler network is analogous to that of a cross-linked organic network on the curing process that results in the accelerated photopolymerization reaction [64,65]. The lowest shrinkage was observed when there was no
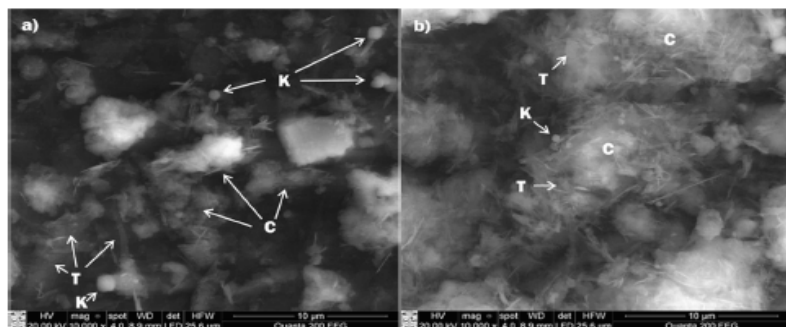

Fig. 2. SEM images of a) uncoated XS filler; b) coated XSM filler. Indices: T – tobermorite, K – katoite, C – C-S-H(I).
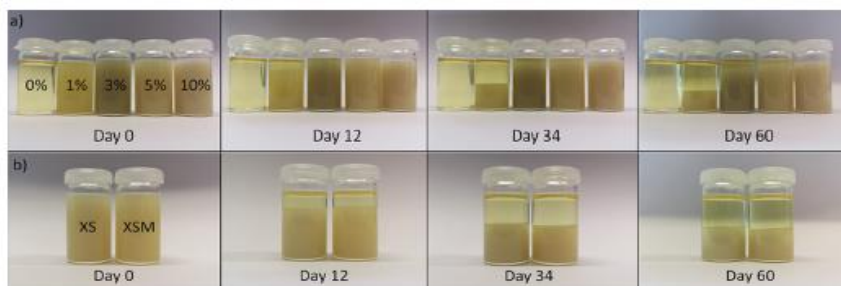
115

Fig. 3. Stability of resins in the 60-day period: resins AS60/I40/0–AS60/I40/X10 with different amounts of X filler (a) and AS40/I60 resin with 5 wt% of XS and XSM fillers (b).
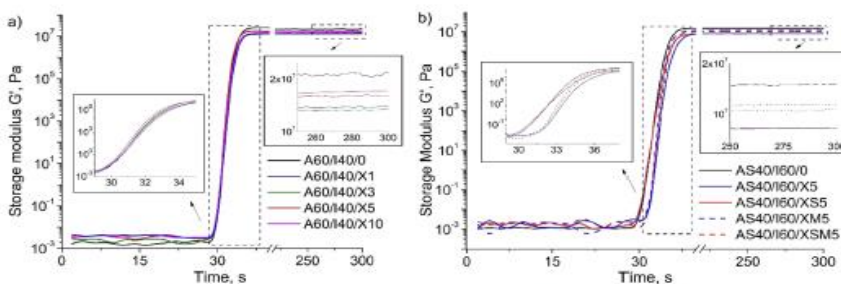

Fig. 4. Storage modulus G′ curves of AS60/I40 (a) and AS40/I60 series (b).

filler in the resin. As resins without fillers showed the slowest photocross-linking reaction with the highest G' values, slower formation of cross-links led to lower polymer shrinkage [66]. The resins with different amounts of X filler showed no dependency between the amount of filler and shrinkage. This irregularity could be caused by inhomogeneous resin, where smaller or larger filler particles were unevenly distributed in the 50 µm gap of the measuring system during the real-time photorheometry test.

Functionalized fillers increased the final values of G' compared to the unmodified ones, confirming the formation of mechanically stiffer composites (Fig. 4b). A significantly higher final value of G' of resin AS40/I60/XSM5 compared to resin AS40/I60/XS5 (Table 3) indicated a successful bonding of the XSM filler to the polymer matrix. In addition, the resins with modified fillers showed a higher t_{gel} and slower photo-curing process, followed by the formation of a stiffer polymer network and a higher final value of G'.

3.3. Characterisation of polymer composites by SEM

SEM images of photocured composite samples with unmodified filler XS (Fig. 5a and 5c) and functionalized filler XSM (Fig. 5b and 5d) show the distribution of tobermorite platelets, C–S–H(I) lumps and katoite 'dots'. The particles of unmodified filler XS tend to agglomerate as they are hydrophilic. The functionalized filler XSM showed better interaction with the polymer, as its particles were better distributed in the hydrophobic matrix.

3.4. Thermal properties of polymer composites

The thermal stability of biobased polymer composites was monitored
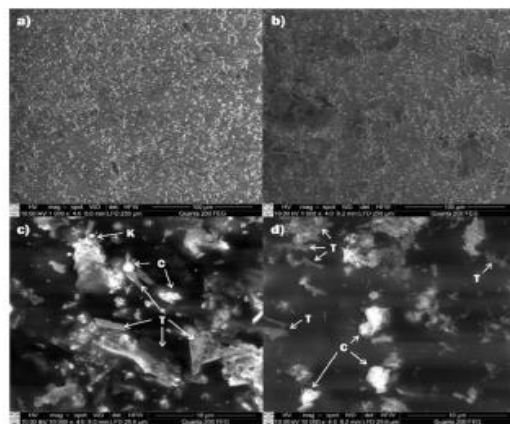
Fig. 5. SEM images of UV-cured composite samples filled with unmodified filler XS (a, c) and functionalised filler XSM (b, d). Indices: T – tobermorite, K – katoite, C – C-S-H(I).

by thermogravimetric analysis (TGA). The TGA curves are presented in Fig. 6. The thermal decomposition temperature was determined at a weight loss of 10 % ($T_{dec.-10\%}$) of the composites was above 308 °C, indicating their high thermal stability (Table 4). It was observed that 1

116
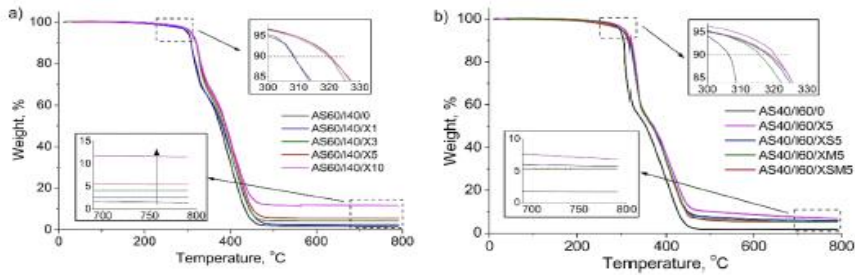
Fig. 6. TGA curves of composite series AS60/I40 (a) and AS40/I60 (b).

Table 4
Thermal characteristics of AESO-based photocross-linked composites.

Sample	TGA		DMTA				
	$T_{dec-10\%}$, °C	Char yield, %	T_g, °C	$tan\delta$ at T_g	E'_{30}[a], MPa	E'_{Tg+50}[b], MPa	v_e, mol m^{-3}
AS60/I40/0	308.5	1.49	99.2	0.644	2155.8	38.5	3655.7
AS60/I40/X1	308.3	2.53	91.6	0.545	1428.3	33.7	3261.8
AS60/I40/X3	320.2	4.09	91.2	0.510	1511.0	36.2	3498.8
AS60/I40/X5	320.2	6.43	91.0	0.499	1693.7	41.3	3999.0
AS60/I40/X10	319.5	11.60	89.4	0.465	1346.9	44.2	4296.9
AS40/I60/0	306.5	1.73	114.8	1.019	3184.1	71.6	6546.0
AS40/I60/X5	320.3	6.88	110.0	0.808	3024.4	93.1	8618.4
AS40/I60/XS5	318.2	5.79	108.5	0.845	2340.8	109.0	10131.3
AS40/I60/XM5	315.9	5.32	106.8	0.755	2628.8	72.1	6727.5
AS40/I60/XSM5	318.8	5.34	111.5	0.963	2511.8	74.5	6872.1

[a] – E' values at 30 °C
[b] – E' values at 50 °C above T_g
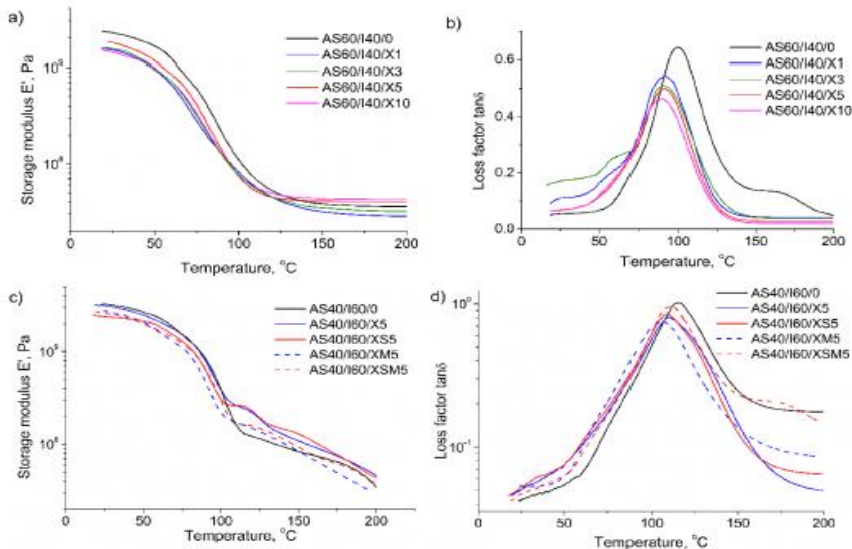
Fig. 7. DMTA curves of polymer composites: AS60/I40 series E' (a) and $tan\delta$ (b) curves, AS40/I60 series E' (c) and $tan\delta$ (d) curves.

7

117

% of filler X did not have an impact on the thermal stability of the compound, while the higher amount of filler X increased $T_{dec.-10\%}$ at more than 12 °C in the AS60/I40 sample series. $T_{dec.-10\%}$ of composite AS40/I60/0 was lower compared to AS60/I40/0 due to the increased loss of isobornyl fragments through ester bond scission [67]. Despite the decreased thermal stability of the polymer matrix, all fillers in the AS40/I60 series significantly increased $T_{dec.-10\%}$. The largest changes in $T_{dec.-10\%}$ were observed between the composites with filler X and filler XM. Almost 5 °C lower $T_{dec.-10\%}$ values were observed when the modified filler was used. This consequential reduction in the thermal stability of the AS40/I60/XM5 composite could be related to the scission of the silane fragments in the composite, as a higher amount of silane coupled to the filler XM was registered, as confirmed by STA (Table 2). The lower char yields of composites with functionalized fillers were related to the loss of silane from the filler.

Thermomechanical properties of photocross-linked composites were carried out by dynamic mechanical analysis (DMTA). In general, for most thermosetting resins, the $tan\delta$ maximum peak appears at T_g, allowing easy and exact monitoring of T_g values [68]. It was observed that T_g values decreased when a higher amount of filler was used in the sample series AS60/I40 (Table 4). The reduced T_g values indicated the high effect of the inert filler on the polymer matrix and its increased flexibility. On the other hand, a higher amount of filler caused higher values of E'_{Tg+50} (Fig. 7a) leading to the enhanced ν_e. Although the inert filler acted as a physical barrier in polymer network formation, causing a reduced T_g value, the mobility of the filler restrained the polymer matrix mobility at higher temperatures and increased thermal stability. Furthermore, since the height of $tan\delta$ peaks is associated with structural homogeneity and chain mobility, cross-linking often decreases $tan\delta$ values in the glass transition region [69]. This relation was clearly seen in the composite series AS60/I40 (Fig. 7b) when the increased amount of filler caused lower $tan\delta$ values at T_g peak resulting in higher ν_e.

The composites of the AS40/I60 series showed a slight peak above 100 °C in the E' curves (Fig. 7c). The most characteristic peaks were obtained in the composites with filler X and filler XS as the peaks in the E' curves of samples with functionalized fillers were barely noticeable. This peak could be related to the unreacted acrylic groups in the polymer because unmodified fillers caused spatial irregularities as a physical barrier that blocked the cross-linking of polymer chains and left residues of unreacted monomers. The smaller peak in the E' curves of the composites with functionalized fillers indicated a more effective composite formation leaving a lower amount of uncured resin. The composites of the AS40/I60 series had lower T_g and E'_{30} compared to the polymer without filler. However, all composites from series AS40/I60 showed higher E'_{Tg+50} values indicating higher polymer stability at higher temperatures compared to the unfilled polymer, as confirmed by TGA. The decreased T_g values of 3D printed polymer composite with functionalized filler were also reported by Liu et al. [70] where T_g of the composite with 5 wt% of functionalized filler was reduced by 8.6 °C. Although lower T_g values were determined for composites AS40/I60, the higher cross-link density was obtained showing improved polymer

matrix rigidity when filler was used. Furthermore, a reduction of ν_e was observed when functionalized filler was used. This could be caused by the slight disablement agglomerates of C-S-H(I) during filler functionalization, which led to a weaker interaction between the filler and polymer matrix, thus reducing not only ν_e but also YIF (Table 5). It was observed that only the composite with functionalized XS filler showed enhanced T_g and E'_{30} values compared to those of the unmodified filler. This showed that filler XSM is superior not just because of its recycled origin but also because of the improved thermomechanical properties of the composite, which distinguishes it as a potential material for O3DP.

3.5. Tensile test of polymer composite specimens

The tensile properties of biobased composites were studied using specimens prepared in Teflon molds. Representative stress-strain curves of the AS60/I40/0-AS60/I40/X10 polymer composite samples (Fig. 8a) showed a reduction in elongation at break (ε) when filler X was used. The AS60/I40/X1 polymer composite specimens showed a slight increase in tensile stress (δ) compared to the polymer specimen without a filler AS60/I40/X0, although increasing the amount of filler resulted in a decrease of δ and ε values. This reduction in mechanical characteristics was observed with an increasing amount of filler due to the weak interaction between an inert filler and the polymer matrix, where the filler acted as a physical barrier for the formation of cross-links [19]. Li et al. [71] reported a similar trend where cellulose nanocrystal reinforced poly(ethylene glycol) diacrylate composites were DLP 3D printed and by the load of 5 wt% of filler significantly reduced the ε and δ.

In the AS40/I60 composite series, fillers significantly increased E_g values. The composite with filler X showed the highest δ and ε values, while the composite AS40/I60/XM5 showed the lowest values of the parameters mentioned. This demonstrated that the filler XM did not form a strong interaction with the AESO-based polymer matrix, leading to deteriorated elasticity and tensile strength. The composite with filler XS showed a significant increase in values of δ and ε when functionalized filler was used. This proved the strong interfacial interaction between the functionalized filler and polymer matrix with increased elasticity, confirming the successful functionalization of XS and allowing the use of it as a reactive filler in photocurable resins for DLP 3D printing.

3.6. DLP 3D printing of polymer composite objects

The resins with fillers XS and XSM were chosen for use in DLP 3D printing due to the highest values of tensile parameters, thermal stability, and cross-linking density of the composites with filler XSM and its recycled origin. For comparison, the resin with the unmodified filler XS was DLP 3D printed as well. DLP 3D printed objects of polymer composites showed high printing accuracy of small details with smooth surface finishing (Fig. 9a). Microscope images of AS40/I60/XSM5 surface top layers at the beginning of the DLP 3D printing and the bottom layers at the end of the DLP 3D printing (Fig. 9c) revealed the sedimentation of the larger particles during the printing process. Sedimentation could be accelerated by the heat generated during an exothermic reaction of the (meth)acrylate photocross-linking reaction [72], which leads to reduced viscosity. SEM images confirmed a good adhesion of the filler/matrix, as the particles were still embedded in the matrix with visible tobermorite and katoite clusters (Fig. 9b).

Furthermore, $(70 \times 10 \times 1) \pm 0.01$ mm samples for the tensile test were DLP 3D printed to determine the adhesion between the printed layers and to compare the mechanical parameters with those of composite specimens prepared in the Teflon mold. Stress-strain curves of DLP 3D printed specimens AS40/I60/XSS-3D and AS40/I60/XSM5-3D and those prepared in the Teflon mold AS40/I60/XS5 and AS40/I60/XSM5 are presented in Fig. 8b. The tensile test showed that DLP 3D printed composite specimens improved mechanical properties compared to mold-prepared composite specimens. Increased δ and ε values of the DLP 3D printed specimens demonstrated strong adhesion

Table 5
Yield of insoluble fraction and tensile characteristics of polymer composites.

Sample	YIF, %	E_g, GPa	δ, MPa	ε, %
AS60/I40/0	98.9	5.6 ± 0.1	177.0 ± 18.3	4.7 ± 1.2
AS60/I40/X1	96.1	6.4 ± 0.3	176.1 ± 16.2	3.9 ± 0.8
AS60/I40/X3	96.0	7.0 ± 0.3	127.5 ± 14.4	2.3 ± 0.3
AS60/I40/X5	95.2	6.8 ± 0.2	95.6 ± 10.1	1.6 ± 0.2
AS60/I40/X10	95.0	6.7 ± 0.6	104.8 ± 22.8	1.9 ± 0.6
AS40/I60/0	99.7	4.8 ± 0.9	69.6 ± 4.1	1.4 ± 0.02
AS40/I60/XS5	94.9	8.9 ± 0.3	103.6 ± 44.5	2.2 ± 0.4
AS40/I60/XS5	93.5	11.0 ± 1.5	75.6 ± 11.3	0.8 ± 0.2
AS40/I60/XS5-3D	94.3	10.1 ± 0.6	128.6 ± 17.4	1.3 ± 0.2
AS40/I60/XM5	94.1	9.1 ± 0.8	48.3 ± 4.6	0.6 ± 0.1
AS40/I60/XSM5	92.7	10.7 ± 0.7	97.4 ± 4.1	1.2 ± 0.3
AS40/I60/XSM5-3D	93.1	10.8 ± 0.2	137.4 ± 5.9	1.3 ± 0.1

118
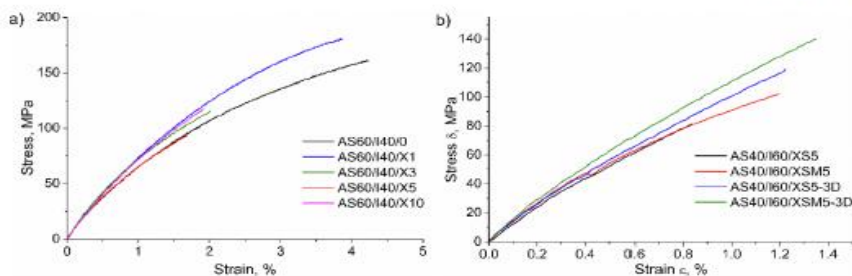
Fig. 8. Stress-strain curves of polymer composites AS60/I40/X0-10 (a); stress-strain curves of AS40/I60/XS5 and AS40/I60/XSM5 3D printed specimens and specimens prepared in the mold (b).
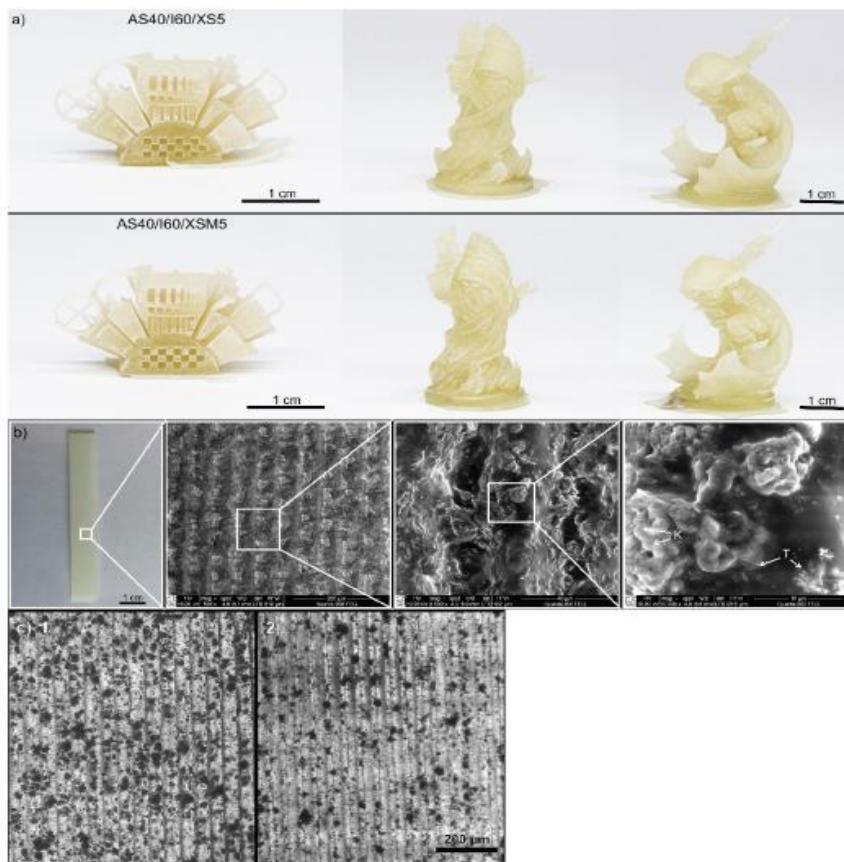
Fig. 9. DLP 3D printed objects of AS40/I60/XS5 (top) and AS40/I60/XSM5 (bottom) (a); SEM pictures of DLP 3D printed AS40/I60/XSM5 (b) microscope pictures of the surface of the specimen AS40/I60/XSM5: 1 – top layers at the beginning of DLP 3D printing, 2 – bottom layers at the end of DLP 3D printing (c);

119

between the photocross-linked layers and increased elasticity of polymer chains [73]. Photocross-linking of the thinner resin layer during O3DP compared to the preparation of the specimen in the mold led to better light penetration following higher YIF and δ with ε values (Table 5). DLP 3D printed specimens with XSM filler attained higher values of all three tensile parameters compared to AS40/I60/XS5-3D due to the use of the functionalized filler and formed covalent bonds between the functionalized filler and the polymer matrix.

3.7. Biodegradability test of polymer composites

The biodegradation of polymer composites was evaluated by measuring oxygen consumption in closed respirometers under laboratory conditions with inoculated test medium. Polymer composites prepared showed biodegradation of (0.7 – 19.6) % after 60 days, and cellulose, a reference material, was biodegraded by 54.4 % after the same period (Fig. 10). The highest biodegradation rate of the investigated polymer composites was observed to be recorded in 14 days. After this period, a relative plateau was reached and the biodegradation process was very slow. The decreased biodegradation rate could be related to the insufficient concentration of microorganisms in the test medium selectively degrading biobased polymer, but monitored oxygen consumption in closed respirometers determined the potential biodegradability of biocomposites in natural environments [52].

The highest biodegradability of the investigated polymer composites was shown by AS40/I60/XSM5 with functionalized filler synthesized from aluminum fluoride production waste. Compared to the polymer composite containing unmodified XS filler, the biodegradability (0.7 %) was the lowest, the functionalization of the filler increased the biodegradability of the polymer composite. Due to the noticeably lower cross-linking density of AS40/I60/XS5 compared to that of AS40/I60/XSM5, the penetration of aqueous test medium and microorganisms or enzymes (i.e., cellulase and lipase) into the specimen was increased and biodegradation increased [74]. It was observed that the polymer composite with the filler X showed a relatively higher biodegradability compared to the polymer composite with the filler XS. This difference could be related to the structure of the fillers, as xonotlite and tobermorite dominated in the filler X, while cuspidine and tobermorite dominated in the filler XS [49]. As the average crystal size of xonotlite is twice that of tobermorite [75], the easier the penetration of microorganisms into polymer composites with the filler X and the higher biodegradation could be registered.

4. Conclusions

In this study, a new way of using of industrial inorganic waste and its conversion into environmentally friendly products by optical 3D printing technology that is applicable in a wide range of areas has been proposed. Novel photocurable biodegradable composites in which the polymer matrix is derived from renewable raw material and the functionalized fillers are derived from industrial inorganic waste material were developed. Acrylated epoxidized soybean oil-based photoresins with calcium silicate hydrate fillers functionalized with acryloxypropyltrimethoxysilane were successfully applied in commercial digital light processing 3D printing.

During the hydrothermal synthesis of calcium silicate hydrate fillers from aluminium fluoride production waste, the remaining hazardous aluminium and fluoride ions were bound into chemically inert compounds. The use of filler synthesized from industrial waste led to an improvement in the characteristics of the composites, such as the glass transition temperature, the cross-linking density, Young's modulus, the tensile strength, and the elongation at break, compared to filler synthesized from impurity-free initial material. The biodegradability of photocured polymer composites reached 19.6 % in 60 days. The high 3D printing accuracy, perfect layer adhesion, and smooth surface finishing of 3D objects printed with a commercial digital light processing 3D
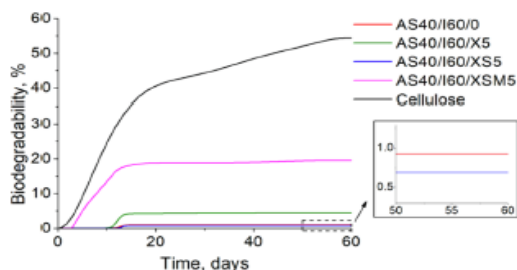

Fig. 10. Biodegradation of polymer composites and reference material cellulose.

printer have been shown by the developed composites. The composite with 5 wt% of functionalized filler synthesized from aluminium fluoride production waste was considered the most suitable for digital light processing 3D printing. The developed composites have the great potential to be a competitive alternative to conventional petroleum-derived ones and reduce the environmental impact.

Funding

CRediT authorship contribution statement

Migle Lebedevaite: Conceptualization, Methodology, Investigation, Validation, Formal analysis, Writing – original draft, Visualization. **Andrius Ginelka:** Conceptualization, Methodology, Investigation, Validation, Formal analysis, Writing – original draft, Visualization. **Valdas Talacka:** Methodology, Investigation, Validation, Visualization. **Kestutis Baltakys:** Conceptualization, Supervision, Writing – review & editing. **Jolita Ostrauskaite:** Conceptualization, Supervision, Writing – review & editing, Project administration, Funding acquisition.

Declaration of Competing Interest

The authors declare that they have no known competing financial interests or personal relationships that could have appeared to influence the work reported in this paper.

References

[1] Skliutas E, Lebedevaite M, Kabouraki E, Baldacchini T, Ostrauskaite J, Vamvakaki M, et al. Polymerization mechanisms initiated by spatio-temporally confined light. Nanophotonics 2021.
[2] Zhang Y, Xu Y, Simon-Masseron A, Lalevée J. Radical photoinitiation with LEDs and applications in the 3D printing of composites. Chem Soc Rev 2021;50(6): 3824–41.
[3] Wang X, Jiang M, Zhou Z, Gou J, Hui D. 3D printing of polymer matrix composites: a review and prospective. Compos B Eng 2017;110:442–58.
[4] Malhotra SK, Goda K, Sreekala MS. Part one introduction to polymer composites. Polym Compos 2012;1:1–2.
[5] Voet VSD, Guit J, Loos K. Sustainable photopolymers in 3d printing: a review on biobased, biodegradable, and recyclable alternatives. Macromol Rapid Commun 2021;42(3):2000475.
[6] Kurimoto M, Yamashita Y, Ozaki H, Kato T, Funabashi T, Suzuoki Y. 3D printing of conical insulating spacer using alumina/UV-cured-resin composite. In: In: 2015 IEEE Conference on Electrical Insulation and Dielectric Phenomena (CEIDP); 2015. p. 463–6.
[7] Kalsoom U, Peristyy A, Nesterenko PN, Paull B. A 3D printable diamond polymer composite: a novel material for fabrication of low cost thermally conducting devices. RSC Adv 2016;6(44):38140–7.
[8] Zhang Y, Li H, Yang Xi, Zhang T, Zhu K, Si W, et al. Additive manufacturing of carbon nanotube-photopolymer composite radar absorbing materials. Polym Compos 2018;39(S2):E671–6.

[9] Sandoval JH, Wicker RB. Functionalizing stereolithography resins: effects of dispersed multi-walled carbon nanotubes on physical properties. Rapid Prototyping J 2006.

[10] Lin D, Jin S, Zhang F, Wang C, Wang Y, Zhou C, et al. 3D stereolithography printing of graphene oxide reinforced complex architectures. Nanotechnology 2015;26(43): 434003.

[11] Totu EE, Cristache CM, Perieanu VS, Burlibasa M, Petre DC, Burlibasa L. Are nano TiO2 inclusions improving biocompatibility of photocurable polydimethylsiloxane for maxillofacial prosthesis manufacturing? Appl Sci 2021;11(9):3777.

[12] Totu EE, Nechifor AC, Nechifor G, Aboul-Enein HY, Cristache CM. Poly (methyl methacrylate) with TiO2 nanoparticles inclusion for stereolitographic complete denture manufacturing – the fututre in dental care for elderly edentulous patients? J Dent 2017;59:68–77.

[13] Eng H, Maleksaeedi S, Yu S, Choong YYC, Wiria FE, Tan CLC, et al. 3D stereolithography of polymer composites reinforced with orientated nanoclay. Procedia Eng 2017;216:1–7.

[14] Saroia J, Wang Y, Wei Q, Lei M, Li X, Guo Y, et al. A review on 3D printed matrix polymer composites: its potential and future challenges. Int J Adv Manuf Technol 2020;106(5-6):1695–721.

[15] Ibrahim F, Mohan D, Sajab MS, Bakarudin SB, Kaco H. Evaluation of the compatibility of organosolv lignin-graphene nanoplatelets with photo-curable polyurethane in stereolithography 3d printing. Polymers 2019;11(10):1544.

[16] Eng CC, Ibrahim NA, Zainuddin N, Ariffin H, Yunus WMZW. Impact strength and flexural properties enhancement of methacrylate silane treated oil palm mesocarp fiber reinforced biodegradable hybrid composites. Scient World J 2014;2014:1–8.

[17] Yun JS, Park T, Jeong YH, Cho JH. Development of ceramic-reinforced photopolymers for SLA 3D printing technology. Appl Phys A 2016;122(6):1–6.

[18] Uysal E, Çakir M, Ekici B. Graphene oxide/epoxy acrylate nanocomposite production via SLA and importance of graphene oxide surface modification for mechanical properties. Rapid Prototyping J 2021;27(4):682–91.

[19] Jeong G, Park CH, Kim B-Y, Kim J, Park S-D, Yang H, et al. Photocurable elastomer composites with SiO2-mediated cross-links for mechanically durable 3D printing materials. ACS Appl Polymer Mater 2020;2(11):5228–37.

[20] Kim K, Zhu W, Qu X, Aaronson C, McCall WR, Chen S, et al. 3D optical printing of piezoelectric nanoparticle-polymer composite materials. ACS Nano 2014;8(10): 9799–806.

[21] Han Y, Wang FuKe, Wang H, Jiao X, Chen D. High-strength boehmite-acrylate composites for 3D printing: reinforced filler-matrix interactions. Compos Sci Technol 2018;154:104–9.

[22] Baltakys K, Iljina A, Bankauskaite A. Thermal properties and application of silica gel waste contaminated with F− ions for CSH synthesis. J Therm Anal Calorim 2015;121(1):145–54.

[23] Gineika A, Siauciunas R, Baltakys K. Synthesis of wollastonite from AlF 3-rich silica gel and its hardening in the CO 2 atmosphere. Sci Rep 2019;9(1):1–10.

[24] Zhao Q, Li T, Cui C, Wang Z, Ding X, Zhang S. Preparation of porous silica powder via selective acid leaching of calcined tobermorite. Powder Technol 2020;375: 420–32.

[25] Smalkys G, Siauciunas R. Peculiarities of xonotlite synthesis from the raw materials with different SiO2 activities. J Therm Anal Calorim 2020;142(5): 1671–9.

[26] Kubátová D, Zezulová A, Rybová A, Nečas R. Application of dilatometric analysis to the study of autoclaved calcium silicate materials. J Therm Anal Calorim 2018;133 (1):399–404.

[27] Tian H, Stephan D, Lothenbach B, Lehmann C. Influence of foreign ions on calcium silicate hydrate under hydrothermal conditions: a review. Constr Build Mater 2021; 301:124071.

[28] Guo X, Meng F, Shi H. Microstructure and characterization of hydrothermal synthesis of Al-substituted tobermorite. Constr Build Mater 2017;133:253–60.

[29] Liao W, Li W, Fang Z, Lu C, Xu Z. Effect of different aluminum substitution rates on the structure of Tobermorite. Materials 2019;12(22):3765.

[30] Różycka A, Kotwica Ł., Małolepszy J. Synthesis of single phase gyrolite in the CaO-quartz-Na2O-H2O system. Mater Lett 2014;120:166–9.

[31] Wu J, Zhu Y-J, Cheng G-F, Huang Y-H. Microwave-assisted preparation of Ca6Si6O17 (OH) 2 and β-CaSiO3 nanobelts. Mater Res Bull 2010;45(4):509–12.

[32] Okuyama T, Maeda H, Ishida EH. Preparation of porous poly (l-lactic acid)/ tobermorite composite membranes via electrospinning and heat treatment. J Mater Sci 2012;47(2):643–8.

[33] Wang L, Guo F, Lin Y, Yang H, Tang SW. Comparison between the effects of phosphorous slag and fly ash on the C-S-H structure, long-term hydration heat and volume deformation of cement-based materials. Constr Build Mater 2020;250: 118807.

[34] Lebedevaite M, Ostrauskaite J. Influence of photoinitiator and temperature on photocross-linking kinetics of acrylated epoxidized soybean oil and properties of the resulting polymers. Ind Crops Prod 2021;161:113210.

[35] Zych A, Tellers J, Bertolacci L, Ceseracciu L, Marini L, Mancini M, Athanassiou A. Biobased, Biodegradable, Self-Healing Boronic Ester Vitrimers from Epoxidized Soybean Oil Acrylate. ACS Applied Polymer Materials 2020.

[36] Guit J, Tavares MBL, Hul J, Ye C, Loos K, Jager J, et al. Photopolymer resins with biobased methacrylates based on soybean oil for stereolithography. ACS Appl Polym Mater 2020;2(2):949–57.

[37] Lebedevaite M, Talacka V, Ostrauskaite J. High biorenewable content acrylate photocurable resins for DLP 3D printing. J Appl Polym Sci 2021;138(16):50233.

[38] Lebedevaite M, Ostrauskaite J, Skliutas E, Malinauskas M. Photoinitiator free resins composed of plant-derived monomers for the optical μ-3d printing of thermosets. Polymers 2019;11(1):116.

[39] Danish M, Vijay Anirudh P, Karunakaran C, Rajamohan V, Mathew AT, Koziol K, Thakur VK, Kannan C, Balan A. 4D printed stereolithography printed plant-based sustainable polymers: Preliminary investigation and optimization. J Appl Polym Sci 2021:50903.

[40] Barkane A, Platnieks O, Jurinovs M, Kasetaite S, Ostrauskaite J, Gaidukovs S, et al. UV-light curing of 3D printing inks from vegetable oils for stereolithography. Polymers 2021;13(8):1195.

[41] Åkesson D, Skrifvars M, Lv S, Shi W, Adekunle K, Seppälä J, et al. Preparation of nanocomposites from biobased thermoset resins by UV-curing. Prog Org Coat 2010;67(3):281–6.

[42] Wang H, Gupta A, Kim BS. Photo-crosslinked polymer networks based on graphene-functionalized soybean oil and their properties. Korean J Chem Eng 2019;36(4):591–9.

[43] Auclair N, Kaboorani A, Riedl B, Landry V. Effects of surface modification of cellulose nanocrystals (CNCs) on curing behavior, optical, and thermal properties of soybean oil bio-nanocomposite. J Coat Technol Res 2020;17(1):57–67.

[44] Dong B, Yuan Y, Luo J, Dong L, Liu R, Liu X. Acryloyl-group functionalized graphene for enhancing thermal and mechanical properties of acrylated epoxidized soybean oil UV-curable based coatings. Prog Org Coat 2018;118:57–65.

[45] Tan K, Lin R, Luo J, Zhu Ye, Wei W, Liu X. Tannic acid functionalized UV-curable carbon nanotube: Effective reinforcement of acrylated epoxidized soybean oil coating. Prog Org Coat 2019;130:214–20.

[46] Wu Y, Li C, Chen T, Qiu R, Liu W. Photo-curing 3D printing of micro-scale bamboo fibers reinforced palm oil-based thermosets composites. Compos A Appl Sci Manuf 2022;152:106695.

[47] Mondal D, Srinivasan A, Comeau P, Toh Y-C, Willett TL. Acrylated epoxidized soybean oil/hydroxyapatite-based nanocomposite scaffolds prepared by additive manufacturing for bone tissue engineering. Mater Sci Eng: C 2021;118:111400.

[48] Liu Z, Knetzer DA, Wang J, Chu F, Lu C, Calvert PD. 3D printing acrylated epoxidized soybean oil reinforced with functionalized cellulose by UV curing. J Appl Polym Sci 2021:51561.

[49] Gineika A, Dambrauskas T, Baltakys K. Synthesis and characterisation of wollastonite with aluminium and fluoride ions. Ceram Int 2021;47(16):22900–10.

[50] Ma G, Yue X, Zhang S, Rong C, Wang Q. Preparation and properties of poly (ether ether ketone) composites reinforced by modified wollastonite grafting with silaneterminated poly (ether ether ketone) oligomers. J Polym Res 2011;18(6): 2045–53.

[51] Ciobotaru I-A, Maior I, Vaireanu D-I, Cojocaru A, Caprarescu S, Ciobotaru I-E. The determination of the optimum hydrolysis time for silane films deposition. Appl Surf Sci 2016;371:275–80.

[52] ISO 14851. Determination of the ultimate aerobic biodegradability of plastic materials in an aqueous medium-Method by measuring the oxygen demand in a closed respirometer. 1999.

[53] Lopes IMF, Abersfelder K, Oliveira PW, Mousavi SH, Junqueira RMR. Flower-like silicon dioxide/polymer composite particles synthesized by dispersion polymerization route. J Mater Sci 2018;53(16):11367–77.

[54] Pantoja M, Velasco F, Broekema D, Abenojar J, Real JCD. The influence of pH on the hydrolysis process of γ-methacryloxypropyltrimethoxysilane, analyzed by FT-IR, and the silanization of electrogalvanized steel. J Adhes Sci Technol 2010;24(6): 1131–43.

[55] Iljina A, Baltakys K, Bankauskaite A, Eisinas A, Kitrys S. The stability of formed CaF 2 and its influence on the thermal behavior of C-S-H in CaO–silica gel waste-H 2 O system. J Therm Anal Calorim 2017;127(1):221–8.

[56] Mostafa NY, Shaltout AA, Omar H, Abo-El-Enein SA. Hydrothermal synthesis and characterization of aluminium and sulfate substituted 1.1 nm tobermorites. J Alloys Compounds 2009;467(1-2):332–7.

[57] Zapata JF, Gomez M, Colorado HA. Structure-property relation and Weibull analysis of calcium aluminate cement pastes. Mater Charact 2017;134:9–17.

[58] Pugh RJ, Bergstrom L. Surface and colloid chemistry in advanced ceramics processing. CRC Press; 2017.

[59] Palucci Rosa R, Rosace G. Nanomaterials for 3D printing of polymers via stereolithography: concept, technologies, and applications. Macromol Mater Eng 2021;306(10):2100345.

[60] Samir A, Saïd MA, Alloin F, Sanchez J, El Kissi N, Dufresne A. Preparation of cellulose whiskers reinforced nanocomposites from an organic medium suspension. Macromolecules 2004;37(4):1386–93.

[61] Yan W, Chen X, Lim JSK, Chen H, Gill V, Lambourne A, et al. Epoxy-assisted ball milling of boron nitride towards thermally conductive impregnable composites. Compos A Appl Sci Manuf 2022;156:106868.

[62] Feist M, Nirschl H, Wagner J, Hirsch G, Schabel S. Experimental results for the settling behaviour of particle-fiber mixtures. Phys Separ Sci Eng 2007;2007:1–6.

[63] Leite JL, Rasteiro M, Salmoria G, Ahrens C, Pouzada A. Epoxy/steel fiber composites—a simple model to predict the fiber sedimentation. Polym Compos 2010;31(8):1378–86.

[64] Li F, Zhou S, Gu G, You Bo, Wu L. Preparation and characterization of ultraviolet-curable nanocomposite coatings initiated by benzophenone/n-methyl diethanolamine. J Appl Polym Sci 2005;96(3):912–8.

[65] Sadej-Bajerlain M, Gojzewski H, Andrzejewska E. Monomer/modified nanosilica systems: photopolymerization kinetics and composite characterization. Polymer 2011;52(7):1495–503.

[66] He Y, Yao M, Nie J. Shrinkage in UV-curable coatings. In: Anonymous Protective Coatings. : Springer; 2017. p. 195-223.

[67] Jaillet F, Darroman E, Boutevin B, Caillol S. A chemical platform approach on cardanol oil: from the synthesis of building blocks to polymer synthesis. OCL 2016; 23(5):D511.

121

[68] Lu J, Hong CK, Wool RP. Bio-based nanocomposites from functionalized plant oils and layered silicate. J Polym Sci, Part B: Polym Phys 2004;42(8):1441–50.

[69] Shnawa HA, Jahani Y, Khalaf MN, Taobi AH. The potential of tannins as thermal co-stabilizer additive for polyvinyl chloride. J Therm Anal Calorim 2016;123(2): 1253–61.

[70] Liu Y, Lin Y, Jiao T, Lu G, Liu J. Photocurable modification of inorganic fillers and their application in photopolymers for 3D printing. Polym Chem 2019;10(46): 6350–9.

[71] Li V-F, Kuang X, Mulyadi A, Hamel CM, Deng Y, Qi HJ. 3D printed cellulose nanocrystal composites through digital light processing. Cellulose 2019;26(6): 3973–85.

[72] Hennessy MG, Vitale A, Cabral JT, Matar OK. Role of heat generation and thermal diffusion during frontal photopolymerization. Phys Rev E 2015;92(2):022403.

[73] Borrello J, Nasser P, Iatridis JC, Costa KD. 3D printing a mechanically-tunable acrylate resin on a commercial DLP-SLA printer. Addit Manuf 2018;23:374–80.

[74] Calabia B, Ninomiya F, Yagi H, Oishi A, Taguchi K, Kunioka M, et al. Biodegradable poly (butylene succinate) composites reinforced by cotton fiber with silane coupling agent. Polymers 2013;5(1):128–41.

[75] Ogur E, Botti R, Bortolotti M, Colombo P, Vakifahmetoglu C. Synthesis and additive manufacturing of calcium silicate hydrate scaffolds. J Mater Res Technol 2021;11:1142–51.

122

10. APPENDIX

10.1. MB "AmeraLabs" Trial production act

AMERALABS

TRIAL PRODUCTION ACT

DLP 3D printing of acrylated epoxidized soybean oil-based resins in the MB "AmeraLabs" production line

In the period 2020-2022 years, novel acrylated epoxidized soybean oil (AESO)-based resins developed by PhD student Migle Lebedevaite supervised by prof. dr. Jolita Ostrauskaite has been applied in digital light processing (DLP) 3D printing by the company "AmeraLabs". The 3D printing parameters have been validated, and the 3D polymeric objects have been DLP 3D printed according to the standardized company procedure. The 3D printing parameters of AESO-based resins were compared with those of commercial petroleum-based resin, and the overall quality of the printed objects was evaluated.

The first set of AESO-based resins was composed of AESO and four different bio-based reactive diluents (RDs): isobornyl methacrylate (IBOMA), metacrylic ester (ME), tetrahydrofurfuryl acrylate (THFA) and tetrahydrofurfurul methacrylate (THFMA), with different biorenewable carbon content (BRC) and suitable viscosity for DLP 3D printing (Table 1). Additionally, for the printing layer thickness control and light absorption, 0.3 % of carbon black pigment was added. AESO-based polymers were 3D printed using a custom AmeraLabs DLP 3D printer equipped with an Acer H6518BD projector 400-600 nm. The 3D printing parameters are presented in Table 2. After printing, the objects were soaked in isopropanol for 15 min and post-cured under LED light ($\lambda = 400$-405 nm, 50 W) for 2 h at room temperature. Commercial petroleum-based resin was also 3D printed for comparison.

Table 1. Characteristics of AESO-based resins

Resin	Ratio of AESO:RD, wt	BRC, %	Viscosity, mPa·s
AESO/IBOMA	60:40	78.5	700
AESO/ME	70:30	81.9	640
AESO/THFA	70:30	76.6	560
AESO/THFMA	70:30	75.3	630

Table 2. 3D printing parameters with custom 3D printer

Parameter	Value
Building volume	71.8 × 40.4 × 230 mm
XY resolution	37.4 µm
Layer thickness	50 µm
Exposure time	6 s

3D printed polymeric objects showed high printing accuracy with smooth surface finishing comparable to commercial petroleum-based resin (Figure 1).

Figure 1. DLP 3D printed object of AESO/IBOMA (left) and 3D printed lower human jaw bone fragments of commercial resin (light) and AESO/THFMA resin (black) (right).

It was noticed that according to the bio-based RD used, different properties of 3D printed objects were obtained. The 3D printed AESO/IBOMA polymer samples were tough and firm, while the AESO/ME polymer samples were soft and elastic (Figure 2).
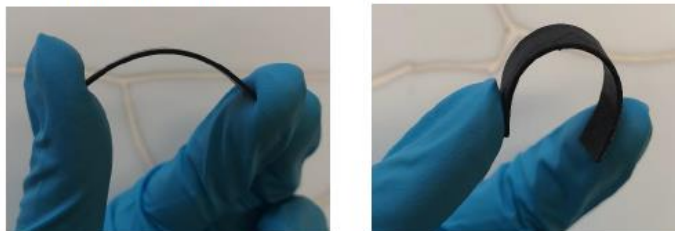

Figure 2. DLP 3D printed specimens of AESO/IBOMA (left) and AESO/ME (right)

Later, AESO-based polymer composites were 3D printed of AESO resins with IBOMA and two different fillers. Fillers were synthesized from local company production waste material (XS) and additionally functionalized with acryl silane (XSM) (Table 3). For light absorption and layer thickness control, 0.08 % of UV blocker 2,5-bis(5-tert-butyl-benzoxazol-2-yl) thiophene was added. DLP 3D printing was performed with a Phrozen Sonic Mini 4K 3D printer. The 3D printing parameters are presented in Table 4. After printing, the objects were soaked in isopropanol for 20 min and post-cured in UV chamber (LED light source: $\lambda = 365$ nm (45 W), $\lambda = 380$ nm (25 W), $\lambda = 395$ nm (70 W)) for 60 min.

Table 3. Characteristics of AESO-based resins

Resin	Ratio of AESO:IBOMA, wt	Amount of filler, wt.%	Viscosity, mPa·s
AS40/I60/XS5	40:60	5	241
AS40/I60/XSM5			266

Table 4. 3D printing parameters with custom 3D printer

Parameter	Value
Building volume	69 × 121 × 132 mm
XY resolution	35 μm
Layer thickness	50 μm
Exposure time	12 s

3D printed polymeric composites were successfully produced from AESO-based resins with fillers derived from local company production waste. The 3D printed objects were highly detailed without any significant marks of filler sedimentation (Figure 3). Due to the incorporated fillers, surface whitening was noticed.

Figure 2. DLP 3D printed AESO-based composites: complex shape object of AS40/I60/XS5 (left) and action figures of AS40/I60/XSM5 (middle and right)

124

AESO-based polymer composites were successfully DLP 3D printed by AmeraLabs for the first time. AESO-based resins could potentially replace commercial petroleum-based 3D printing resins. Such an innovation would benefit the environment by reducing the consumption of petroleum-based materials and providing competitive properties for 3D printed objects.

Conclusions

1. Acrylated epoxidized soybean oil-based resins with different bio-based reactive diluents were 3D printed with a custom-made DLP 3D printer. Printed objects indicated high printing accuracy and appearance similar to those printed of the commercial petroleum-based resin. Depending on the chosen reactive diluent, different properties of 3D printed bio-based polymer objects can be obtained.
2. Acrylated epoxidized soybean oil-based composites with fillers developed from the local company production waste material were 3D printed with a commercial DLP 3D printer. Printed polymeric composite objects were highly detailed without significant filler sedimentation noticed and could potentially replace commercial petroleum-based products in DLP 3D printing.

MB "AmeraLabs" representative: KTU representatives:

Co-founder   Prof. dr. J. Ostrauskaite
V. Talacka

                                                  PhD student
                                                  M. Lebedevaite

125

10.2. JSC "3D Creative" Trial production act

saulius@3dcreative.lt
+370 604 96962
3dcreative.lt

TRIAL PRODUCTION ACT
Optical 3D printing of medical fittings from acrylated epoxidized soybean oil-based resins on the JSC "3D Creative" production line

In 2021, a novel acrylated epoxidized soybean oil (AESO)-based resin developed by PhD student Migle Lebedevaite supervised by prof. dr. Jolita Ostrauskaite of Kaunas University of Technology (KTU) has been applied in the industrial line of JSC 3D Creative". Before this, AESO-resin was tested for a small optical 3D printing at the Laser Research Center (LRC) of Vilnius University (VU) by PhD student E. Skliutas supervised by prof. dr. M. Malinauskas.

Computer Aided Design (CAD) models of medical fittings were created using the 3D scanning technique readily available at JSC 3D Creative. They were converted to STL models and adjusted for specific 3D printers: Asiga Pico 2 UV (VU) and later for Zortrax Inkspire (3D Creative) (Figure 1).
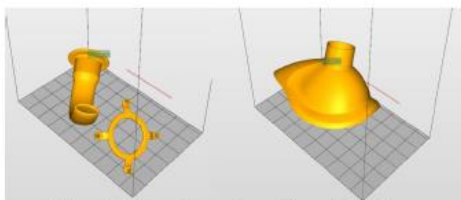

Figure 1. STL model previews of the medical fittings.

Firstly, a small-scale medical fitting was produced in VU LRC from commercial standard resin Asiga PlasGray (Figre 2a) to evaluate the STL models and to find the most appropriate 3D printing parameters like layer height and exposure duration. Then the chosen manufacturing conditions were adjusted to the AESO-based resin to produce quality 3D printed objects (Figure 2b).

Figure 2. Reduced size 3D printed medical fittings of commercial resin Asiga PlasGray (a) and AESO-based resin (b) using Asiga Pico UV 3D printer at VU LRC

After the developed AESO-based resin fulfilled the requirements for the produced objects, the manufacturing was transferred to JSC 3D Creatice. Despite the differences in the equipment switching from Digital Light Processing (DLP) to Liquid Crystal Display (LCD) techniques and from 385 to 405 nm irradiation wavelengths, judging from geometrical and mechanical properties, the produced objects revealed suitability for the intended use (Figure 3).

126

Figure 3. 3D printed medical fittings produced in 3D Creative by Zortrax Inkspire 3D printer.

True to shape with smooth surface finishing 3D printed medical fittings of the developed novel AESO-based resin proved its suitability for replacing commercial petroleum-based resins for rapid prototyping and additive manufacturing.

Conclusions

Acrylated epoxidized soybean oil-based resin produced lookalike 3D printed objects as the commercial standard resin Asiga PlasGray. Real-scale 3D printed medial fittings of developed bioresin were produced in the industrial line of JSC 3D Creative demonstrating its suitability for the intended use.

JSC "3D Creative" representative:

General manager
S. Lileikis

KTU representatives

Prof. dr. J. Ostrauskaite

PhD student
M. Lebedevaite

VU LRC representatives

Prof. dr. M. Malinauskas

PhD student
E. Skliutas

10.3. Life Cycle Assessment. Optical 3D printing of dental models using acrylic resin on soybean oil

Rathish Rajan, Egidija Rainosalo, Migle Lebedevaite, Ostrauskaitė Jolita, Vaidas Talačka

Life Cycle Assessment

OPTICAL 3D PRINTING OF DENTAL MODELS USING ACRYLIC RESIN BASED ON SOYBEAN OIL

Rathish Rajan and Egidija Rainosalo – Centria University of Applied Sciences, Finland
Migle Lebedevaite and Ostrauskaitė Jolita – Kaunas University of Technology, Lithuania
Vaidas Talačka – AmeraLabs Ltd, Lithuania

Life Cycle Assessment

OPTICAL 3D PRINTING OF DENTAL MODELS USING ACRYLIC RESIN BASED ON SOYBEAN OIL

centria
University of Applied Sciences
ammattikorkeakoulu

129

CONTENTS

131

1 INTRODUCTION

To facilitate the current transition toward a circular economy, the availability of renewable materials for additive manufacturing also becomes increasingly important. Additive manufacturing started in the 1980s with the development of the stereolithography apparatus (SLA) by Hull at 3D Systems (Hull 1984, Gross 2014). SLA printing is the layer-by-layer curing of liquid photopolymer resins using a focused laser beam. When a light projector is applied instead, exposing the entire layer to UV light simultaneously, the process is named digital light processing (DLP). Additive manufacturing via SLA or DLP process is applicable for high-resolution prototyping and fabrication of biomedical devices, for example, dental implants (l'Alzit 2022). The commercialized photopolymer resins used in SLA/DLP process are expensive and fossil fuel-based (Gross 2014, Voet 2021).
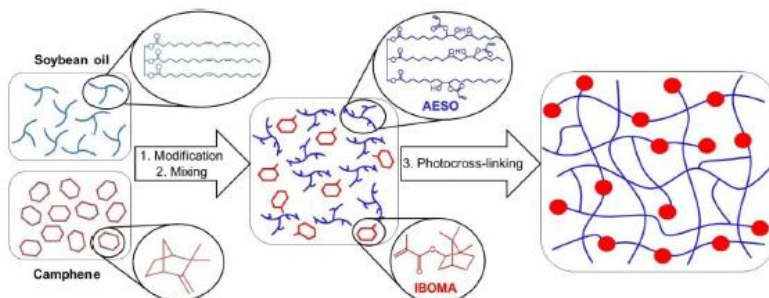

Figure 1: Schematic representation of curing of modified soybean oil-based resin during SLA/DLP method

The increased interest in bio-based products lead to active research and development that resulted in the development of vegetable oil-based 3D printable resin formulations. It is important to ensure that the new bio-based resin formulations do not have unintended environmental or health impacts from emissions during the production of novel ingredients, during the product use phase and during end-of-life disposal. Therefore, it is necessary to apply a holistic assessment tool to measure the sustainability of the resin formulation and the product made of it on a life cycle basis.

Life Cycle Assessment (LCA) is a tool to assess the potential environmental impacts and resources used throughout a product's life cycle, considering all potentially hazardous emissions and multiple categories of health and environmental impacts that result from those emissions (International Organization for Standartisation 2006). LCA can be used to investigate the most important contributors to environmental impacts by identifying the processes or materials in product life. Thus, it will provide data for designers to guide material selection, assist in supply chain management efforts, compare alternate designs or formulations, and provide product-level assessments that can be used for technology development and marketing (Montazeri 2018).

The advancement in digital technology has increased the options available for dental treatment. To produce solid casts from digital data, there are two types of 3D manufacturing processes. Subtractive manufacturing is one of the processes that can produce 3D models (Kafle 2021). The other fabrication method being used is additive manufacturing such as 3D printing. This method of fabrication includes many advantages such as a minimum material usage with diminished waste accumulation during the production and the ability to create multiple products at a time (Kafle 2021).

Dental model printing generally requires exceptional surface quality and very high accuracy as these models are used by dental technicians and dentists not only for a visual purpose but for the planning of dental treatment as well. Optical 3D printing here is also very beneficial as most of these prints are personalized, unique and applied to a specific customer only. Currently, the dental models are made from petroleum-based acrylic resins. Cradle-to-gate LCA results are compared across multiple impact categories to highlight potential environmental benefits or impacts of printing a batch of dental models from soybean oil-based resin formulation and provide recommendations for further improvements applicable to different life cycle phases of the product.
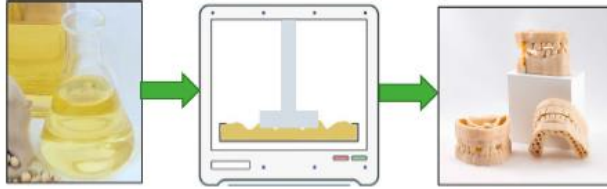
x 11,69 in

132

Figure 2: Representation of the SLA 3D-printing of dental models from resin formulation based on soybean oil

2 METHODS

The LCA model is built according to the international standards ISO 14040 and ISO 14044 (International Organisation for Standartisation, 2006). To conduct the LCA, the SimaPro 9.0 software and ILCD midpoint+ method was used.

2.1 GOAL AND SCOPE

The goal of this study is to compare the life cycle environmental impacts of bio-based photocurable acrylic resin for 3D printing dental models with existing conventional photocurable acrylic resins. The acrylated epoxidized soybean oil (AESO) is used as the main component of the bio-based photocurable resin with approx. 87.7% of bio-renewable carbon (BRC) content. The functional unit of this study is set to 3D-printing of a batch containing 17 dental models using 0.25 kg of photocurable acrylic resin (bio-based or conventional) by digital light processing method. The optical 3D printing using both resins consumes 0.24 kg of isopropanol (IPA) and 5 g of gloves.

Since this LCA aims to compare the environmental impacts in the production phase of bio-based and conventional acrylic resins used for the production of dental models, the use-phase and EOL (End of Life) of the dental models are excluded. These stages are excluded due to the lack of data about the emissions during production and because of similarities of end-of-life scenarios for both types of resins considered. Thus, a cradle-to-gate approach has been adopted which begins from the raw material extraction and ends with the printed part ready for packing. The life cycle phases and the unit processes of 3D printing dental models with bio-based resin and conventional resin are presented in Figure 3. Capital equipment, infrastructure and employee travel are excluded. Since the factories and infrastructure are used for producing vast amounts of 3D printed products, the environmental impacts allocated to one batch of the dental model are extremely low. Therefore, these processes are excluded.
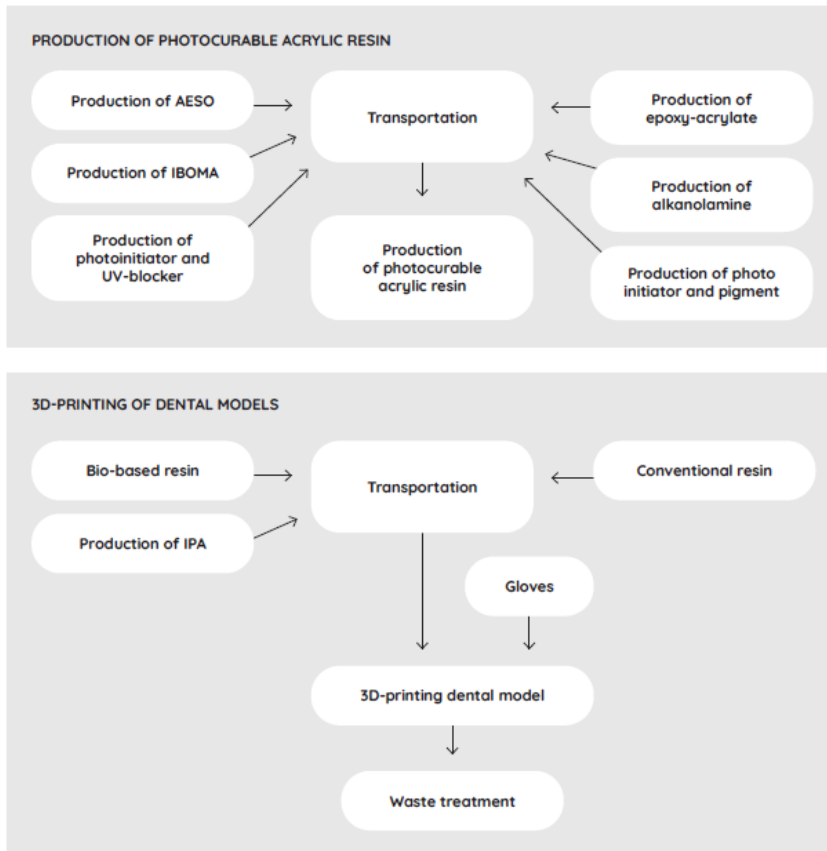
PRODUCTION OF PHOTOCURABLE ACRYLIC RESIN

Production of AESO → Transportation ← Production of epoxy-acrylate

Production of IBOMA → ← Production of alkanolamine

Production of photoinitiator and UV-blocker → ↓ ← Production of photo initiator and pigment

Production of photocurable acrylic resin

3D-PRINTING OF DENTAL MODELS

Bio-based resin → Transportation ← Conventional resin

Production of IPA →

Gloves

3D-printing dental model

Waste treatment

Figure 3: System boundary considered for 3D printing dental models from soybean oil-based resin and conventional acrylic resin

2.2 LIFE CYCLE INVENTORY

The main processes modelled for the study are described in the following sub-sections. Priority was given to measured/calculated data obtained from the ECOLABNET partners (KTU and AMERALABS). Other secondary data used in the study is collected from Ecoinvent 3.1. database and the literature. Literature and internet pages, as well as expert judgement and personal communications, were used as a source of information to construct the needed processes and materials. When the secondary data was not available or data was not available, estimates are applied to ensure the completeness of the study. Simapro 9.1 software was used to model the cradle to gate life cycle of 3D printing the dental models. The country-specific Ecoinvent datasets of the electricity grid mix have been used for modelling the electricity consumed during the 3D printing, and production of the photocurable acrylic resin. The inventory results and the impact assessment are calculated using Simapro 9.1.

2.2.1 MODELLING OF BIO-BASED PHOTOCURABLE ACRYLIC RESIN

The resins were prepared by mixing AESO (58.45%) with bio-based reactive diluent (IBOMA) (38.97%) to achieve the required resin viscosity for DLP 3D printing technology. The added amount of photoinitiator was 2.5%. 0.08% of UV blocker was used to control the UV light absorption.

Table 1. Composition of photocurable AESO resin

Formulation	(%)
acrylated epoxidized soybean oil (monomer)	58,45
isobornylmethacrylate (monomer)	38,97
diphenyl(2,4,6-trimethylbenzoyl) phosphine oxide (photoinitiator)	2,5
2,5-bis(5-tert-butyl-benzoxazol-2-yl)thiophene (UV blocker)	0,08

The modelling of the bio-based acrylic resin was done based on the data provided by the resin producer (KTU). The composition of the photocurable AESO resin is tabulated in Table 1. The AESO and IBOMA were not available in the Ecoinvent database. The AESO was modelled using epoxidized soybean oil (ESO), acrylic acid, hydroquinone and triethylamine (Habib 2011, Saithai 2011). In addition, epoxidized soybean oil was modelled and used in the modelling of AESO. The literature data was followed for the selection of raw materials for AESO. The modelling of the process for the production of 1 kg of AESO is tabulated in Table 2. The electricity and heat data required for producing 1 kg of organic chemical excluding the upstream process is included in the modelling due to lack of data (Kim 2003).

The production of IBOMA was modelled using methacrylic acid, camphene, hydroquinone, and zirconia sulfuric acid. Camphene and zirconia sulfuric acid are not modelled but replaced with 'chemical organic' available in the Ecoinvent database. The raw materials used for modelling are based on the process of preparation of IBOMA in the US. Patent US5719314A (Riondel 1998). The material input and the data used can be found in Table 3.

Table 2: Modelling of the process for producing 1 kg AESO

Materials/fuels	Data used	Amount	Unit
Epoxidized soybean oil	Epoxidized soybean oil (Modelled)	1000	g
Acrylic acid	Acrylic acid {RER}| production	Cut-off, U	141	g
Hydroquinone monomethyl ether	Hydroquinone {RER}| production	Cut-off, U	0,45	g
Triethylamine	Triethyl amine {RER}| production	Cut-off, U	5,7	g
Production			
Electricity	Electricity, medium voltage {LT}| electricity voltage transformation from high to medium voltage	Cut-off, U	0,166	kWh
Heat - steam	Heat, from steam, in chemical industry {RER}| steam production, as energy carrier, in chemical industry	Cut-off, U	7,7	MJ
Heat - fuel	Heat, district or industrial, other than natural gas {LT}| heat and power co-generation, oil	Cut-off, U	0,15	MJ

136

Table 3: Modelling of the process for producing 1 kg of IBOMA

Materials/fuels	Data used	Amount	Unit
Zirconia sulfuric acid (catalyst)	Chemical, organic {GLO}| market for	Cut-off, U	121	g
Hydroquinone monomethyl ether	Hydroquinone {RER}| production	Cut-off, U	0,107	g
Methacrylic acid	Methacrylic acid {RER}| production	Cut-off, U	554,34	g
Camphene	Chemical, organic {GLO}| market for	Cut-off, U	808,05	g
Production			
Electricity	Electricity, medium voltage {LT}| electricity voltage transformation from high to medium voltage	Cut-off, U	0,166	kWh
Heat - steam	Heat, from steam, in chemical industry {RER}| steam production, as energy carrier, in chemical industry	Cut-off, U	7,7	MJ
Heat - fuel	Heat, district or industrial, other than natural gas {LT}| heat and power co-generation, oil	Cut-off, U	0,15	MJ

The modelling of the bio-based acrylic resin was done according to the formulation provided by KTU (Table 1). The UV-blocker (0.08%) and diphenyl(2,4,6-trimethylbenzoyl) phosphine oxide (2.5%) was not modelled. It was replaced with the 'chemical organic' unit process from the Ecoinvent database. The data used for the production of bio-based photocurable resin can be seen in Table 4.

Table 4: Modelling of the process for producing 1 kg of photocurable bio-based acrylic resin

Materials/fuels	Data used	Amount	Unit
AESO (Monomer)	Acrylated epoxidized soybean oil (Modelled)	584,5	g
IBOMA (Monomer)	Isobornyl methacrylate (Modelled)	389,7	g
diphenyl(2,4,6-trimethylbenzoyl phosphine oxide (photoinitiator) +UV-blocker	Chemical, organic {GLO}| production	Cut-off, U	25,8	g
Production			
Electricity	Electricity, medium voltage {LT}| electricity voltage transformation from high to medium voltage	Cut-off, U	0,166	kWh
Heat - steam	Heat, from steam, in chemical industry {RER}| steam	7,7	MJ

137

2.2.2 MODELLING OF CONVENTIONAL PHOTOCURABLE ACRYLIC RESIN

The modelling of conventional acrylic resin was done by following formulations of a commercial resin's material safety data sheet from Ameralabs. The average energy consumption for 1 kg of organic chemicals was also included in modelling (Kim 2003).

Table 5: Modelling of the process for producing 1 kg of photocurable conventional acrylic resin

Materials/fuels	Data used	Amount	Unit
Epoxy-acrylate	Conventional photocurable_Epoxy acrylate (Modelled)	950	g
Alkanolamine	Triethanolamine {RER}| ethanolamine production	Cut-off, U	20	g
Photoinitiator	Chemical, organic {GLO}| production	Cut-off, U	10	g
Pigment	Chemical, organic {GLO}| production	Cut-off, U	20	g
Production			
Electricity	Electricity, medium voltage {LT}| electricity voltage transformation from high to medium voltage	Cut-off, U	0,166	kWh
Heat - steam	Heat, from steam, in chemical industry {RER}| steam production, as energy carrier, in chemical industry	Cut-off, U	7,7	MJ
Heat - fuel	Heat, district or industrial, other than natural gas {LT}| heat and power co-generation, oil	Cut-off, U	0,15	MJ

138

2.2.4. MODELLING OF PRODUCTION STAGE

The details about modelling of 3D printing of 1 batch of dental models by DLP method using bio-based and conventional, photocurable acrylic resins are provided in this sub-section. One batch of dental models containing 17 models takes 38 minutes to complete DLP 3D printing. The resin consumed during the printing of one batch of dental models and the final weight of the cured models is 255 g. There is assumed to be 30 g/batch wastage of resin during printing. Around 3.7 L of isopropanol (IPA) is used for washing and IPA is assumed to be replaced after the production of 200 parts (Mele 2020). The modelling of bio-based and conventional acrylic resin can be seen in Table 6 and Table 7.

Table 6: Modelling of the process for 3D printing 1 batch of dental models using bio-based resin

Materials/fuels	Data used			Amount	Unit
Bio-based acrylic resin	Bio-based (Modelled)	acrylic	photo resin	255	g
IPA for washing	Isopropanol Cut-off, U	{RER}	production		245,86	g
Gloves	Latex {RER} market for latex	Cut- off, U			5	g
Production					
Electricity - Printing	Electricity, low voltage {LT} electricity voltage transformation from medium to low voltage	Cut- off, U			0,0361	kWh
Waste treatment					
Waste treatment IPA	Process-specific burdens, hazardous waste incineration plant {CH} processing	Cut-off, U			245,86	g
Waste treatment gloves	Process-specific burdens, hazardous waste incineration plant {CH} processing	Cut-off, U			5,0	g
Waste resin during printing	Process-specific burdens, hazardous waste incineration plant {CH} processing	Cut-off, U			30,0	g
Transportation					
Transportation of resin from a distance of 100 km	Transport, freight, lorry >32 metric ton, EURO5 {RER} transport, freight, lorry >32 metric ton, EURO5	Cut-off, U			0,025	tkm
Transportation of IPA from a distance of 100 km	Transport, freight, lorry >32 metric ton, EURO5 {RER} transport, freight, lorry >32 metric ton, EURO5	Cut-off, U			0,024	tkm

139

Table 7: Modelling of the process for 3D printing 1 batch of dental models using conventional resin

Materials/fuels	Data used	Amount	Unit
Conventional acrylic resin	Conventional photo curable acrylic resin (Modelled)	255	g
IPA for washing	Isopropanol {RER}| production	Cut-off, U	245,86	g
Gloves	Latex {RER}| market for latex	Cut- off, U	5	g
Production			
Electricity - Printing	Electricity, low voltage {LT}| electricityvoltage transformation from medium to low voltage	Cut- off, U	0,0361	kWh
Waste treatment			
Waste treatment IPA	Process-specific burdens, hazardous waste incineration plant {CH}| processing	Cut-off, U	245,86	g
Waste treatment gloves	Process-specific burdens, hazardous waste incineration plant {CH}| processing	Cut-off, U	5,0	g
Waste resin during printing	Process-specific burdens, hazardous waste incineration plant {CH}| processing	Cut-off, U	30,0	g
Transportation			
Transportation of resin from a distance of 100 km	Transport, freight, lorry >32 metric ton, EURO5 {RER}| transport, freight, lorry >32 metric ton, EURO5	Cut-off, U	0,025	tkm
Transportation of IPA from a distance of 100 km	Transport, freight, lorry >32 metric ton, EURO5 {RER}| transport, freight, lorry >32 metric ton, EURO5	Cut-off, U	0,024	tkm

140

3 LIFE CYCLE IMPACT ASSESSMENT METHOD

The life cycle impact assessment method chosen in this study is ILCD Midpoint+. The full title of this method is ILCD recommendations for LCIA in the European context. The European Commission analysed several methodologies for LCIA and made some effort toward harmonization. The endpoint methods, however, are not included in the ILCD method in Simapro, because the list is far from complete. However, in this study, all the type of LCI results are linked to 16 midpoint categories and is connected through endpoint indicators to the areas of protection such as human health, natural environment and natural resources as per the ILCD handbook recommendation (Figure 4).
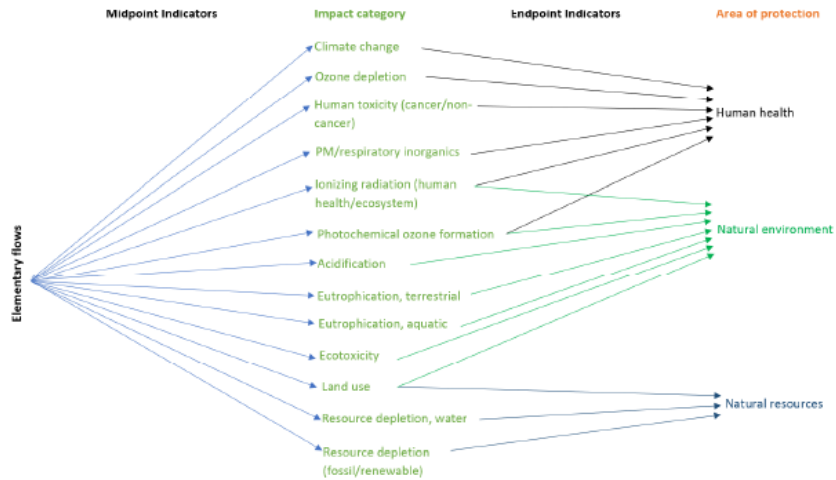

Figure 4: Overall scheme of the ILCD Midpoint+ method showing the link through midpoint indicators and endpoint indicators towards three areas of protection

141

4 LIFE CYCLE IMPACT ASSESSMENT

Life cycle impact assessment (LCIA) results are presented in this section. The results of the inventory analysis have been characterized, and impact assessment results are calculated using Simapro. LCIA results are always relative expressions and represent the potential environmental impact. According to ISO 14040 and ISO 14044, normalization and weighting are voluntary parts of the impact assessment phase. In this study, the LCIA results have not been weighted or normalization has been done.

In the characterization step, all the impacts are sorted into 16 midpoint categories according to the effect they have on the environment. The global warming potential is calculated for each of the different greenhouse gases and expressed relative to the CO_2 which is therefore defined as unity. The results show that there is a small savings of 0,15 kg CO_2 eq in terms of the climate change category. The main process contributing to this impact category in terms of bio-based resin is crude soybean oil. The lower savings in this category is due to the modification process of soybean oil. The main midpoint categories that showed increased impact for bio-based resin were land occupation, marine eutrophication and water resource depletion. This is obviously due to the land occupation and other agricultural practices during the cultivation of the soybean. The fertilizer run-off into the water bodies due to agricultural practices is accountable for the increased impact of bio-based resin in the eutrophication category. However, the dental models printed with bio-based resin showed reduced impact in 12 out of 16 categories when compared to those made from conventional acrylic resin.

Table 8: Characterization results expressed in 16 midpoint categories for a batch of dental models printed with conventional and bio-based acrylic resins

Midpoint impact category	Unit	Dental model-Conventional acrylic resin	Dental models-Bio-based acrylic resin
Climate change	kg CO2 eq	2,30E+00	2,15E+00
Ozone depletion	kg CFC-11 eq	2,72E-07	1,55E-07
Human toxicity, non-cancer effects	CTUh	4,26E-07	4,56E-08
Human toxicity, cancer effects	CTUh	8,93E-08	7,37E-08
Particulate matter	kg PM2.5 eq	1,25E-03	1,01E-03
Ionizing radiation HH	kBq U235 eq	1,68E-01	1,24E-01
Ionizing radiation E (interim)	CTUe	5,73E-07	4,48E-07
Photochemical ozone formation	kg NMVOC eq	7,80E-03	6,46E-03
Acidification	molc H+ eq	1,00E-02	8,94E-03
Terrestrial eutrophication	molc N eq	1,78E-02	1,58E-02
Freshwater eutrophication	kg P eq	5,71E-04	4,09E-04
Marine eutrophication	kg N eq	1,70E-03	3,45E-03
Freshwater ecotoxicity	CTUe	3,13E+01	2,01E+01
Land use	kg C deficit	1,85E+00	1,32E+01
Water resource depletion	m3 water eq	3,09E-03	4,63E-03
Mineral, fossil & renewable resource depletion	kg Sb eq	3,66E-05	6,60E-05

A reduced impact was found in terms of freshwater ecotoxicity for bio-based resins. The process that influences this impact category was crude soybean oil used in the modelling of bio-based acrylic resin. Chemicals can be emitted to the environment (air, water, soil) during all life cycle stages of products. Emission inventories of different products may contain hundreds of chemicals, of which many will have the potential to cause ecotoxic impacts on aquatic and terrestrial ecosystems, leading to damage to ecosystem quality. It can be concluded that by using the soybean-based resin, fewer chemicals are emitted into the environment during resin production. This should eventually improve the ecosystem quality.

15

142

The three areas of protection linked through midpoint indicators are human health, natural environment and natural resources as seen in Figure 4. As seen in Figure 5, the dental models based on bio-based resin have a negative environmental impact on endpoint indicator natural resources. This is because the midpoint categories (land use, water resource depletion and mineral, fossil & renewable resource depletion) assigned to this endpoint indicator are related to soybean oil cultivation. The bio-based resin seems to be a better option than conventional resin in the case of endpoint indicator human health.
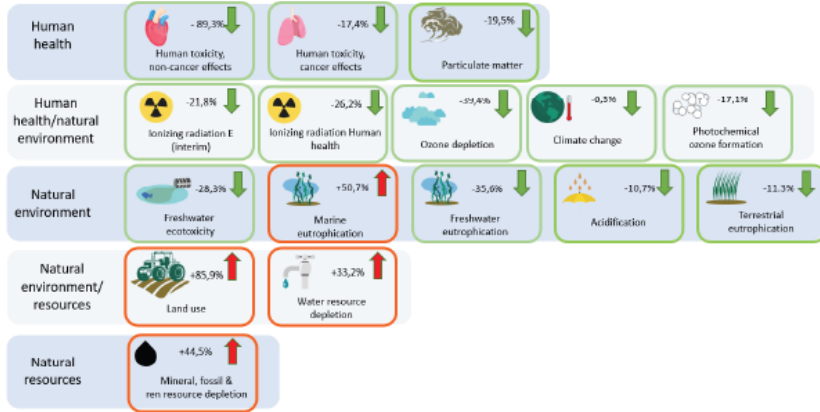

Figure 5: The environmental impacts of using bio-based resin compared to conventional resin to print the dental models presented in terms of three areas of protection

5 CONCLUSIONS

A cradle-to-gate life cycle assessment of optical 3D printing a batch of dental models by using bio-based and conventional acrylic resin was conducted to compare the environmental impact of both resins. The inventory compilation was based on Ecoinvent 3.1. database in Simapro software. Literature and internet pages, as well as expert judgement and personal communications, were used as a source of information. The life cycle impact assessment method chosen in this study is ILCD Midpoint+.

The bio-based resin has shown reduced impact on human health but increased impact on natural resources. The emissions from agricultural activities, especially the sulphur-containing diesel burned in farm equipment and the surface runoff of nitrogen and phosphorus compounds to water bodies due to fertilizer use, deteriorating air and water quality as seen from the overall LCIA results. Additionally, aromatic, aliphatic and chlorinated compounds added during soybean crushing and degumming, oil refining, and resin production all contribute to the increased environmental impacts when the soybean oil-based resin is considered. Land use is the major contributor to the endpoint indicator, natural resources and is due obvious reason for land occupation for soybean cultivation.

The results from this study clearly show the benefit of using bio-based chemicals for formulating the resin. However, replacing petrochemical components with renewable chemical substitutes in new bio-based resin formulations should not just consider the amount of bio-based content, but ideally should consider more sustainable bio-based feedstock and the processing conditions with low environmental impact to ensure environmentally preferable resin formulations.

144

REFERENCES

Gross, B. C., Erkal, J. L., Lockwood, S. Y., Chen, C., & Spence, D. M. (2014). Evaluation of 3D printing and its potential impact on biotechnology and the chemical sciences.

Habib, F., & Bajpai, M. (2011). Synthesis and characterization of acrylated epoxidized soybean oil for UV cured coatings. Chem. Chem. Technol, 5(3), 317-326.

Hull, C. W. (1984). Apparatus for production of three-dimensional objects by stereolithography. United States Patent, Appl., No. 638905, Filed.

International Organization for Standardization. (2006). Environmental management: life cycle assessment; Principles and Framework. ISO.

International Organization for Standardization. (2006). Environmental management: life cycle assessment; requirements and guidelines (Vol. 14044). Geneva, Switzerland: ISO.

Kafle, A., Luis, E., Silwal, R., Pan, H. M., Shrestha, P. L., & Bastola, A. K. (2021). 3D/4D Printing of polymers: Fused deposition modelling (FDM), selective laser sintering (SLS), and stereolithography (SLA). Polymers, 13(18), 3101.

Kim, S., & Overcash, M. (2003). Energy in chemical manufacturing processes: gate-to-gate information for life cycle assessment. Journal of Chemical Technology & Biotechnology: International Research in Process, Environmental & Clean Technology, 78(9), 995-1005.

l'Alzit, F. R., Cade, R., Naveau, A., Babilotte, J., Meglioli, M., & Catros, S. (2022). Accuracy of commercial 3D printers for the fabrication of surgical guides in dental implantology. Journal of Dentistry, 117, 103909.

Mele, M., Campana, G., & D'Avino, G. (2020). Life cycle impact assessment of desktop stereolithography. Journal of Cleaner Production, 244, 118743.

Montazeri, M., & Eckelman, M. J. (2018). Life cycle assessment of UV-Curable bio-based wood flooring coatings. Journal of Cleaner Production, 192, 932-939.

Riondel, A. (1998). U.S. Patent No. 5,719,314. Washington, DC: U.S. Patent and Trademark Office.

Saithai, P., Tanrattanakul, V., Chinpa, W., Kaewtathip, K., & Dubreucq, E. (2011). Synthesis and characterization of triglyceride-based copolymer from soybean oil. In Materials Science Forum (Vol. 695, pp. 320-323). Trans Tech Publications Ltd.

Voet, V. S., Guit, J., & Loos, K. (2021). Sustainable photopolymers in 3d printing: A review on biobased, biodegradable, and recyclable alternatives. Macromolecular Rapid Communications, 42(3), 2000475.

Life Cycle Assessment
OPTICAL 3D PRINTING OF DENTAL MODELS USING ACRYLIC RESIN BASED ON SOYBEAN OIL

Green chemistry and green engineering concepts have been combined to develop novel sustainable polymeric materials by formulating bio-based UV-curable 3D-printable resins. The bio-based resin is composed of acrylated epoxidized soybean oil (AESO), isobornyl methacrylate (IBOMA), photo-initiator and UV-blocker. Our previous studies have shown that these resins show comparable properties to the fossil-based optical 3D printing resins by providing the additional benefit of using bio-based feedstock materials.

Life cycle assessment is a tool used to measure environmental sustainability. This study aims to compare the environmental impact of 3D printing a batch of dental models using UV-curable, bio-based and fossil-based acrylic resins. This is a cradle-to-gate study which covers the raw material extraction and production of a batch of the dental model that is ready to pack. The software used for modelling the study is Simapro 9.1. The life cycle impact assessment (LCIA) method used is ILCD midpoint+. All the 16 midpoint impact categories are linked to three areas of protection (Human health, natural environment, and natural resources).

The dental models printed with bio-based resin show reduced impact in 12 out of 16 categories when compared to those made from conventional petroleum-based acrylic resin. There was no large difference between the two resins when the climate change impact category is considered. The four impact categories in which bio-based resin had relatively higher environmental impact are eutrophication, land-use, water resource depletion, mineral, fossil & renewable resource depletion. This is certainly due to the cultivation practices, processing of soybean oil, and production of AESO which contributes to the higher environmental impact of dental models printed by bio-based resin. The results from this study clearly show the benefit of using bio-based materials for formulating the UV-curable 3D-printing resin. In addition, the results also point out the importance of selecting more sustainable bio-based feedstock and processing conditions with low environmental impact when formulating new bio-based resins.